US DOT - PHMSA

Final Report No. 16-025

Threat/Anomaly Mitigation Decision-Making Process

Jing Ma, PhD

February 23, 2016

0339-1402

Intentionally blank

Final Report No. 16-025

Final Report

on

THREAT / ANOMALY MITIGATION DECISION-MAKING PROCESS

to

U.S. DEPARTMENT OF TRANSPORTATION – PIPELINE AND HAZARDOUS MATERIALS SAFETY ADMINISTRATION

February 23, 2016

Prepared by

Jing Ma, PhD
Senior Engineer I

Approved by

John F. Kiefner, PhD, PE
Senior Advisor

Kiefner and Associates, Inc.
4480 Bridgeway Avenue, Suite D
Columbus, OH 43219

0339-1402

DISCLAIMER

This document presents findings and/or recommendations based on engineering services performed by employees of Kiefner and Associates, Inc. The work addressed herein has been performed according to the authors' knowledge, information, and belief in accordance with commonly accepted procedures consistent with applicable standards of practice, and is not a guaranty or warranty, either expressed or implied.

The analysis and conclusions provided in this report are for the sole use and benefit of the Client. No information or representations contained herein are for the use or benefit of any party other than the party contracting with Kiefner. The scope of use of the information presented herein is limited to the facts as presented and examined, as outlined within the body of this document. No additional representations are made as to matters not specifically addressed within this report. Any additional facts or circumstances in existence but not described or considered within this report may change the analysis, outcomes and representations made in this report.

TABLE OF CONTENTS

INTRODUCTION 1
CONCLUSIONS 1
Flaw Interaction Criteria 1
Excavation and Re-Assessment Scheduling 3
Scheduling Mitigations of Corrosion Regions 3
Scheduling Mitigations of Crack-like Anomalies 4
Scheduling Mitigations of Mechanical Damage 5
LIST OF ANNEXES 6

Intentionally blank

Threat/Anomaly Mitigation Decision-Making Process

Jing Ma, PhD

INTRODUCTION

Pipeline operators must excavate and examine anomalies discovered through in-line inspection (ILI) and direct assessment (DA) such as ECDA, ICDA, or SCCDA in a timely manner to assure that critical flaws are repaired before they become severe enough to cause a pipeline to fail at its maximum operating pressure. They must also periodically re-assess their pipelines that are located in or could affect high consequence areas.

Prescriptive regulations often require examinations or re-assessments of anomalies to be carried out after specific time periods. Pipeline integrity management standards such as ASME B31.8S and API 1160 provide guidance to operators with respect to identifying threats to pipeline integrity, gathering data for estimating risks associated with different threats, prioritizing pipeline segments, conducting engineering critical assessments, evaluating remaining lives, and scheduling future re-assessments.

While these standards have served the industry well, they could be strengthened in two areas, i.e. Interaction of Threats/Anomalies and Guidance for Scheduling of Excavations and Re-Assessments. To specifically enhance these two aspects, this project was supported by PHMSA under DOT agreement DTPH5614H00005 – "Threat/Anomaly Mitigation Decision-Making Process". The work involved reviewing and assessing approaches to flaw interaction and probabilistic evaluation methods. Three categories of anomalies, corrosion, crack-like, and mechanical damage were investigated in sequential order. Improvements to the above-mentioned pipeline standards were described and demonstrated in each milestone interim report submitted to PHMSA. The findings are summarized hereinafter and detailed in individual annex reports.

CONCLUSIONS

Flaw Interaction Criteria

The flaw interaction criteria were found through a comprehensive literature review encompassing 18 standards, 23 technical reports and 44 journal articles. Among these reports and articles, 23 were experimental projects, 32 involved purely analytical work, and 12 were

combined experimental and analytical projects. Conclusions drawn from the review are as follow:

- For corrosion-with-corrosion interaction, only the load-controlled failure mode exists, i.e. plastic collapse. Analytical studies generally yielded much larger threshold interaction distances than experimental tests. All the experimental results point to 6***t*** where ***t*** is the pipe wall thickness as the upper bound of interacting distance. However, when the spacing is as large as 6***t***, the experiments consistently found that the interaction of corroded areas does not occur. Therefore, ASME B31G 3***t***-by-3***t*** condition serves properly as the in-ditch interaction condition, which is also validated by its safe use in the actual historical pipeline operation. For ILI indications, with the consideration of tool sizing threshold and tolerance, at least 6***t***-by-6***t*** should be selected as the clustering criterion.

- For crack-with-crack interaction, both toughness-controlled and load-controlled failure mechanisms exist, e.g. fatigue, brittle fracture, ductile tearing and plastic collapse. For the offset distance between two surface cracks, experiments involving flaws that failed by fatigue pointed to the crack depth ***a*** as the interacting separation; analytical studies produced the value close to ***a*** for the stress intensity factor (SIF) and J-integral, and 1.8***a*** for plastic collapse. For the in-plane distance between two surface cracks, experiments yielded the threshold distance being ***a*** for cleavage and zero for fatigue; analytical studies generated the upper bound as the crack length 2***c*** for the SIF and 0.5***a*** for the J-integral and plastic collapse. With regard to embedded cracks, only analytical investigations on the SIF are available. For one embedded crack with one surface crack, the critical in-plane distance is 2***c*** along the length direction and 2***a*** along the depth direction. For two embedded cracks, the critical in-plane distance is ***a*** along both the length and depth directions. Overall, BS 7910: 2013 matches well with journal article findings for both surface and embedded cracks, and stands on the conservative side. Since the majority of experimental validations are based on fatigue tests, BS 7910: 2013 reflects the interaction during the crack growth before coalescence. Since brittle fracture utilizes the same SIF as fatigue, the interaction criterion can be interpreted similarly. No systematic experiments were conducted to define the threshold distance for ductile failures. However, burst tests on groove-groove defects by Kiefner (1969) and Advantica (2005) provide guidance to infer crack-like interaction in the plastic collapse regime, particularly for very long cracks. This means 6***t*** is a proper conservative estimation under such a circumstance. The interacting distance for ductile tearing is a load-dependent parameter, and the value should be between that for brittle fracture and that for plastic collapse.

- For dent-with-dent interaction, Francini and Yoosef-Ghodsi (2008) suggested the interaction criterion being the edge-to-edge distance less than $2\sqrt{Rt}$ (where R is the radius of the pipe and t is the wall thickness). For dent-with-corrosion interaction, the experimental work

conducted by Kiefner and Alexander (1999) provided the ASME B31.8 guidance. Al-Muslim (2010) performed the sensitivity study to fit equations for burst pressure and fatigue life prediction. For dent-with-weld interaction, Rosenfeld (1999) recommended applying the dent stress concentration factor (SCF) with a representative weld S-N (cyclic stress vs. number of cycles to failure) curve. In addition, Dinovitzer (2007) derived a dent-girth weld interaction factor. For dent-with-gouge interaction, the European Pipeline Research Group (EPRG) model was adopted by API 579-1/ASME FFS-1: 2007. For dent-with-crack interaction, an analytical model was proposed by Bai (1998) to incorporate certain crack SIFs accompanying some dent SCFs. Experimental tests on ten specimens exhibited a decent correlation with the model predictions. The essential idea is to treat the dent-caused stress and moment concentration as a nominal load magnification on the crack. Analogous methodology can be extended to the fatigue analysis.

Excavation and Re-Assessment Scheduling

In the second part of this project, the remediation plan for each of three anomaly categories was executed from both deterministic and probabilistic perspectives. Deterministic methods tend to use fixed values of each parameter, e.g. nominal or conservative estimation, and typically employ a standard assessment algorithm. To account for inherent uncertainties, arbitrary factors of safety are applied to the calculations of failure pressure and remaining life to remediate critical flaws and to establish re-assessment intervals. As a counterpart, probabilistic methods involve actual statistical variations of various parameters and consider the degree of error associated with the algorithms. The results are statistical distributions of failure pressure and remaining life, from which the operator may select upper or lower bound values with a desired degree of confidence level. Further, the influence from possible flaw interactions was discussed for future mitigation planning. “Tailored” interaction criteria for immediate repair were recommended to minimize the likelihood of an interaction occurring within the re-assessment interval. This part of the investigation demonstrated the flexibility of the existing guidelines by incorporating parameters reflecting the actual condition of pipeline, revealed potential problems of deterministic assessment prescribed by regulations, exemplified the capacity of probabilistic-based methods, and highlighted the improved reliability and risk mitigation. In the following, the conclusions for each type of anomaly mitigation are summarized based on the completed work.

Scheduling Mitigations of Corrosion Regions

ASME B31.8S is referenced by CFR 192 Subpart O for managing gas pipeline integrity. Liquid operators implement ASME B31.8S on a voluntary basis. The immediate response and re-assessment intervals are defined in Section 7 Figure 4 and Section 5 Table 3 in ASME B31.8S: 2010 for the mitigation of time-dependent growth of internal and external metal loss. The safety factor is described by the failure pressure ratio (FPR). According to the probabilistic

assessment, the probability of failure (POF) with an FPR of 1.1 is relatively small for an operating pressure level corresponding to 72% of SMYS, but the value of POF associated with the same FPR of 1.1 increases with decreasing operating stress levels.

By the same token, confidence levels vary significantly for every re-assessment requirement in the ASME B31.8S: 2010, Section 5 Table 3. To achieve the same POF as the immediate repair at the 72%-of-SMYS operating stress level when the specified time for re-assessment approaches, the required FPRs are generally higher than those prescribed values in the table for each operating condition and each re-assessment interval. The difference is greater for a lower operating pressure and/or a longer re-assessment interval when the corrosion growth uncertainty is taken into account.

Scheduling Mitigations of Crack-like Anomalies

With regard to the mitigation of crack-like anomalies, several issues were discussed in the finished work, such as interacting patterns of hook cracks, appropriate interaction criteria to determine repair, composite model of SCC and fatigue growth, and probabilistic fatigue life assessment.

On the basis of Kiefner's experience in inspection and failure analysis, it is quite common for seam weld crack-like defects to be located close to each other. The most frequent pattern is two hook cracks individually extending from the ID and OD surfaces. Through a sensitivity study, it was found that with twice the pipe wall thickness, $2t$, as the critical interaction spacing, those defects not interacting at present will be unlikely to interact until the end of five years for a typical liquid pipeline operating condition.

Traditional integrity management programs treat the growth mechanisms of SCC and pressure-cycle-induced fatigue separately. However, some prior research experiments and certain historical pipeline in-service failure data indicated independent analysis of the two phenomena could lead to non-conservative results. The superposition of SCC and fatigue growth mechanisms is a conservative description for remaining life prediction of SCC. Case studies have been carried out to understand this complex behavior dependent on multiple variables, such as SCC growth rate, pressure cycling severity, and crack shape. The comparison between exemplary gas pipelines and liquid pipelines provides insight into the superposition of and competition between SCC and fatigue behaviors.

The probabilistic fatigue life analysis was conducted on an operator's real case example in light of variabilities of material strength and toughness, crack-like anomaly size, and burst pressure model error. Defect size distributions were established from the in-ditch UT phased array and TOFD inspection during the ILI validation and repair program. The risk levels of fatigue failure before the next re-assessment associated with defects detected and missed by ILI were

separately calculated to identify the ILI effectiveness for mitigating the pipeline seam weld threat. Over time, the risk may be decreased or increased depending on the balance between the mitigation effort and the fatigue growth rate.

This approach proved to be particularly meaningful when the fatigue lives from the deterministic calculation for all pipeline segments cannot be differentiated. The probability of fatigue failure before the subsequent re-assessment provides a more holistic picture of the pipeline integrity condition. Thereby it expedites the prioritization process and optimizes the resources available for integrity assessment and remediation. It can be straightforwardly implemented into the pipeline risk management system even with a dynamic segmentation.

Scheduling Mitigations of Mechanical Damage

Mechanical damage is separated into two groups, i.e. immediate failures and delayed failures. An immediate failure is one which occurs at the instant the damage is done to the pipeline. A puncture, for example, is an immediate failure. Delayed failures involve damage that is not sufficient to cause a leak or a rupture at the time it is inflicted. On average, 15% of the mechanical damage incidents in gas transmission pipelines and 13% of the mechanical damage incidents in hazardous liquid pipelines can be classified as delayed failures.

The immediate failures are generally minimized through the preventative measures and design efforts. For instance, it is shown herein that the puncture probability can be calculated through the comparison between the likelihood of any given external load being imposed and inherent pipe resistance. While preventative measures serve to reduce the occurrences of delayed failures as well as the occurrences of immediate failures, there is also an opportunity to mitigate delayed failures through ILI and timely remediation actions.

The fact that the assessment methods for mechanical damage are generally not as robust as those for cracks and corrosion tends to limit the reliability of deterministic calculations of response times. Therefore, risk-based approaches to minimizing delayed failures were developed. Three different approaches to deciding which dents need to be excavated after an ILI were pursued. One involved the use of reportable incident rates based on the PHMSA statistics in conjunction with the number of ILI dent indications per mile to determine a POF. The second consisted of a probability-of-exceedance calculation of fatigue life by the ILI-reported dent dimension. The third involved a decision-making process based on successive excavations of dents located by ILI, in which the Bayesian method was applied to compare predicted versus actual severity and thereby determine the POF associated with stopping after a specific number of excavations.

LIST OF ANNEXES

Annex A - Review of Existing Rules and Methods for Evaluating Interaction
Authors: Jing Ma, Benjamin Zand and Robert Francini

Annex B - Deterministic and Probabilistic Approaches for Scheduling Mitigations of Corrosion Regions
Author: Jing Ma

Annex C - Deterministic and Probabilistic Approaches for Scheduling Mitigations of Crack-like Anomalies
Authors: Jing Ma and M.J. Rosenfeld

Annex D - Deterministic and Probabilistic Approaches for Scheduling Mitigations of Mechanical Damage
Authors: Jing Ma, Fan Zhang and Guy Desjardins

US DOT - PHMSA

Final Report No. 16-025

Final Report

Threat/Anomaly Mitigation Decision-Making Process – Annex A. Review of Existing Rules and Methods for Evaluating Interaction

Jing Ma, Benjamin Zand, and Robert Francini

February 23, 2016

Kiefner Applus RTD

0339-1402

Intentionally blank

Final Report No. 16-025

Final Report

on

THREAT/ANOMALY MITIGATION DECISION-MAKING PROCESS ANNEX A. REVIEW OF EXISTING RULES AND METHODS FOR EVALUATING INTERACTION

DTPH5614H00005

to

U.S. DEPARTMENT OF TRANSPORTATION – PIPELINE AND HAZARDOUS MATERIALS SAFETY ADMINISTRATION

February 23, 2016

by

Jing Ma, Benjamin Zand, and Robert Francini

Kiefner and Associates, Inc.
585 Scherers Ct.
Columbus, OH 43085

0339-1402

DISCLAIMER

This document presents findings and/ or recommendations based on engineering services performed by employees of Kiefner and Associates, Inc. The work addressed herein has been performed according to the authors' knowledge, information, and belief in accordance with commonly accepted procedures consistent with applicable standards of practice, and is not a guaranty or warranty, either expressed or implied.

The analysis and conclusions provided in this report are for the sole use and benefit of the Client. No information or representations contained herein are for the use or benefit of any party other than the party contracting with Kiefner. The scope of use of the information presented herein is limited to the facts as presented and examined, as outlined within the body of this document. No additional representations are made as to matters not specifically addressed within this report. Any additional facts or circumstances in existence but not described or considered within this report may change the analysis, outcomes and representations made in this report.

EXECUTIVE SUMMARY

The work described herein is part of PHMSA Project #DTPH5614H00005 – "Threat/Anomaly Mitigation Decision-Making Process". The objective of the project is to enhance the understanding of flaw interaction and provide better guidance of scheduling examinations and estimating re-assessment intervals.

The following document specifically covers Task 2 consisting of a literature review and a pipeline operator and ILI vendor interview. The literature reviewed covers analytical and experimental studies of multiple types of interactions, e.g. between adjacent corroded areas, between cracks, between corrosion and cracks, between dents and gouges, between dents and dents, between dents and cracks, and between dents and corrosion, etc. The reviewed literature is comprised of 18 standards, 23 technical reports and 44 journal articles. Among these 23 are experimental studies, 32 are analytical investigations and 12 are a combination. Appendix C lists the reference summary related to three groups of interactions, i.e. corrosion, cracks, and mechanical damage, respectively.

For one flaw interacting with another one in its proximity such as crack-with-crack or corrosion-with-corrosion, if assuming the primary stress is along the hoop direction, various relative positions are represented by in-plane distance S along the axial direction and off-set distance H along the circumferential direction in Figure ES1. Four typical configurations, i.e. coplanar, coparallel, parallel and overlapping are shown in Figure ES2 by combining different values of S and H. For surface flaws, the interaction is determined by the values of S and H only. For embedded flaws, the interaction is also determined by the distance along the depth direction as exemplified by Figure ES3.

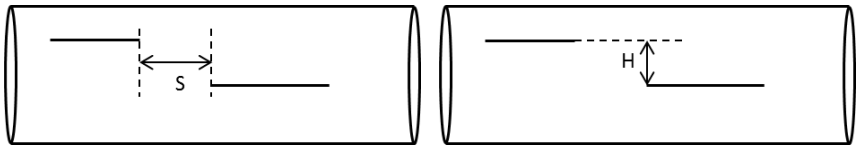

Figure ES1. Plan View of In-plane Distance S and Off-set Distance H

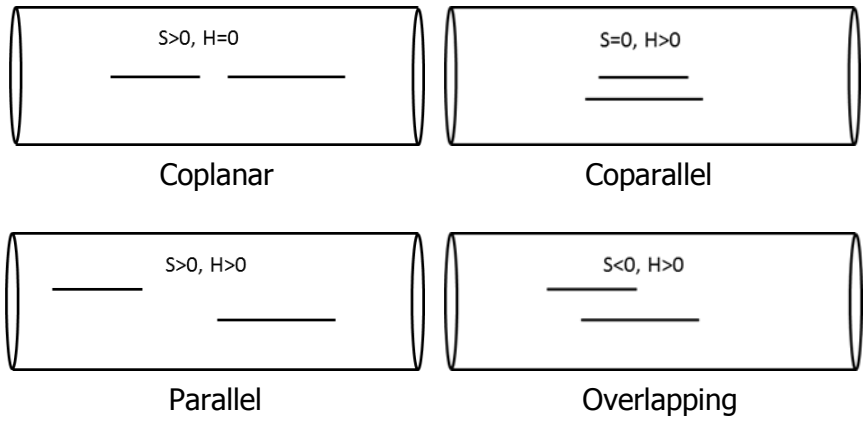

Figure ES2. Configurations of Flaw Interaction in Close Proximity

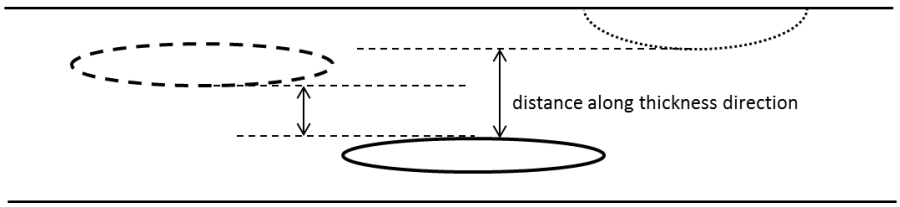

Figure ES3. Elevation View of Distance along Wall Thickness Direction

Based on the literature review, preliminary conclusions are drawn as the following.

- For corrosion-with-corrosion interaction, only load-controlled failure mode exists, i.e. plastic collapse. The analytical work generally produced much larger threshold distance of interaction than the experimental tests, particularly the linear finite element analyses. On the other hand, all the experimental results point to 6t (where t is the wall thickness of the pipe) as the upper bound of interacting distance. Experiments conducted by Advantica on axially separated groove-groove defects led to the upper bound 6t. However, the authors stated that 6t is probably over-conservative. When the spacing is as large as 6t, the experiments consistently found that the interaction of corrosion areas does not occur. Therefore ASME B31G 3t-by-3t condition serves properly as the in-ditch corrosion interacting criteria, which is also validated by its safe use in the actual pipeline operation.
- For crack-with-crack interaction, both toughness-controlled and load-controlled failure mechanisms exist, e.g. fatigue, brittle fracture, ductile tearing and plastic collapse. For the offset distance between two surface cracks, experiments failed by fatigue referred to the crack depth ***a*** as the interacting separation; analytical studies produced the value close to ***a*** for stress intensity factor and J-integral, and 1.8***a*** for plastic collapse. For the in-plane distance between two surface cracks, experiments yielded the threshold distance being ***a*** for cleavage and zero for fatigue; analytical studies generated the

upper bound as the crack length 2***c*** as for stress intensity factor and 0.5***a*** for J-integral and plastic collapse. With regard to embedded cracks, only analytical investigations on stress intensity factor are available. For one embedded crack with one surface crack, the critical in-plane distance is 2***c*** along the length direction and 2***a*** along the depth direction. For two embedded cracks, the critical in-plane distance is ***a*** along both the length and depth directions. Overall, BS 7910: 2013 matches well with journal article findings for both surface and embedded cracks, and stands on the conservative side taking into account the fact that the embedded cracks usually don't interact as strongly as the surface cracks. Since the majority of experimental validations are based on fatigue tests, BS 7910: 2013 reflects the interaction during the crack growth before coalescence. Considering brittle fracture utilizes the same stress intensity factor as fatigue, the interaction criterion can be interpreted similarly. No systematic experiments were conducted to define the threshold distance for ductile failures. However, burst tests on groove-groove defects by Kiefner and Advantica provide guidance to infer crack interaction in the plastic collapse region, particularly for long cracks. This means 6t is a proper conservative estimation under such a circumstance. The interacting distance for ductile tearing is a load dependent parameter, and the value should be between that for brittle fracture and that for plastic collapse.

- For corrosion-with-crack interaction, limited information on experiments and analysis is available. The underlying failure mode and interaction mechanism have not been elucidated. University of Waterloo is conducting more research in this area.
- For dent-with-dent interaction, Francini and Yoosef-Ghodsi suggested the interaction criterion being the edge-to-edge distance less than $2\sqrt{Rt}$. Al-Muslim performed the sensitivity study to fit equations for burst pressure and fatigue life prediction. The formulae are presented in this document.
- For dent-with-corrosion interaction, the experimental work conducted by Kiefner and Alexander provides ASME B31.8 guidance. Al-Muslim performed the sensitivity study to fit equations for burst pressure and fatigue life prediction. The formulae are presented in this document.
- For dent-with-crack interaction, the experiment done by Ghaednia showed that a crack shallower than 24% wall thickness in a 4% OD deep dent had the burst pressure greater than the pipe yielding design pressure. This is consistent with ASME B31.4 grinding criterion. An analytical model was proposed by Bai and Song to incorporate the Bilby-Cottrell-Swinden crack intensity factor and the Shannon dent stress concentration factor. Experimental tests on ten specimens exhibited a decent correlation with the model prediction. The essential idea is to treat the dent-caused stress and moment concentration as the nominal load magnification on crack. Similar methodology can be tailored to the fatigue analysis, such as the work conducted by Martin and Andrew.

- For dent-with-gouge interaction, the EPRG model is adopted by API 579-1/ASME FFS-1: 2007 and PDAM: 2003.
- For dent-with-weld interaction, Rosenfeld recommends applying the dent stress concentration factor with a representative weld S-N curve. The approach is adopted by PDAM: 2003. The recent PRCI project performed by Dinovitzer et al. derived an interaction factor for dent-girth weld interaction.

Since multiple PRCI projects are underway to understand the dent-with-defect interaction including full-scale tests and numerical modeling, the corrosion-with-crack interaction is identified as a knowledge gap at this point.

TABLE OF CONTENTS

INTRODUCTION 1
LITERATURE REVIEW OF CORROSION INTERACTIONS 1
LITERATURE REVIEW OF PLANAR FLAW INTERACTIONS 27
LITERATURE REVIEW OF CRACK WITHIN CORROSION 73
LITERATURE REVIEW OF MECHANICAL DAMAGE INTERACTIONS 75
RESULTS OF QUESTIONNAIRE ON INTERACTING ANOMALIES 96
APPENDIX A 103
APPENDIX B 105
APPENDIX C 108

LIST OF FIGURES

Figure 1. Corrosion Interaction Patterns 2
Figure 2. Sizing of Multiple Metal Losses in an Adjacent Region 5
Figure 3. Flaws 1, 2 Combined Based on Figure 2 into the Same Assessment 6
Figure 4. Corrosion Pit Interaction Distances 7
Figure 5. Type I Interaction 8
Figure 6. Type II Interaction 8
Figure 7. Corrosion Depth Adjustment for Background Corrosion 11
Figure 8. Projection of Circumferentially Interacting Defects 11
Figure 9. Formation of a Composite Defect by Projection of Overlapping Sites 12
Figure 10. Formation of a Composite Defect by Projection of Overlapping Internal and External Defects 12
Figure 11. Combining Interacting Defects 13
Figure 12. Example of Grouping of Adjacent Defects for Interaction to Find the Lowest Failure Pressure 13
Figure 13. Interaction between LTAs 15
Figure 14. Corrosion Interaction Diagram 16
Figure 15. Configuration of Axially Spaced Corrosion Defects for Colony 1 and 2 17
Figure 16. Configuration of Rhombus Shaped Defects for Colony 3 and 4 18
Figure 17. Secondary Assessment of Interaction 22
Figure 18. Guideline Flowchart of Corrosion on Welds 24
Figure 19. Girth Weld Defect Limits for Tier 3 29

Figure 20. Assessment of Branched Cracking 30
Figure 21. Assessment of Multiple Crack-like Flaws 31
Figure 22. Interaction of Coplanar Flaws 32
Figure 23. Interaction of Coplanar Flaws (Continued) 33
Figure 24. Alignment Rules for Non-coplanar Flaws 34
Figure 25. Interaction Rules for Coplanar Flaws 35
Figure 26. Interaction Rules for Coplanar Flaws (Continued) 36
Figure 27. Imperfection Interaction Criteria 37
Figure 28. Flaw Combination Criteria 38
Figure 29. Flaw Alignment Criteria 39
Figure 30. Interaction Zone around a Defect 40
Figure 31. Geometry Layout of a Two-Crack Configuration 42
Figure 32. Normalized Crack Driving Force for Two Coplanar Cracks 43
Figure 33. Normalized Crack Driving Force for Two Coparallel Cracks 44
Figure 34. Normalized Crack Driving Force for two Cracks at 2b/t=1 46
Figure 35. Experimental Setup with Units in mm 47
Figure 36. Crack Growth and Coalescence under Fatigue Loading 48
Figure 37. Ratio of Stress Intensity Factors between Free Surface Positions C and E 48
Figure 38. Fracture Surfaces of Ductile Tearing 49
Figure 39. Two Interacting Cracks Failed in the Lower Shelf Regime at -196 °C 50
Figure 40. Specimen S10 and Its Corresponding Re-characterized Defect on FAD 50
Figure 41. Beach Markings on a Fracture Surface 51
Figure 42. Deviation of Adjacent Crack Tips before Coalescence 51
Figure 43. Configuration and Dimension of Two Cracks 52
Figure 44. Geometry of Notched Specimen 55
Figure 45. Two Cracks with S=2.5 mm and H=2.5 mm Fractured Before Coalescence 57
Figure 46. Fracture Surfaces for Two cracks with S=0 mm and H=5 mm and 10 mm 58
Figure 47. Fracture Surfaces for Two Coplanar Cracks with S=5 mm 58
Figure 48. Criteria to Judge Smaller Crack Arrest 59
Figure 49. Type 1 Configuration between Two Coplanar Embedded Cracks 64
Figure 50. Type 2 Configuration between Two Coplanar Embedded Cracks 64
Figure 51. Interaction Factor of Type 1 Configuration 64
Figure 52. Interaction Factor of Type 2 Configuration 65

Figure 53. One Embedded Crack with One Surface Crack in a Pressurized Cylinder 65
Figure 54. Schematic of Non-Coplanar Embedded Crack with Surface Crack.....66
Figure 55. Defect of EDM Notch-within-Groove Machined by Kiefner Lab 74
Figure 56. Dent Spring-back and Depth Change under Internal Pressure 76
Figure 57. Dent Width Measurement for Dent SCF Calculations 77

LIST OF TABLES

Table 1. Interaction Critical Distance Determination 18
Table 2. Failure Location and Failure Pressure for Interacting Defects.....19
Table 3. Four Specimens under Burst Tests.....20
Table 4. Corrosion Defect Interaction Criteria Based on Experimental and Analytic Studies.....25
Table 5. Corrosion Defect Interaction Criteria Listed in Various Codes, Standards, and Handbooks.....26
Table 6. History of Flaw Interaction of BS 7910 27
Table 7. Matrix of Initial Crack Geometries with Units in mm.....53
Table 8. Fatigue Test Matrix under Cyclic Tensile Loads 56
Table 9. A_{nm} Fitted Values for the Interaction Factor ɣ.....61
Table 10. C_n Fitted Values for the Interaction Factor ɣ.....62
Table 11. Coefficients of A_{nm} to Calculate Interaction Factor $\beta_{P,Q}$.....67
Table 12. Crack Interaction Criteria Listed in Various Codes, Standards, and Handbooks.....69
Table 13. Crack Interaction Criteria Based on Experimental and Analytic Studies 70
Table 14. Comparison between Journal Articles and BS 7910:2013.....72
Table 15. Burst Test Results for EDM Notch with/without Groove by Kiefner 74
Table 16. Dent-Girth Weld Interaction Coefficients.....90
Table 17. Dent-Dent Interaction Coefficients 92
Table 18. Dent-Metal Loss Interaction Coefficients.....93
Table 19. Values of a_p, b_p and c_p for Dent Stress Intensity Factor Calculations.....104
Table 20. Reference Related to Corrosion-with-Corrosion/Crack 108
Table 21. Reference Related to Crack-with-Crack.....109
Table 22. Reference Related to Mechanical Damage 110

Intentionally blank

Threat/Anomaly Mitigation Decision-Making Process – Annex A. Review of Existing Rules and Methods for Evaluating Interaction

Jing Ma, Benjamin Zand, and Robert Francini

INTRODUCTION

This interim report on DTPH5614H00005, "Threat/Anomaly Mitigation Decision-Making Process" presents the results of a review of existing defect interaction rules. The purposes of the work described herein were to determine what types of defect interactions are covered by the current rules and whether or not the current rules have been thoroughly validated. To the extent the current rules appear to be inadequate, subsequent work on this project will be done to develop and validate improved interaction rules. The types of interaction addressed herein are:

- Interaction between closely spaced corrosion pits
- Interaction between closely spaced cracks
- Interaction between cracks and corrosion pits where the two overlap
- Interaction between dents and gouges
- Interaction between dents and cracks
- Interaction between dents and corrosion pits

The focus of this project is to evaluate available defect interaction criteria and bring them into a single document. Through reviewing standards/codes, research projects, and publications, the interactions related to corrosion, planar flaws, and mechanical damage are covered in this interim report.

LITERATURE REVIEW OF CORROSION INTERACTIONS

To accurately predict the failure pressure of a pipeline section, the complex geometry of corrosion needs to be taken into account. In general, corrosion is composed of a group of intermittent pits with or without interaction between each other. The term "pits" hereinafter refers to the localized metal loss with dimensions, i.e. diameter greater than the order of pipe wall thickness.

Multiple interaction rules have been given based on experimental studies and numerical analysis. As early as 1969 Kiefner published some experimental data on defect interaction[1]. The experiments were done on longitudinally spaced flaws, circumferentially spaced flaws, and corrosion-like pits. In 1990 Kiefner and Vieth summarized the results of the first two groups and classified the interaction into three categories[2]. The specimens were fabricated from an X60 pipe with 36-inch diameter and 0.4-inch wall thickness. Flaws on the pipe were all notches with a length of 4.8 inches and a depth of 0.3 inch. This research resulted in the interaction rule for three types of corrosion defect combinations shown in Figure 1.

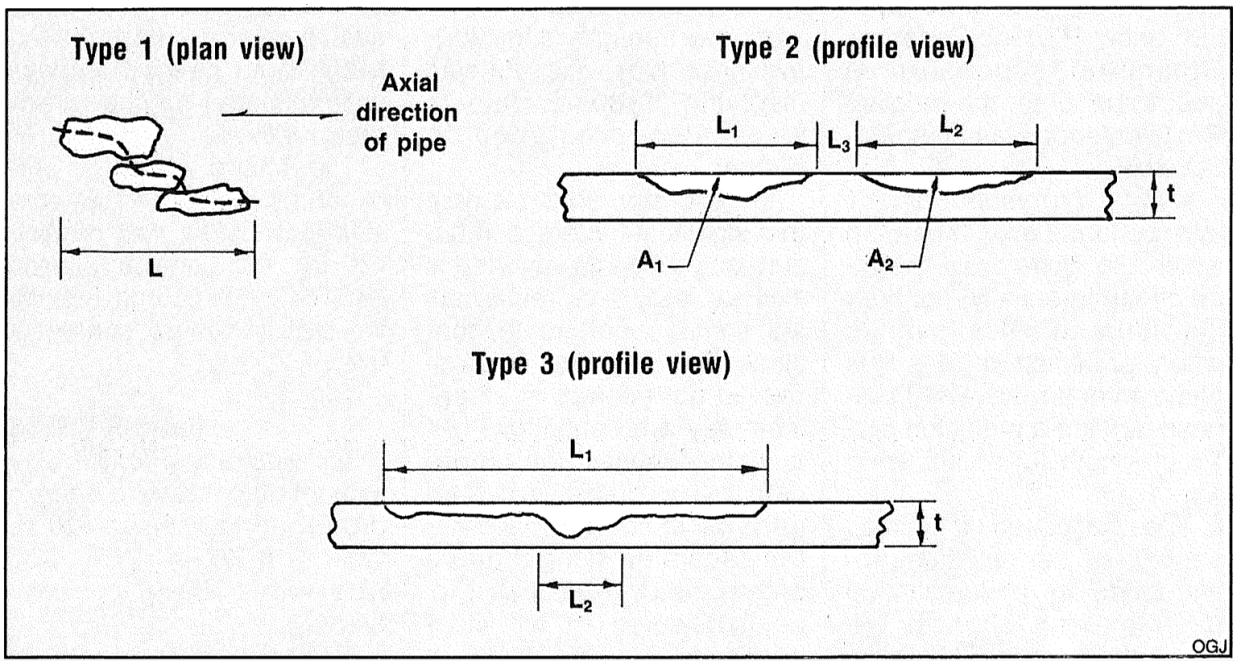

Figure 1. Corrosion Interaction Patterns

- Type 1 defects are those separated circumferentially with projected overlapping onto a common axial plane. Experiments indicated that a separation of 6t, where t is the wall thickness of the pipe, is a critical distance for interaction. If circumferential spacing is greater than 6t, each defect can be assessed individually; otherwise, they have to be treated as a single one.
- Type 2 defects are those lying on the same axial plane with a separation of some full wall thickness pipe. Experiments suggested that significant interaction occurs only when the spacing is 1 inch or less.

[1] Kiefner, J.F., Fourth Symposium on Line Pipe Research, American Gas Association, Catalog No. L30075, Nov. 1969.
[2] Kiefner, J.F. and Vieth, P.H., "Evaluating Pipe – Conclusion: PC Program Speeds New Criterion for Evaluating Corroded Pipe", OGJ Special, Oil and Gas Journal, August 20, 1990.

- Type 3 defects are those in which a corrosion defect is contained within another defect. Two methods are valid: Method 1 is to treat the short deep defect in a pipe with a reduced wall thickness equal to the net thickness beneath the long defect. Method 2 is to use the effective area method RSTRENG by iteration to find the minimum failure pressure.

Using methods similar to the above research, Coulson and Worthingham studied the interaction of machined grooves of various lengths with a depth equal to 40% of wall thickness and a width equal to 1 inch[3,4]. They suggested the following criteria for the longitudinal oriented defects:

- Defects separated by a longitudinal distance greater than the length of the shortest defect don't interact.
- Defects separated by a circumferential distance greater than the width of the narrowest defect don't interact.

Hopkins and Jones at British Gas conducted experiments on long grooves and single pits in 1992[5]. The results demonstrated that:

- Grooves aligned in the longitudinal direction don't interact with spacing greater than 3 wall thicknesses.
- Grooves oriented in the longitudinal direction don't interact with circumferential spacing greater than 1 wall thickness or 1 inch.
- Pits don't interact with each other with spacing greater than 1 wall thickness in either the longitudinal or circumferential direction.

In 1993 Chouchaoui and Pick found that simple corrosion pits only interact if they touch in the circumferential direction or are within one wall thickness in the longitudinal direction[6]. In 1996 Cronin, Roberts and Pick performed some additional numerical analysis on a series of single pits in a longitudinal groove. The result exhibited that the interaction started with a longitudinal separation equal to 6 wall thicknesses and became pronounced with the separation below 2

[3] Coulson, K. and Worthingham, R., "New Guidelines Promise More Accurate Damage Assessment", Oil and Gas Journal, April 16, 1990, Page 41-45.
[4] Coulson, K. and Worthingham, R., "Standard Damage-Assessment Approach Is Overly Conservative", Oil and Gas Journal, April 9, 1990, Page 54-58.
[5] Hopkins, P. and Jones, D.G., "A Study of the Behavior of Long and Complex-shaped Corrosion in Transmission Pipelines", OMAE, Pipeline Technology, Volume V-A, ASME 1992.
[6] Chouchaoui, B.A. and Pick, R.J., "Interaction of Closely Spaced Corrosion Pits in Line Pipe", OMAE, Vol. V, Pipeline Technology, Page 203-214, 1993.

wall thicknesses[7]. In the same year through a numerical study Sims and DePadova found that defects don't interact with a separation greater than a tenth of diameter[8].

Three forms of defect interaction criteria for corrosion are based on the critical distance as a function of: (1) the pipe wall thickness, (2) the dimensions of two adjacent defects, and (3) the pipe diameter or a combination of the pipe diameter and wall thickness. Below the current standards/codes regarding corrosion interaction are reviewed.

API 579-1/ASME FFS-1 2007 Fitness-For-Service

In Part 4 – Assessment of General Metal Loss and Part 5 – Assessment of Local Metal Loss, API 579-1 adopts the rules as shown in Figure 2 to assess multiple metal losses in close proximity to each other. For each local thin area (LTA) with a maximum longitudinal extent s and a maximum circumferential extent c, a rectangular with the dimension 2s×2c is drawn around it. If any other LTA is within this rectangle, these two LTAs are determined to interact with each other. This process has to be iterated until there is no other LTA within the increasing box.

Once the interaction between flaws is determined, the average thickness value or Critical Thickness Profiles (CTPs) can be easily established as illustrated in Figure 3. The Level 1 and Level 2 assessments for the interacting defects follow the same procedure as for the single flaw situation.

[7] Cronin, D.S., Roberts, K.A. and Pick, R.J., "Assessment of Long Corrosion Grooves in Line Pipe", ASME International Pipeline Conference, Vol. 1, Page 401-408, 1996.
[8] Sims, J.R. and DePadova, T.A., "Fitness for Continued Service: Local Thin Areas", International Conference on Pressure Vessel Technology, Volume 2, ASME 1996, Page 175-181.

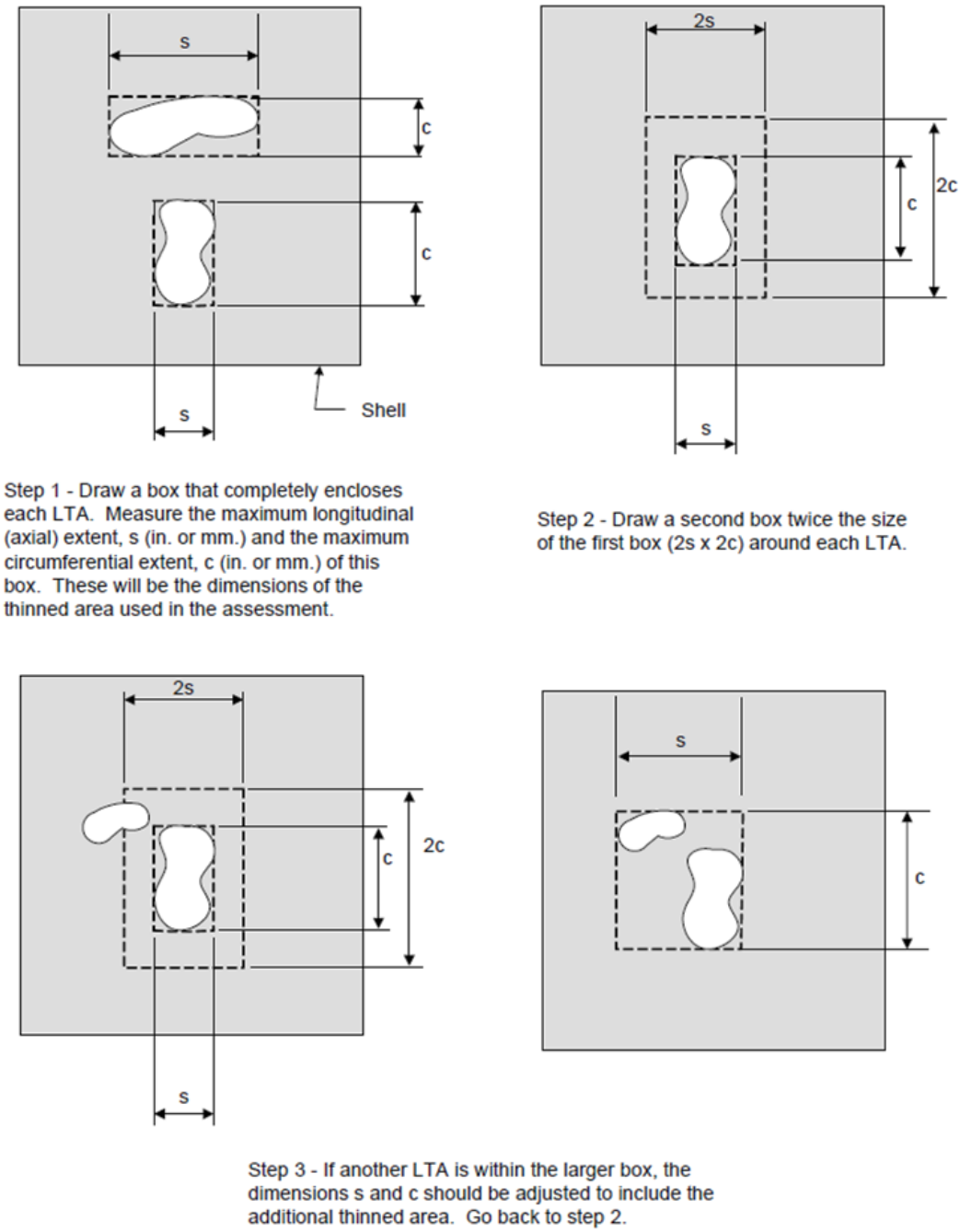

Step 1 - Draw a box that completely encloses each LTA. Measure the maximum longitudinal (axial) extent, s (in. or mm.) and the maximum circumferential extent, c (in. or mm.) of this box. These will be the dimensions of the thinned area used in the assessment.

Step 2 - Draw a second box twice the size of the first box (2s x 2c) around each LTA.

Step 3 - If another LTA is within the larger box, the dimensions s and c should be adjusted to include the additional thinned area. Go back to step 2.

Figure 2. Sizing of Multiple Metal Losses in an Adjacent Region

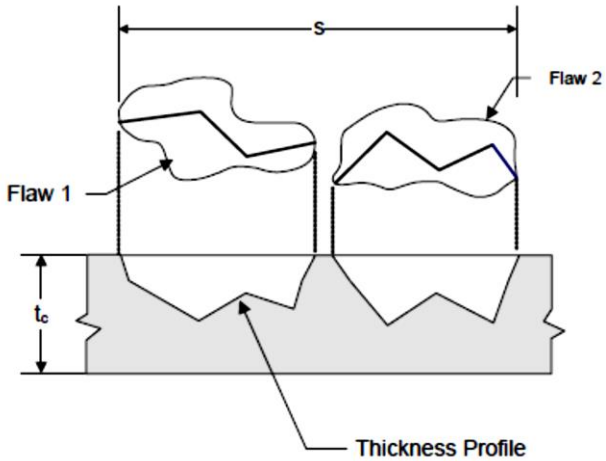

Figure 3. Flaws 1, 2 Combined Based on Figure 2 into the Same Assessment

ASME B31G 2009 Manual for Determining the Remaining Strength of Corroded Pipelines

Section 1.12 – Flaw Interaction gives the following guidelines:

- Flaws are considered interacting if they are spaced longitudinally or circumferentially from each other within a distance of 3 times the wall thickness (3t). Interacting flaws should be evaluated as a single flaw combined from all interacting flaws.
- Flaws are considered non-interacting if spaced outside of the above dimensions. Non-interacting flaws should be evaluated as separated flaws.

This rule is commonly known as "3t×3t" is shown in Figure 4. The standard also emphasizes that caution should be used when grouping or clustering flaws in in-line inspection. Careful consideration should be given to minimum thresholds of reliable detection, sizing and reporting, and the expected mode of coating failure. In the current practice of in-line inspection, different spacing criteria are provided for the operator to choose, e.g. 3t×3t, 6t×6t, and 12t×12t.

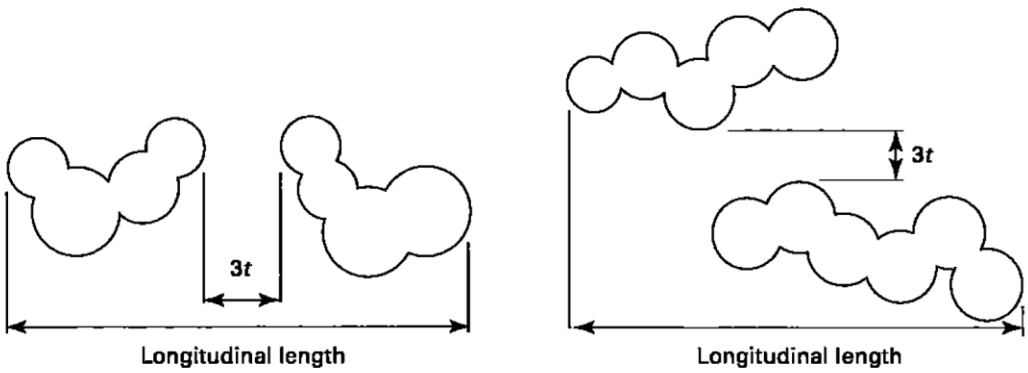

Figure 4. Corrosion Pit Interaction Distances

The Effective Area Method or the RSTRENG method for Level 2 Evaluation is the approach to assess the irregular shaped area of corrosion. It is accomplished through the iterations of all possible combinations of local metal loss by calculating

$$S_F = S_{flow}\left[\frac{1 - A/A_0}{1 - (A/A_0)(M^{-1})}\right], \qquad \text{Equation 1}$$

where A is the local metal loss area, A_0 is the corresponding original area, M is the Folias factor to account for the bulging effect, S_{flow} is the flow stress of the material (usually taken to be SMYS+10,000 psi), D is the pipe diameter, t is the pipe wall thickness, and L is the effective length of the corrosion defect which gives the lowest failure pressure for all iterations.

$$M = \left(1 + 0.6275\frac{L^2}{Dt} - 0.003375\frac{L^4}{D^2t^2}\right)^{\frac{1}{2}} \quad \text{for } L \le \sqrt{50Dt}, \qquad \text{Equation 2}$$

$$M = 3.3 + 0.032\frac{L^2}{Dt} \quad \text{for } L > \sqrt{50Dt}. \qquad \text{Equation 3}$$

Two ways are allowed in the standard to implement the calculation. One is to simply follow the "river bottom" by projecting the deepest local regions around the circumference onto the same longitudinal plane with the consideration of 3t criterion; the other is to repeat the analysis along each meridian.

As to whether RSTRENG can capture the corrosion interaction with some full wall thickness separation, different opinions exist. If postulating the adjacent defects as a whole complex shaped defect, it seems plausible to use RSTRENG to assess the region provided that the validation experimental database includes multiple examples of actual irregularly shaped corrosion having some very shallow regions.

ASME B31.4 2012 Pipeline Transportation Systems for Liquids and Slurries

Section 451.6.2.2 – Corrosion, lists the rules of Interaction of Corrosion-caused Metal Loss Areas in Subsection (d). It concludes that in general, neighboring regions of metal loss separated by areas of full wall thickness may interact in a manner that reduces the remaining strength to a greater extent than the reduction resulting from the individual areas.

Two types of interaction are possible and each should be assessed as follows:

- Type I Interaction (see Figure 5). If the circumferential separation distance C is greater than or equal to 6 times the wall thickness required for design, the areas A_1 and A_2 should be evaluated as separate anomalies. If the circumferential separation distance is less than 6 times the wall thickness, the composite area ($A_1 + A_2 - A_3$) and the overall length L should be used.
- Type II Interaction (see Figure 6). If the axial separation distance L_3 is greater than or equal to 1 inch, the areas A_1 and A_2 should be evaluated as separate anomalies. If the axial separation distance is less than 1 inch, area A_1 plus A_2 should be used and the length L should be taken as $L_1 + L_2 + L_3$.

This interaction criteria is the same as the paper of Kiefner and Vieth in 1990[2] (i.e., interaction must be considered if C in Figure 5 is less than 6t or if L_3 in Figure 6 is less than 1 inch).

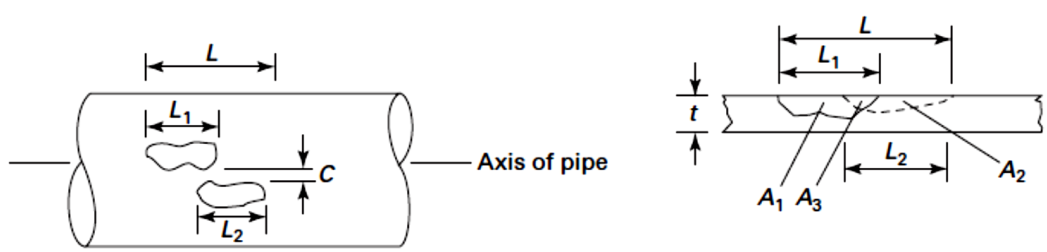

Figure 5. Type I Interaction

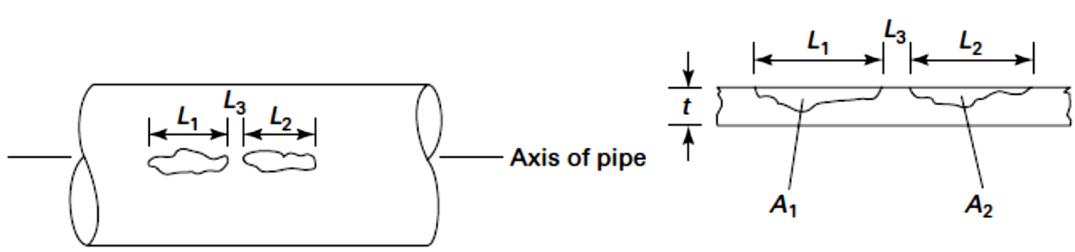

Figure 6. Type II Interaction

DNV-RP-F101 October 2010 Corroded Pipelines

The recommended practice describes two alternative approaches to assess corroded pipelines: Part A - the calibrated safety factor approach and Part B - the allowable stress design approach. The former includes Chapter 4 for a single defect and Chapter 5 for interacting defects; the latter includes Chapter 8 for a single defect and Chapter 9 for interacting defects. Since the two approaches are essentially the same, only Part B is explained here to be more comparable with other standards/codes.

The interaction criterion was developed by Fu and Batte. As explained in Chapter 8, a defect can be treated as an isolated defect, and interaction with other defects need not be considered, if either of the following conditions is satisfied:

- The circumferential angular spacing between adjacent defects,

$$\phi > 360\sqrt{\frac{t}{D}} \text{ (degrees) ;}$$

- The axial spacing between adjacent defects,

$$s > 2.0\sqrt{Dt} \text{ .}$$

If defects are determined to be interacting based upon the above equations, Chapter 9 should be followed. The basic idea is to assess the interacting defects by the single defect equation with the total length and the "effective" depth. Concrete steps are listed in the standard:

(1) For regions with background metal loss less than 10% of the wall thickness, the local pipe wall thickness and defect depths can be used (see Figure 7).

(2) The corroded pipe should be divided into sections of a minimum length of $5.0\sqrt{Dt}$ with a minimum overlap of $2.5\sqrt{Dt}$. Steps (3) through (12) should be repeated for each sectioned length to determine the lowest failure pressure.

(3) Construct the parallel axial lines with a circumferential angular spacing of:

$$Z = 360\sqrt{\frac{t}{D}} \text{ (degrees)} \qquad \text{Equation 4}$$

(4) Consecutively consider the plane through the wall at each axial line. If defects lie within ±Z, their profile should be projected onto the current projection plane (see Figure 8).

(5) Overlapping defects should be combined to form a composite defect. For each composite defect, the depth is equal to the deepest defect. For instance, in Figure 9, two composite defects are individually formed by four overlapping defects and two overlapping defects. If the composite defect consists of an internal and external defect,

the depth is the sum of the maximum depth of the internal and external defects (see Figure 10).

(6) Calculate the failure pressure (P_1, P_2, · · ·, P_N) of each defect or composite defect as a single one:

$$P_i = \frac{2tf_u}{(D-t)} \frac{\left(1-\frac{d_i}{t}\right)}{\left(1-\frac{d_i}{tQ_i}\right)}, \mathrm{i} = 1,...\mathrm{N}, \text{ where } Q_i = \sqrt{1+0.31\left(\frac{l_i}{\sqrt{Dt}}\right)^2}. \qquad \text{Equation 5}$$

Here f_u is the tensile strength used in design. d_i and l_i are the depth and length of each defect or composite defect.

(7) Calculate the combined length of all combinations of adjacent defects (see Figure 11 and Figure 12). For defects n to m the total length is given by:

$$l_{nm} = l_m + \sum_{i=n}^{i=m-1}(l_i + s_i), \mathrm{n, m} = 1...\mathrm{N}, \qquad \text{Equation 6}$$

where s_i is the axial spacing between two adjacent defects.

(8) Calculate the effective depth of the combined defect from all of the interacting defects from n to m, as shown in Figure 11.

$$d_{nm} = \frac{\sum_{i=n}^{i=m} d_i l_i}{l_{nm}} \qquad \text{Equation 7}$$

(9) Calculate the failure pressure of the combined defect from n to m using l_{nm} and d_{nm}.

$$P_{nm} = \frac{2tf_u}{(D-t)} \frac{\left(1-\frac{d_{nmi}}{t}\right)}{\left(1-\frac{d_{nm}}{tQ_{nm}}\right)}, \text{ where } Q_{nm} = \sqrt{1+0.31\left(\frac{l_{nm}}{\sqrt{Dt}}\right)^2}. \qquad \text{Equation 8}$$

(10) The failure pressure for the current projection line is

$$P_f = MIN(P_1, P_2, ...P_N, P_{nm}) \qquad \text{Equation 9}$$

(11) The safe working pressure of the current project line is

$$P_{SW} = F \times P_f, \qquad \text{Equation 10}$$

where F is the total usage factor.

(12) The minimum of the safe working pressures for each of the projection lines around the whole circumference is the safe working pressure for the section of corroded pipe.

(13) Repeat Steps (3) to (12) for the next section of the corroded pipeline.

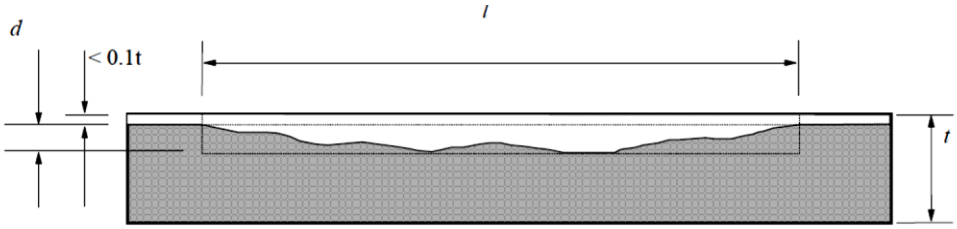

Figure 7. Corrosion Depth Adjustment for Background Corrosion

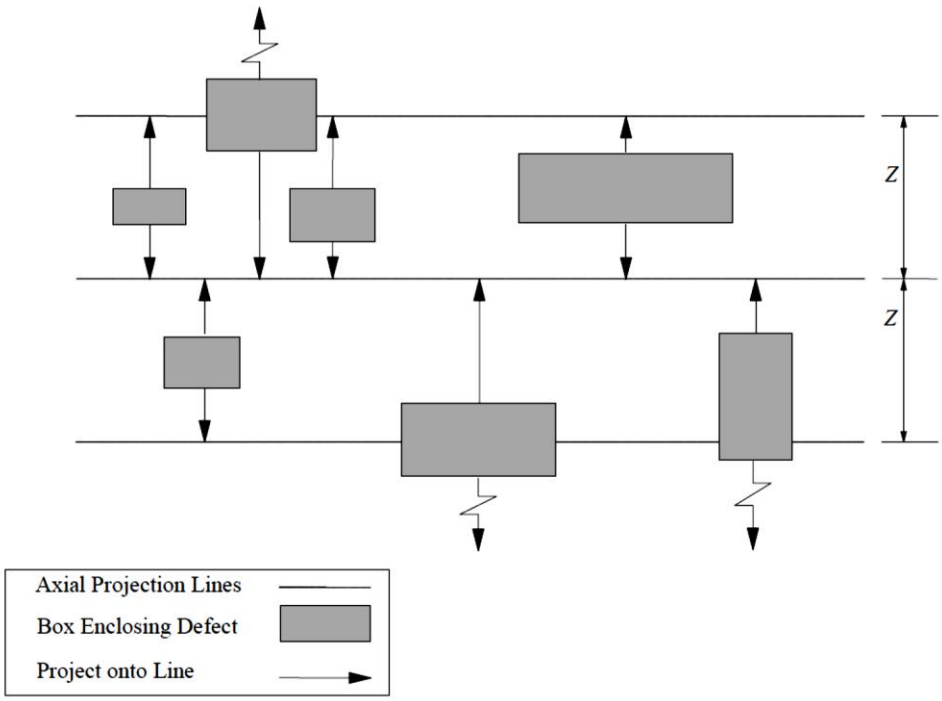

Figure 8. Projection of Circumferentially Interacting Defects

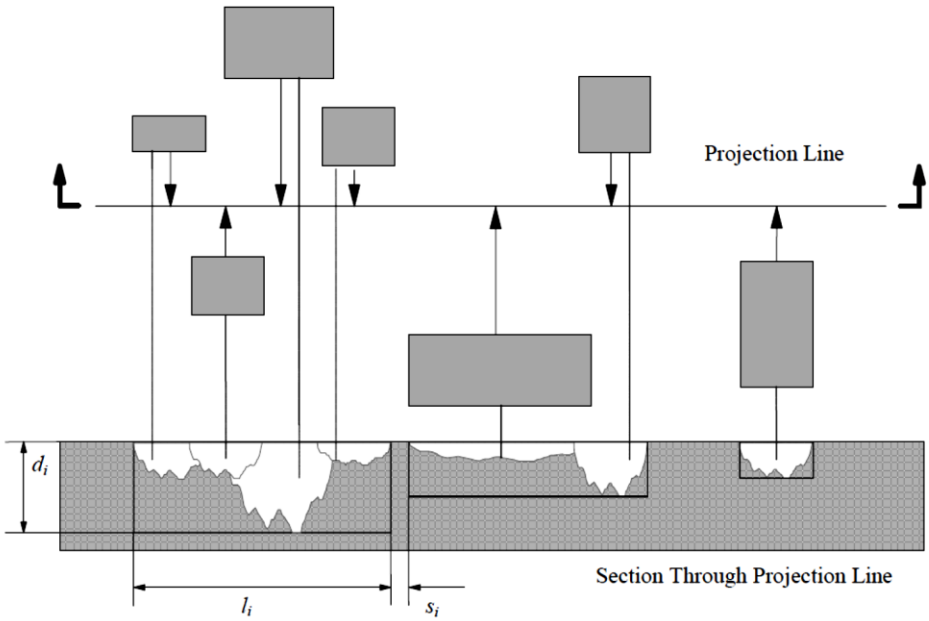

Figure 9. Formation of a Composite Defect by Projection of Overlapping Sites

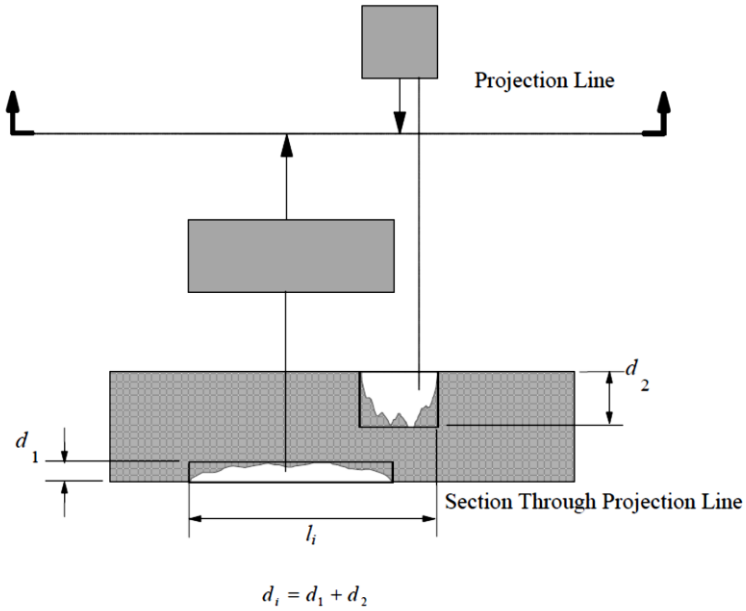

Figure 10. Formation of a Composite Defect by Projection of Overlapping Internal and External Defects

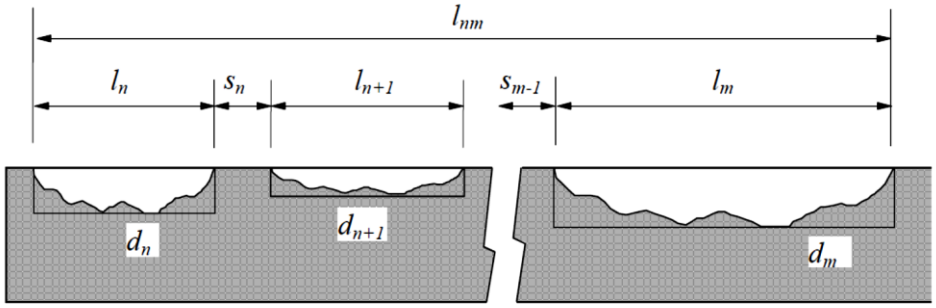

$$l_{nm} = l_m + \sum_{i=n}^{i=m-1}\left(l_i + s_i\right) \qquad d_{nm} = \frac{\sum_{i=n}^{i=m} d_i l_i}{l_{nm}}$$

Figure 11. Combining Interacting Defects

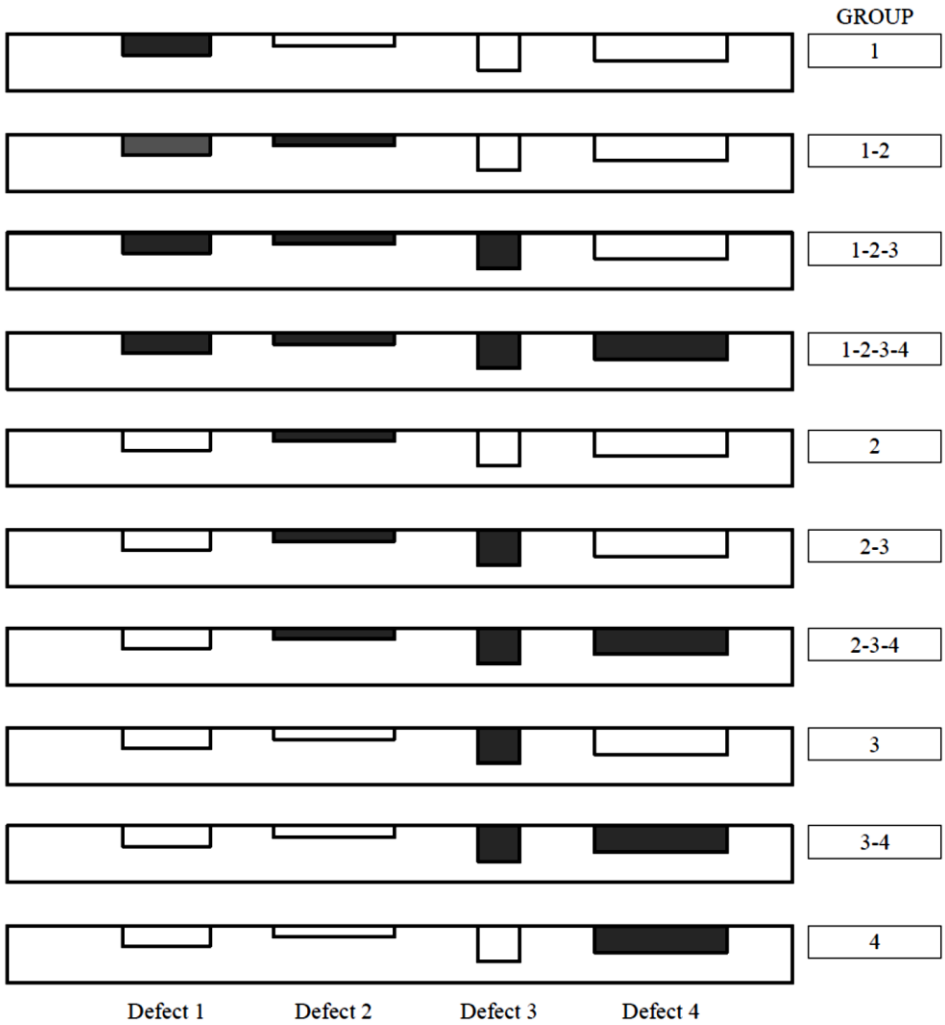

Figure 12. Example of Grouping of Adjacent Defects for Interaction to Find the Lowest Failure Pressure

BS 7910 2013 Guide to Methods for Assessing the Acceptability of Flaws in Metallic Structures

In Annex G – The Assessment of Local Thinned Areas (LTAs), Annex G.7.2 illustrates the conditions of adjacent LTAs to interact with each other in Figure 13.

- The axial spacing between the LTAs is less than or equal to the axial or circumferential length of the smaller LTA; or
- The circumferential spacing between the LTAs is less than or equal to the axial or circumferential length of the smaller LTA; or
- The spacing is less than 3 times wall thickness.

It is emphasized in Annex G that the interaction rule should be applied with the dimension of individual LTAs, not the dimensions of a cluster of interacting LTAs, which means that this rule is only needed for the first round grouping. This is quite distinct from API 579.

The combined size of interacting LTAs is defined as a rectangle enveloping all the LTAs, i.e. the depth equal to the deepest LTA for the LTAs sharing a common surface, whereas it is equal to the sum of the depth of the deepest LTAs on the two opposite surfaces.

Schematic flaws	Criteria for interaction	Effective dimensions after interaction
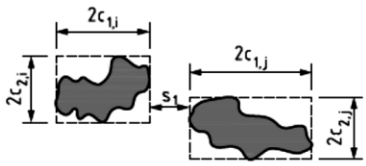	$s_1 \le 2c_{1,i}$ $(c_{1,i} < c_{1,j})$	$a = \max(a_i, a_j)$ $2c_1 = 2c_{1,i} + 2c_{1,j} + s_1$
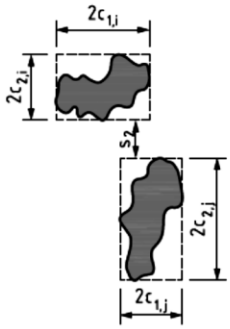	$s_2 \le 2c_{2,i}$ $(c_{2,i} < c_{2,j})$	$a = \max(a_i, a_j)$ $2c_2 = 2c_{2,i} + 2c_{2,j} + s_2$
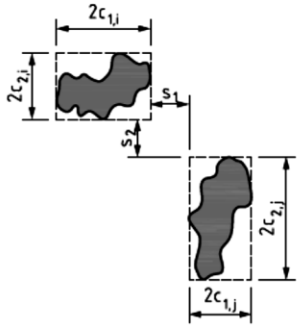	$s_1 \le 2c_{1,i}$ $(c_{1,i} < c_{1,j})$ and $s_2 \le 2c_{2,i}$ $(c_{2,i} < c_{2,j})$	$a = \max(a_i, a_j)$ $2c_1 = 2c_{1,i} + 2c_{1,j} + s_1$ $2c_2 = 2c_{2,i} + 2c_{2,j} + s_2$

Figure 13. Interaction between LTAs

CSA Z662 2011 Oil and Gas Pipeline Systems

Section 10.10.2.1 discusses the corrosion imperfections on pipelines. As exhibited in Figure 14, corroded areas in close proximity shall be considered to interact if the distance G between them is less than the longitudinal length of the smallest area. For internal corrosion areas, it is recommended that the maximum depth of corroded area C be increased and the separation G be decreased to compensate for any uncertainty in measurement.

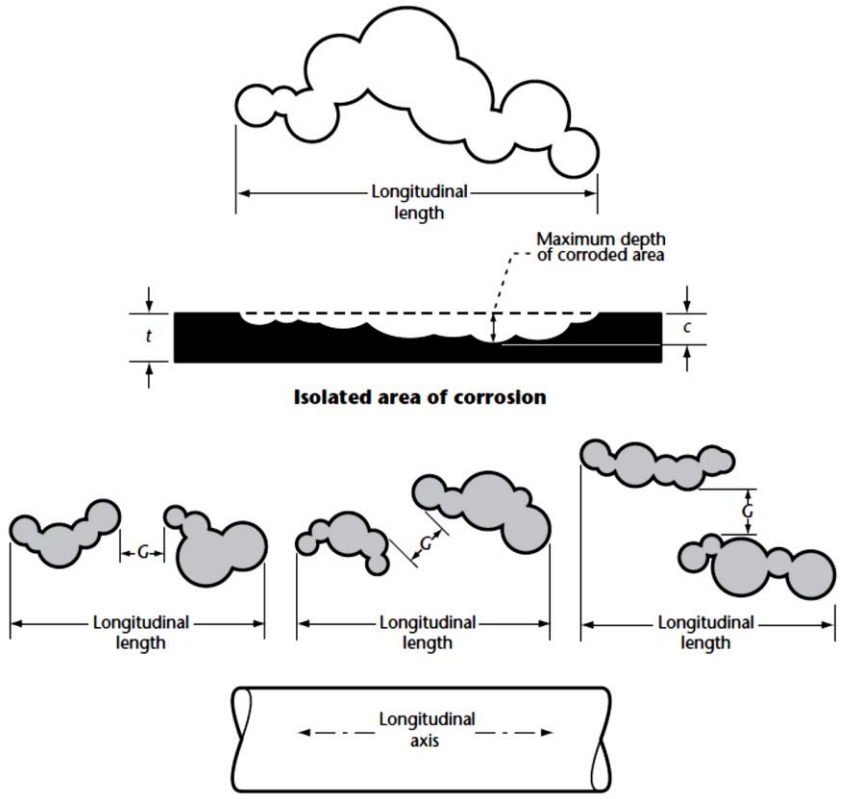

Figure 14. Corrosion Interaction Diagram

Section 10.10.2.4 mentions that corroded areas that contain cracks, or that are concentrated in the seams of electric resistance welded or flash welded pipe, or that are located in material likely to exhibit brittle fracture initiation, shall be rejected.

Pipeline Defect Assessment Manual (PDAM) 2003

Section 20.12.2.3 of PDAM recommends using one of two criteria for interacting corrosion assessment, i.e. DNV-RP-F101 and RSTRENG for the wall thickness no greater than 1 inch, and otherwise specialist advice should be sought. The method given in DNV-RP-F101 should not be applied:

(1) if the 2/3 thickness size upper shelf Charpy V-notch impact energy is less than 18 J (13 ft·lbf), i.e. the full size equivalent is 27 J (20 ft·lbf),
(2) if the minimum elongation requirements in API 5L are not satisfied, or
(3) to line pipe steels of grades A or B, or to any steels that are suspected to be 'dirty'.

RSTRENG can be applied even if Requirement No. (3) is not met.

Review of Journal Articles and Technical Reports

Studies sponsored by PETROBRAS have investigated interacting corrosion defects by means of both numerical and experimental efforts[9, 10, 11, 12, 13, 14]. Multiple identical defects were arranged into different configurations, such as axially aligned, circumferentially aligned, rhombus shaped, "X" shaped, "V" shaped, etc.

The "ligament stress criterion" was applied for the failure determination in FEA. It requires that the Von Mises stress along a radial direction including all points situated across the thickness within the colony of defects exceeds the true ultimate tensile stress[12]. The pipe material under study was API 5L X80 steel, 18-inch-OD, and 0.312-inch-wall thickness. Two kinds of configurations were simulated: two identical defects axially aligned and four identical defects in a rhombus shape (see Figure 15 and Figure 16). Each defect had geometry parameters: length=39.6 mm, width=31.9 mm, and depth=5.39 or 4.05 mm. Since the circumferential spacing S_C was kept fixed and small enough to guarantee an interaction in the second configuration, the only variable was axial spacing S_L.

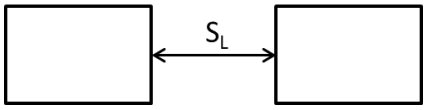

Figure 15. Configuration of Axially Spaced Corrosion Defects for Colony 1 and 2

[9] Benjamin, A. C., Freire, J. L. F., Vieira, R. D., Diniz, J. L. C. and Andrade, E. Q., 2005, "Burst Tests On Pipeline Containing Interacting Corrosion Defects", 24th International Conference on Offshore Mechanics and Arctic Engineering, OMAE 2005, June 2005.
[10] Benjamin, A. C., Freire, J. L. F., Vieira, R. D. and Andrade, E. Q., 2006, "Burst Tests On Pipeline Containing Closely Spaced Corrosion Defects", 25th International Conference on Offshore Mechanics and Arctic Engineering, OMAE 2006, June 2006.
[11] Andrade, E. Q., Benjamin, A. C., Machado Jr., P. R. S., Pereira, L. C., Jacob, B. P., Carneiro, E. G., Guerreiro, J. N. C., Silva, R. C. C. and NoronhaJr., D. B., 2006, "Finite Element Modeling of the Failure Behavior of Pipelines Containing Interacting Corrosion Defects", 25th International Conference on Offshore Mechanics and Arctic Engineering, OMAE 2006, June 2006.
[12] Benjamin, A. C., Andrade, E. Q., Jacob, B. P., Pereira, L. C., Machado Jr. and P. R. S., "Failure Behavior of Colonies of Corrosion Defects Composed of Symmetrically Arranged Defects", Proceedings of IPC 2006, 6th International Pipeline Conference, September 25-29, 2006, Calgary, Alberta, Canada.
[13] Andueza, A. and Pontual, T., "Structural Integrity Evaluation for the Analysis of Corroded Pipelines with Multiple Corrosion Defects", Proceedings of IPC 2006, 6th International Pipeline Conference, September 25-29, 2006, Calgary, Alberta, Canada.
[14] Benjamin, A. C., Franzoi, A.R., Freire, J. L. F., Vieira, R. D. and Diniz, J.L.C., "Burst Tests on Pipeline Containing Irregular Shaped Corrosion Defects", Proceedings of IPC 2008, 7th International Pipeline Conference, September 29 – October 3, 2008, Calgary, Alberta, Canada.

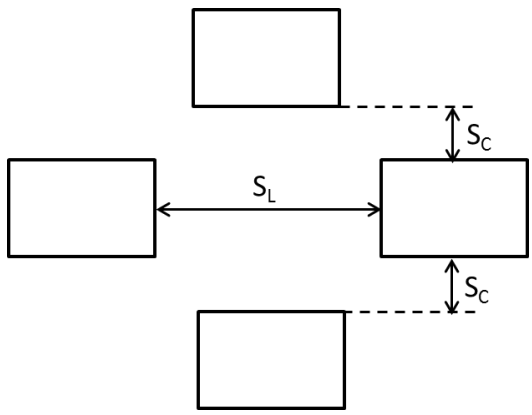

Figure 16. Configuration of Rhombus Shaped Defects for Colony 3 and 4

Three interaction rules were evaluated for 26 cases, including the Kiefner-Vieth rule[2], the Pipeline Operators Forum (POF) rule[3, 4], and the DNV rule. In the FEA the interaction was identified as occurring when the failure pressure relative to a single defect was less than 99%. It turned out that the DNV rule gave the highest percentage of right diagnoses equal to 96.2%, followed by 42.3% for the Kiefner-Vieth rule and 53.8% for the POF rule. From the 26 cases Table 1 extracts the relevant data of critical longitudinal distance for interaction. It can be seen that the separation needs to be greater than 18t on average to avoid interaction.

Table 1. Interaction Critical Distance Determination

Colony	Case	S_L/t	Interacting (Y/N)
1	GD311110	14	Y
1	GD311150	19	N
2	GD32100	12	Y
2	GD32150	19	N
3	GD61300	16	Y
3	GD61400	22	N
4	GD62200	10	Y
4	GD62400	22	N

Two groups of burst tests have been undertaken by PETROBRAS to examine the interaction of corrosion defects, also termed irregular shaped corrosion defects[9, 10, 14]. The experiments were done with external flat bottomed defects machined by spark erosion. The first group of 12 burst tests included single defects and group defects on a similar 18-inch-OD, 0.312-inch-wall thickness, API 5L X80 pipe. In Table 2, the failure location is designated by the shadowed rectangle, and the failure pressure is normalized by that of a single defect. S_L is the longitudinal separation and S_C is the circumferential separation. The interaction is determined by the failure pressure less than either 90% or 80% of the single defect result. The critical distance is inferred to be: S_L=2.5t and S_C=1.2t.

Table 2. Failure Location and Failure Pressure for Interacting Defects

Specimen ID	Defect Configuration	Wall Thickness (mm)	S_L (mm)	S_C (mm)	Normalized Burst Pressure	S_L/t	Sc/t	Interaction Defined by 90% Relative	Interaction Defined by 80% Relative
IDTS3		8.1	20.50	-31.90	0.896	2.5	-3.9	N	N
IDTS4		8.1	-39.60	9.90	0.932	-4.9	1.2	N	N
IDTS5		8.1	-9.50	10.00	0.920	-1.2	1.2	N	N
IDTS6	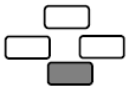	8.1	20.50	9.60	0.823	2.5	1.2	Y	N
IDTS7		8.1	20.40	10.00	0.828	2.5	1.2	Y	N
IDTS9		8.0	-9.88	9.88	0.953	-1.2	1.2	N	N
IDTS10	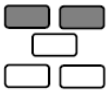	8.0	19.98	10.01	0.960	2.5	1.3	N	N
IDTS11	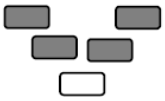	8.0	19.84	10.03	0.879	2.5	1.3	Y	N
IDTS12	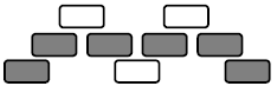	8.0	20.06	9.99	0.833	2.5	1.2	Y	N

The second group included burst tests on four specimens from the same pipe as shown in Table 3. Each region consisted of eight short and deep corrosion defects within a long and shallow corrosion patch. The dark region represents the failure location. If applying the average separation values of 2.0t and 4.3t, the critical interaction distance is about 3t.

Table 3. Four Specimens under Burst Tests

Specimen	Defect Top View	Separation
ISTS 1	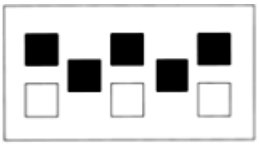	1.2t
ISTS 2	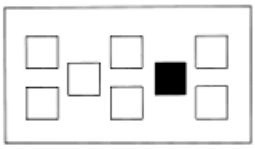	4.3t
ISTS 3	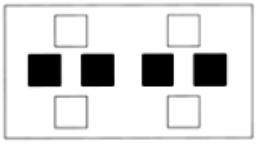	2.0t
ISTS 4	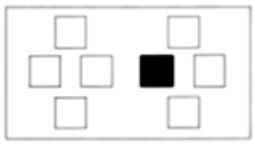	14.3t

A series of PRCI projects done by Advantica have investigated the corrosion interaction rules through reviewing historical test data[15, 16], conducting non-linear finite element simulations[17] and full-scale validation burst tests[18]. The axial and circumferential pit-pit, pit-groove, and groove-groove combinations were examined for three X65 pipe materials under the FEA sensitivity study of the separation dependence. The detailed pipe geometries were:

- Pipe Diameter, D, 32″ (812.8mm) and wall thickness, t, ¾″ (19.05mm) [D/t=43]
- Pipe Diameter, D, 36″ (914.4mm) and wall thickness, t, ½″ (12.7mm) [D/t=72]
- Pipe Diameter, D, 22″ (558.8mm) and wall thickness, t, 3/8″ (9.5mm) [D/t=58]

The experiments were done on 24-inch-OD, 0.312-inch-WT, API 5L grade B/X42 pipes. The conclusions were drawn as below.

[15] Fu, B., Stephens, D., Ritchie, D., Jones, C.L. "Methods for Assessing Corroded Pipeline – Review, Validation and Recommendations", PRCI Catalog No. L51878, Contract PR-273-9803, October 2000.
[16] Fu. B, Jones, C.L. and Chauhan, V. "Guidance for Assessing the Remaining Strength of Corroded Pipeline", PRCI Catalog No. L51958, Contract PR-273-9803, August 2002.
[17] Chauhan, V. and Grant, R., "Improved Methods for the Assessment of the Remaining Strength of Corroded Pipelines (Phase 4)", PRCI Catalog No. L51968, Contract PR-273-9803, 2003.
[18] Chauhan, V. and Wood, A., "Experimental Validation of Methods for Assessing Closely Spaced Corrosion Metal Loss Defects in Pipelines", Prepared for Gas Research Institute, 2005.

- Interaction of small diameter (2t) axially separated pit-pit combinations is insignificant. The difference in failure pressure between a pit separation of 1t and 6t is less than 5%.
- Interaction of larger diameter (8t) axially separated pit-pit combinations is more noticeable. However, the difference in failure pressure for defects spaced 1t and 6t apart is still less than 10%.
- Interaction of small diameter (2t) pit and groove (8t and 16t long), separated either axially, circumferentially or a combination of both, is insignificant, even when the defects are spaced as close as 1t from each other. The failure is dominated by the groove only.
- Interaction of groove-groove defects (8t long) separated axially is more marked than for pit-groove combinations. A reduction in failure pressure of approximately 26% is predicted as the defect spacing reduces from 6t to 1t. For similar groove-groove defects that are circumferentially spaced, the failure pressure increased significantly when the spacing was changed from 1t to 3t.
- Similar conclusions can be drawn for pipelines with (D/t) ratios of 43, 58 and 72.

Cunha proposed a corrosion interaction rule based on an analytical solution in the linear elastic domain[19]. The stress-strain solutions were expressed as relative perturbations produced by some hypothesized flaws on an intact pipe. Two straining modes of a cylindrical shell under internal pressure were taken into account: bending strain was simulated by an axis-symmetric flaw and membrane strain was simulated by a very narrow axial flaw. The range of non-negligible flaw induced stress concentration in its vicinity is defined as the possible interaction region. Two levels of flaw interaction criteria were recommended. The initial screening is based on the axial spacing no less than half of pipe radius or the circumference spacing no less than π/4. The secondary level presented by Figure 17 is more complicated. It involves considering individual flaw dimensions. L is half of the flaw length, l is half of the flaw width, d is the flaw depth, t_1 is the remaining wall thickness after corrosion, t_2 is the full wall thickness, and R is the pipe radius. The procedure is as follows. For two corrosion defects with indexes *j* and *k*, calculate the critical axial distance precluding interaction $\hat{S}_{j,k}$ and the critical angular distance precluding interaction $\hat{\Theta}_{j,k}$ from the analytical solutions. If the axial distance between these two corrosions no less than $\hat{S}_{j,k}$ or the angular distance between these two corrosions no less than $\hat{\Theta}_{j,k}$, there is no interaction. Otherwise, interaction is deemed between these two corrosions. The analytical rules were compared to the usual industry practice, e.g. ASME, DNV, and POF. It was found out that in certain situations, the existing interaction rules may give the unsafe predictions and disregard the possible interactions.

[19] Sérgio B. Cunha, "An Analytical Interaction Rule for Corrosion Flaws", IPC2008-64023, Proceedings of IPC 2008, 7th International Pipeline Conference, September 29-October 3, 2008, Calgary, Alberta, Canada.

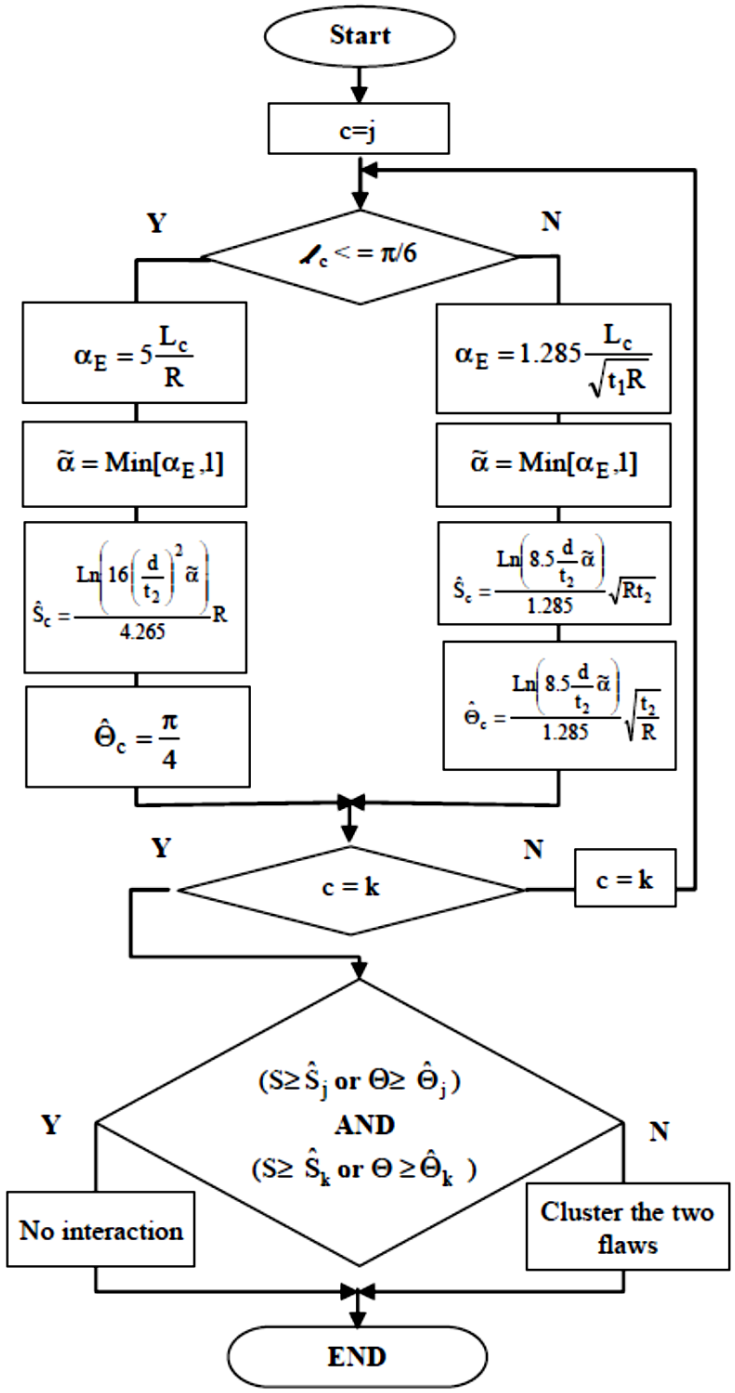

Figure 17. Secondary Assessment of Interaction

Artificial neural network technology was employed to study the corrosion interaction[20]. FEA simulations were carried out on a pipe containing two identical 80×32 mm corrosion defects

[20] Silva, R.C.C., Guerreiro, J.N.C., Loula, A.F.D., "A Study of Pipe Interacting Corrosion Defects Using the FEM and Neural Networks", Advances in Engineering Software, 38, 2007, Page 868-875.

with different depths separated by various spacing along both the axial and the circumferential directions. Afterwards, the results were used in the training and the validation phases of the neural network conception. This methodology had been applied successfully in a single defect assessment under bending or pressure loads[21, 22]. Consequently the neural network achieved experience to be able to give appropriate responses for new interacting situations, for instance, other corrosion geometries. From the limited database of 43 nonlinear finite element analyses, a three-layered neural network was built. The interaction spacings along the axial and the circumferential directions were determined to be $2\sqrt{Dt}$ and $3\sqrt{Dt}$ respectively, where D is the pipe diameter and t is the pipe wall thickness.

Corrosion defects interacting with longitudinal seams or girth welds were explored, and guidelines were formulated by B.N. Leis, et al.[23] The safe use of existing pipe body remaining strength prediction methods for corrosion on welds was investigated and validated by full-scale tests, laboratory tests, and in-service failures. Criteria were developed by trending empirical results from both lab and field to identify common traits for cases where pipe body criteria were used successfully. The circumstances where this adaption is inappropriate were highlighted through consideration of material fabrication defects, the presence of high shape-induced constraint, fracture toughness of weld and HAZ, local residual stresses from welding, and multi-axial loading conditions, etc. Particularly, all the results indicated that body criteria should not be used where vintage autogenous seam welds are involved. However, results for very large simulated metal loss on DSA girth welds exhibited very high tolerance, without distress even under nominal equibiaxial and other loadings up to or slightly beyond SMYS. The constraint effects due to the defect geometry excludes the applications in pitting corrosion and corrosion located in sharp strain or stress gradients with local biaxiality or triaxiality. Generally the defect width has to be at least three times its depth. The ultimate flow chart is presented in Figure 18. To test the flowchart viability, some experimental results of corrosion on welds were evaluated. The outcome is that (1) the failure pressure was conservatively predicted for all cases ending with "pipe body criteria viable" in the flow chart; (2) the failure pressure was not conservatively predicted for all cases ending with "pipe body criteria not viable without ECA" in the flow chart; (3) For the SSAW seams, the flow chart can be overly conservative.

[21] Han, Y.L., Shen S.M., Dai, S.H., "Artificial Neural Network Technology As a Method to Evaluate the Failure Bending Moment of a Pipe with a Circumferential Crack", Int J Pres Ves Pip, 1996, 68:1-6.
[22] Han, L., Han, L., Liu, C., "Neural Networks Applied to Prediction of the Failure Stress for a Pressurized Cylinder Containing Defects", Int J Pres Ves Pip, 1997, 76: 215-219.
[23] Leis, B.N., Clark, E.B., Zhu, X.K., and Galliher, R.D., "Guidelines for Assessing Corrosion Associated with Girth and Long-Seam Welds", PRCI Report GRI-8521, October 2004.

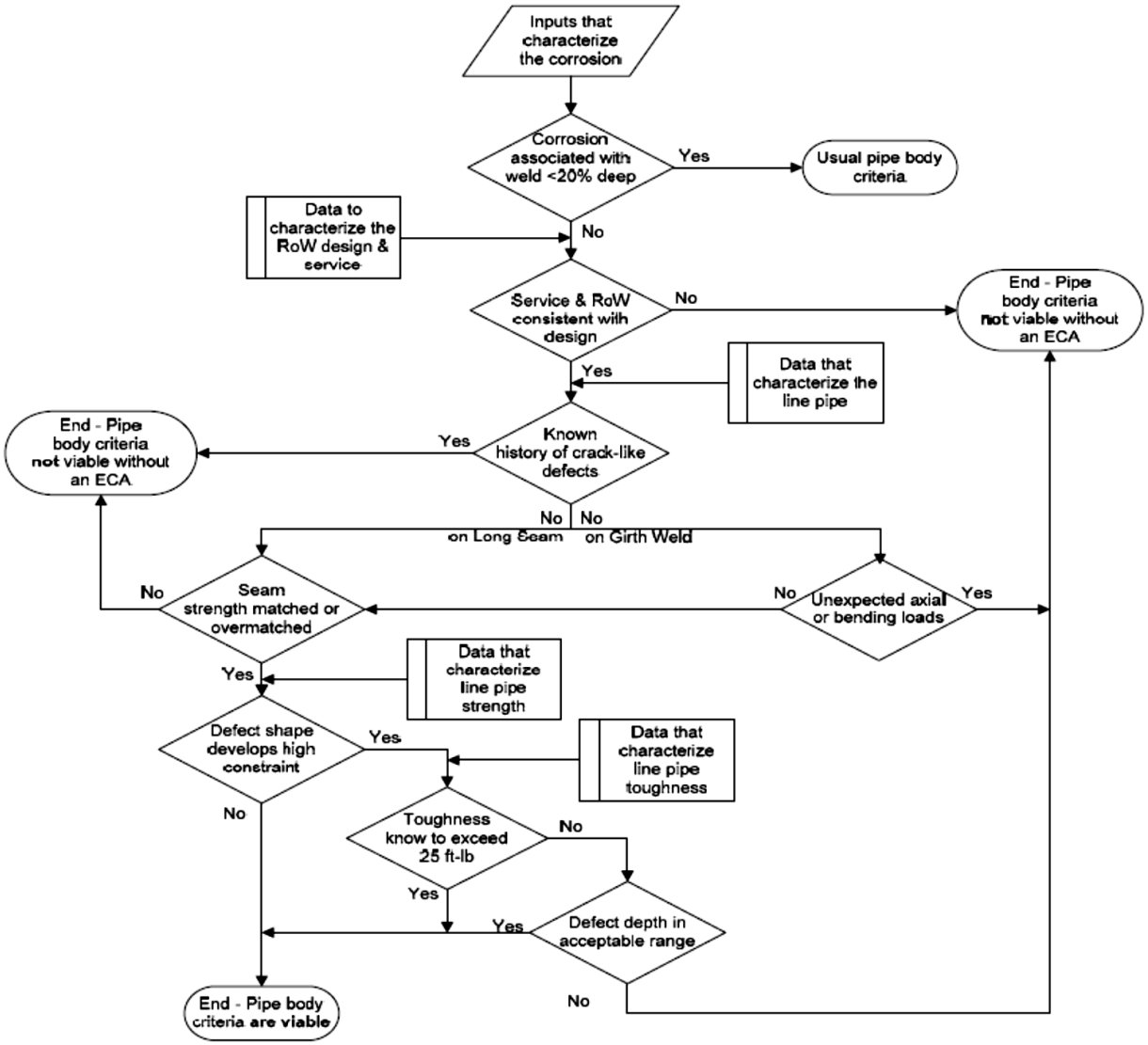

Figure 18. Guideline Flowchart of Corrosion on Welds

Summary of Interaction Criteria for Corrosion Defects

From several studies discussed in conjunction with corrosion defect interaction, it is seen that the resulting criteria for interaction were quite varied. The results from these studies are summarized in Table 4.

Table 4. Corrosion Defect Interaction Criteria Based on Experimental and Analytic Studies

Reference Numbers	Type of Study	Minimum Spacing to Avoid Type 1 Interaction (See Figure 1)	Minimum Spacing to Avoid Type 2 Interaction
1,2	Experimental	6t	1 inch
3,4	Experimental	The width of the narrowest defect	The length of shortest defect
5	Experimental	1t or 1 inch	3t
6	Experimental	0 for circular pits	1t for circular pits
7	Analytical		6t
8	Analytical	One tenth of pipe diameter	One tenth of pipe diameter
9	Experimental	1.2t*	2.5t*
12	Analytical		18t**
14	Experimental		3t
18	Experimental		6t
19	Analytical	One eighth of circumference	One fourth of pipe diameter
20	Analytical	$3\sqrt{Dt}$	$2\sqrt{Dt}$

Note: * Interaction defined as the burst pressure less than 80% of that for the single defect.
** Interaction defined as the burst pressure less than 99% of that for the single defect; if defining interaction as less than 85%, the critical distance is 2.5t.

It is not surprising that the analytical results differ widely from one another, and why some vary widely from the experimental results. Some of the analyses were elastic analyses while others accounted for the elastic-plastic behavior of the material near the defects. It seems likely that in some cases, experimental results may have been used to calibrate the analysis. Even within the experimental results there was disagreement between the various sets of experiments. That may be due to the fact that different defect configurations and different materials were used by the various investigators. However, the upper bound experimental result of 6t suggests that the larger separation distances established by some of the analytical studies are excessively conservative. It is significant that all experimental results point to 6t as being the most conservative separation distance to avoid having to consider the overall dimensions of a pair or a group of non-touching corrosion defects in calculating the failure pressure. The criteria for interaction of corrosion defects listed in various codes, standards, and handbooks are listed in Table 5.

Table 5. Corrosion Defect Interaction Criteria Listed in Various Codes, Standards, and Handbooks

Code, Standard or Handbook	Minimum Circumferential Spacing to Avoid Interaction	Minimum Longitudinal Spacing to Avoid Interaction
API 579-1/ASME FFS-1:2007	Half the larger circumferential dimension of two defects	Half the larger longitudinal dimension of two defects
ASME B31G:2009	3t	3t
ASME B31.4:2012	6t	1 inch
DNV-RP-F101:2010	$360\sqrt{t/D}$ degrees	$2\sqrt{Dt}$
BS 7910:2013	The smaller circumferential dimension of two defects	The smaller longitudinal dimension of two defects
CSA Z662:2011	The longitudinal dimension of the smaller defect	The longitudinal dimension of the smaller defect
PDAM:2003	$360\sqrt{t/D}$ degrees	$2\sqrt{Dt}$

The consistent experimental finding that interaction of corrosion defects does not occur when the spacing is as large as 6t suggests that the ASME standards are pretty close to the mark and that the limits contained in other standards and handbooks are over-conservative. The ASME B31.4 limitation of 1 inch for Type 2 defects should probably be changed to 3t to agree with the ASME B31G standard. It does not seem necessary to change the limits to 6t because the authors of Reference [18] who came up with the most conservative experimental results, state that 6t is probably over-conservative. Moreover, there is no evidence from actual pipeline experience that the 3t values in ASME B31G or even the 1-inch limit in ASME B31.4 lead to unsafe conditions.

It can be concluded from this review that there is no need for further analytical work on the subject of corrosion defect interaction. The analytical studies thus far, except in one case, have produced results that are far more conservative than the separation distances confirmed by experiments. Therefore, it is recommended that the analytical work to come should be focused on the interaction of defect types other than corrosion.

LITERATURE REVIEW OF PLANAR FLAW INTERACTIONS

In 2011 TWI published a paper describing the historical evolution of BS 7910 flaw interaction criteria.[24] The multiple refinement since the 1980 version of the BS 7910 predecessor PD 6493 was explained by the support of the experimental data and numerical analysis.

Table 6. History of Flaw Interaction of BS 7910

Document	Flaw Interaction Criterion
PD 6493: 1980	$s \leq 0.5\times(2c_1+2c_2)$
PD 6493: 1991	$s \leq 2c_1$, if $c_1<c_2$
BS 7910: 1999	$s=0$, for $a_1/c_1<1$ and $a_2/c_2<1$
BS 7910: 2005	$s=0$, for $a_1/c_1<1$ and $a_2/c_2<1$

Note: s is the edge-to-edge distance between two flaws along the length direction. $2c_1$ and $2c_2$ are two flaw lengths. a_1 and a_2 are two flaw depths.

As summarized in Table 6 about coplanar surface flaws, the interaction criterion has become more generous to avoid the unnecessary conservatism. It changes from the average flaw length, to the smaller flaw length, until two flaws touch.

PD 6493: 1980 used the fatigue crack growth data to derive the stress intensity factors of two identical interacting flaws under bending loading[25, 26]. The interaction factor is defined as a ratio of the stress intensity factors for the adjacent to the remote crack tips. This factor decreases from 1.6 to 1 for various samples within a spacing s of about 0.2 times the average length. A safety factor of around 5 is built in the rule. Similar fatigue growth tests were conducted recently. The onset of the coalescence of two flaws happens when the adjacent tips are very close to each other[27, 28, 29]. PD 6493:1991 adopts the smaller flaw length criterion so as to be consistent with the limiting state of one infinitesimal flaw.

[24] Bezensek, B., Sharples, J., Hadley, I., and Pisarski, H., "The History of BS 7910 Flaw Interaction Criteria", ASME 2011 Pressure Vessels and Piping Division Conference, Baltimore, Maryland, USA, Page 17-21.
[25] Bezensek, B. and Hancock, J.W., "The Re-characterization of Complex Defects, Part I: Fatigue and Ductile Tearing", Engng. Fract. Mech., 2004, 71:1000-1020.
[26] Bezensek, B., and Hancock, J.W., "Brittle Fracture from Interacting Surface Breaking Defects", 2001 ASME Pressure Vessels and Piping Conference, Atlanta, USA, July 2001, Page 25-31, Vol. 423.
[27] Sharples, J.K., Wilkes, M.A., Yellowlees, S.F., Beardsmore, D.W., Melvin, G.T., Hurlston, R., and Watson, C.T., "Analysis of Multiple Co-planar Surface Breaking Flaws Loaded in Tension under Cleavage Failure Conditions", 2006 ASME Pressure Vessels and Piping Conference, Vancouver, Canada, July 2006.
[28] Sharples, J.K., Wilkes, M.A., Beardsmore, D.W., Melvin, G.T., Sherry, A.H., Goldthorpe, M.R., and Watson, C.T., "Further Analysis of Multiple Co-planar Flaws under Cleavage Failure Conditions", 2007 ASME Pressure Vessels and Piping Conference, San Antonio, USA, July 2007.
[29] Sharples, J.K., Wilkes, M.A., Beardsmore, D.W., Melvin, G.T., Sherry, A.H., and Jackson, M., "Further Studies of Multiple Co-planar Surface Breaking Flaws for Cleavage Fracture", 2008 ASME Pressure Vessels and Piping Conference, Chicago, USA, July 2008.

In the late 1990s a study carried out by the ASME Boiler and Pressure Vessel Code, Section XI, concluded that the flaw interaction is not negligible within the distance comparable to the flaw depth.

Since 1999, BS 7910 has allowed the adjacent flaws to touch prior to combining them. Since the bounding flaw size is greater than the sum of the two flaws, not using flaw interaction for closely spaced flaws is compensated for. Even with ductile tearing, this criterion is still conservative[25]. Meanwhile, there is another change in the 1999 version compared to the previous ones. The requirement of determining the interaction of a combined flaw with others is no longer needed.

However, recent studies found that touching flaw characterization is not always conservative for cleavage[30,27,28,29]. At a given failure probability, a lower failure load can be attained for touching flaws comparing to a combined one. This offers one reason for the modification of the flaw interaction rule in BS 7910:2013.

In 1996, European Pipeline Research Group (EPRG) published the guidelines for pipeline girth weld assessment[31]. The accumulation and interacting criteria were considered in the allowable defect length. In terms of Figure 19, the allowable length of planar defects, no matter whether they are interacting or not, had the cutoff of 25% of the pipe circumference. This is twice the cutoff of API 1104. The three limit criteria for individual, interacting and all defects are different.

If a planar, slag or porosity defect is separated from a planar defect by a distance less than the shorter length of the two defects, then it is categorized as a single defect of length equal to the sum of two individual lengths and separation.

[30] Bezensek, B., and Hancock, J.W., "The Re-characterization of Complex Defects, Part II: Cleavage", Engng. Fract, Mech., 2004, 71:1021-1040.
[31] Knauf, rer. nat. Gerhard and Hopkins, Phil, "The EPRG Guidelines on The Assessment of Defects in Transmission Pipeline Girth Welds", Sonderdruck aus 3R international, 35. Jahrgang, Heft 10-11/1996, S. 620-624.

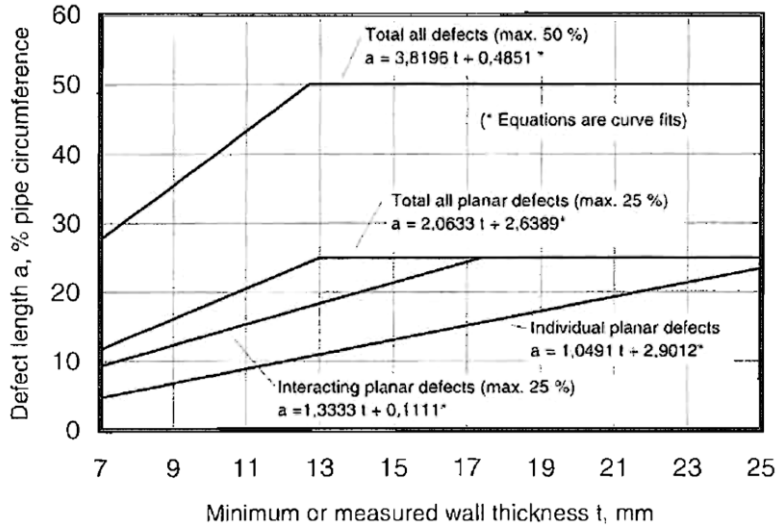

Figure 19. Girth Weld Defect Limits for Tier 3

API 579-1/ASME FFS-1 2007 Fitness-For-Service

Section 9.3.6.4 characterizes branched cracks as a single equivalent one. Figure 20 details the procedure:

(1) Draw a rectangle around the affected region with the measured flaw length $2c_m$.

(2) Define an effective flaw length $2c$ perpendicular to the maximum principal stress σ_1 by following Section 9.3.6.2.

(3) Measure the maximum through-wall depth of the branched network a_0. If an actual depth measurement is made, the effective depth is 1.2 times a_0. Otherwise, conservative default values can be used, which for example is equal to wall thickness.

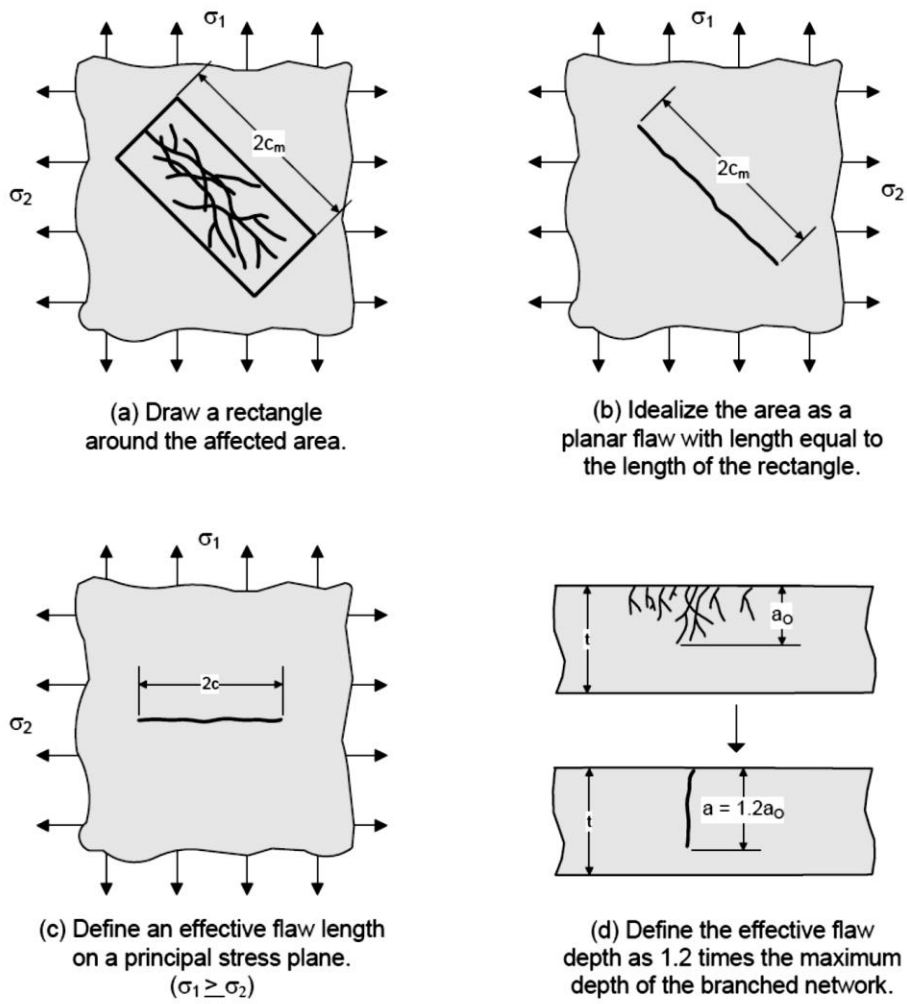

Figure 20. Assessment of Branched Cracking

Section 9.3.6.5 characterizes multiple flaws in close proximity to one another. The procedure is illustrated below with the support of Figure 21 and Figure 22.

(1) Project each discrete flaw on the plan perpendicular to maximum principal stress σ_1 as Figure 21 (b). Effective length should be calculated by following Section 9.3.6.2.
(2) Apply criteria in Figure 22 to check the interaction between parallel flaws, and project the interacting flaws onto a single plane as Figure 21 (c).
(3) Estimate the depth of a single flaw or a combined flaw produced from Step (2). For combined flaws, each depth is defined as the width of an inscribed rectangle as Figure 21 (d). Effective depth should be calculated by following Section 9.3.6.3.
(4) Apply the criteria in Figure 22 to check for interaction between flaws on a given plane. If interaction exists, the dimensions of the combined flaw are derived from the inscribed rectangle.

This section also mentions that multiple flaws do not have to be combined for evaluation if a stress intensity factor and limit load can be obtained for the interacting flaw geometries. From Figure 22, it is straightforward to determine that the interaction criteria are essentially the comparison between the spacing and the average length or depth of two "embedded" flaws along the same direction, assuming that a real surface flaw with the depth a is equivalent to an embedded flaw with the depth $2a$.

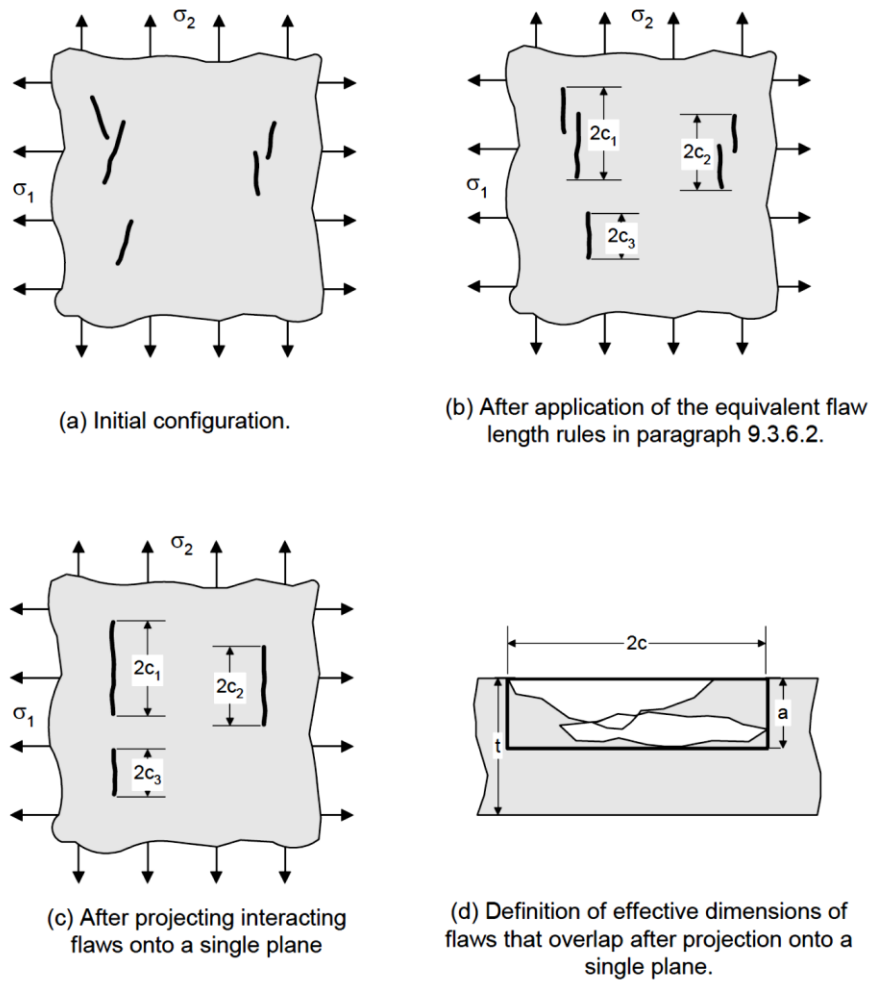

(a) Initial configuration.

(b) After application of the equivalent flaw length rules in paragraph 9.3.6.2.

(c) After projecting interacting flaws onto a single plane

(d) Definition of effective dimensions of flaws that overlap after projection onto a single plane.

Figure 21. Assessment of Multiple Crack-like Flaws

Multiple Crack-Like Flaw Configuration	Criterion For Interaction	Effective Dimensions After Interaction
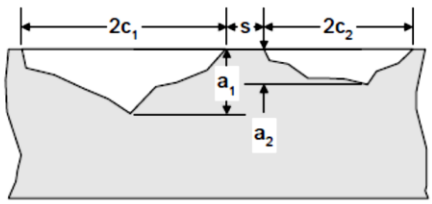	$c_1 + c_2 \geq s$	$2c = 2c_1 + 2c_2 + s$ $a = \max[a_1, a_2]$
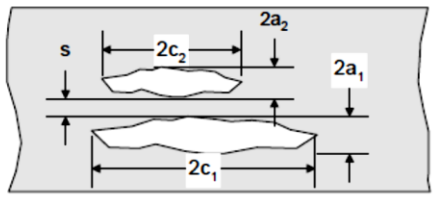	$a_1 + a_2 \geq s$	$2a = 2a_1 + 2a_2 + s$ $2c = \max[2c_1, 2c_2]$
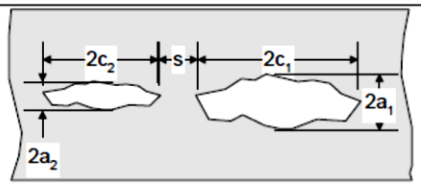	$c_1 + c_2 \geq s$	$2c = 2c_1 + 2c_2 + s$ $2a = \max[2a_1, 2a_2]$
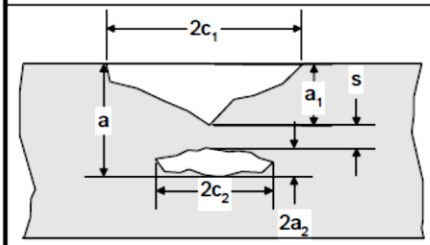	$a_1 + a_2 \geq s$	$a = a_1 + 2a_2 + s$ $2c = \max[2c_1, 2c_2]$

Figure 22. Interaction of Coplanar Flaws

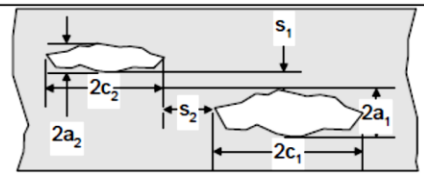	$c_1 + c_2 \geq s_2$ *and* $a_1 + a_2 \geq s_1$	$2c = 2c_1 + 2c_2 + s_2$ $2a = 2a_1 + 2a_2 + s_1$
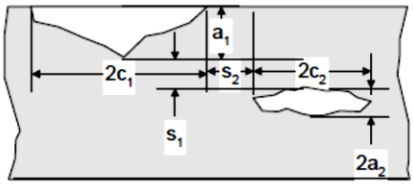	$c_1 + c_2 \geq s_2$ *and* $a_1 + a_2 \geq s_1$	$2c = 2c_1 + 2c_2 + s_2$ $a = a_1 + 2a_2 + s_1$
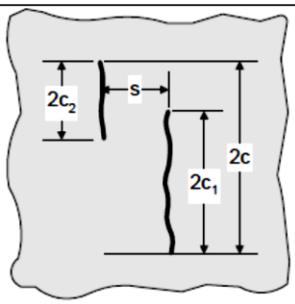	$c_1 + c_2 \geq s$	Project flaws onto the same plane. $2c$ = total length of projection based on cracks defined by $2c_1$ and $2c_2$
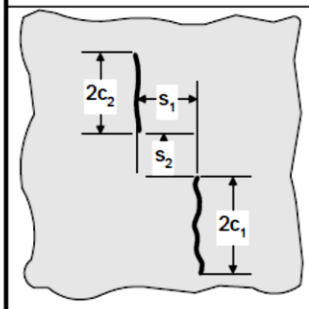	$c_1 + c_2 \geq s_1$ *and* $c_1 + c_2 \geq s_2$	Project flaws onto the same plane. $2c = 2c_1 + 2c_2 + s_2$

Figure 23. Interaction of Coplanar Flaws (Continued)

BS 7910 2013 Guide to Methods for Assessing the Acceptability of Flaws in Metallic Structures

Section 7.1.2 – Flaw Dimensions and Interaction, provides the interaction rules in Subsection 7.1.2.3. The basic procedure consists of two steps as illustrated in Figure 24 and Figure 25. Flaws on the different cross-section planes should first be checked by the alignment criteria as shown in Figure 24. If the distance between two flaw planes is not greater than the average depth of two flaws, they are deemed to interact and need to be projected onto the same principal plane for the further assessment. Aligned flaws or flaws originally occurring on the same plane should be checked against the combination criteria as shown in Figure 25.

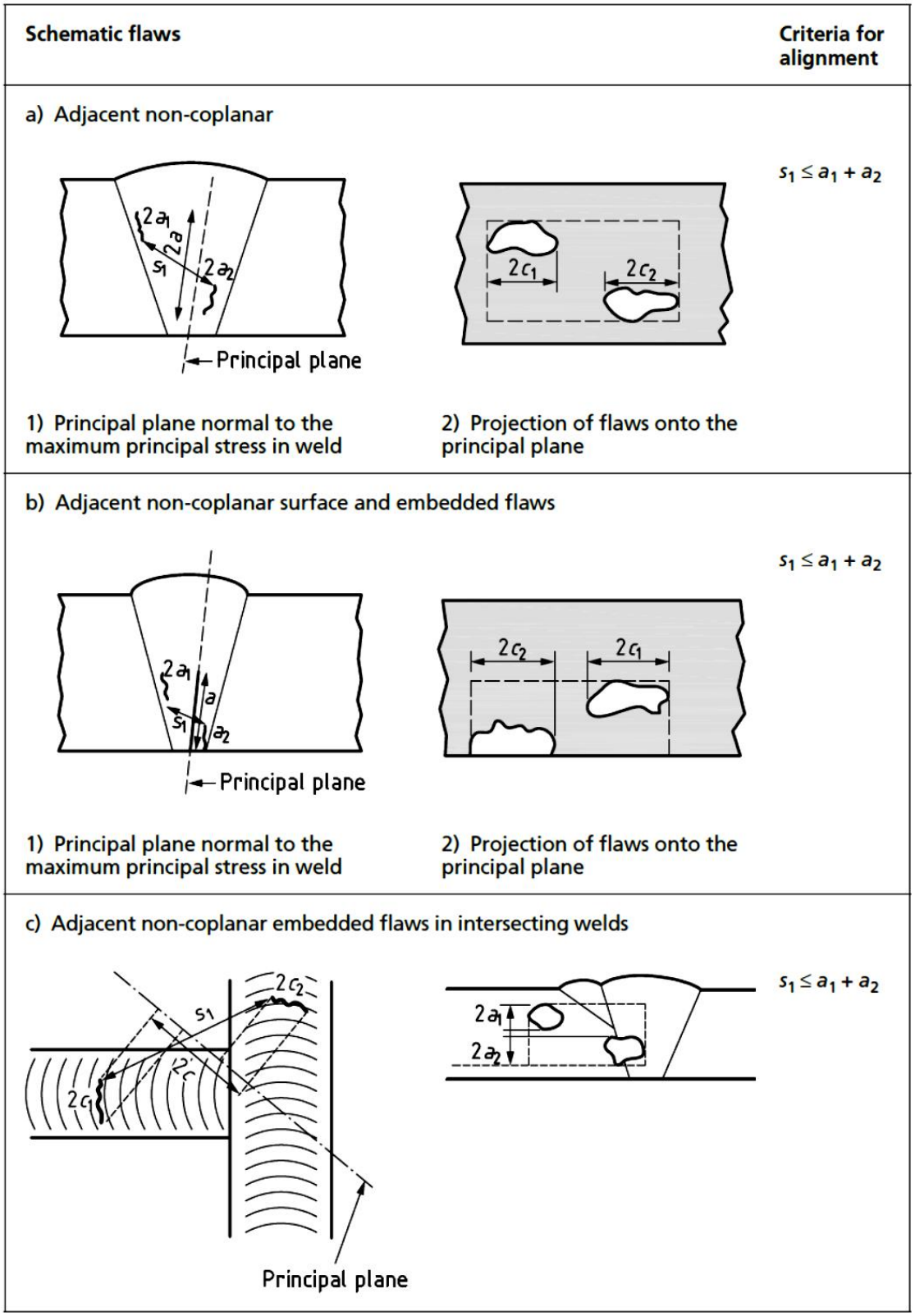

Figure 24. Alignment Rules for Non-coplanar Flaws

Schematic flaws	Criteria for interaction	Effective dimensions after interaction
i) Coplanar surface flaws 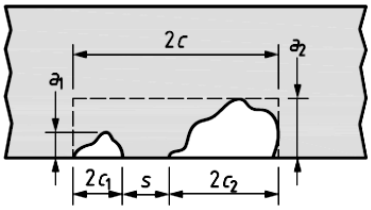	$s \le 2c_1$ for a_1/c_1 or $a_2/c_2 > 1$ $s \le$ max. $\{0.5a_1, 0.5a_2\}$ for a_1/c_1 and $a_2/c_2 < 1$ $(c_1 < c_2)$	a = max. $\{a_1, a_2\}$ $2c = 2c_1 + 2c_2 + s$
ii) Coplanar embedded flaws (interaction in thickness direction) 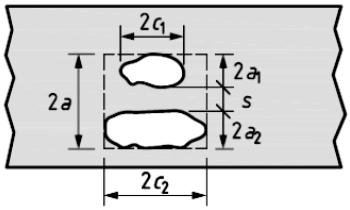	$s \le a_1 + a_2$	$2a = 2a_1 + 2a_2 + s$ $2c$ = max. $\{2c_1, 2c_2\}$
iii) Coplanar embedded flaws (interaction in width direction) 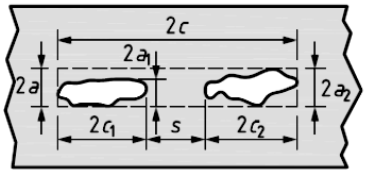	$s \le 2c_1$ for a_1/c_1 or $a_2/c_2 > 1$ $s \le$ max. $\{a_1, a_2\}$ for a_1/c_1 and $a_2/c_2 < 1$ $(c_1 < c_2)$	$2a$ = max. $\{2a_1, 2a_2\}$ $2c = 2c_1 + 2c_2 + s$
iv) Coplanar surface and embedded flaws (interaction in thickness direction) 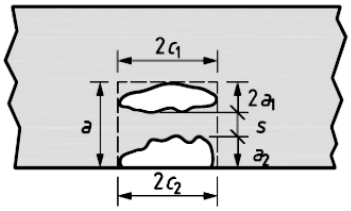	$s \le a_1 + a_2$	$a = 2a_1 + a_2 + s$ $2c$ = max. $\{2c_1, 2c_2\}$
v) Coplanar embedded flaws (interaction in thickness and width direction) 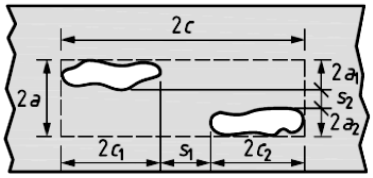	$s_1 \le$ max. $\{a_1, a_2\}$ for a_1/c_1 and $a_2/c_2 < 1$ $s_1 < 2c_1$ for a_1/c_1 or $a_2/c_2 > 1$ and $s_2 \le a_1 + a_2$ $(c_1 < c_2)$	$2c = 2c_1 + 2c_2 + s_1$ $2a = 2a_1 + 2a_2 + s_2$

Figure 25. Interaction Rules for Coplanar Flaws

Schematic flaws	Criteria for interaction	Effective dimensions after interaction
vi) Coplanar surface and embedded flaws (interaction in both thickness and width direction) 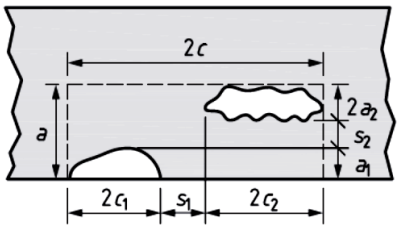	$s_1 \leq 2c_1$ for a_1/c_1 or $a_2/c_2 > 1$ $s_1 \leq$ max. $\{a_1, a_2\}$ for a_1/c_1 and $a_2/c_2 < 1$ and $s_2 \leq a_1 + a_2$ $(c_1 < c_2)$	$a = a_1 + 2a_2 + s_2$ $2c = 2c_1 + 2c_2 + s_1$

Figure 26. Interaction Rules for Coplanar Flaws (Continued)

Note: It is not normally necessary to consider the additional interaction of a combined flaw with the neighboring flaws. For fatigue assessment, it is not necessary to apply flaw interaction criteria. However, if there is any uncertainty as to whether flaws are separate they should be combined or specific calculations carried out.

Compared to API 579, BS 7910 gives more complicated rules about coplanar flaw interaction. The criteria depend on the aspect ratio of relevant flaw geometries, i.e. the depth/length ratio for each flaw. For the spacing in the depth direction, it is always compared to the average depth of two "embedded" flaws by treating any real surface flaw with the depth a equivalent to an embedded flaw with the depth $2a$. When both flaws have a depth/length ratio less than 1, the spacing along the length direction is compared to the half of the maximum depth of two "embedded" flaws on the condition that at least one flaw is really embedded. It is then compared to the quarter of the maximum depth of two "embedded" flaws on the condition that both flaws are surface breaking; otherwise it is compared to the smaller length of two flaws.

CSA Z662 2011 Oil and Gas Pipeline Systems

In Annex K – Standards of Acceptability for Circumferential Pipe Butt Welds Based upon Fracture Mechanics Principles, Section K.7.2 explains the interaction rule between imperfections. Coplanar imperfections shall be considered to interact if the circumferential distance between their indications is less than the length of the smaller indication. For such imperfections, the effective length shall be the sum of the dimensions of the two indications plus the distance between them.

In the Commentary on CSA Z662-11, Section K.7.2 states that the criterion for interaction of imperfections is consistent with Figure 9 of BSI BS 7910:1999.

API 1104 21ST Edition 2013 Welding of Pipelines and Related Facilities

Annex A – Alternative Acceptance Standards for Girth Welds illustrates the imperfection interaction in Figure 27. For the spacing along the length direction, it is the same as CSA Z662; for the spacing along the depth direction, it is similar to BS 7910.

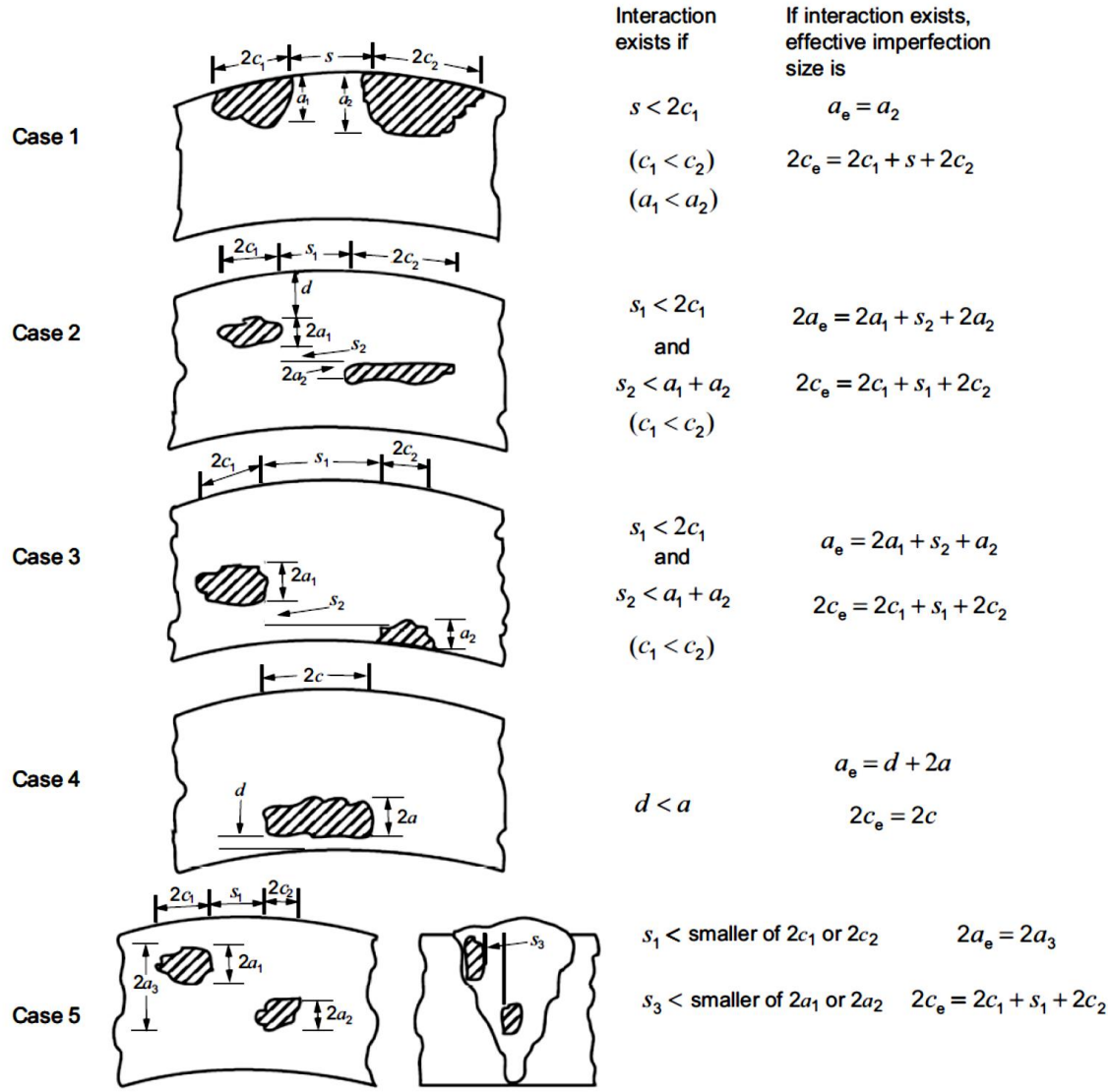

Figure 27. Imperfection Interaction Criteria

FITNET Fitness-for-Service Procedure 2006: A unified European procedure for structural integrity assessment

Annex F – Interaction of Multiple Planar Flaws: Alignment and Combination Rules, is similar to BS 7910, but not the same, especially regarding the alignment criteria (see Figure 28 and

Figure 29). It uses the minimum of real flaw depths regardless of embedded or surface breaking rather than the average depth value.

CASE	COMBINATION CRITERIA	EFFECTIVE DEFECT DIMENSIONS
A 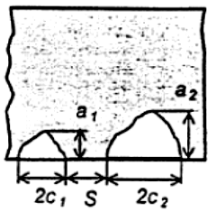	For a_1/c_1 or $a_2/c_2 > 1$: $S \le \min(2c_1, 2c_2)$ OR $S \le \max(0.5a_1, 0.5a_2)$ else: $S \le \max(0.5a_1, 0.5a_2)$	$a = \max(a_1, a_2)$ $2c = 2c_1 + s + 2c_2$
B 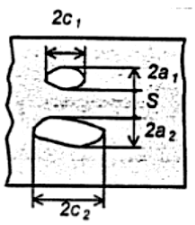	$S \le a_1 + a_2$	$2c = \max(2c_1, 2c_2)$ $2a = 2a_1 + s + 2a_2$
C 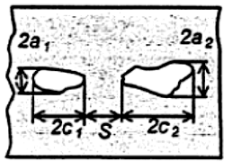	For a_1/c_1 or $a_2/c_2 > 1$: $S \le \min(2c_1, 2c_2)$ OR $S \le \max(a_1, a_2)$ else: $S \le \max(a_1, a_2)$	$2a = \max(2a_1, 2a_2)$ $2c = 2c_1 + s + 2c_2$
D 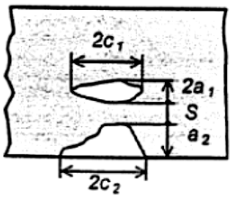	$S \le \frac{2a_1 + a_2}{2}$	$2c = \max(2c_1, 2c_2)$ $a = 2a_1 + s + a_2$

Figure 28. Flaw Combination Criteria

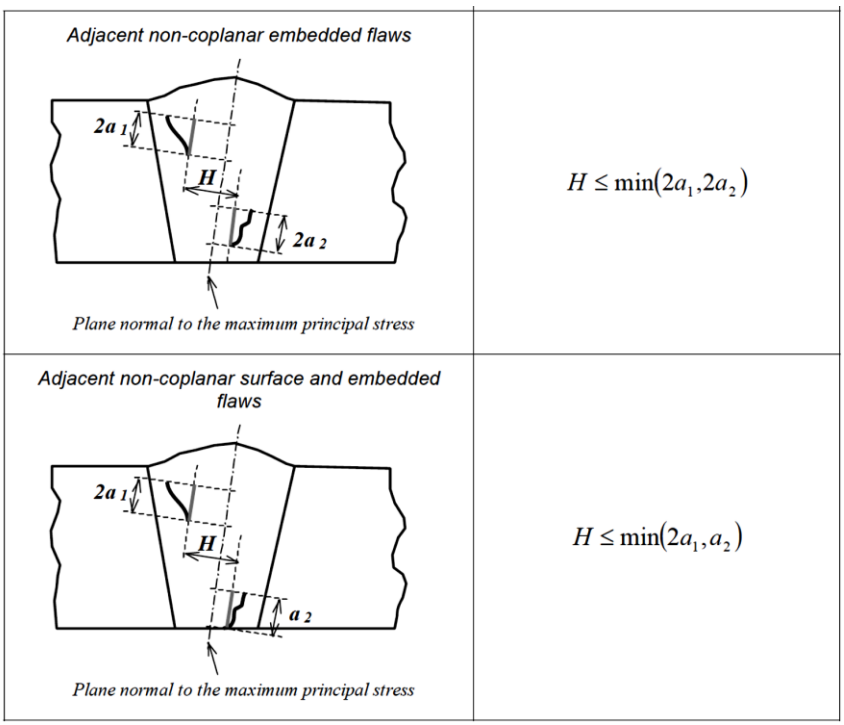

Figure 29. Flaw Alignment Criteria

Pipeline Defect Assessment Manual (PDAM) 2003

Section 36.4.1 – Part-wall Defects has the interaction rule for crack-like defects.

- Adjacent part-wall defects should be considered to interact if the spacing in any direction on the surface of the pipe between the defects is less than the major dimension (i.e. length or width, whichever is the greater) of the smaller defect. This interaction rule is similar to those given in BS 7910 and API 579. To be clearer, Figure 30 defines a zone of interaction around a defect. Adjacent defects will interact if larger (length or width) defects lie within the interaction zone of the smaller defect.
- The minimum interaction distance should be taken as three times the wall thickness.
- The effective dimensions of the cluster of adjacent interacting defects are the minimum dimensions of the enveloping rectangle. For interacting defects on a common surface, the effective depth is defined as the maximum depth; for interacting defects on opposite surfaces, the effective depth is defined as the sum of the maximum depth on both surfaces.

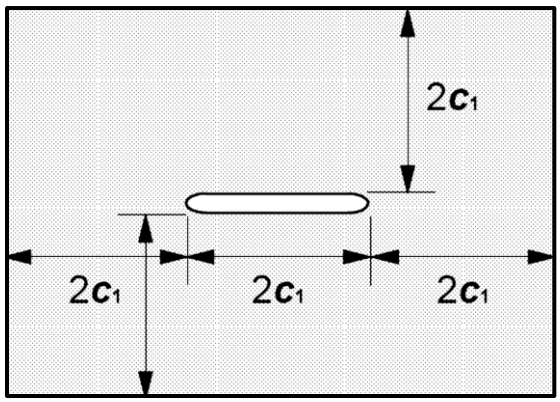

Figure 30. Interaction Zone around a Defect

SCC Recommended Practices, 2nd Edition, 2007 CEPA

Section 8.2.1.1 describes the physics of SCC Interaction as the overlap of stress fields around neighboring crack tips. The interaction is determined in both the longitudinal and circumferential directions by checking

$$Y \leq \frac{0.14(l_1 + l_2)}{2}, \qquad \text{Equation 11}$$

and

$$X \leq \frac{0.25(l_1 + l_2)}{2}, \qquad \text{Equation 12}$$

where X, Y are the longitudinal and circumferential spacing. l_1 and l_2 are the SCC lengths.

Both conditions have to be satisfied to guarantee if the interaction exists. When a third SCC feature is to be assessed adjacent to two SCC features already determined to be interacting, the non-interacting lengths of adjacent SCC features are to be used in consecutive assessments. This requirement is the same as NACE SP0204 Direct Assessment Methodology.

Characterization of Axial Flaws in Pipelines With a Focus on Stress Corrosion Cracking, PRCI 1997, Catalog No. L51807

Leis conducted a comprehensive research on the characterization of axial flaw interaction and coalescence[32,33], essentially being the basis of the CEPA criterion. Finite element simulation was

[32] Leis, B. N., "Characterization of Axial Flaws in Pipelines, With a Focus on Stress Corrosion Cracking", PRCI, Catalog No. L51807, Contract NG-18 Report No. 212, December 1997.

implemented to investigate the stress intensity factor change of a single crack due to the existence of other cracks in the close proximity. The conclusion is that the SCC pattern is dominated by circumferential spacing between cracks rather than their depth and length. Spacing equal to 20% of the wall thickness divides SCC into dense and sparse groups. Cracks in dense shallow patches, i.e. a large length/depth ratio stay dormant with negligible growth in depth, since the driving force vanishes as the depth increases. On the contrary, cracks in sparse deep patches, i.e. a length/depth ratio around 2 keep growing in both length and depth direction, and eventually fail by leaks or ruptures. For dense patches, the augmented compliance effect elevates the failure pressure compared to an isolated crack. For regular pipeline conditions, with regard to the shielding effect, the in-depth tips begin to interact for crack depths equal to ~7.5% of the wall thickness, and the surface tips begin to interact for crack depths equal to ~2% of the wall thickness. Some numerical examples were given to demonstrate the effects of the axial and circumferential spacing on the crack driving force. The geometry configuration is illustrated in Figure 31. Two identical cracks have a length of 2c and a depth of a. The axial spacing between them is 2d, and the circumferential spacing between them is 2b. In the cases studied, the crack depth is fixed to be 50% wall thickness (a/t=0.5), and the crack length/depth ratio is fixed to be 6 (c/a=3). Coplanar cracks are aligned in the same axial plane with 2b=0; coparallel cracks are stacked above each other around the pipe circumference with 2d=-3t.

[33] Stonesifer, R.B., Brust, F.W., and Leis, B.N., "Mixed-Mode Stress Intensity Factors for Interacting Semi-Elliptical Surface Cracks in a Plate", Engineering Fracture Mechanics, Vol. 45, No.3, Page 357-380,1993.

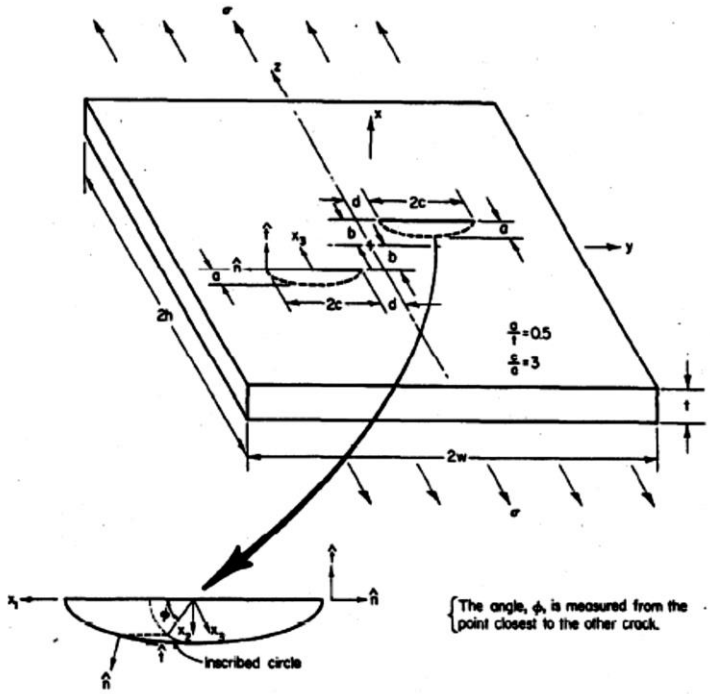

Figure 31. Geometry Layout of a Two-Crack Configuration

Under a hoop loading, two coplanar cracks only have the Mode I behavior. Figure 32 shows the stress intensity factor F_I along the whole crack front at three axial separations, 2d/t=0.25, 0.5, 1.0, normalized by the isolated crack value. The angle φ is measured from the crack tip closest to the other crack, i.e. inner crack tip.

The result of an isolated crack is drawn with solid triangle symbols. Since all the other curves lie above that for the isolated crack, the interaction with the adjacent coplanar crack increases the driving force. With a smaller separation, the interaction becomes stronger. Compared with an isolated crack, F_I increases less than 20% from φ=0° to φ=90° at 2d/t=0.25. It implies that in order to generate enough interaction to start coalescence, the axial spacing between two coplanar cracks needs to be less than 25% WT.

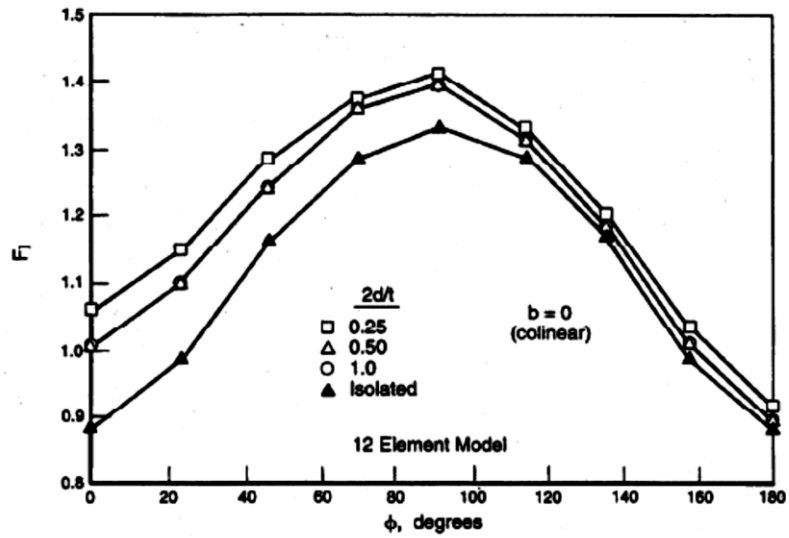

Figure 32. Normalized Crack Driving Force for Two Coplanar Cracks

A pair of coparallel cracks has a mixed-mode behavior, which is different from a pair of coplanar cracks. Figure 33 exhibits three components of the crack driving force for two coparallel cracks. Only the portions of 0°≤φ≤90° are shown due to the symmetry along φ=90°. Shear components, i.e. the Mode II and Mode III values are much smaller than the Mode I value, within 30% and 5% respectively. The sign convention is: "+" means cracks growing away and "-" means cracks growing together. For the Mode I component, all other curves lie below that for an isolated crack. The existence of an adjacent coparallel crack decreases the driving force, and this decrease is more substantial for a larger circumferential separation. For the Mode II component, all the values are positive, which means that cracks tend to grow away from each other. For the Mode III component, even though there are some negative values, the magnitudes are too small to be effective. Thus it is unlikely that coparallel pairs of cracks would grow much more than an isolated crack. In addition, the coparallel configuration is very rare in practice, as many arbitrary factors can lead to one crack growing differently from the other.

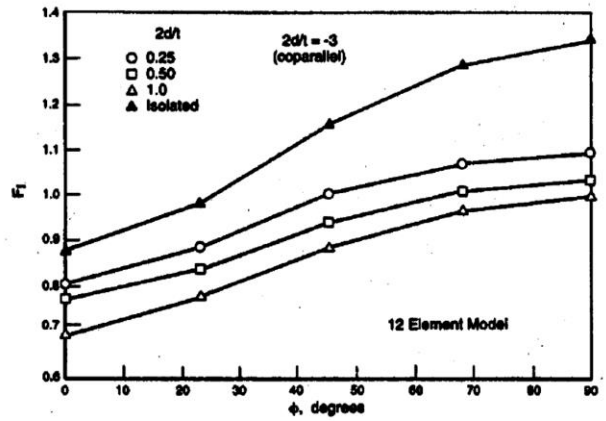

a Mode I cracking

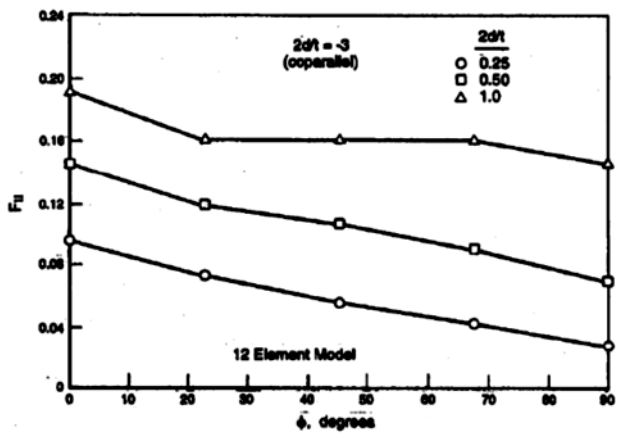

b Mode II cracking

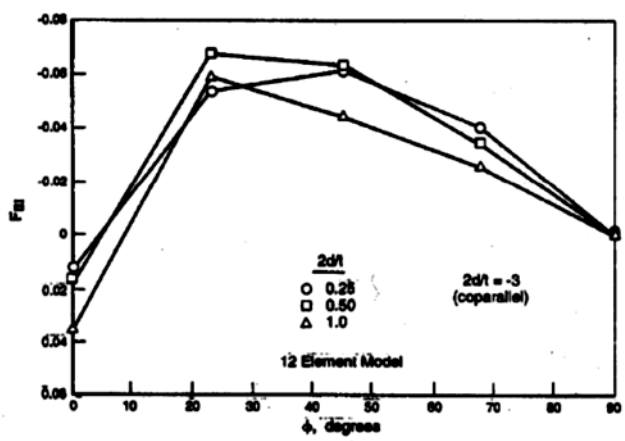

c Mode III cracking

Figure 33. Normalized Crack Driving Force for Two Coparallel Cracks

A more general case is illustrated in Figure 34 for two cracks with a fixed circumferential spacing equal to the wall thickness. The axial spacing 2d changes from -3t to 0.5t. Similarly, for all the cases, the Mode II and Mode III values are much smaller than the Mode I value. For the cracks that do not overlap axially, i.e. 2d/t>0, the curves are above the isolated crack solution, and the driving force becomes stronger with a smaller axial spacing. When 2d/t=0.25, the curve is almost identical with that for 2d/t=0 for two contacted cracks. For partially overlapped cracks, e.g. 2d/t=-0.5 and 2d/t=-1, when φ is less than a certain value φ_0, the curves are below the isolated crack solution; otherwise, the curves are above the isolated crack solution. For instance, with 2d/t=-0.5, the transition occurs at φ_0=35°; with 2d/t=-1, the transition occurs at φ_0=60°. Along the crack front, the shielding effect is strongest at the inner surface tip φ=0°, and the positive interaction is strongest at the deepest point φ=90°. When approaching the outer surface tip φ=180°, the curves collapse to the isolated crack solution. For fully overlapped cracks 2d/t=-3, the average driving force is dramatically less.

Comparing the coparallel situation in Figure 33, the Mode II behavior for partially overlapped cracks tends to cause the adjacent tips to grow towards rather than away from each other. For the Mode II, the largest value occurs at 2d/t=-0.5 and is about 15% of the corresponding the Mode I value. For the Mode III, except for the fact that the maximum values occur at points other than the surface point, the discussion related to the Mode II also applies.

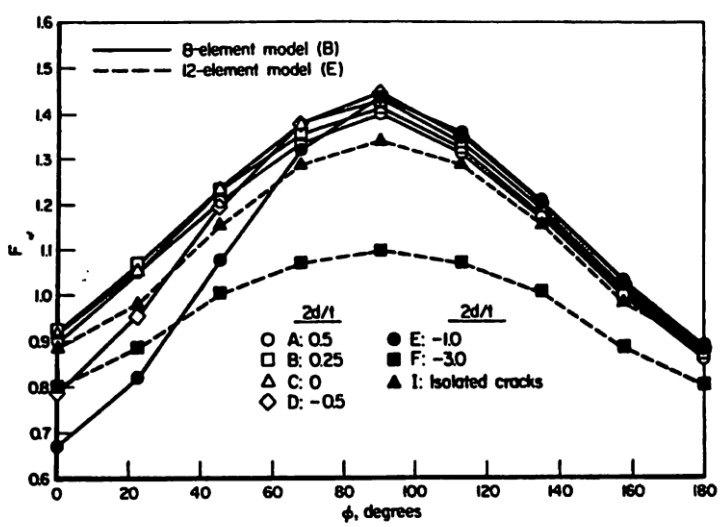

(a) Mode I

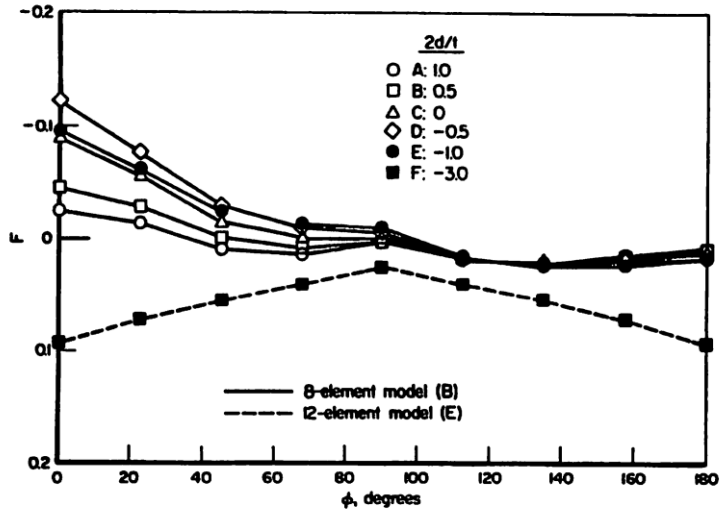

(b) Mode II

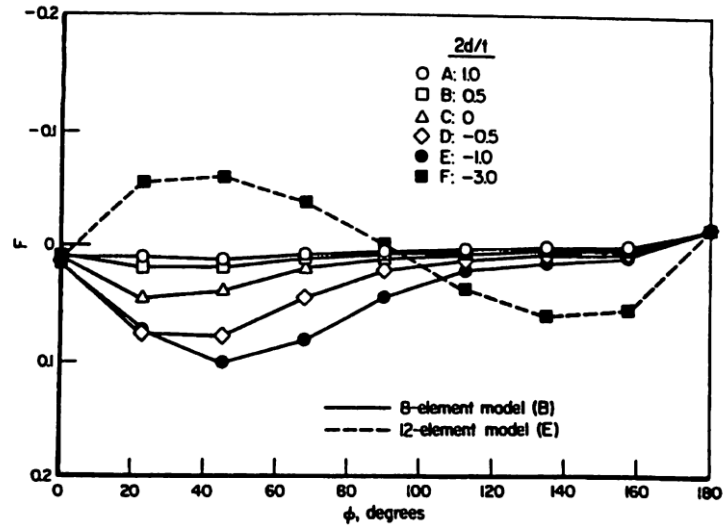

(c) Mode III

Figure 34. Normalized Crack Driving Force for two Cracks at 2b/t=1

Review of Journal Articles and Technical Reports

The procedures invoked by various codes allow for multiple interacting or complex defects idealized as a single contouring one. A family of representative defects was analyzed numerically and experimentally in regard to the interaction and failure mechanisms. The

conservatism level of the re-characterization in fatigue and ductile tearing[34] and the possibility of non-conservatism in cleavage[35] were revealed.

Experiments were employed on a plain carbon manganese steel plate with two surface breaking defects under three point bending. The defects were produced by the fatigue of two coplanar circular shallow slitting notches. The setup dimensions were illustrated schematically in Figure 35. Under the fatigue loading, semi-elliptical cracks were developed and extended in both length and depth directions after the initial growth in depth direction. In Figure 36 the progression was retrieved from the striations on the fracture surface. The largely uniform spacings of adjacent beachmarks along the crack fronts are the evidence that two separate cracks grew almost independently of each other until they touched. Subsequently a sharp re-entrant sector was formed on the coalescence plane and evolved towards a convex bounding shape quickly. In all fatigue tests, the surface crack path deviated locally from the notch plane. The cracks either overlapped and isolated a small cone-shaped piece of metal, or coalesced by shearing the small ligament and forming a step in the crack front. The phenomenon was explained by Melin[36] as that it is energetically unfavorable for any two adjacent crack tips to extend without the out-of-plane deviations.

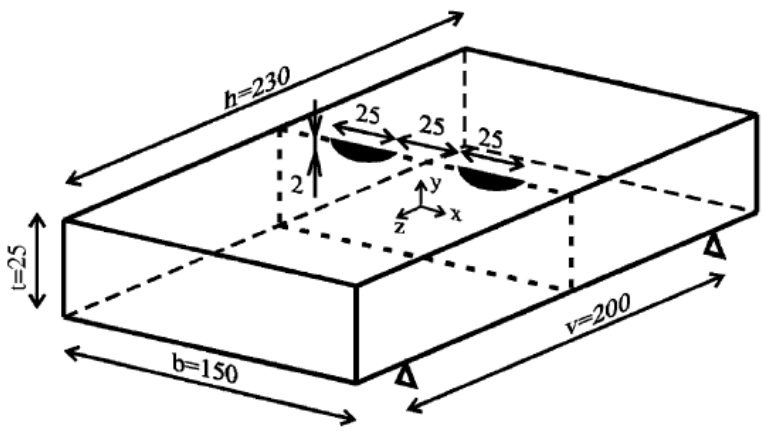

Figure 35. Experimental Setup with Units in mm

[34] Bezensek, B. and Hancock, J.W., "The Re-characterization of Complex Defects Part I: Fatigue and Ductile Tearing", Engineering Fracture Mechanics, 71 (2004) 981-1000.
[35] Bezensek, B. and Hancock, J.W., "The Re-characterization of Complex Defects Part II: Cleavage", Engineering Fracture Mechanics, 71 (2004) 1001-1019.
[36] S. Melin, International Journal of Fracture 23, 37 (1982).

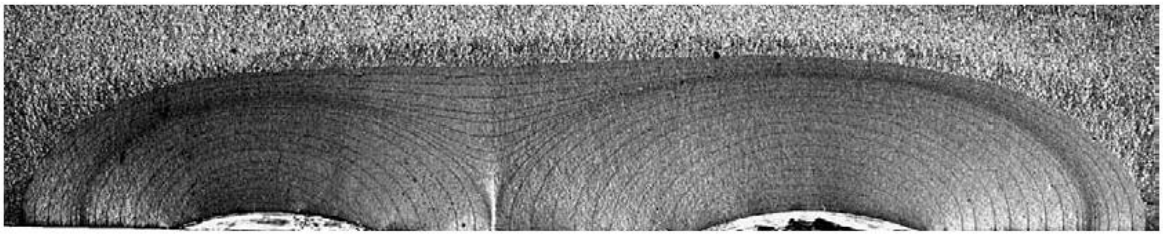

Figure 36. Crack Growth and Coalescence under Fatigue Loading

However, small interaction influence did occur before the crack tips came in contact. To get a better understanding of interaction between two separated cracks before coalescence, the ratio of stress intensity factor between the surface position E and C was plotted in Figure 37. Interaction becomes remarkable when the crack tip spacing becomes less than half the depth of the deepest defect (s<d/2). The magnitude of interaction is related to the thickness of the out-of-plane ligament between the adjacent crack tips, which determines the coalescence modes: overlap or shear step. When two cracks get touched with each other ($s \cong 0$), the stress intensity factor is enhanced by 20% from overlap or by 40% from a shear step in comparison with an isolated crack.

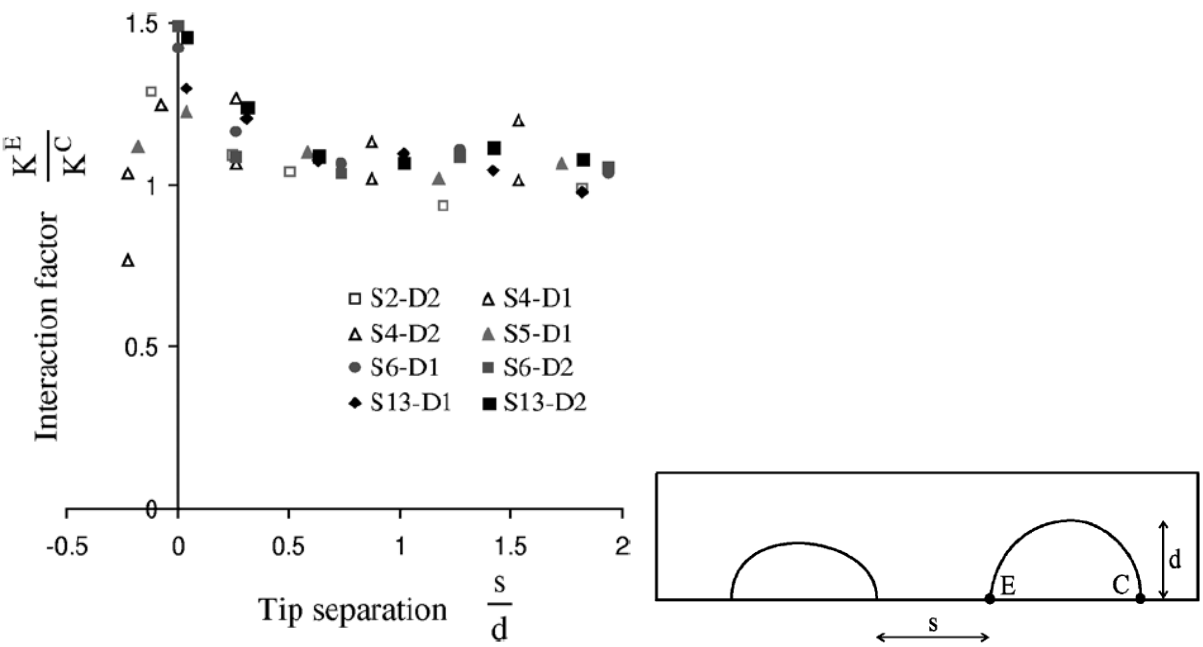

Figure 37. Ratio of Stress Intensity Factors between Free Surface Positions C and E

Ductile tearing experiments were performed at 20 °C with three dissimilar crack configurations generated by the fatigue process. As shown in Figure 38, the arrows point to the tearing boundary. Two stages of displacement-controlled loadings were applied. Ductile tearing started in the re-entrant sector, allowing for the cracks to develop towards a single smooth one.

A negligible amount of extension was observed on the remaining crack front. Once an encompassing crack was established, it advanced nearly along the whole front. Only one specimen was tested containing two separated cracks. The non-coplanar crack tips were connected by a shear force into a planar crack front with a modest re-entrant portion. The initial spacing of these two cracks was very tiny, and the interaction was assured during the ductile failure. No other data implied the critical spacing for the onset of interaction during ductile tearing. Both the fatigue and ductile tearing tests exhibited the elevated crack driving force in the re-entrant sector of coalescing complex defects and the crack front advancement in a similar way towards the re-characterized convex shape, therefore the inherent conservatism in the re-characterization procedure of BS 7910: 1999 and R6/4: 2001 was confirmed.

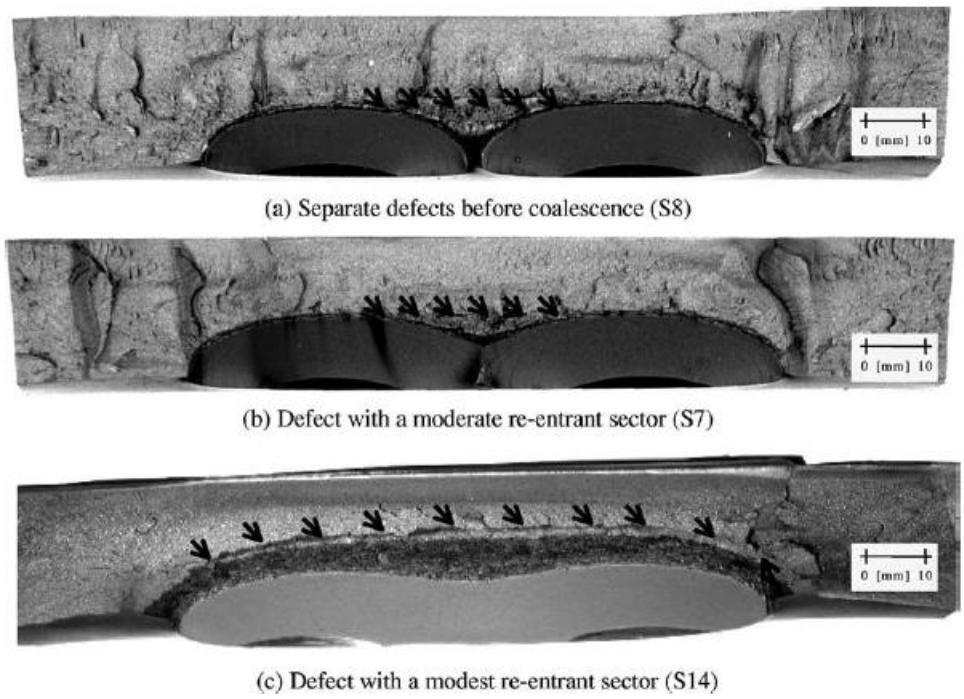

(a) Separate defects before coalescence (S8)

(b) Defect with a moderate re-entrant sector (S7)

(c) Defect with a modest re-entrant sector (S14)

Figure 38. Fracture Surfaces of Ductile Tearing

Another group of cleavage tests was pursued on the close separate cracks and the coalescing complex cracks with certain re-entrant sectors. On the lower shelf at -196 °C, for the complex cracks, the experimental failure loads were up to 23 percent lower than those estimated for the hypothetical bounding crack from the re-characterization. In contrast, in the brittle-ductile transition regime at -100 °C, the experimental failure loads were greater. In other words, the non-conservatism was discovered for the re-characterization on the lower shelf for the coalescing configurations. It was elucidated by the fact that the diverse failure behaviors between the lower shelf and the transition regime are owing to the constraint induced toughness difference. The enhanced toughness effect induced by the loss of constraint is more pronounced in the transition region than the lower shelf. On the lower shelf, localized crack

driving force from the re-entrant sector exceeds the constraint enhanced toughness; whereas on the transition region, it is vice versa.

Two separate cracks in close proximity, such as exemplified in Figure 39, were tested in the lower shelf regime at -196 °C, where the spacing between adjacent tips is equal to the crack depth. The Failure Assessment Diagram for this case was plotted in Figure 40 by two fracture toughness inputs: (a) standard test result; (b) standard test result with the constraint correction. The experimental failure load is only 3% higher than that derived from the re-characterized defect with standard test toughness in Figure 40 (a). However, taking into account of spatial variation of toughness along the crack front, the failure locus of the re-characterized defect is much further away from Failure Assessment Curve (FAC) in Figure 40 (b) than that of two cracks. Therefore, it was suggested by the authors that when the crack separation s is greater than the larger defect depth d, s>d, only a slight interaction is present and the assessment of individual defects is more realistic. As the cracks approach each other, for instance s<d, interaction becomes significant and should be included in the assessment.

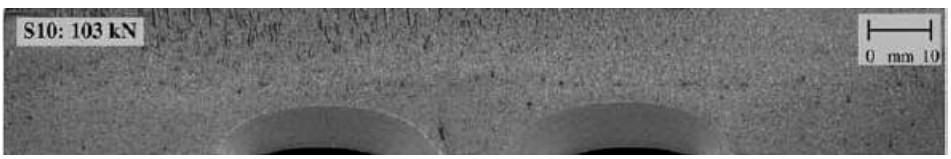

Figure 39. Two Interacting Cracks Failed in the Lower Shelf Regime at -196 °C

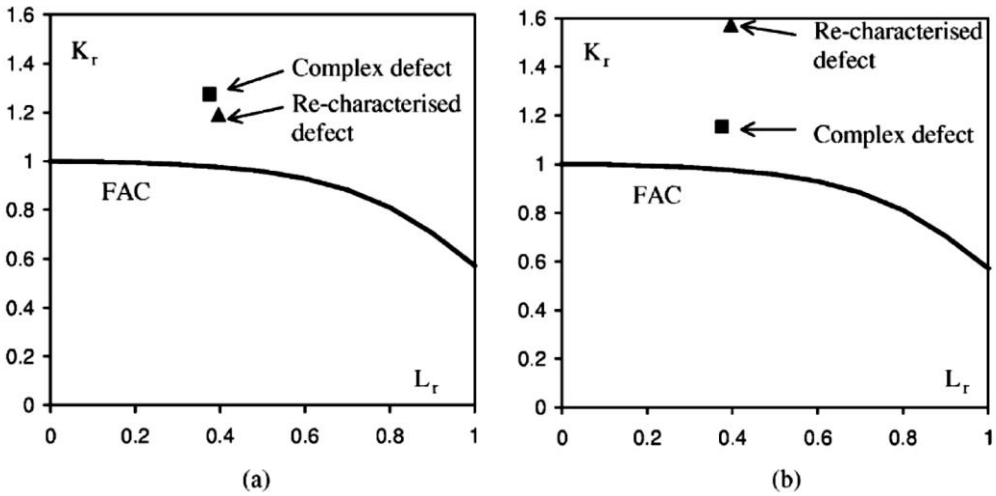

Figure 40. Specimen S10 and Its Corresponding Re-characterized Defect on FAD

Fatigue tests subjected to the pure bending were carried out for stress ratios of 0.2, 0.5, and 0.7 on a servohydraulic testing machine[37]. Crack growth rates were monitored by the direct current potential difference. The specimens were composed of two coplanar semi-elliptical cracks with an initial depth of 1 mm and initial separations of 4 mm, 8 mm, and 16 mm. A common beachmarked fracture surface was illustrated in Figure 41. The deviation of adjacent crack tips before the coalescence was clearly observed in Figure 42. It was pointed out that the adjacent tips generally grew past each other before the cracking occurred across the high stress intensified deviation region.

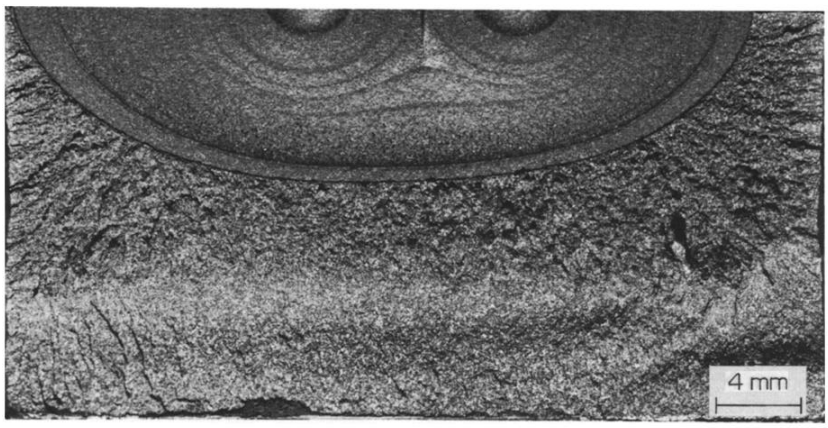

Figure 41. Beach Markings on a Fracture Surface

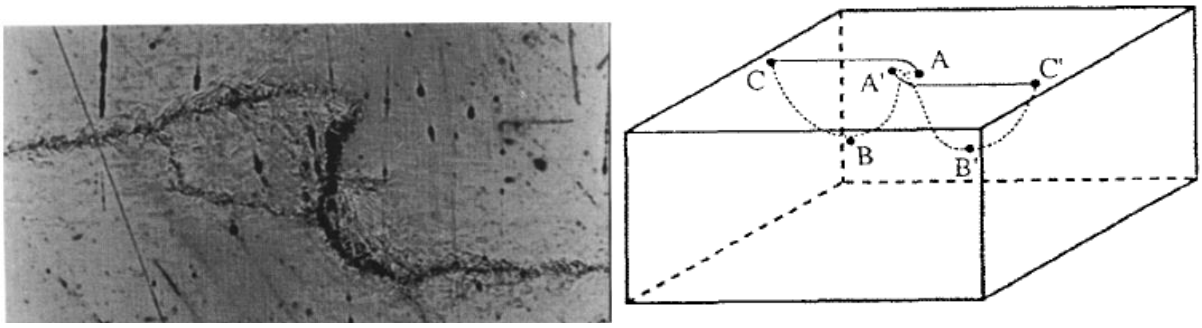

Figure 42. Deviation of Adjacent Crack Tips before Coalescence

According to the tests, the cracks grew almost independently until their adjacent tips came into contact. The linear FEA simulation on two identical coplanar cracks with aspect ratio a/c of 0.83 and 0.67 implied that the interaction occurs when the spacing is less than 12.5% of crack length with a stress intensity factor magnified by around 10%. Through the comparison between experiments and numerical studies, the investigation concluded that it is acceptable to

[37] Soboyejo, W.O., Knott, J.F., Walsh, M.J., and Cropper, K.R., "Fatigue Crack Propagation of Coplanar Semi-Elliptical Cracks in Pure Bending", Engineering Fracture Mechanics, 37 (1990) 323-340.

treat two cracks separately before contact. The encompassing procedure, e.g. spacing no greater than twice the maximum depth in ASME Section XI: 1980, is overly conservative.

Eighteen fatigue tests on surface cracked plane plates under either pure bending or pure tensile cyclic loads were examined[38]. As described in Figure 43 and Table 7, $a_{1,2}$, $c_{1,2}$ are the depth and the half length of two semi-elliptical cracks, s is the distance between adjacent crack tips projected to the plane normal to the principal stress, and d is the offset distance between crack planes.

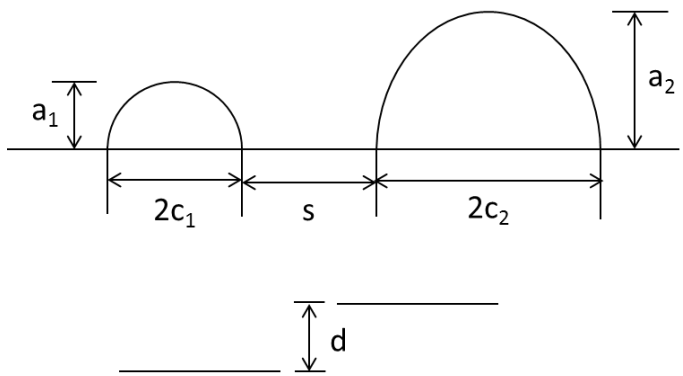

Figure 43. Configuration and Dimension of Two Cracks

[38] Leek, T.H. and Howard, I.C., "An Examination of Methods of Assessing Interacting Surface Cracks by Comparison with Experimental Data", International Journal of Pressure Vessels and Piping, 68 (1996) 181-201.

Table 7. Matrix of Initial Crack Geometries with Units in mm

Test no.	a1	c1	a2	c2	s	d
T1MS*	10.0	17.13	-	-	-	-
B1MS*	9.5	17.52	-	-	-	-
B2MS*	7.5	11.53	-	-	-	-
T2MS	7.2	15.28	8.5	14.73	10.0	-0.23
T3MS	11.0	16.63	8.2	15.43	8.0	12.91
T4A508	9.3	14.8	9.7	14.73	10.9	4.84
T5A508	8.8	14.51	8.9	14.74	9.18	0.01
T6A508	9.5	14.68	9.7	15.02	9.06	9.71
T7A508	9.4	14.64	9.2	14.73	9.3	17.93
B3A508	8.3	15.33	8.5	14.96	9.5	12.4
B4A508	8.3	15.05	8.2	14.98	21.6	11.89
B5A508	5.6	10.65	9.7	16.55	8.7	12.13
B6A508	9.4	14.1	9.4	13.93	3.4	11.94
B7A508	6.6	10.65	7.2	11.25	17.65	6.35
B8A508	9.3	16.15	5.6	10.43	9.2	2.87
B9A508	5.1	10.3	5.1	10.53	18.75	20.14
B10A508	6.0	10.5	5.5	10.81	18.5	-0.03
B11A508	5.5	10.35	5.6	10.45	10.85	5.9

* denotes a single crack test.

The specimens included patterns of one single crack (T1MS*, B1MS*, B2MS*), coplanar cracks (T2MS, T5A508, B10A508), and non-coplanar cracks (T3MS, T4A508, T6-7A508, B3-9A508, B11A508). The single crack tests were intended to justify the validity of system arrangement, and material properties utilized to determine the Paris law constants. Among these eighteen experiments, there were three tests (T3MS, B5A508, B8A508) related to two cracks initially having distinct sizes. So the conclusion drawn here to some extent may be suitable to demonstrate the interaction of cracks with dissimilar sizes, nevertheless it is not appropriate to warrant the universal safety for other aspect ratios of crack shapes.

The growth profiles of coplanar cracks were quite analogous to those aforementioned. Through the comparison of growth rates between experiments and those predicted from diverse interaction rules, it appeared that even though it may not be safe, neglecting the interaction between coplanar cracks can give a realistic approximation for crack growth. The safety can be improved by taking into account the slight magnification of crack driving force when two cracks approach very closely. The interacting criteria, such as twice the maximum crack depth in ASME: 1992 code or the minimum crack length in BSI PD6493: 1991 are overly conservative.

For two parallel cracks in different planes, prior to overlapping, cracks grew straight in their initial planes. Once overlapped, the crack faces rapidly curved towards each other, and a piece of material was isolated between them similar to Figure 42. This material region usually had a

flattened cone shape with its edges at the position where two cracks met. For non-coplanar cracks with an offset distance d, the combination rule of 1 inch in ASME: 1992 code or average of crack depths in BSI PD6493: 1991 was only adequate for a small d under pure bending. New criteria were proposed to judge whether the cracks should be assumed to be coplanar[39, 40]. The cracks are independent if:

When $a/t > 0.8 : d > 0.5\bar{c}$

When $0.5 \le a/t \le 0.8 : d > 1.61\bar{c}$, or $d > 7.72\bar{a}$, or $d^2 > 5.95\bar{a}\bar{c}$

When $a/t \le 0.5 : d > 1.41\bar{c}$, or $d > 2.49\bar{a}$, or $d^2 > 1.63\bar{a}\bar{c}$.

Here a is the depth of each crack and t is the wall thickness. For a/t greater than 0.8, the condition was derived from the through-wall cracks. The conditions were built upon the interaction factor less than 1.05, which was defined as mode I crack stress intensity factor with the influence of interaction normalized by that for an isolated crack. Otherwise the cracks are deemed to be coplanar. These conditions are valid when $0.1 \le a/c \le 2.0$ under tension, bending, or combined tension and bending. $\bar{a}$ and $\bar{c}$ are the average depth and average semi-length of two cracks.

Fatigue crack growth tests subjected to cyclic tensile loads were conducted on stainless steel plate specimens with surface notches[41]. A good correlation between the crack driving force and the area change was exposed for both discrete and interacting cracks. When the magnitude of interaction is sufficiently large, the crack driving force can be predicted precisely by replacing two pre-existing cracks with a semi-elliptical crack of the same area on the projected plane.

[39] Leek, T. H. and Howard, I. C., Rules for the assessment of interacting surface cracks under mode I loading, Int. J. Pres. Ves. and Piping, 60 (1994) 323-339.
[40] Leek, T. H., The interaction and growth of two surface cracks under fatigue loading, Ph.D. Thesis, (1990) University of Sheffield, UK.
[41] Kamaya, M., "Growth Evaluation of Multiple Interacting Surface Cracks Part I: Experiments and Simulation of Coalesced Crack", Engineering Fracture Mechanics, 75 (2008) 1336-1349.

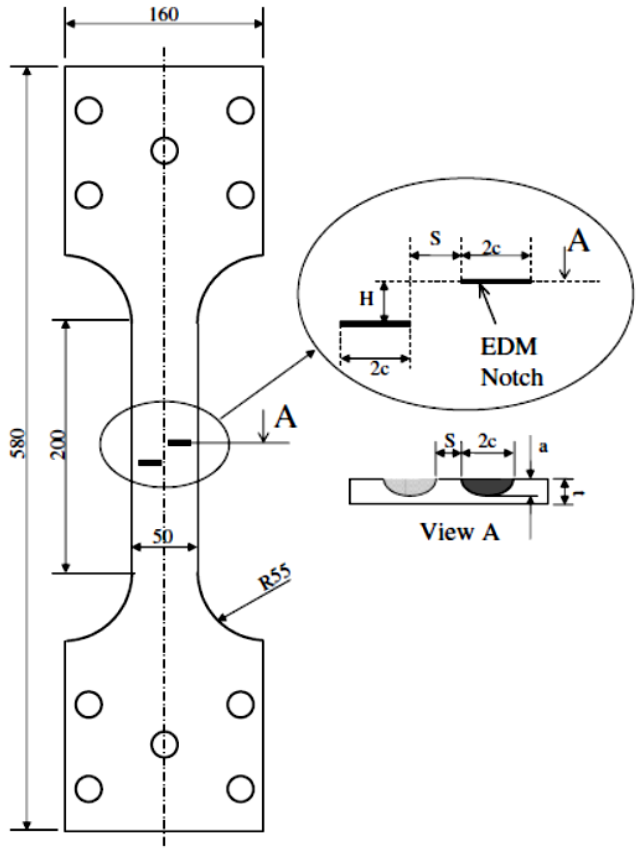

Figure 44. Geometry of Notched Specimen

The plate specimen is sketched in Figure 44, where the relative crack position is denoted by an in-plane distance S and an offset distance H. The test matrix is tabulated in Table 8. Three representative groups of fatigue growth and eventual fracture configuration are incorporated: non-coplanar cracks without initial horizontal overlapping (S>0, H>0), non-coplanar cracks having initial adjacent tips touched in the projected plane (S=0, H>0), and coplanar cracks (S>0, H=0), corresponding to Figure 45, Figure 46, and Figure 47 respectively.

Table 8. Fatigue Test Matrix under Cyclic Tensile Loads

Specimen	Number of notches	Relative position (mm)		Initial notch size (mm)		Number of beachmarks	Plate thickness (mm)	Stress range (Mpa)
		H	S	c	a			
A-Single	1			2.5	2.5	4	10	180
A-H0S5	2	0	5	2.5	2.5	5	10	180
A-H2.5S2.5	2	2.5	2.5	2.5	2.5	3	10	180
A-H2.5	2	2.5	0	2.5	2.5	3	10	180
A-H2.5C2A4	2	2.5	0	2	4	4	10	180
A-H2.5C4A2	2	2.5	0	4	2	3	10	180
B-Single	1			5	5	5	15	120
B-H0S5	2	0	5	5	5	5	15	120
B-H2.5(1)	2	2.5	0	5	5	6	15	120
B-H2.5(2)	2	2.5	0	5	5	5	15	120
B-H5	2	5	0	5	5	8	15	120
B-H10	2	10	0	5	5	8	15	120

For two non-coplanar cracks (S>0, H>0), as they approached close to each other, the inner crack tips curved and the outer crack tips kept almost straight. The rupture happened before the coalescence, e.g. Figure 45. It was mentioned that the interaction becomes important when the offset distance H is less than 0.8a[42]. Based on this criterion, all the non-coplanar cracks in this study started tangible interaction after the first beachmark.

In the fracture surface in Figure 46 for two cases (S=0, H>0), only one crack maintained a continuous profile. The distortion and deviation of crack shape from a semi-ellipse caused by the out-of-plane interaction is apparent. The crack growth arrest of the overlapped region due to the shielding effect is discernible, which is more severe in H=5 mm than in H=10 mm. Another study shows that the shielding effect is stronger when two initial crack sizes are dissimilar[43]. The smaller crack stops growing when the size difference of interacting cracks is large enough. After the smaller crack stops growing, the interaction effect on the fatigue life of the larger crack becomes minor. Figure 48 clarifies the arrest criteria to be: (1) two cracks fully overlap; and (2) at two closer crack tips, the stress intensity factor of the larger crack is greater than that of the smaller crack.

[42] Kamaya, M., "Flaw Proximity Rules for Parallel Surface Cracks Based on Elastic, Elastic–Plastic Fracture Mechanics and Limit Load Analyses", PVP2006-ICPVT11-93341, 2006.
[43] Kamaya, M., Miyokawa, E., and Kikuchi, M., "Growth Prediction of Two Interacting Surface of Dissimilar Sizes", Engineering Fracture Mechanics, 77 (2010) 3120-3131.

For coplanar cracks (S>0, H=0), the cracks progressed straight on the surface before coalescence. The beachmark interval before the crack tips touched was nearly uniform along the whole crack fronts, which implied the negligible interaction influence on the growth.

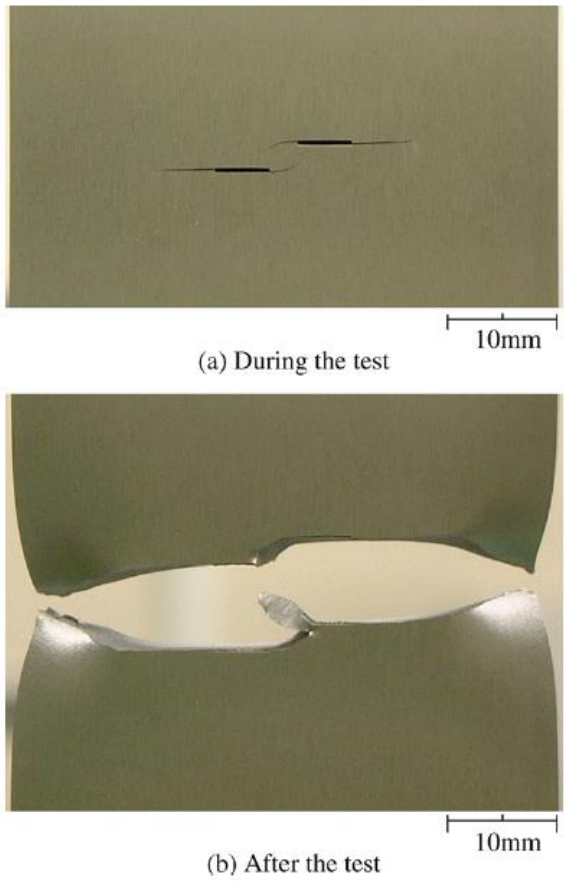

Figure 45. Two Cracks with S=2.5 mm and H=2.5 mm Fractured Before Coalescence

(a) B-H5 (initial condition: $S = 0$mm, $H = 5$mm)

(b) B-H10 (initial condition: $S = 0$mm, $H = 10$mm)

Figure 46. Fracture Surfaces for Two cracks with S=0 mm and H=5 mm and 10 mm

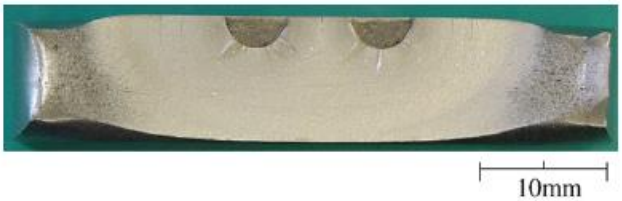

(a) A-H0S5 (initial condition: $S = 5$mm, $H = 0$mm)

(b) B-H0S5 (initial condition: $S = 5$mm, $H = 0$mm)

Figure 47. Fracture Surfaces for Two Coplanar Cracks with S=5 mm

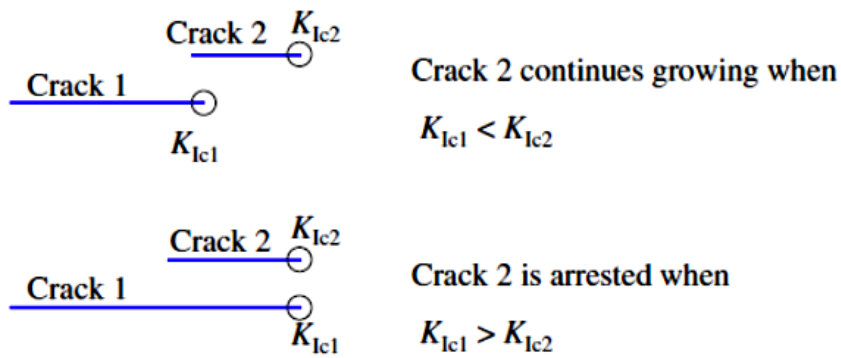

Figure 48. Criteria to Judge Smaller Crack Arrest

Three dimensional linear elastic and elastic-plastic finite element analyses were used to study the geometric variables affecting the crack interaction under tension, e.g. the relative distance between two cracks and the crack aspect ratios[44]. The elastic and elastic-plastic J-integral values along the crack fronts were examined. Simulations were done for two cracks in the same plane perpendicular to the loading direction. The depths were fixed to be 50% of the wall thickness for one crack and 30% of the wall thickness for another crack. The aspect ratios of two cracks were kept equal and chosen to be c/a= 0.5, 1, and 3, which was defined as the half crack length divided by the crack depth.

The separation varied between 20% of the wall thickness and twice the wall thickness. The results show that the interaction between two cracks with aspect ratio of 3 and with aspect ratio of 1 follow the similar trend. For the larger and deeper crack, the stress intensity factor along the crack front is only elevated by interaction within 60° away from the inner crack tip, and the value at the deepest point is not affected at all. However, for the smaller and shallower crack, the stress intensity factor along the whole crack front is intensified. When the aspect ratio reduces to be as small as 0.5, the interaction is much less substantial than the above two cases. The elastic-plastic analysis was performed with the applied nominal stress equal to yield stress. The material behavior was assumed to follow the Ramberg-Osgood relationship. The overall tendency of J-integral is identical to that of the linear elastic analysis regardless of aspect ratios. These observations drew the remarks that BS7910: 2005 seems to provide a relevant crack combination rule for two coplanar surface cracks, if the interaction condition is set to be 10% relative increase of crack driving force.

The linear-elastic fracture, elastic-plastic fracture, and limit load analyses were systematically conducted for two identical interacting surface cracks by finite element method under a tensile

[44] Kim, Jong-Min and Huh, Nam-Su, "On Crack Interaction Effects of In-Plane Surface Cracks Using Elastic and Elastic-Plastic Finite Element Analyses", Nuclear Engineering and Technology, Vol. 42, No. 6 (2010), 680-689.

and bending load[45]. The effects on interaction from the crack relative position and the crack aspect ratios were studied, particularly the offset distance between two parallel crack planes.

The shielding effect only occurs near the inner crack tip region for two cracks with projected overlapping, and the stress relaxation becomes more prominent as the offset distance decreases. The stress intensification occurs in the other region of crack front for overlapped cracks and the entire crack front for non-overlapped cracks. For non-coplanar cracks, the relative stress intensity factor increase due to the interaction is bounded by 15% for two cracks even getting contacted in the projected plane; for coplanar cracks, the relative increase is bounded by 7% for in-plane distance greater than half of crack depth.

The J-integrals were obtained for interacting cracks under multiple loading magnitudes. The dependence on the crack relative position is quite similar to the stress intensity factor, whereas greater loading amplitude gives rise to stronger interaction. The sharp change of J-integral by varying loads takes place at nominal stress equal to 70% of yield stress. For coplanar cracks, the relative increase of J-integral is bounded by 10% for in-plane distance larger than half of crack depth.

Assuming that the condition of interaction incipience is defined as 7% increase of stress intensity factor and 10% increase of J-integral, for any in-plane distance the threshold offset distance is 80% and 70% of crack depth. Limit load for ductile collapse is dominated by the projected equivalent area of two cracks. Thereby the maximum limit load occurs when two cracks fully overlap. The critical offset distance is determined to be 1.8 times crack depth to guarantee the relative limit load decrease within 10% when the in-plane distance is equal to half the crack depth. In summary,

$S \leq 0.5a$ for stress intensity factor, J-integral and plastic collapse,
$H \leq 0.8a$ for stress intensity factor, $\leq 0.7a$ for J-integral, $\leq 1.8a$ for plastic collapse.

A sensitivity study was done by linear finite element analyses for two identical parallel surface cracks under tension and bending loads[46]. The in-plane distance S/c and the offset distance H/2c were extended from -2 to 2 and from 0.3 to 1 respectively. The crack depth a/t and aspect ratio a/c are kept constants as 0.2 and 0.3. The interaction factor ɣ was defined as the ratio of stress intensity factor with interaction to that without interaction. At the end ɣ was condensed into a simple least-squares-fit function in terms of S/c and H/2c with less than 2.5% deviation from the FEA values.

---

[45] Kamaya, M., "Flaw Proximity Rules for Parallel Surface Cracks Based on Elastic, Elastic-Plastic Fracture Mechanics and Limit Load Analyses", Proceedings of PVP2006-ICPVT-11, 2006 ASME Pressure Vessels and Piping Division Conference, July 23-27, 2006.
[46] Moussa, W.A., Bell, R., and Tan, C.L., "The Interaction of Two Parallel Non-coplanar Identical Surface Cracks under Tension and Bending", International Journal of Pressure Vessels and Piping, 76 (1999) 135-145.

$$\gamma = \sum_{n=0}^{2}\sum_{m=0}^{2} A_{nm}\left(\frac{S}{c}\right)^{n}\left(\frac{H}{2c}\right)^{m}$$

The coefficients A_{nm} are enclosed in Table 9. The maximum ɣ value along the crack front may not be at the position of the highest stress intensity factor. When H/2c is decreasing, the shielding effect magnifies for the overlapping situations S/c<0. For all cases, the interaction effect diminishes as the value of S/c approach 2. Nevertheless, if treating two cracks as a bounding crack when S/c is close to 2, it is excessively conservative.

Table 9. A_{nm} Fitted Values for the Interaction Factor ɣ

A_{nm}	Tension ϕ = 180°	Tension ϕ = 90°	Tension ϕ = 0°	Bending ϕ = 180°	Bending ϕ = 90°	Bending ϕ = 0°
A_{00}	1.056	1.214	1.100	1.023	1.269	1.095
A_{01}	0.272	-0.148	-0.003	0.350	-0.160	-0.022
A_{02}	-0.181	0.075	-0.006	-0.224	0.070	0.006
A_{10}	0.433	-0.083	-0.084	0.407	-0.116	-0.066
A_{11}	-0.749	0.006	0.118	-0.679	0.066	0.075
A_{12}	0.451	-0.004	-0.061	0.404	-0.056	-0.035
A_{20}	-0.365	-0.174	-0.032	-0.317	-0.193	-0.052
A_{21}	0.194	0.194	-0.102	0.080	0.179	-0.035
A_{22}	-0.102	-0.105	0.054	-0.041	-0.072	0.014
A_{30}	-0.094	0.040	0.037	-0.091	0.056	0.030
A_{31}	0.170	-0.022	-0.054	0.159	-0.060	-0.038
A_{32}	-0.105	0.008	0.027	-0.097	0.037	0.018
A_{40}	0.083	0.023	-0.005	0.073	0.020	0.002
A_{41}	-0.057	-0.032	0.038	-0.034	-0.016	0.019
A_{42}	0.033	0.020	-0.019	0.020	0.004	-0.008

Similarly, the interaction factor ɣ was resolved for a wide range of crack geometric dimensions and relative position configurations[47]. Two cracks under consideration are self-similar and coplanar subjected to remote tension. The shape aspect ratio (0.3≤a/c≤1.2), depth (1.25≤t/a≤6), in-plane distance (0.33≤2c/d≤0.9), and location on the crack front (0≤2φ/π≤2) were meant for deriving an empirical expression for ɣ. Here d refers to the center-to-center distance between two cracks d=S+2c, and φ starts from zero at the inner crack tip position.

The equation of ɣ at the surface and deepest points is

$$\gamma = C_1 + C_2\left(\frac{t}{a}\right)^{C_9} + C_3\left(\frac{a}{c}\right)^{C_{10}} + C_4\left(\frac{2c}{d}\right)^{C_{11}} + C_5\left(\frac{t}{a}\right)^{C_{12}}\left(\frac{a}{c}\right)^{C_{13}} + C_6\left(\frac{a}{c}\right)^{C_{14}}\left(\frac{2c}{d}\right)^{C_{15}} + C_7\left(\frac{2c}{d}\right)^{C_{16}}\left(\frac{t}{a}\right)^{C_{17}} + C_8\left(\frac{t}{a}\right)^{C_{18}}\left(\frac{a}{c}\right)^{C_{19}}\left(\frac{2c}{d}\right)^{C_{20}},$$

in which constants are given in Table 10. The deviations from the FEA results are within ±2%.

[47] Sethuraman, R., Reddy, G.S.S., and Ilango, I.T., "Finite Element Based Evaluation of Stress Intensity Factors for Interactive Semi-Elliptic Surface Cracks", International Journal of Pressure Vessels and Piping, 80 (2003), 843-859.

The equation of γ throughout the entire crack front is estimated by

$$\gamma = C_1 + C_2\left(\frac{t}{a}\right)^{C_3}\left(\frac{a}{c}\right)^{C_4}\left(\frac{2c}{d}\right)^{C_5}\left(\frac{2\phi}{\pi}\right)^{C_6},$$

where C_1=1.009163, C_2=0.211629, C_3=-0.813784, C_4=0.102877, C_5=3.647398, and C_6=-0.464392. It gives values within ±5% deviation from FEA for 4≥t/a>2, and ±9.5% for 2≥t/a≥1.25. It was noticed that for all the considered ranges of a/c and 2c/d, when t/a increases, the interaction factor decreases at the inner and outer crack tips but remains the same at the deepest point.

Table 10. C_n Fitted Values for the Interaction Factor γ

Constants	2ϕ/π = 0 (max. dev. = 2.02%)	2ϕ/π = 1 (max. dev. = 0.58%)	2ϕ/π = 2 (max. dev. = 1.09%)
C_1	1.005	0.009	-0.002
C_2	0.052	0.467	1.039
C_3	-0.006	4.099	5.111
C_4	4.048	0.573	10.534
C_5	-0.019	-3.242	-5.140
C_6	76.736	-20.187	9.732
C_7	-128.376	-2.851	-12.478
C_8	48.763	22.204	-7.602
C_9	-1.334	0.667	-0.239
C_{10}	-0.907	0.198	-0.018
C_{11}	8.996	1.301	2.339
C_{12}	-7.168	0.319	-0.039
C_{13}	5.169	0.067	-0.019
C_{14}	-0.015	0.132	0.091
C_{15}	6.367	0.101	1.992
C_{16}	6.566	0.454	2.278
C_{17}	0.052	0.145	0.004
C_{18}	0.125	0.054	0.004
C_{19}	0.024	0.092	0.115
C_{20}	6.735	0.127	2.001

Stress corrosion cracking is a particular example of interacting cracks. UTCD in-line inspection generally matches well with the overall crack colony layout and reports the maximum depth for cracks within the colony. For crack fields, field length, width, longest indication, and maximum depth are usually reported. The recent development keeps evolving on the individual crack detection and its depth profile sizing which are hindered by the signal noise interference. Burst tests and in-the-ditch NDT are conducted to assist and validate the signal filtering analysis. These efforts help mitigate the excessive conservatism for non-interacting cracks to be treated

as a whole and allow operators to reduce the unnecessary digs and repairs. Three samples of X65 line pipes were burst tested that had a range of crack colonies with various crack alignments and densities[48]. The fracture surfaces were measured for accurate crack mapping. The ILI results were refined and optimized through signal filtering by comparing the crack maps to match the individual cracks. The mapping information was applied to calculate failure pressure by several assessment methods under diverse interaction rules, and was compared to the actual experiment results. The API 579 Level II and CorLAS® assessment methods were used with crack interaction rules from the API 579, CEPA, 2005 BS 7910, and Leis & Mohan[49]. The CEPA interaction rule gave the most accurate prediction.

Some analytical investigations were carried out related to embedded cracks. The hybrid boundary element method was utilized to explore the interaction. A total of 42 crack configurations were analyzed for two embedded cracks in a finite thickness plate under a uniform tension[50]. Two types of interactions were considered individually: Type 1 in Figure 49 refers to the long principal axes of two cracks in the alignment; Type 2 in Figure 50 refers to the short principal axes of two cracks in the alignment. The geometry ratio b_1/a_1 and b_2/a_2 are either 0.25 or 1.0, and the distance between two cracks s_1/b_{min} and s_2/b_{min} ranges from 0.5 to 2.0. If defining the interaction factor $\overline{M}_{1\max}$ as the ratio of the maximum value of stress intensity factor along two crack fronts to that for a single crack. The results are exhibited in Figure 51 and Figure 52. For Type 1, two equal circular cracks have the strongest interactions and the $\overline{M}_{1\max}$ values are 1.085, 1.038, and 1.012 for s_1/b_{min}=0.5, 1.0, and 2.0 respectively. For Type 2, the strongest interaction occurs for two cracks of b_1/a_1=1.0, b_2/a_2=0.25, and a_2/a_1=1.0. The corresponding $\overline{M}_{1\max}$ values are 1.157, 1.089, and 1.017 for s_2/b_{min}=0.5, 1.0, and 2.0 respectively. When s_1/b_{min} and s_2/b_{min} are the same, Type 2 interaction is stronger than Type 1. Assuming the interaction criteria is 15% increase of that for an isolated crack, the critical separation between two embedded cracks is around b_{min}, half of crack depth. This criterion is similar to the BS 7910:2013 for Type 1 condition, whereas more amenable than the BS 7910:2013 for Type 2 condition.

[48] Kariyawasam, S., Arumugam, U., Callar, G., Clarke, C., Hugger, A., Senf, P., and Law, M., "Stress Corrosion Crack Detection, Analysis, and Assessment Improvements for Effective Integrity Management", 16th Biennial Pipeline Research Joint Technical Meeting of APIA EPRG and PRCI, March, 2007.
[49] Leis, B. N. and Mohan, R., "Failure Criteria for Semicircular Flaws", Eight Symposium on Line Pipe Research, Houston, 1993.
[50] Chai, Guozhong, Zhang, Kangda, and Wu, Dongdi,"Interactions of Two Coplanar Elliptical Cracks Embedded in Finite Thickness Plates under Uniform Tension", Engineering Fracture Mechanics, Vol. 53, No. 2, 179-191, 1996.

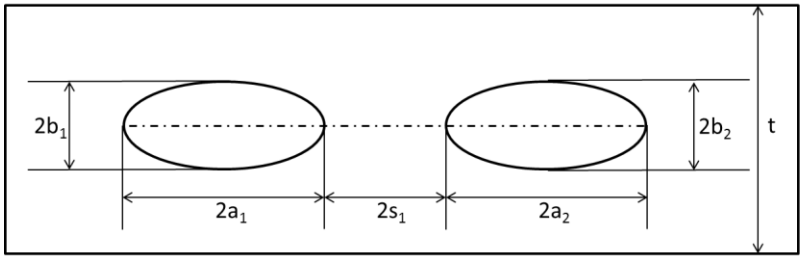

Figure 49. Type 1 Configuration between Two Coplanar Embedded Cracks

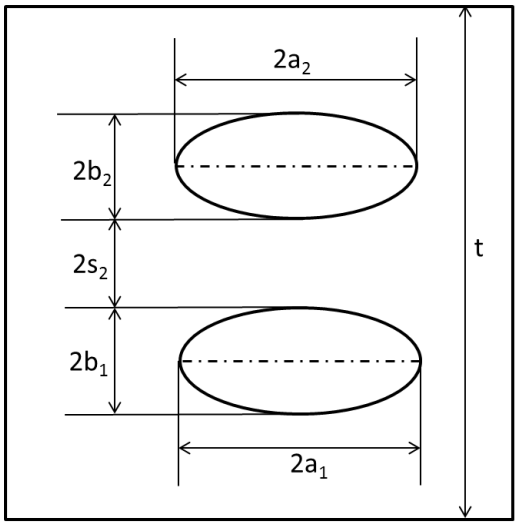

Figure 50. Type 2 Configuration between Two Coplanar Embedded Cracks

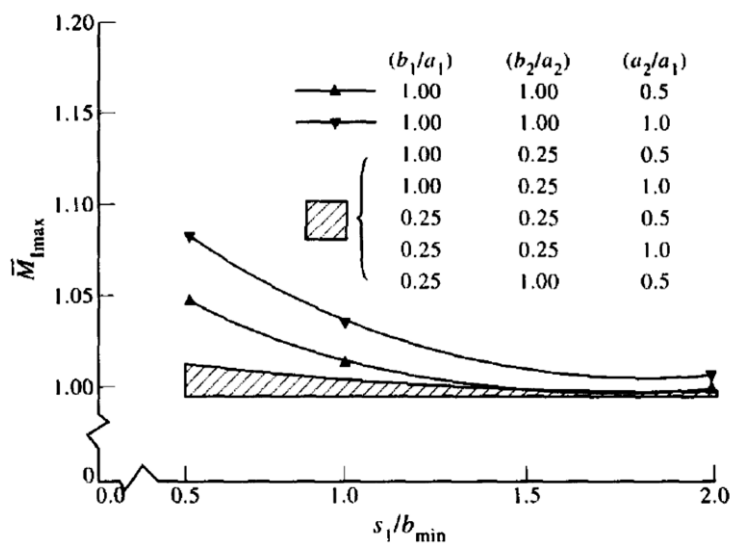

Figure 51. Interaction Factor of Type 1 Configuration

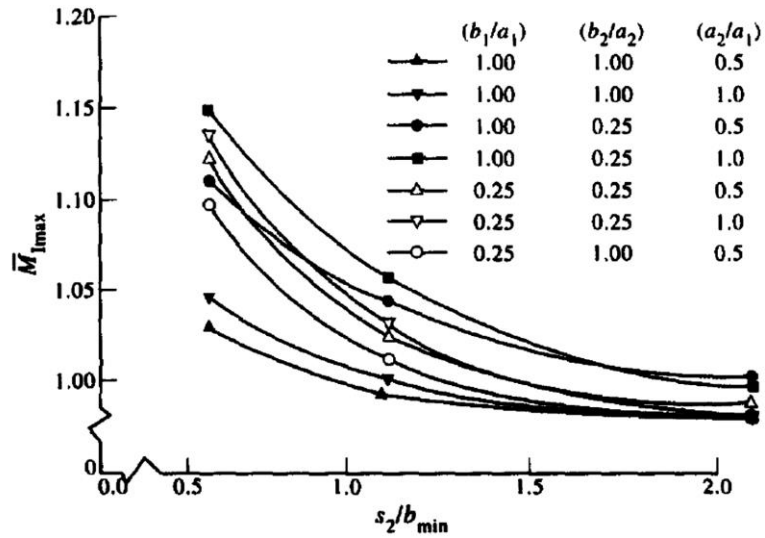

Figure 52. Interaction Factor of Type 2 Configuration

Similar research was produced for one embedded crack with one surface crack in the same plane. A total of 54 cases in a pressurized cylinder were analyzed for the crack arrangement in Figure 53, where the depth-to-length ratio equal to 0.25, 0.5 and 1.0[51]. The distance varies from 0.5 to 2.0 relative to the minimum value of half depth of the embedded crack and whole depth of the surface crack. Compared with the single surface crack and single embedded crack, the interaction increases the stress intensity factors along both crack fronts. With decreasing the separation, the intensification effect is magnified. The critical distance of interaction is at most $2b_{min}$.

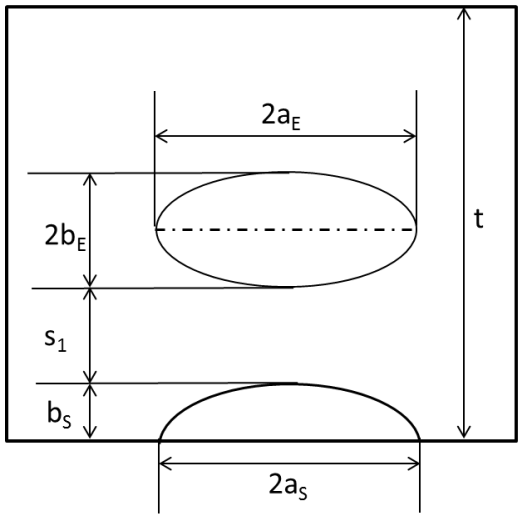

Figure 53. One Embedded Crack with One Surface Crack in a Pressurized Cylinder

[51] Chai, Guozhong and Zhang, Kangda, "Stress Intensity Factors for Interaction of Surface Crack and Embedded Crack in a Cylindrical Pressure Vessel", International Journal of Pressure Vessels and Piping, 77 (2000) 539-548.

Another numerical research was conducted for a non-coplanar embedded crack under a weld toe and surface crack[52]. In Figure 54, both crack depths $a_{P,Q}$ were fixed to be 0.2t and the shape aspect ratio $a_{P,Q}/c_{P,Q}$ varies from 1.0 to 0.33. The offset distance $h/2c_Q$ is kept as 0.3. The results provided an empirical function to estimate the interaction factor $\beta_{P,Q}$ relative to an isolated embedded or surface crack.

$$\beta_{P,Q} = \sum_{n=0}^{1}\sum_{m=0}^{2} A_{nm}\left(\frac{a_{Q,P}}{c_{Q,P}}\right)^n\left(\frac{s}{c_Q}\right)^m ,$$

where the values of A_{nm} are listed in Table 11. The value $\beta_{P,Q}$ is bounded by 20% at the surface point when s/c_Q=2.0.

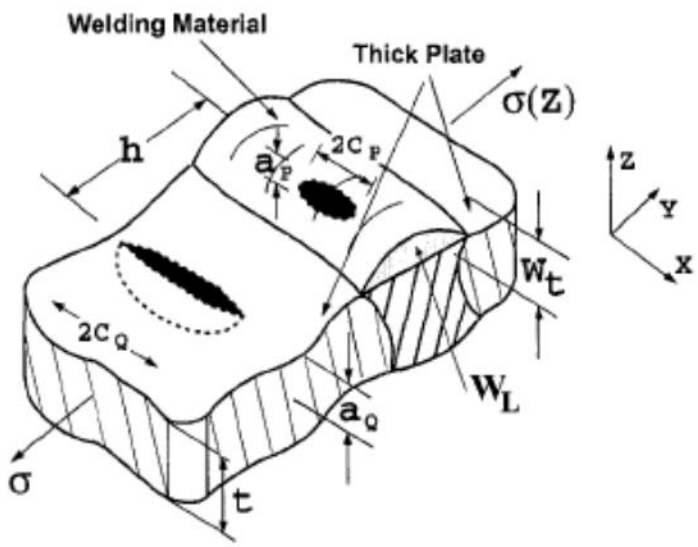

Figure 54. Schematic of Non-Coplanar Embedded Crack with Surface Crack

[52] Moussa, W.A., "On the Interaction of Non-Coplanar Embedded Crack with Surface Crack in 3D Using FE and Multi-Level Sub-Structure", Proceedings of PVP 2002, 2002 ASME Pressure Vessels and Piping Conference, August 5-9 2002, Vancouver, BC, Canada.

Table 11. Coefficients of A_{nm} to Calculate Interaction Factor $\beta_{P,Q}$

$A_{n,m}$	$\phi_Q = 180^\circ$	$\phi_Q = 90^\circ$	$\phi_Q = 0^\circ$
$A_{0,0}$	0.48710	1.36659	0.52303
$A_{0,1}$	1.20667	-0.00641	0.80374
$A_{0,2}$	-0.20310	-0.16179	0.70072
$A_{0,3}$	-0.05250	0.08572	-0.54071
$A_{1,0}$	0.14009	-0.06848	-0.03427
$A_{1,1}$	0.10921	-0.08869	0.07378
$A_{1,2}$	0.17058	0.06706	-0.34561
$A_{1,3}$	-0.09289	-0.01924	0.22070
$A_{2,0}$	-0.05602	-0.12511	-0.01133
$A_{2,1}$	-0.71887	-0.10328	0.05418
$A_{2,2}$	0.46852	0.14399	-0.66595
$A_{2,3}$	-0.16060	-0.07004	0.41064
$A_{3,0}$	-0.03151	0.02145	0.00855
$A_{3,1}$	-0.03011	0.07818	-0.00596
$A_{3,2}$	0.01791	-0.08591	0.13309
$A_{3,3}$	-0.01670	0.03307	-0.08869
$A_{4,0}$	0.01627	0.02032	0.00382
$A_{4,1}$	0.14531	-0.01303	-0.03251
$A_{4,2}$	-0.11267	0.01279	0.12691
$A_{4,3}$	0.04419	-0.00330	-0.07369

$A_{n,m}$	$\phi_P = 0^\circ$	$\phi_P = 90^\circ$	$\phi_P = 180^\circ$
$A_{0,0}$	0.44981	1.40626	0.47996
$A_{0,1}$	0.98467	-0.24467	0.63110
$A_{0,2}$	-0.17020	0.09609	0.62348
$A_{0,3}$	0.00390	0.01981	-0.42412
$A_{1,0}$	0.12956	-0.06750	-0.03040
$A_{1,1}$	0.08174	-0.07235	0.07301
$A_{1,2}$	0.14060	0.03754	-0.31545
$A_{1,3}$	-0.06377	-0.00661	0.19752
$A_{2,0}$	-0.05296	-0.12953	-0.00928
$A_{2,1}$	-0.62747	-0.08399	0.03497
$A_{2,2}$	0.44195	0.13109	-0.54789
$A_{2,3}$	-0.17352	-0.07110	0.33499
$A_{3,0}$	-0.02914	0.02207	0.00781
$A_{3,1}$	-0.02297	0.06937	-0.00775
$A_{3,2}$	0.01624	-0.07314	0.11854
$A_{3,3}$	-0.01741	0.02826	-0.07720
$A_{4,0}$	0.01512	0.02078	0.00316
$A_{4,1}$	0.12589	-0.01496	-0.02636
$A_{4,2}$	-0.10318	0.01409	0.10607
$A_{4,3}$	0.04432	-0.00323	-0.06124

Summary of Interaction Criteria for Cracks

Similar to the corrosion defects, the interaction criteria for cracks varied a lot. Table 12 and Table 13 summarize the findings within codes, standards, handbooks, and journal publications. Overall, for general cracks, the BS 7910: 2013 provides the most advanced interaction criterion built on relevant numerical and experimental efforts. It extends the fatigue-based conditions in the previous 1999 and 2005 versions to the consideration of cleavage, and is more consistent with the FITNET: 2006.

For two surface cracks, with the exception of Reference [39] and [40], the analytical and experimental work in the journal article review points to the crack depth a as the critical offset distance covering fatigue, brittle fracture and ductile tearing. For plastic collapse, only Reference [45] is available and results in 1.8a. Hence the magnitude of a_1+a_2 prescribed in the BS 7910:2013 provides the universal conservative condition taking account of all the failure mechanisms. For cracks with aspect ratio $a/c \leq 1$, the critical in-plane distance is bounded by max (a_1, a_2) in the experimental studies, and is recommended to be zero mostly for the reasonable crack growth prediction. However, the upper bound of the analytical studies is 2c for the arbitrary aspect ratio $a/c \leq 2$.

For two embedded cracks, the in-plane interacting distance along both depth and length directions is the half crack depth a. For an embedded crack with another surface crack, the in-plane distance along the length direction is the crack length 2c and along the depth direction is

the crack depth 2a. Since there have been only analytical investigations for embedded cracks, the validation of embedded crack interaction still needs experimental verification.

As a further step, Table 14 lists the comparison between the complete journal article findings and the BS 7910: 2013 regarding to the critical interacting distance. There is general consistency for two surface cracks. Discrepancy exists in two circumstances: (1) in-plane distance along the length direction for one embedded crack with one surface crack; (2) in-plane distance along depth direction for two embedded cracks. Additionally, for Case (2) the BS 7910: 2013 still stands on the conservative side. In the journal articles reviewed, no information is available about the offset distance related to the embedded cracks. However, for two embedded cracks or one embedded crack with another surface crack, under the same amount of the offset distance, the interaction perpendicular to the crack plane should be weaker than two surface cracks. Hence it is plausible to assume the offset threshold of two surface cracks serving as that associated with embedded cracks, which is stated as the same as the BS 7910: 2013. Similar logic applies to the in-plane distance along the length direction for one embedded crack with one surface crack. In a word, the BS 7910: 2013 provides an optimal guidance of crack interaction determination.

Table 12. Crack Interaction Criteria Listed in Various Codes, Standards, and Handbooks

Code, Standard or Handbook	Offset Distance	Two Surface Cracks	One Embedded Crack with One Surface Crack or Two Embedded Cracks	
		In-plane Distance	In-plane Distance along Length	In-plane Distance along Depth
API 579-1/ASME FFS-1:2007	c_1+c_2	c_1+c_2	c_1+c_2	a_1+a_2
BS 7910:2013	a_1+a_2	If a_1/c_1 or $a_2/c_2>1$, min($2c_1$, $2c_2$); otherwise, 0.5 max(a_1, a_2)	If a_1/c_1 or $a_2/c_2>1$, min($2c_1$, $2c_2$); otherwise, max(a_1, a_2)	a_1+a_2
CSA Z662:2011*		min($2c_1$, $2c_2$)	min($2c_1$, $2c_2$)	
API 1104:2013*	min($2a_1$, $2a_2$)	min($2c_1$, $2c_2$)	min($2c_1$, $2c_2$)	a_1+a_2
FITNET:2006	min($2a_1$, a_2) for one embedded crack with one surface crack; min($2a_1$, $2a_2$) for two embedded cracks	If a_1/c_1 or $a_2/c_2>1$, min($2c_1$, $2c_2$) or 0.5 max(a_1, a_2) ; otherwise, 0.5 max(a_1, a_2)	If a_1/c_1 or $a_2/c_2>1$, min($2c_1$, $2c_2$) or max(a_1, a_2); otherwise, max(a_1, a_2) for two embedded cracks	$a_1+a_2/2$ for one embedded crack with one surface crack; a_1+a_2 for two embedded cracks
PDAM:2003	If $2c_1<2c_2$, max(a_1, $2c_1$) for a surface crack or max($2a_1$, $2c_1$) for an embedded crack ; otherwise, max(a_2, $2c_2$) for a surface crack or max($2a_2$, $2c_2$) for an embedded crack	If $2c_1<2c_2$, max(a_1, $2c_1$); otherwise, max(a_2, $2c_2$)	If $2c_1<2c_2$, max(a_1, $2c_1$) for a surface crack or max($2a_1$, $2c_1$) for an embedded crack ; otherwise, max(a_2, $2c_2$) for a surface crack or max($2a_2$, $2c_2$) for an embedded crack	If $2c_1<2c_2$, max(a_1, $2c_1$) for a surface crack or max($2a_1$, $2c_1$) for an embedded crack ; otherwise, max(a_2, $2c_2$) for a surface crack or max($2a_2$, $2c_2$) for an embedded crack
CEPA SCC:2007	0.07 ($2c_1+2c_2$)	0.125 ($2c_1+2c_2$)		

Note: (1) *: is for girth welds only. (2) a stands for half depth for an embedded crack and whole depth for a surface crack; 2c stands for crack length regardless if it is a surface or embedded one.

Table 13. Crack Interaction Criteria Based on Experimental and Analytic Studies

Reference Numbers	Type of Study	Failure Mode	Critical Offset Distance Hc	Critical In-Plane Distance Sc	Aspect Ratio a/c	Crack Configuration
Two Surface Cracks						
34	Experimental	Fatigue		0.5 max(a_1, a_2)	<1	Coplanar
35	Experimental	Cleavage		max(a_1, a_2)	<1	Coplanar
37	Experimental	Fatigue		0	<1	Coplanar
37	Analytical	SIF		12.5% max($2c_1$, $2c_2$)	<1	Coplanar
38	Experimental	Fatigue		0	<1	Coplanar
38	Experimental	Fatigue	1" or 0.5(a_1+a_2)		<1	Non-Coplanar
39, 40	Analytical	SIF	a/t>0.8, 0.5c; 0.5≤a/t≤0.8, 1.61c or 7.72a or 5.95ac; a/t≤0.5, 1.41c or 2.49a or 1.63ac		≤2	Non-Coplanar
41	Experimental	Fatigue		0	1	Coplanar
41	Experimental	Fatigue	0.8a for in-plane distance>0; a for in-plane distance=0		1	Non-Coplanar
44	Analytical	SIF and J-integral		If a_1/c_1 or a_2/c_2>1, min($2c_1$, $2c_2$); otherwise, 0	≤2	Coplanar
45	Analytical	SIF, J-integral and Plastic Collapse	0.8a for SIF; 0.7a for J-integral; 1.8a for Plastic Collapse	0.5a	≤1	Coplanar and Non-Coplanar
46	Analytical	SIF		2c	<1	Coplanar and Non-Coplanar

Two Embedded Cracks or One Embedded Crack with One Surface Crack						
50	Analytical	SIF		a for two embedded cracks along both length and depth directions	≤1	Coplanar
51	Analytical	SIF		2a for one embedded crack and one surface crack along depth direction	≤1	Coplanar
52	Analytical	SIF	0.6c*	2c for one embedded crack and one surface crack along length direction	≤1	Non-Coplanar

Note: (1) SIF stands for elastic stress intensity factor. (2) a stands for half depth for an embedded crack and whole depth for a surface crack; 2c stands for crack length regardless it is a surface or embedded one. (3) *: means interaction is guaranteed, however 0.6c being the critical threshold value of the offset distance is not ensured.

Table 14. Comparison between Journal Articles and BS 7910:2013

Critical Separation for Interaction	Two Surface Cracks		One Embedded Crack with One Surface Crack		Two Embedded Cracks	
	Journal Article	BS 7910: 2013	Journal Article	BS 7910: 2013	Journal Article	BS 7910: 2013
Offset Distance	a or 1.8a	a_1+a_2	NA	a_1+a_2	NA	a_1+a_2
In-Plane Distance along Length Direction	2c for $a/c\leq 2$; a or 0 for $a/c\leq 1$	If a_1/c_1 or $a_2/c_2>1$, min($2c_1$, $2c_2$); otherwise, 0.5 max(a_1, a_2)	2c for $a/c\leq 1$	If a_1/c_1 or $a_2/c_2>1$, min($2c_1$, $2c_2$); otherwise, max(a_1, a_2)	a for $a/c\leq 1$	If a_1/c_1 or $a_2/c_2>1$, min($2c_1$, $2c_2$); otherwise, max(a_1, a_2)
In-Plane Distance along Depth Direction			2a for $a/c\leq 1$	a_1+a_2	a for $a/c\leq 1$	a_1+a_2

LITERATURE REVIEW OF CRACK WITHIN CORROSION

A numerical study was undertaken to investigate cracks residing in corrosion defects[53, 54]. Finite element simulation calculated the burst pressure for longitudinally oriented cracks within uniformly deep corrosion grooves in the same orientation. Three groups of analyses were performed. For infinitely long crack within infinitely long corrosion, the failure pressure fell between that of a pure crack and that of a pure corrosion having the same total defect depth of 60% of the wall thickness.

The transition to the corrosion behavior only occurred when the corrosion depth is greater than 75% of the total defect depth, whilst the crack is less than 25% deep of the whole defect. The finite length effect of a crack coincident with an infinitely long corrosion was also considered for the total depth of 40% of the wall thickness. Interestingly, the collapse pressure of the hybrid defect was found to be lower than a single crack with equivalent total depth. This reduction was attributed to the surrounding corrosion-caused stress increase. When the length of corrosion decreased and approached the length of crack, the failure pressure increased towards the crack-only value.

Furthermore, the NG-18 and BS7910 Level-2A FAD assessments were attempted to solve the failure pressure for crack-in-corrosion defects. Both approaches treated the hybrid defect to be a hypothetical flaw with the same maximum size. By comparing with the finite element calculation, neither approach was recommended, as tangible amounts of non-conservatism were discovered for both methods.

Kiefner has conducted burst tests to compare the burst capacity of an EDM crack-like defect and an identical EDM crack-like defect within a significantly machined groove to simulate corrosion less deep than the tip of the crack-like defect. The defect configuration is shown in Figure 55. When the corrosion depth is 70% of the total hybrid defect depth, the burst pressure is only 1.35% higher than a single crack-like defect. The results are listed in Table 15. This tiny difference may be due to the high toughness of pipe, which could cause the crack-like defect failed prone to plastic collapse. To further investigate this complex behavior and maximize the difference of burst pressure between crack-like and corrosion-like flaws, the less tough pipe material is recommended.

[53] Cronin, Duane, Plumtree, Alan, Sen, Millan, and Kania, Richard, "Assessment of Crack in Corrosion Defects in Natural Gas Transmission Pipelines", IPC2008-64339, Proceedings of IPC 2008, 7th International Pipeline Conference, September 29-October 3, 2008, Calgary, Alberta, Canada.
[54] Seyed Aliakbar Hosseini, "Assessment of Crack in Corrosion Defects in Natural Gas Transmission Pipelines", a M.S. Thesis in Mechanical Engineering, University of Waterloo, Ontario, Canada, 2010.

Figure 55. Defect of EDM Notch-within-Groove Machined by Kiefner Lab

Table 15. Burst Test Results for EDM Notch with/without Groove by Kiefner

Defect Type	EDM Notch Dimensions	Buffing Depth	Failure Pressure, psig
Without groove	6” x 50% WT	0	1,780
With groove	6” x 50% WT	35% of WT	1,804

Dent Assessment

Dent assessment methods under fatigue loading are based on experimental or semi-analytical stress solutions that give a maximum stress at the apex of the dent. Extensive experimental data indicates that the burst pressure of a pipe is not affected by dents that are shallower than 10% pipe diameter[55, 56]. Mechanical damage, on the other hand, is a combined defect that usually consists of a deformed area with metal loss, i.e. gouge and sometimes cracking. Unlike a plain dent, the burst pressure capacity of a pipe with mechanical damage can be significantly lower than that of an intact pipe. Mechanical damage is a major cause of pipeline failure due to third party damage[57]. API 579 and PDAM contain assessment methods for dent–with-gouge combination under static or fatigue loading that can be used for mechanical damage.

A common cause of dents in buried pipelines is the presence of rock fragments in the backfill soil or rock outcroppings in the bottom of the trench with no soil between the pipe and the rock. For this reason dents may appear in large numbers along a portion of a pipeline that is backfilled with a soil full of rock fragments or where the ditch has been dug to expose a rock outcropping and no soil or padding is placed on the ditch bottom before the pipe is lowered in. Rock dents usually are plain dents, at least initially with no gouging or cracking because the bearing area between the rock and the pipe metal is usually large enough to prevent gouging. Mechanical damage is usually accompanied with a damaged pipe coating, but a damaged pipe coating does not necessarily indicate mechanical damage to the pipe itself (pipe coating can get damaged at a plain dent also). Although dents that are shallower than 6% of pipe diameter are known to have little effect on the pipe's ability to withstand static pressure, under certain conditions fatigue crack growth can initiate from a dent. Liquid pipelines are particularly susceptible to fatigue crack growth due to frequent pressure fluctuations. Several factors, including Bauschinger's effect, plastic dent re-rounding under repeated cyclic loads and re-rounding due to material creep renders the fatigue life prediction of a dent challenging.

When a dent is formed on a pipe due to a localized force or an object pressing against the pipe, the deformation involves elastic and plastic parts. The maximum dent depth during the indentation process is called instantaneous depth. The term "spring back" is the decrease of a dent depth after removal of the indenter. Actual dents usually occur under internal pressure.

---

[55] Rosenfeld, M.J., "Proposed New Guidelines for ASME B31.8 on Assessment of Dents and Mechanical Damage", Des Plaines, IL: Gas Research Institute, 2001, GRI-01/0084.
[56] Cosham, Andrew and Hopkins, Phil, "The Pipeline Defect Assessment Manual (PDAM)", Newcastle: Penspen Ltd, 2003, NR00018/4238.1.10/R1.01.
[57] Database reflects recent trends in European gas pipeline failures. Bolt, R.: PennWell Corporation, 2001, Oil and Gas Journal, Vol. 99, pp. 48-54.

Spring-back may involve some plastic deformation due to the action of the internal pressure, if the internal pressure is sufficiently high. If the internal pressure of a dented pipe is removed the dent depth increases elastically (Figure 56), and when the internal pressure increases dent depth decreases (re-rounding). Re-rounding under internal pressure can be elastic or plastic. Plastic re-rounding is permanent leading to a permanent reduction of dent depth, length and width. Under repeated loading a dent that is initially experiencing plastic re-rounding may "shake down" to a dent with an entirely elastic response. Sometimes plastic re-rounding can lead to almost complete and permanent removal of a dent.

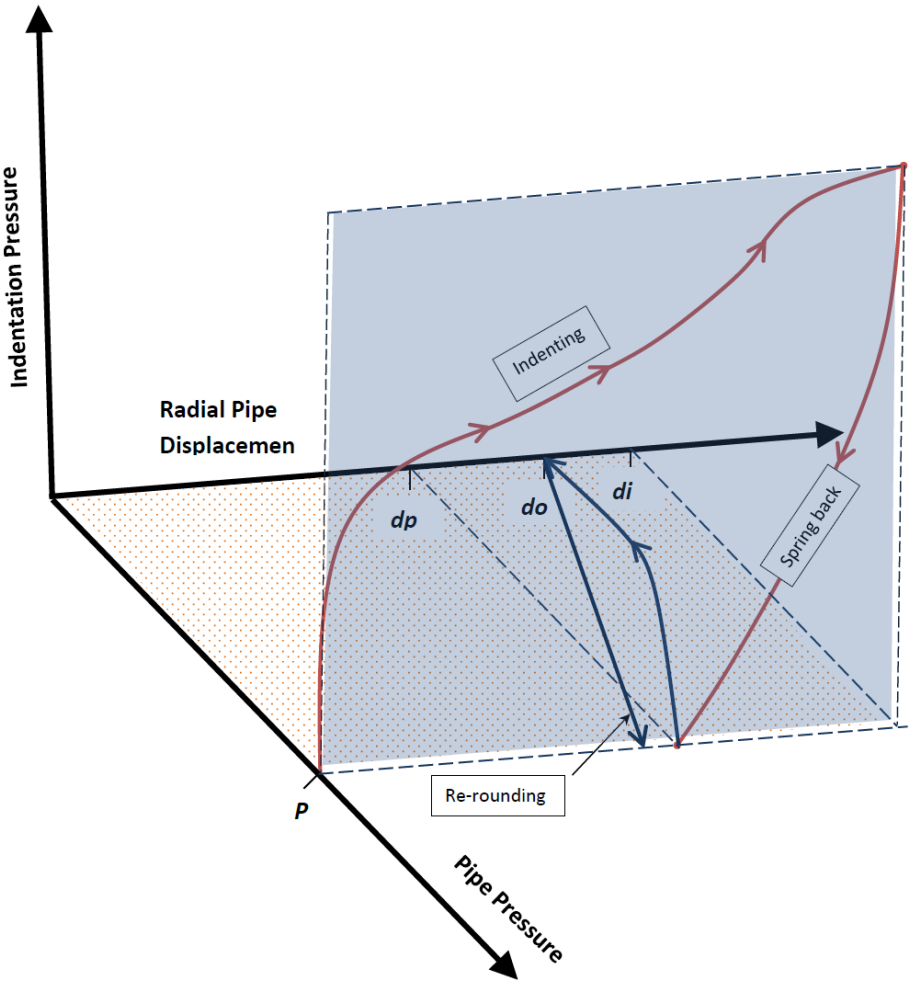

Figure 56. Dent Spring-back and Depth Change under Internal Pressure

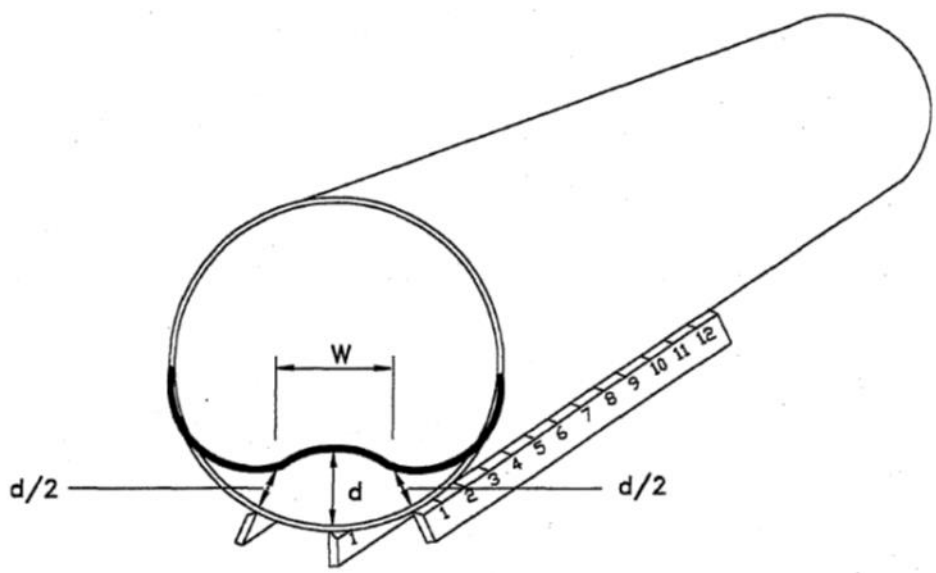

Figure 57. Dent Width Measurement for Dent SCF Calculations

Dent re-rounding and spring back affect the stress concentration at dent location and should be taken into account in dent assessment. Dent re-rounding models have been developed by Battelle, Gasunie, EPRG[56] and a number of other researchers. Rosenfeld developed a semi-empirical model[58] that is briefly described here:

$$d_0 = \frac{d_p}{f \cdot g} \qquad \text{Equation 14}$$

$$f = \frac{1.04}{1 + 0.0875(x)^{-3.2}} - 0.052 \qquad \text{Equation 15}$$

$$g = \frac{0.88\left(\frac{D}{w}\right)}{1 + 0.59\left(\frac{D}{w}\right) + 0.041\left(\frac{D}{w}\right)^2} \qquad \text{Equation 16}$$

[58] Rosenfeld, M.J., "Guidelines for the Assessment of Dents on Welds", PRCI, 1999, Catalog No. L51810.

$$x = \frac{\left(\frac{D}{w}\right)^{0.3}}{\left(\frac{D}{t}\right)^{0.7}\left(\frac{P}{E}\right)^{0.2}} \qquad \text{Equation 17}$$

where

w is the circumferential width of the dent measured between two points at half the dent depth (see Figure 57),
P is internal pressure,
E is pipe elastic modulus,
d_0 is the dent depth under zero internal pressure, and
d_p is the measured dent depth under internal pressure.

The PDAM recommends the following equations for dent spring back and re-rounding:

$$\frac{d_0}{D} = 0.624\frac{d_p}{D} - 0.628 \qquad \text{Equation 18}$$

$$\frac{d_0}{D} = 1.43\frac{d_P}{D}$$

The above equation does not account for pressure variations and is a simplification for a phenomenon that is complex in nature. In addition to the above mentioned methods, Reference [59] contains a rigorous method for shake down analysis of dents subjected to repeated pressure cycles. Reference [60] is another experimental and analytical work on this topic.

Rosenfeld also developed a stress concentration factor for plain dents that is included in Appendix A. Furthermore, Rinehart and Keating developed a semi-analytical model for dent stress concentration calculations[61]:

[59] Rosenfeld, M.J., "Development of a Model for Fatigue Rating Shallow Unrestrained Dents", PRCI, 1997, Catalog No. L51741.
[60] Avigaele Le Bastard, "Influence of Internal Pressure for Depth Measurement on a Dent", Calgary, Alberta, Canada: ASME, September 25-29, 2006, Proceedings of IPC2006: International Pipeline Conference.
[61] Rinehart, A.J. and Keating, P.B.," Stress Concentration Solution for a 2D Dent in an Internally Pressurized Cylinder", ASCE, 2007, Journal of Engineering Mechanics, Vol. 133, pp. 792-800.

$$k_d = 1 - 1.74\frac{d_P}{D} + 5.22\frac{d_P}{t}$$ Equation 19

References [62] and [63] are more recent examples on development of a dent stress concentration factor. Dent depth in the assessment should always be defined with respect to the undented pipe geometry. Since dents are usually accompanied by some pipe ovality, the dent depth as defined above is greater than the distance between the dent apex and the ridge around the apex on the pipe circumference. The parameters that are measured in a field inspection are usually the depth of the dent from the peak to the apex of the dent and dent width. There are analytical models that estimated the true dent depth from measured parameters[61]. Data from ILI using a caliper tool is usually a superior means for calculating the true dent depth as it can provide the entire inner pipe surface profile. In either case, contrary to what has been suggested by some investigators, it is inappropriate to deduct pipe ovality from a measured dent depth[59].

Gouge Assessment

Gouges are generally serious threats to pipe integrity whether accompanied with a dent or not. The combined effect of a gouge in a dent is significantly more severe that a gouge with no dent or a dent of the same depth with no gouge. Part 12 of API 579: 2007 contains an assessment method for gouges under static and fatigue loading, which is based on fracture mechanics. If a gouge has a smooth surface with no cracking or metallurgically altered layer at the base, it is possible to assess a gouge as metal loss. However, a gouge usually contains a layer of metallurgically altered metal at the base with properties similar to those of a cold-worked metal. If this work hardened layer contains cracking (often it does if the dent has been re-rounded plastically due to internal pressure) the effective gouge depth is defined as the depth of the gouge plus the depth of cracking at the base. If the gouge depth meets acceptable metal loss limits it may be dressed to remove the surface layer and any small cracks. Afterward, gouge assessment should be conducted using the increased depth of a gouge after dressing. Because a gouge is accompanied by coating damage, the pipe is susceptible to corrosion. The existing standards do not contain an assessment method for the combined effect of a corroded gouge. A simple approach for assessing a corroded gouge is to add the corrosion depth to the gouge depth.

[62] Carvalho Pinheiro, Bianca and Paranhos Pasqualino, Ilson, "Stress Concentration Factors of Dented Pipelines", Calgary, Alberta, Canada, September 25-29, 2006, Proceedings of IPC2006: 6th International Pipeline Conference.
[63] Khazhinskii, G.M., "Approximate Evaluation of Stresses in Dents of Cylindrical Shells", pp. 3-4, 2005, Chemical and Petroleum Engineering, Vol. 41.

The PDAM recommended method for assessment of a gouge is similar to that of a metal loss[56], but it recommends increasing the measured depth by at least 0.5 mm to account for cracking. For fatigue analysis of a gouge, PDAM recommends the BS 9710: 1990 fatigue analysis method.

ASME B31.4 2012 Pipeline Transportation Systems for Liquids and Slurries

Section 451.6.2.3 provides guidelines for gouges, grooves, and arc burns. The code recommends that gouges and grooves be evaluated by nondestructive examination. Superficial grinding (not to exceed 12.5% of the nominal pipe wall thickness) to form a smooth surface for nondestructive examination may become necessary, which also has the added benefit of removing stress concentrators. Upon completion of superficial grinding, the absence of any cracking shall be confirmed by using dye penetrant or magnetic particle inspection. The code sets a maximum depth of 12.5% of the nominal pipe wall thickness for gouges or grinding area and if this limit is exceeded an assessment becomes necessary. Any dent deeper than 6% of the pipe nominal diameter or those with metal loss deeper than 12.5% of the pipe nominal wall thickness or crack-like defects shall be removed unless API 1160 methods are used to reduce the risk. Any dent that can obstruct pig inspection should be removed. The code requires that arc burns be removed or repaired by grinding and examined by etching to confirm complete removal of the altered material.

ASME B31.8 2010 Gas Transmission and Distribution Piping Systems

ASME B31.8 also sets a maximum depth of 6% of the nominal pipe diameter for plain dents. According to this standard dents that contain stress concentrators (dent with cracks, dent with sharp gouges, mechanical damage) shall generally be repaired or mitigated at a reduced internal pressure for safety reasons during the repair process. Paragraph 851.4.1 and paragraph 860.2(a) of ASME B31.8: 2012 state that a dent less deep than 6% of the pipe outside diameter that contains a blunt metal-loss can be assessed similarly to an isolated metal loss following the assessment method of ASME B31G.

CSA Z662 2011 Oil and Gas Pipeline Systems

The Canadian Standard states that gouges, grooves and arc burns are defects that shall be repaired. Dents are considered to be defects unless an engineering analysis proves otherwise. Dents with stress concentrators are defects unless an engineering analysis shows that they are acceptable. Dents in mill or field welds that exceed 2% of the pipe's outside diameter for pipes with OD greater than 323.9 mm (12.75 inches), and dents deeper than 6 mm (0.236 inch) in smaller diameter pipes are defects. A dent with a metal loss greater than 10% wall thickness is generally a defect unless the length of the metal loss area is less than the maximum allowable corrosion length per Level 1 analysis table of ASME B31G. Dents with corrosion greater than

40% of wall thickness are defects regardless of the corrosion length. Cracks are always defects, whether inside a dent or isolated. According to this standard, defects should be repaired unless an engineering analysis proves that they are acceptable.

Pipeline Defect Assessment Manual (PDAM) 2003

PDAM provides a comprehensive review of pipe defect assessment methods. Furthermore, it contains experimental data from failure testing of defective pipe specimens. Chapter 25 of the report provides assessment method for dent and gouge combination, which is a very common feature of mechanical damage. The fatigue life and burst pressure capacity of a dent with a gouge can be significantly lower than that of a plain dent with the same depth or a similar isolated gouge. A gouge can cause a local stress concentration, which intensifies the already high stresses in a dent. The base of a gouge usually possesses mechanical properties similar to those of a cold worked metal and it is less ductile than scrounging areas possibly containing many small cracks.

Furthermore, it is not uncommon to find larger cracks at the base of a mechanical damage, and thus PDAM recommends grinding and inspecting a gouge for cracks. Experimental evidence indicates that dressing a gouge will increase both static and fatigue strengths of dent-gouge combination (it should be noticed that some codes do not allow for the dressing of a gouge inside a dent). Chapter 25 of the report provides analytical methods and recommendations for the assessment of dent-gouge combination.

The recommended assessment method for static strength is the semi-empirical method developed by British Gas and adopted by European Pipeline Research Group (EPRG), which in turn has evolved from an earlier work by Kiefner et al.[64, 65]. EPRG 1995 reports numbered 12[66], 13[67], 14[68], 15[69] and 16[70] as well as AGA PR-201-927[71] report provide insight into the historical development of the method. The assessment method uses both the material flow stress and

---

[64] Roovers, P., Bood, R., Galli, M., Marewski, U., Steiner, M., and Zarea, M., "EPRG Methods for Assessing the Tolerance and Resistance of Pipelines to External Damage", Brügge, Belgium: Pipeline Technology, 2000, The Proceedings of the Third International Pipeline Technology Conference, Vol. II, pp. 405-425.
[65] Ghaednia, Hossein, et al., "Pressure Tests on 30-inch Diameter X65 Grade Pipes with Dent-Crack Defects", First Quarter, 2013, The Journal of Pipeline Engineering, pp. 61-67.
[66] Colder, I. and Chatain, P., "EPRG Recommendations for the Assessment of the Resistance of Pipelines to External Damage", European Pipeline Research Group, Paper No 12, 1995.
[67] Colder, I. and Chatain, P., "Towards EPRG Recommendations for the Assessment of the Tolerance and Resistance of Pipelines to External Damage", European Pipeline Research Group, Paper No 13, 1995.
[68] Eiber, R.J and Leis, B.N., "Line Pipe Resistance to Outside Force", European Pipeline Research Group, Paper No 14, 1995.
[69] Fowler, J.R., Alexander, C.R., Kovach, P.J., and Connelly, L.M., "Fatigue Life of Pipelines with Dents and Gouges Subjected to Cyclic Internal Pressure", European Pipeline Research Group, Paper No 15, 1995.
[70] "A Fatigue Crack-initiation Criterion for the Assessment of the Residual Life of Gas Transmission Pipelined with "Gouge Only" or "Gouge in Dent" Defects", European Pipeline Research Group, Paper No 16, 1995.
[71] Fowler, J.R., Alexander, C.R., Kovach, P.J., and Connelly, L.M., "Cyclic Pressure Fatigue Life of Pipelines with Plain Dents, Dents with Gouges, and Dents with Welds", Stress Engineering Services, Inc., Prepared for American Gas Association, AGA Report Nos PR-201-927 and PR-201-9324.

fracture toughness, and it is primarily developed based on experimental data. It is recommended to increase the depth of a gouge by at least 0.5 mm (0.02 inch) to account for possible cracking. This assessment method has also been adopted by API 579: 2007, and will be described later on. PDAM states that the fatigue life of a dent with a gouge can be estimated as one hundredth of that of a plain dent with the same depth. This assessment method is recommended for dents with a maximum unpressurized depth of 4% (~2.8% under pressure) of the pipe diameter and a gouge depth less than 20% of the pipe wall thickness with an upper shelf V-notch impact energy of at least 47 Joules (of 35 ft-lb).

Chapter 26 of the PDAM contains assessment methods and recommendations for combined dent with other defects (such as crack-like defects, mechanical damage and inclusions). A dent caused by mechanical damage may contain a layer of severely cold worked metal with a reduced ductility. The static strength and fatigue life of a smooth dent containing a defect can be significantly lower than that of a plain dent of the same depth or a similar isolated defect. As opposed to dent-gouge combinations, there is no experimental work for a dent that contains multiple gouges or altered material properties (e.g. hard spots) and very little data on blunt defects in a dent. It is clear that assuming the defect to be sharp is conservative, but such assumption can lead to overly conservative conclusions. For the assessment of dent and defect combinations PDAM recommends increasing the depth of the defect by at least 0.5 mm (0.02 inch) to account for possible cracking. PDAM recommends the same methodology that is proposed for the dent-gouge combination for the dent-defect combination. PDAM does not offer a direct method for assessment of dents containing areas with different material properties such as hard spots.

A dented weld usually contains stress concentrators and it is more difficult to inspect it for cracking. A dented weld usually has a significantly shorter fatigue life and a lower static strength as compared to a similar weld with no dent or a plain dent of the same depth on base metal. It is difficult to predict the fatigue life of a dented weld due to the possibility of damage during denting or re-rounding processes. It is common practice to repair dented welds unless they are minor (depth<2%OD). Assessment can be performed using guidelines from Reference [58] that is based on a dent stress concentration factor combined with a representative S-N curve for the weld.

API 579-1/ASME FFS-1 2007 Fitness-For-Service

The assessment method described in Part 12 of API 579 can be applied to isolated plain dents or mechanical damages away from welds. The assessment method can also account for a uniform corrosion metal loss across the entire pipe circumference. Other defect types such as cracks within a dented area are not included. API 579 sets a maximum allowed dent depth of

7% of the pipe OD for all dents. For the burst pressure calculation of a dent-gouge defect API 579 has adopted the EPRG method:

$$RSF = \frac{2}{\pi}\cos^{-1}\left(\exp\left(-\frac{C_1 \cdot C_3}{C_2^2}\right)\right)\cdot\left(1-\frac{d_g}{t}\right) \qquad \text{Equation 20}$$

$$C_1 = \frac{1.5\pi U_1 E}{\sigma_f A_{CVN} d_g} \qquad \text{Equation 21}$$

$$C_2 = Y_1\left(1-\frac{1.8d_0}{D}\right)+Y_2\frac{10.2d_0}{2t} \qquad \text{Equation 22}$$

$$C_3 = \exp\left(\frac{\ln\left(U_2 CVN\right)-1.9}{0.57}\right) \qquad \text{Equation 23}$$

$$\sigma_f = 1.15\sigma_y\left(1-\frac{d_g}{t}\right) \qquad \text{Equation 24}$$

$$Y_1 = 1.12-0.23\left(\frac{d_g}{t}\right)+10.6\left(\frac{d_g}{t}\right)^2-21.7\left(\frac{d_g}{t}\right)^3+30.4\left(\frac{d_g}{t}\right)^4 \qquad \text{Equation 25}$$

$$Y_2 = 1.12-1.39\left(\frac{d_g}{t}\right)+7.32\left(\frac{d_g}{t}\right)^2-13.1\left(\frac{d_g}{t}\right)^3+14.0\left(\frac{d_g}{t}\right)^4 \qquad \text{Equation 26}$$

where

RSF is the remaining strength factor,
A_{CVN} is the fracture are of a 2/3 Charpy specimen; A_{CVN} = 53.33 mm^2 (0.083 inch^2),
CVN is Charpy V-notch energy,
d_g is maximum gouge depth,
σ_f is the gouge flow stress,
U_1 is unit conversion factor, U_1 = 113.0 if E and σ_f are in MPa, A_{CVN} is in mm^2, and d_0 is in mm, while U_1 = 1.0 if E and σ_f are in psi, A_{CVN} is in inch^2, and d_0 is in inches, and
U_2 is unit conversion factor, U_2 = 0.738 for units of Joules and U_2 = 1.0 for units of ft-lb.

The remaining strength factor RSF is defined as the ratio of the plastic collapse load of the pipe with defect to that of an intact pipe. The remaining fatigue life of a dented pipe with gouge is calculated as:

$$N_c = 562.2\left(\frac{\sigma_{uts}}{2\sigma_A K_d K_g}\right) \qquad \text{Equation 27}$$

$$\sigma_A = \sigma_{hm}\left(1-\left(\frac{\sigma^C_{\mathrm{m,max}} - \sigma_{hm}}{\sigma_{uts}}\right)^2\right)^{-1} \qquad \text{Equation 28}$$

$$\sigma_{hm} = \frac{\sigma^C_{\mathrm{m},max} - \sigma^C_{\mathrm{m,min}}}{2} \qquad \text{Equation 29}$$

$$K_d = 1 + C_s\sqrt{\frac{t}{D}\left(d_0 \cdot C_{ul}\right)^{3/2}} \qquad \text{Equation 30}$$

$$C_s = \left|\begin{matrix} 2.0 & \text{for smooth dents, } r_d \geq 5t \\ 1.0 & \text{for kinked dents, } r_d < 5t \end{matrix}\right. \qquad \text{Equation 31}$$

$$K_g = 1 + 9\left(\frac{d_g}{t}\right) \qquad \text{Equation 32}$$

where

N_c is the expected number of stress cycles to failure, including the past stress cycles,
σ_{hm} is circumferential membrane stress,
σ_{uts} is the ultimate tensile strength,
$\sigma^C_{\mathrm{m,max}}$ is the maximum circumferential membrane stress accosted with P_{max},
$\sigma^C_{\mathrm{m,min}}$ is the minimum circumferential membrane stress accosted with P_{min}, and
C_{ul} is a conversion factor, C_{ul} = 1.0 if d_0 is in mm and C_{ul} = 25.4 if d_0 is in inches.

This document sets the following criteria for dent and joint weld interaction:

$$L_w \geq \max\left[2t, 25mm\right] \qquad \text{Equation 33}$$

where

t is pipe wall thickness, and
L_w is the distance to the nears joint weld.

Review of Journal Articles and Technical Reports

Kiefner and Alexander[72] conducted experimental work on dent-defect interaction, which was sponsored by American Petroleum Institute. They performed 8 tests on 12.75-inch OD by 0.188-inch WT Grade X52 pipe with two dents separated by 0.5, 1, 2, and 3 times indenter diameter (indenter diameters of 4 inches and 8 inches were used). They defined dent interaction based on dent geometry as formation of a flat area between two adjacent dent apexes. They concluded that such dents should be removed due to very short fatigue lives. However, no attempt was made to determine an interaction rule based on dent and pipe parameters. They also tested five pipe specimens with corrosion inside dents and found that corrosion inside a dent will not affect the burst pressure capacity of a pipe more than it affects the burst pressure of a pipe with no dent. Essentially, this means that the burst pressure of a dented pipe with corrosion inside dent can be estimated using the same methods pertinent to corroded pipe burst capacity estimation.

The authors reported that they could not create unrestrained dents with residual depths greater than about 3% pipe OD in pipes that were pressurized to 72% SMYS, due to the re-rounding effect of internal pressure. Thus, they concluded that a deep dent in a pipeline that has experienced high pressures after the dent formation is likely to be a restrained dent (e.g. a rock dent). In this respect a very narrow dent may also act like a restrained dent due to high radial stiffness. They also observed that minor stress concentrators such as girth welds or seam welds can reduce the fatigue life of a dent; however the reduction was relatively insignificant when the intrinsic scatter in the data was considered. In particular, the fatigue life of a dent on good quality ERW weld was observed to be in the same order of that of a plain dent. This research also confirmed that removing a gouge by grinding would improve the fatigue life of a gouge-dent combination, but it was still shorter than the fatigue life of a similar plain dent.

Ghaednia et al.[65] reported the results of pressure test on 30-inch OD by 0.322-inch WT Grade X65 pipe specimens with dent-crack combinations. The cracks were initiated on the test

[72] API 1156, "Effects of Smooth and Rock Dents on Liquid Petroleum Pipelines", Kiefner and Alexander, API Publication 1156, First Edition, November 1997; Addendum October 1999.

specimens by machining a 10-mm long by 1 to 1.5-mm deep V-notch in the longitudinal direction of pipe samples and exposing the notch to fatigue load. The fatigue load was a half sine-wave applied to each pipe through an actuator at a location approximately 200 mm away from the V-notch to stimulate crack growth from the notch-tip into the pipe wall thickness. Crack depths were regularly verified using ultrasonic measurements and fatigue loading was stopped once a desired depth was achieved. A dent was pressed in each pipe at the location of the crack in such a way to fit the crack inside the dent. The experiment used two different dent geometries produced using a sharp 100-mm long diamond-shaped indenter and a 500-mm long blunt elliptical indenter while an internal pressure ranging from 0 to 1105 psig was applied. This experimental work concluded that the shape of the indenter and the internal pressure during the indentation did not affect the burst pressure (The number of specimens tested may not be sufficient to firmly establish this conclusion). Cracks shallower than 2 mm (24% wall thickness) did not affect the static burst pressure capacity of pipe, while 4 mm deep cracks (50% wall thickness) reduced the burst pressure by about 40%.

Bai and Song[73] developed an analytical model for the prediction of burst pressure of dented pipe with cracks. They used a modified version of the Bilby-Cottrell-Swinden crack intensity factor solution[74] with a dent stress concentration factor of Shannon[75] to develop an analytical solution for circumferential and axial cracks in a dent. The bending moment and uniaxial tensile stress in a dented pipe were calculated as:

$$\sigma = \sigma_H \left(1 - 1.8\frac{d_d}{D}\right) \qquad \text{Equation 34}$$

$$M = 0.85\sigma_H \cdot t \cdot d_d \qquad \text{Equation 35}$$

where

σ_H is the hoop stress,
d_d is the dent depth under pressure,
σ is the axial stress at dent apex, and
M is the through thickness bending moment at dent apex.

The crack stress intensity factor was calculated using the following equation:

[73] Bai, Yong and Song, Ruxin, "Fracture Assessment of Dented Pipes with Cracks and Reliability-based Calibration of Safety Factors", volume 74, Elsevier, 1998, International Journal of Pressure Vessels and Piping, pp. 221-229.
[74] Bilby, B. A., Cottrell, A. H. and Swinden, K. H., "The Spread of Plastic Yield from a Notch", 1963, Proc. Roy. Soc., Vol. A272, pp. 304.
[75] Shannon, R. W., "The Mechanics of Low Stress Failure Which Occurs as a Result of Severe Mechanical Interface - a Preliminary Hypothesis", 1973, ERS Report 571.

$$K = \frac{F}{\sqrt{Q}}\sigma\sqrt{\pi a} + H\frac{F}{\sqrt{Q}}\cdot\frac{6M}{t^2}\sqrt{\pi a}$$ Equation 36

where

K is the stress intensity factor,
σ is the axial stress at dent apex,
M is the through thickness bending moment at dent apex,
Q is the shape factor for elliptical crack,
F is the crack boundary correction factor, and
H is the correction factor for bending moment.

The authors used the solution developed by Newman and Raju to determine the factors Q, F, and H. They applied a reliability-based model to account for uncertainties in the model parameters such as crack size and pipe properties. They compared their results with the experimental results of ten specimens and showed good agreement between the model predictions and experimental observations.

Blachut and Iflefel[76] conducted the experimental investigation on the burst pressure of pipes with plain and gouged dents under combined bending moment and internal pressure. They tested five dented pipe specimens with a diameter to wall thickness ratio of 40 and dent depth to pipe diameter ratios of 15% to 23%. The dents were applied to the pressurized specimens using a hemispherical indenter with a diameter of 41% pipe diameter. Three out of the five tested specimens had a longitudinally oriented gouge inside the dent area. The first two gouges possessed a depth of 50% wall thickness and a length of 25% pipe diameter, while the last gouge had a depth of 25% wall thickness and a length of 81% pipe diameter. The specimens were subjected to a four point bending test to plastic failure with internal pressure maintained constant. Then the internal pressure was increased to burst the specimens. They compared their test results (pipe displacement-load responses and burst pressures) to finite element analysis (FEA) results and concluded that FEA can predict the behavior of dented pipes fairly well but does not provide equally good predictions when gouges were introduced.

Been et al. [77] studied the growth of cracks located at the apex of restrained and unrestrained dents using an elastic-plastic finite element analysis. They simulated indentation of 36-inch and 42-inch OD, 0.375-inch wall thickness, and Grade X-65 pipes using rigid hemispherical indenters

[76] Blachut, J. and Iflefel, I. B.," Collapse of Pipes with Plain or Gouged Dents by Bending Moment", 2007, The International Journal of Pressure Vessels and Piping, pp. 507-581.
[77] Been, J., Carroll, B., Dinovitzer, A., and Sutherby, R., "Stress Intensification and Crack Growth in the Presence of Dents on Pipelines", Calgary, Alberta, Canada: ASME, September 2006, Proceedings of IPC 2006 International Pipeline Conference, pp. 1-7.

with diameters ranging from 50 to 200 mm to create 6% OD deep dents. Their analysis calculated a stress concentration factor of about 2 for unrestrained dents and about 1.6 for restrained dents. The calculated stress concentration factors were more or less independent of the indenter width. The high stress zone of the dents was determined to be at the apex area, and while restrained dents had lower stress concentration factors, they possessed larger high stress zones. They studied the growth of an axial 0.5-mm deep and 2.5-mm long crack located within the high stress zone under internal pressure fluctuations of a typical liquid line. They concluded that the crack growth rate is slightly higher for unrestrained dents and it increases with decreasing indenter diameters. The analysis predicted moderate crack growth rates; for example, the cracks inside the restrained dents formed with 50-mm and 100-mm indenter grew to through-wall cracks within 13 and 33 years, respectively. They did not conduct any experimental validation of the results, neither did they account for far-field stress redistribution due to crack growth.

Martin and Andrews[78] developed a time dependent model for failure prediction of mechanical damage under internal pressure variations. The model combined BS 7910 crack failure assessment diagram with an R5[79] creep approach to predict time to failure for combined dent-crack defects. The model used a two-dimensional analysis of the defect with crack growth in the through-thickness direction only. The authors concluded that their approach can predict the sensitivity of the failure pressure and the fatigue life of a mechanical damage defect to input parameters such as pipe pressure fluctuations.

The review of the literature on the dent interaction shows that there are experimental data and theoretical models for assessment of dent-gouge-crack combinations. The method, developed by EPRG from earlier work and adopted by API 579: 2007, is semi-empirical based on experimental data and uses both fracture toughness and flow stress as input parameters. The literature contains other assessment methods that typically combine fracture mechanics with the dent stress concentration factor determined from finite element analyses. Currently the primary factor that renders uncertainty in the assessment of dent-gouge-crack combination is the difficulty of measuring geometrical gouge and crack parameters. However, with the emerging ultrasonic and ILI technology it is likely that in near feature such measurements can be taken with higher accuracy levels.

The codes address the metallurgically altered local areas by requiring the operator to remove the defect (e.g. arc burns) or otherwise by setting allowance limits for such defects. Since

[78] Martin, Michael and Andrews, Bob, "A Time Dependent Model for Assessing the Significance of Mechanical Damage", Calgary, Alberta, Canada, September 25-29, 2006, Proceeding of IPC 2006: 6th International Pipeline Conference.
[79] British Energy, Assessment Procedure R5, Issue 3, 2003.

there is no exiting mathematical model to assess such defects, the interaction of metallurgically altered areas within a dent and mechanical damage cannot be addressed analytically.

Dinovitzer et al.[80] defined a dent-dent interaction parameter as the distance between the two dent apexes divided by the dent depth. They considered the two dents to be interacting dents when the parameter was less than one. Francini and Yoosef-Ghodsi (2008) suggested that two dents were interacting dents when their edge-to-edge distance was less than $2\sqrt{Rt}$ [81].

Dinovitzer et al.[82] presented dent-weld interaction criteria for a pressurized, dented pipe. Aiming to develop fatigue life interaction criteria for weld-dent interaction, the authors conducted a series of finite element analyses on restrained dents on or near a pipe seam and/or a girth welds. The presence of the weld was accounted for by assuming that it would act as a stress raiser with a stress concentration factor of 3. However, the weld geometry and material properties were not included explicitly. They developed the following criterion for dent-girth weld interaction distance:

$$I_{axial} = \left(A_1 \left(\frac{\sigma_y}{\sigma_{ref}} \right)^2 + B_1 \left(\frac{\sigma_y}{\sigma_{ref}} \right) + C_1 \right) + \left(A_2 \left(\frac{D}{t} \right)^2 + B_2 \left(\frac{D}{t} \right) + C_2 \right) + \left(A_3 \cdot d^2 + B_3 \cdot d + C_3 \right) + \left(A_4 \left(\frac{d}{\sqrt{L}} \right)^2 + B_4 \left(\frac{d}{\sqrt{L}} \right) + C_4 \right) + \left(A_5 \left(\frac{l}{\sqrt{L}} \right)^2 + B_5 \left(\frac{l}{\sqrt{L}} \right) + C_5 \right) \qquad \text{Equation 37}$$

where

A_i, B_i, and C_i values are regression coefficients (Table 16),
D is pipe OD,
t is pipe wall thickness,
d is dent depth in mm,
L is the length of the dent shoulder in mm, and
l is the distance between dent apex and the location of half depth in mm.

[80] Dinovitzer et al., "Geometric Dent Characterization", ASME, IPC2002-27076, Proceedings of the International Pipeline Conference, Calgary, Alberta, 2002.
[81] Francini and Yoosef-Ghodsi, "Development of a Model for Predicting the Severity of Pipeline Damage Identified by In-line Inspection", Final report to Pipeline Research Council International, Inc. Report No PR-218-063511-B, 2008.
[82] Dinovitzer, A., Fregj, A., Carroll, B., Semiga, V., Asavare, M., Tiku, S., "Evaluation of Interaction of Mechanical Damage on Welds", Pipeline Research Council International, Inc., Report No PR-214-0326, 2007.

The regression coefficients (A, B, and C) of the last two terms in the above equation are sensitive to the units. The values given in Table 16 are valid for mm.

Table 16. Dent-Girth Weld Interaction Coefficients

Pressure Range (%MOP)	Regression Coefficients						Mean Error, mm	Max. Error, mm	Min. Error, %
	Coeff.	1	2	3	4	5			
75-100	A	415.82	0.02	66.46	265.25	-406.98	22	15	-11
	B	336.06	-4.56	-698.62	-350.33	1680.98			
	C	233.33	233.33	233.33	233.33	233.33			
50-100	A	87.16	-0.02	-157.18	-299.73	-7435.48	31	19	-12
	B	-252.71	2.23	1180.18	776.62	8277.58			
	C	-682.75	-682.75	-682.75	-682.75	-682.75			
25-100	A	183.85	-0.03	-167.01	-274.63	-8206.91	28	16	-9
	B	-255.83	4.11	1218.56	737.45	9402.45			
	C	-743.21	-743.21	-743.21	-743.21	-743.21			
0-100	A	-16.15	0.05	43.98	470.19	-7448.47	18	8	-4
	B	115.58	-10.07	-811.53	-600.68	10166.21			
	C	265.54	265.54	265.54	265.54	265.54			

Al-Muslim[83]developed an interaction model for two adjacent dents by conducting a series of probabilistic finite element analyses. He studied the effect of dent-to-dent distance and orientation and concluded that the maximum dent stress increases with decreasing distance between the two dents, and with increasing orientation angle with respect to the pipe axial direction. That is, two dents that are aligned in the transverse direction will have a higher stress as compared to two dents with identical shapes aligned in the axial direction. The results of the parametric study were regressed to express various output parameters as functions of dent parameters in the following format:

[83] "Impact of Ccombined Mmechanical Ddamage on the Iintegrity of Ppipelines", Husain Muhammed Al-Muslim, PhD Dissertation, King Fahd University of Petroleum & Minerals, Dhahran, Saudi Arabia.

$$\text{Output Parameter} = a_0 + b_1\frac{D}{t} + b_2\frac{d}{D} + b_3\frac{l}{D} + b_4\frac{w}{d} + b_5\frac{l\cdot d\cdot w}{D^2 t} + b_6\frac{\sigma_{flow}}{E_{avg}} +$$
$$b_7\frac{E_t}{E_l} + b_8\frac{d_{e-e}}{\sqrt{0.5D\cdot t}} + b_9\phi + b_{10}\frac{P_{\max}-P_{\min}}{P_{SMYS}} + c_1\left(\frac{D}{t}\right)^2 + c_2\left(\frac{d}{D}\right)^2 + c_3\left(\frac{l}{D}\right)^2 +$$
$$c_4\left(\frac{w}{D}\right)^2 + c_5\left(\frac{l\cdot d\cdot w}{D^2 t}\right)^2 + c_6\left(\frac{\sigma_{flow}}{E_{avg}}\right)^2 + c_7\left(\frac{E_t}{E_l}\right)^2 + c_8\left(\frac{d_{e-e}}{\sqrt{0.5D\cdot t}}\right)^2 +$$
$$+c_9\Phi^2 + c_{10}\left(\frac{P_{\max}-P_{\min}}{P_{SMYS}}\right)^2$$

Equation 38

where

a_0, b_i, and c_i values are regression coefficients for various output parameters,
D is pipe diameter,
t is pipe wall thickness,
d is dent depth (in the study both dents had the same depth),
l is dent width at half depth,
w is dent width at half depth,
d_{e-e} is the apex-to-apex distance of the two dents,
ϕ is the orientation of the line connecting the two dents with respect to axial pipe direction in radians,
σ_{flow} is the flow stress,
E_t is Young's modulus in hoop direction,
E_l is Young's modulus in axial direction,
E_{avg} is the average of E_t and E_l,
P_{max} is the maximum internal pressure,
P_{min} is the minimum internal pressure, and
P_{SMYS} is the internal pressure corresponding to material SMYS.

The regression coefficients are presented in Table 17. The output parameters that are used in this table are:

ε_{atp} is the strain at dent apex,
σ_{atp} is the axial stress at dent apex,
σ_{rp} is Von Mises stress range at dent apex,
σ_{mp} is the mean Von Mises stress at dent apex,
σ_{ra} is the maximum Von Mises stress range along a line in the longitudinal direction of the pipe,
σ_{ma} is the mean Von Mises stress at the location of σ_{ra},

σ_{rh} is the maximum Von Mises stress range along a line in the hoop direction of the pipe,
σ_{mh} is the mean Von Mises stress at the location of σ_{rh},
N is the number of cycles to fatigue failure.

Table 17. Dent-Dent Interaction Coefficients

	ε_{atp}	$\frac{\sigma_{atp}}{\sigma_y}$	$\frac{\sigma_{rp}}{\sigma_y}$	$\frac{\sigma_{mp}}{\sigma_y}$	$\frac{\sigma_{am}}{\sigma_y}$	$\frac{\sigma_{ra}}{\sigma_y}$	$\frac{\sigma_{mh}}{\sigma_y}$	$\frac{\sigma_{rh}}{\sigma_y}$	$\ln(N)$
a_0	-3.90E-01	2.61E-01	-3.89E-01	6.82E-01	-2.46E+01	1.51E+00	-7.45E-01	1.83E+00	9.39E+01
b_1	-1.70E-03	-3.60E-03	-8.72E-04	1.07E-02	-4.70E-03	4.90E-03	2.10E-03	6.90E-03	3.78E-02
b_2	1.06E+01	4.45E+01	1.06E+01	2.68E+01	1.83E+00	1.32E+01	1.92E+00	1.33E+01	4.95E+02
b_3	1.63E-01	3.29E-01	-2.05E-01	-5.15E-01	-1.33E-01	-6.01E-01	-2.36E-01	-6.20E-01	2.02E+01
b_4	-5.65E-01	5.40E+00	1.13E+00	3.53E+00	5.50E-01	6.55E+00	5.15E-01	7.40E+00	1.13E+02
b_5	3.88E-01	2.21E-01	4.93E-01	-8.43E-03	4.83E-01	-2.49E-01	5.28E-01	-1.69E-01	2.58E+01
b_6	1.74E+02	7.35E+01	5.02E+02	6.62E+02	3.09E+02	8.07E+02	2.64E+02	8.15E+02	5.08E+04
b_7	2.79E-01	3.31E-01	1.17E+00	-1.02E-02	-6.37E-01	6.85E-01	-6.32E-01	4.41E-01	4.67E+01
b_8	1.70E-03	-1.11E-01	-8.60E-03	3.57E-02	-1.45E-01	2.42E-01	-5.74E-02	-4.10E-03	1.05E+00
b_9	-1.44E-02	-2.84E-01	4.73E-02	1.23E-02	-1.74E-01	1.36E-01	-2.12E-02	2.70E-03	4.67E+00
b_{10}	-	-	1.27E+00	1.86E+00	-4.06E-02	-4.12E-01	2.30E+00	1.03E+00	6.99E+01
c_1	6.80E-06	2.45E-05	2.45E-06	-6.47E-05	-4.86E-05	-2.26E-05	-2.63E-05	-4.87E-05	3.91E-05
c_2	7.34E+01	5.16E+02	1.96E+02	3.86E+02	8.92E+01	1.48E+02	8.53E+01	2.10E+02	9.78E+03
c_3	-4.55E-02	-7.01E-02	1.94E-02	1.24E-01	4.10E-02	1.03E-01	7.90E-02	7.80E-02	2.93E+00
c_4	5.08E-02	6.53E+00	1.03E+00	5.55E+00	2.14E+00	8.38E+00	-8.63E-01	1.12E+01	1.18E+02
c_5	-1.88E-01	-1.31E-01	-2.21E-01	2.74E-02	-1.86E-01	2.07E-01	-2.62E-01	2.68E-01	9.00E+00
c_6	2.08E+04	1.86E+04	7.47E+04	9.43E+04	3.96E+04	1.04E+05	3.48E+04	1.08E+05	8.02E+06
c_7	-9.48E-02	-2.12E-01	5.34E-01	-2.08E-02	3.39E-01	-4.06E-01	3.38E-01	-3.00E-01	2.00E+01
c_8	-1.43E-02	2.10E-02	2.47E-02	1.04E-04	8.26E-02	-8.92E-02	3.26E-02	-1.62E-02	-3.11E-01
c_9	-2.58E-02	1.02E-01	2.83E-01	-4.03E-02	1.31E-01	-7.45E-02	1.84E-02	4.95E-02	1.70E+00
c_{10}	-	-	-9.03E-01	1.84E+00	3.02E-01	6.81E-02	1.87E+00	5.84E-01	6.30E+01
R^2	0.78	0.9	0.55	0.64	0.4	0.72	0.54	0.76	0.66

Al-Muslim[83] developed similar probabilistic-based criteria for dent-metal loss interaction as below.

$$\text{Output Parameter} = a_0 + b_1\frac{D}{t} + b_2\frac{d}{D} + b_3\frac{l}{D} + b_4\frac{w}{d} + b_5\frac{l\cdot d\cdot w}{D^2 t} + b_6\frac{\sigma_{flow}}{E_{avg}} +$$
$$b_7\frac{E_t}{E_l} + b_8\frac{d_m}{w_m} + b_9\frac{P_{\max}-P_{\min}}{P_{SMYS}} + c_1\left(\frac{D}{t}\right)^2 + c_2\left(\frac{d}{D}\right)^2 + c_3\left(\frac{l}{D}\right)^2 +$$
$$c_4\left(\frac{w}{D}\right)^2 + c_5\left(\frac{l\cdot d\cdot w}{D^2 t}\right)^2 + c_6\left(\frac{\sigma_{flow}}{E_{avg}}\right)^2 + c_7\left(\frac{E_t}{E_l}\right)^2 + c_8\left(\frac{d_m}{w_m}\right)^2 +$$
$$+c_9\left(\frac{P_{\max}-P_{\min}}{P_{SMYS}}\right)^2$$

Equation 39

In the above equation w_m and d_m are the width and depth of the metal loss area and all the other parameters are as defined previously. Table 18 contains the corresponding regression coefficients.

Table 18. Dent-Metal Loss Interaction Coefficients

	ε_{atp}	$\frac{\sigma_{atp}}{\sigma_y}$	$\frac{\sigma_{rp}}{\sigma_y}$	$\frac{\sigma_{mp}}{\sigma_y}$	$\frac{\sigma_{ma}}{\sigma_y}$	$\frac{\sigma_{ra}}{\sigma_y}$	$\frac{\sigma_{mh}}{\sigma_y}$	$\frac{\sigma_{rh}}{\sigma_y}$	$\ln(N)$
a_0	-1.02E-01	-8.48E-01	1.32E+00	1.55E+00	-1.10E-01	1.76E+00	-3.79E-01	2.63E+00	1.13E+02
b_1	1.62E-03	2.03E-02	3.00E-03	2.60E-03	3.50E-03	-9.80E-03	4.40E-03	-1.38E-02	-2.72E-01
b_2	-4.86E-01	-3.58E-01	2.93E+00	7.32E+00	3.15E+00	6.20E+00	3.47E+00	5.80E+00	9.61E+01
b_3	-1.45E-03	1.57E+00	1.38E+00	1.21E+00	5.65E-02	1.42E+00	6.15E-01	1.96E+00	6.45E+01
b_4	2.83E-01	1.02E+01	2.94E+00	5.75E+00	3.70E-01	2.69E+00	-9.45E-02	3.51E+00	2.03E+02
b_5	2.55E-01	3.78E+00	1.29E+00	5.00E-01	1.15E+00	-8.18E-01	6.98E-01	1.30E-01	1.04E+02
b_6	4.65E+01	4.73E+00	6.78E+02	1.63E+02	6.89E+01	1.34E+02	1.39E+02	1.66E+01	4.17E+04
b_7	-2.91E-02	1.28E+00	6.22E-01	-9.37E-01	6.00E-03	7.22E-01	1.65E-01	5.41E-01	1.03E+01
b_8	-5.05E-02	1.19E+00	-4.27E-01	1.19E+00	-3.12E-02	1.73E+00	1.57E-01	1.31E+00	3.73E+01
b_9	-	-	-2.94E+01	-7.50E-01	-9.47E-01	-9.53E-02	1.35E+00	4.54E+00	5.65E+01
c_1	-9.75E-06	-1.17E-04	-1.63E-05	-6.93E-06	-2.53E-05	6.40E-05	-3.13E-05	8.42E-05	1.90E-01
c_2	4.95E+00	1.55E+02	1.13E+01	1.66E+01	7.04E+00	4.88E+01	4.07E+01	9.82E+01	3.84E+02
c_3	9.38E-02	-7.85E-01	9.65E-01	1.56E+00	-4.68E-02	7.53E-01	-3.03E-01	7.73E-01	7.13E+01
c_4	2.80E+00	2.60E+01	9.00E+00	2.88E+01	-1.60E+00	5.05E+00	2.49E+00	5.03E+00	9.95E+02
c_5	-1.08E-01	2.19E+00	-5.81E-01	-1.41E-01	-3.86E-01	4.23E-01	-1.63E-01	-3.69E-02	4.41E+01
c_6	6.92E+03	1.00E+05	9.34E+04	2.40E+04	6.90E+00	2.00E+04	2.16E+04	6.29E+02	5.88E+06
c_7	1.14E-02	5.02E-01	-2.38E-01	4.06E-01	-5.40E-03	-3.47E-01	-7.41E-02	-2.78E-01	2.30E+00
c_8	5.94E-02	9.45E-01	5.06E-01	1.32E+00	6.06E-01	7.81E-01	-7.37E-02	1.03E+00	3.65E+01
c_9	-	-	5.37E-01	7.74E-01	1.34E+00	-8.62E-01	-9.58E-01	3.69E+00	5.07E+01
R^2	0.68	0.61	0.35	0.51	0.63	0.60	0.53	0.46	0.31

A research project sponsored by PRCI, currently in progress, is focused on fatigue life assessment of dents and dents interacting with joint welds and metal loss defects[84]. Included in this effort is compiling a database for full scale experimental data for dents interacting with girth welds, seam welds and metal loss defects[85]. The dents in this experimental program were introduced at zero internal pressure. The dents were exposed to an initial pressure cycle of either 80% or 100% SMYS, followed by 10 pressure cycles of zero to 80% SMYS, after which they were exposed to pressure cycles of 10% to 80% SMYS until failure. The results of the experiments on plain dents denoted that unrestrained dents underwent spring-back from an initial depth of 15% to a residual depth of 5.9% after the removal of indenter under zero internal pressure. Average dent depth after two pressure cycles of 80% to 100% SMYS were measured to be only 2.5%. Also, the results of plain dent fatigue tests indicate that those dents that underwent an initial pressure cycle (one cycle) of 100% SMYS possessed longer fatigue lives as compared to those which underwent an initial pressure cycle of 80% SMYS. The longer fatigue life of a dent that was initially exposed to one cycle of a greater internal pressure was due to re-rounding and reduction of dent depth after the initial cycle. The test data on dent-weld interaction indicated that the presence of a girth weld near a dent apex did not cause a significant reduction in dent fatigue life, while a girth weld at some offset from dent apex (50.8 mm offset was used in the experiments) could reduce the fatigue life by 30%. This might be due to the fact that fatigue failure usually initiates near the perimeter of a dent rather than dent apex.

There are three ongoing PRCI projects that, upon completion, will address various elements of dent-defect interaction assessment. These projects are:

1- MD 4-2, full scale demonstration of the interaction of dents with localized effects[86],

2- MD 4-3, mechanical damage instantaneous failure model – numerical simulation of physical tests[87],

3- MD 4-9, fatigue screening and life assessment of pipelines, dents and dent interacting with welds[88],

---

[84] "Fatigue Screening and Life Assessment of Pipelines, Dents and Dents Interactions with Welds", Project status update September 2013, PRCI Project MD 4-9.
[85] Brock Bolton et al., "Full Scale Cyclic Fatigue Testing of Dented Pipelines and Development of a Validated Dented Pipe Finite Element Model", Calgary, Alberta, Canada: ASME, September 2010, Proceedings of IPC 2010 International Pipeline Conference, IPC2010-31579.
[86] MD 4-2, "Full Scale Demonstration of the Interaction of Dents with Localized Effects", Status Update Report April 2014.
[87] MD 4-3, "Mechanical Damage Instantaneous Failure Model – Numerical Simulation of Physical Tests", Andrew Francis & Associates Limited, May 2013, Pipeline Research Council International, Inc., Contract No. PR-408-124500.
[88] MD 4-9, "Fatigue Screening and Life Assessment of Pipelines, Dents and Dents Interacting with Welds", Status Update Report September 2013.

The review of the literature has identified the following knowledge gaps concerning interaction of dent and mechanical damage with other defects:

- There is very limited experimental data for dents and mechanical damage under axial load and global bending.
- Most of experimental data are obtained by testing pipes with dents created at zero pressure. There are limited experimental data that compare the strength of a mechanical damage formed under pressure with that of a mechanical damage formed without pressure.
- Experimental data or analytical models for interaction of a dent or a mechanical damage adjacent to crack-like defects have not been found at this time.
- Any analytical model for interaction of a dent and metal loss when the metal loss is located inside the dent has not been found. API 579 indicates that it is always conservative to replace a blunt metal loss with a crack. However, such an assessment can be overly conservative.
- In general there are limited experimental data on dent-defect interaction. The ongoing PRCI research project is expected to partially address this issue.

RESULTS OF QUESTIONNAIRE ON INTERACTING ANOMALIES

As part of Project DTPH5614H00005, "Threat/Anomaly Mitigation Decision-Making Process", a questionnaire was sent to a total of 21 pipeline operators and in-line inspection (ILI) service vendors regarding the relative frequency of their finding various types of interacting anomalies during integrity assessments of pipelines using ILI. The full text of the questionnaire is presented in Appendix B. Copies of the questionnaire were sent to the designated recipients on June 18, 2014. Meaningful replies were received from four pipeline operators (three hazardous liquid and one gas) and one ILI service vendor.

The Answers to the Questions

In Question No. 1 the respondent was asked to state how often they had to deal with interacting defects such as dents with metal loss, closely spaced dents, dents with cracks, closely spaced corrosion, closely spaced cracks, etc. Four respondents indicated "frequently" and one (the gas pipeline operator) responded "occasionally". These responses suggest that interacting defects are encountered frequently during integrity assessments of pipelines via ILI.

In Question No. 2 the respondents were asked to rank (1 through 7) the relative frequency with which the following types of interactions were encountered.

a. Dents with metal loss
b. Closely spaced dents
c. Dents with cracks or gouges
d. Closely spaced corrosion
e. Closely spaced cracks
f. Dents near welds
g. Other

The results were as follows.

Type of Interaction	Liquid Pipeline Operator	Liquid Pipeline Operator	Liquid Pipeline Operator	Gas Pipeline Operator	ILI Service Vendor	Total Across Row
Dents with metal loss	1	1	2	5	5	14
Closely spaced dents	6	5	3	4	3	21
Dents with cracks or gouges	2	4	4	3	7	20
Closely spaced corrosion	3	2	1	1	1	8
Closely spaced cracks	5	6	5	2	6	24
Dents near welds	7	3	6	6	4	26
Other	4	7	7	7	2	27

The totals of these rankings across each row in the table provide a crude measure of the relative importance of these types of interaction. On this basis, closely spaced corrosion appears to be the most frequently encountered type of defect interaction. Dents with metal loss would seem to be the second most frequently encountered type of interaction.

The questionnaire sought opinions on the category of "other", and five answers received are shown below in the order of the position of the respondent from left to right in the table.

1. In terms of "other" the first liquid pipeline operator described "other" as "cracks near or on welds" and ranked it No. 4.
2. The second liquid pipeline operated stated the following regarding "other". "Many dents with metal loss features (approx. 1 per 5 miles inspected with ILI each year). Most are dents with shallow corrosion, but sometimes still discover latent construction damage or new third party damage. Closely spaced corrosion can be an issue on some segments. Other features are more rare."
3. The third liquid pipeline operator provided no comment on "other".
4. The gas pipeline operator mentioned "crack on corrosion" as an important "other" interacting defect.
5. The ILI service vendor mentioned "manufacturing anomalies" as an important "other" interacting defect.

From these "other" responses it can be inferred that analysis methods for the following types of interaction need to be addressed:

- Cracks near or on welds
- Cracks in combination with corrosion (covered in the literature review)
- Manufacturing defects (apparently in conjunction with other defects, otherwise, not a subject for an interaction study)

In **Question No. 3** the respondent was asked: "How does your company prioritize interacting defects if they are discovered?" The answers (again in left to right order of operators in the table) were:

1. "Interacting defects are higher priority than non-interacting defects, especially if they are dissimilar defects, i.e. a dent with metal loss is a higher priority than a metal loss near another metal loss. If there were an area with 3 or more interacting defects (a crack in a dent on a weld) that would be a higher priority than a area with 2 interacting defects (a crack in a dent)."
2. Dents with metal loss are handled per Part 195.452 Section (h) criteria (immediate and 60-day conditions). Most other interacting defects are handled as other conditions, prioritized based on risk and time to re-assessment.
3. Most are prioritized based on 195.452 guidelines for anomalies in HCA's. Additionally, we have guidelines for prioritizing some interacting defects in non-HCA's. This process is based mostly on threat evaluations of the defects.
4. Because there is no reliable assessment method available to assess the severity of interacting defects, if any interacting defects are discovered in our pipeline, we remove them from our system.
5. Customer criteria

Answer No. 4 to Question No. 3 shows a conservative approach to interacting defects, and it indicates that there is a need for defect interaction criteria for assessing the integrity of a pipeline when interacting defects are found. Answers No. 1, 2, and 3 suggest that these particular operators are concerned with interacting defects, and that their responses to such anomalies are prioritized by the nature of the interaction. The ILI service vendor relies on the customer's criteria (Answer No. 5).

In **Question No. 4** the respondent was asked: "Does your company have a method for determining the re-assessment interval for interacting defects if they are discovered?

1. The first liquid pipeline operator indicated that for interacting metal loss defects and interacting cracks they have a way to determine the re-assessment interval. They do not have a re-assessment interval calculation for dissimilar interacting defects such as a crack at a metal loss in a dent. In such a case they would fix all of them.
2. No answer was provided.
3. We evaluate the level of threat of the defects to determine a timeframe for re-assessment. We complete a growth analysis to predict when certain growth digs are due and to help understand when the next ILI assessment needs to be completed.
4. No.
5. Industry Standards and or Corrosion Growth Assessment Interval Calculation

A possible explanation for Answer No. 1 to Question No. 4 is that the operator may be combining corroded areas and cracked areas (probably SCC) and then assessing remaining life based on the combined defects. This would seem to be a reasonable approach for same-type defects. Answer No. 2 and Answer No. 4 to Question No. 4 tend to reflect the reality that analysis methods for interaction of dissimilar defects do not exist.

Question No. 5 was as follows. Would a set of rules for prioritizing interacting defects be useful for your company?

1. Yes.
2. Yes.
3. No answer was provided.
4. Yes.
5. Yes.

This is an endorsement of the need for research on defect interaction leading to the ability to predict failure pressure and remaining life.

There was no **Question No. 6**.

In **Question No. 7**, if the answer to Question No. 5 was yes, the respondent was asked to check off the desired format for rules of prioritizing interacting defects. If the answer to Question 5 is yes, what would be the best format for these rules: a. Equations b. Pictorial c. Procedural d. Other i. If other, please describe the preferred method

1. Equations + pictorial + procedural + decision path flow chart.
2. Equations + procedural.
3. No answer was provided.
4. Equations + procedural.
5. Procedural.

One interpretation of these answers is that while equations would be desirable, operators and vendors at a minimum would like to have a standardized procedure for addressing the various types of defect interaction when they appear in ILI data. That could mean a set of criteria that indicate for cases of overlapping dissimilar anomalies how the operator should proceed, i.e., when should such anomalies be excavated and examined versus when should they be examined in the future or simply monitored by means of future ILI tool runs.

In **Question No. 8** the respondent was asked if a set of rules for determining re-assessment intervals for interacting defects would be useful.

1. Very much so, rules bring every operators and engineers into a common frame of reference, set a standard that becomes an industry benchmark, and provide defensibility if a failure occurs when an operator took industry guidance to decide appropriate response actions.
2. Not as important as equations to estimate remaining strength of an interacting defect ILI anomaly call.
3. A set of guidelines not necessarily "rules" would be useful. We feel an adequate data integration program should allow us to manage these threats. If these were "rules" then certain anomalies with lesser integrity threats may get prioritized over more injurious anomalies.
4. Yes.
5. Yes.

These answers tend to suggest that absolute numerical solutions for re-assessment intervals are less important than general guidelines for when to address potentially interacting defects when they are identified in ILI data.

In **Question No. 9**, if the answer to Question No. 8 was yes, the respondent was asked to check off the desired format for rules to determine re-assessment intervals for interacting defects.

1. Equations +pictorial + procedural + decision path flow chart
2. No answer was provided.
3. No answer was provided.
4. Equations + procedural.
5. Procedural.

The answers can be interpreted as suggesting a greater need for procedures for responding to interacting dissimilar anomalies when revealed in ILI data than for numerical solutions to calculate re-assessment intervals.

In **Question No. 10** the respondent was asked whether rules for prioritizing defect interaction and for determining re-assessment intervals should be incorporated into a standard or compiled as a stand-along document.

1. Standard.
2. Stand-alone.
3. Stand-alone.
4. Stand-alone.
5. Standard.

The majority prefer stand-alone guidelines from this work.

In **Question No. 11** the respondent was asked to describe specific needs with respect to prioritizing defect interaction or for determining re-assessment intervals that were not previously addressed in this questionnaire.

1. Calculating reassessment intervals on cracks in welds seems to be something the industry needs additional help with. Pipelife is a great tool for calculating reassessment intervals for cracks in ductile materials from pure pressure cycling fatigue, but is non-conservative for brittle materials and doesn't include a calculation of reassessment intervals for selective seam corrosion defects.
2. No answer was provided.
3. No answer was provided.
4. How to address interacting threats such as ground movement and construction defects, and preferential corrosion on ERW / FW long seam.
5. No answer was provided.

Question No. 12 solicited additional comments, if any.

1. None.
2. Biggest issue for us is a sense of over-response to deformations containing shallow metal loss, particularly corrosion. Particularly as most hazardous liquid operators are into 2nd/3rd/4th ILI assessments since a baseline inspection, unless suspected to be new third party damage, treatment as an immediate condition for a top-side deformation containing shallow corrosion requiring a de-rate seems too conservative. Being able to scientifically determine a safe operating pressure and/or justifying a non-immediate investigation would be extremely helpful in managing these defects.
3. None.
4. None.
5. None.

Conclusions

Although answers were acquired from only five respondents, four of the five indicated that they frequently encountered situations involving interacting defects when conducting pipeline integrity assessments via ILI. This would seem to indicate that pipeline operators have to deal with significant numbers of interacting defect situations, and that rules to deal with such situations could be quite useful.

The responses to the question on what the operators are finding suggest that the most common kinds of interacting defects are closely spaced corrosion anomalies and dents

containing corrosion. As the literature review shows, the current practices for judging the interaction and calculating the failure pressure levels of closely spaced corrosion anomalies as embodied in various standards appear to be adequate. However, finding a solution for the case of dents containing corrosion should take on the highest importance. Other types of interaction such as cracks in combination with corrosion, closely spaced dents, dents on or near welds, and cracks on or near welds appear to rank next in importance. As shown in the literature review, a method exists for assessing the failure pressure of a gouge in a dent, and rules for handling closely spaced cracks appear in at least one standard. It is noted that these latter methods may not be adequate for judging such anomalies solely on the basis of ILI-provided dimensions. More work confirming the methodology for these latter two types of interaction would be welcome, but it should be recognized that ILI-based dimensions involve inherent errors that need to be taken into account.

Apparently, pipeline operators and ILI service vendors see the need for criteria to define the interactions of dissimilar types of anomalies appearing in ILI data in order to know whether to excavate and examine them. Secondarily they would like to have methods to predict failure pressures and remaining life.

APPENDIX A

The SCF (dent stress concentration factor) can be calculated according to the methodology described in the PRCI Report L51810, "Guidelines for the assessment of dents on welds" by M. Rosenfeld[58]. This method was originally developed for fatigue analysis of dented girth welds but can also be used for the base metal. Dent SCF generally increases with pipe D/t and dent depth, while it decreases with increasing mean pressure level (as a result of re-rounding effect of internal pressure). Dent SCF is calculated for a unique combination of D/t, d/D and P_m as below:

$$k_d = 1 + \left(\frac{d_0}{t} m_y + b_y\right)\frac{2t}{D} \qquad \text{Equation 36}$$

$$b_y = \begin{cases} -5 \quad if\ \frac{D}{t} \leq 30 \\ b_a + \frac{b_b}{D/t} + \frac{b_c}{(D/t)^2} + \frac{b_d}{(D/t)^3} \quad if\ \frac{D}{t} > 30 \end{cases} \qquad \text{Equation 37}$$

$$b_a = 2.215 + 0.0166P_m - 0.00002946(P_m)^2 \qquad \text{Equation 38}$$

$$b_b = -526.3 - 3.299P_m + 0.004133(P_m)^2 \qquad \text{Equation 39}$$

$$b_c = 180400 + 70.11P_m - 0.1527(P_m)^2 \qquad \text{Equation 40}$$

$$b_d = -5069500 + 290.5P_m + 1.708(P_m)^2 \qquad \text{Equation 41}$$

$$m_y = \begin{cases} a_p + \frac{b_p}{D/t} + \frac{c_p}{(D/t)^2} \quad if\ \frac{D}{t} \leq 50 \\ a_p + b_p\frac{D}{t} \quad if\ \frac{D}{t} > 50 \end{cases} \qquad \text{Equation 42}$$

where

d_0 is dent depth under zero internal pressure, inch,

D is pipe OD, inch,

t is pipe wall thickness, inch, and

P_m is the mean pressure, psig.

The values of a_p, b_p, and c_p are calculated according to Table 19. The dent SCF tends to decrease by increasing pressures due to re-rounding effect of internal pressure, therefore conducting the analysis for the maximum operating pressure (MOP) may not cover the whole spectrum of pressures. It is recommended repeating the assessment for several intermediate pressures in addition to MOP. Moreover, extrapolation beyond the following limits is not recommended:

$P_m \leq 1{,}500$ psig,

$D/T \geq 20$,

$d_p/D \leq 0.06$.

Table 19. Values of a_p, b_p and c_p for Dent Stress Concentration Factor Calculations

	D/t≤ 50		**D/t > 50**	
	P≤900	**P>900**	**P≤900**	**P>900**
a_p	$-6.87P_m+4490$	P_m-2580	$-3P_m+3475$	$-0.0775P_m+848$
b_p	$309P_m-118100$	$-80P_m+231500$	$0.02P_m-20.7$	$-0.00065P_m-2.03$
c_p	$-3472P_m+930700$	$1154P_m-3233000$	NA	NA

APPENDIX B

Threat/Anomaly Mitigation Decision-Making Process Questionnaire

Prepared by:
Bob Francini
Phone: (614) 410-1605
Email: bob.francini@applusrtd.com

Kiefner and Associates, Inc. is working on a project for PHMSA on the threat/anomaly mitigation decision making processes. The objective of this project is to strengthen pipeline industry consensus standards such as ASME B31.8S and API Standard 1160 by providing enhanced guidance for conducting the technical aspects of a pipeline integrity management program. Specifically, better guidance is needed for deciding when the combined effects of two or more threats and the associated anomalies create a higher probability of failure than the individual threats/anomalies themselves. This project builds on the existing technology for defect assessment. New approaches to defect interaction and probabilistic methods are being explored. If successful, the technology could be applied to enhance the above-mentioned consensus standards.

1. How often does your company deal with interacting defects such as dents with metal loss, closely spaced dents, dents with cracks, closely spaced corrosion, closely spaced cracks, etc.?

2. If the answer to Question 1 is a. or b. please rank the frequency of each type of defect:

a. Dents with metal loss
b. Closely spaced dents
c. Dents with cracks or gouges
d. Closely spaced corrosion
e. Closely space cracks
f. Dents near welds
g. Other

If other, please describe the types of defects

3. How does your company prioritize interacting defects if they are discovered?

4. Does your company have a method for determining the re-assessment interval for interacting defects if they are discovered?

If yes, can you briefly describe the approach your company takes for determining re-assessment intervals?

5. Would a set of rules for prioritizing interacting defects be useful for your company?

6. If the answer to Question 5 is yes, what would be the best format for these rules:

   a. Equations
   b. Pictorial
   c. Procedural
   d. Other

   If other, please describe the preferred method:

7. Would a set of rules for determining re-assessment intervals for interacting defects be useful for your company?

8. If the answer to Question 7 is yes, what would be the best format for these rules:

   a. Equations
   b. Pictorial
   c. Procedural
   d. Other

   If other, please describe the preferred method:

9. Would you like to see rules for prioritizing and determining re-assessment intervals for interacting defects incorporated into Standards or as stand-alone guidelines?

a. Incorporate into standards
b. Stand-alone guidelines

10. Do you have specific needs with regard to prioritizing and/or determining re-assessment intervals that have not been covered by this questionnaire?

If yes, please describe briefly.

11. Additional comments

APPENDIX C

Table 20. Reference Related to Corrosion-with-Corrosion/Crack

Reference Number	Standard, Technical Report, or Journal Article	Year of Publication	Interaction Type	Experimental or Analytical of Both
1	Journal Article	1969	corrosion-with-corrosion	Experimental
2	Journal Article	1990	corrosion-with-corrosion	Both
3	Journal Article	1990	corrosion-with-corrosion	Experimental
4	Journal Article	1990	corrosion-with-corrosion	Experimental
5	Journal Article	1992	corrosion-with-corrosion	Experimental
6	Journal Article	1993	corrosion-with-corrosion	Experimental
7	Journal Article	1996	corrosion-with-corrosion	Analytical
8	Journal Article	1996	corrosion-with-corrosion	Analytical
9	Journal Article	2005	corrosion-with-corrosion	Experimental
10	Journal Article	2006	corrosion-with-corrosion	Experimental
11	Journal Article	2006	corrosion-with-corrosion	Analytical
12	Journal Article	2006	corrosion-with-corrosion	Analytical
13	Journal Article	2006	corrosion-with-corrosion	Analytical
14	Journal Article	2008	corrosion-with-corrosion	Experimental
15	Technical Report	2000	corrosion-with-corrosion	Experimental
16	Technical Report	2002	corrosion-with-corrosion	Experimental
17	Technical Report	2003	corrosion-with-corrosion	Analytical
18	Technical Report	2005	corrosion-with-corrosion	Experimental
19	Journal Article	2008	corrosion-with-corrosion	Analytical
20	Journal Article	2007	corrosion-with-corrosion	Analytical
23	Technical Report	2004	corrosion-with-weld	Both
53	Journal Article	2008	corrosion-with-crack	Analytical
54	Technical Report	2010	corrosion-with-crack	Experimental
API 579-1	Standard	2007	corrosion-with-corrosion	NA
ASME B31G	Standard	2009	corrosion-with-corrosion	NA
ASME B31.4	Standard	2012	corrosion-with-corrosion	NA
DNV-RP-F101	Standard	2010	corrosion-with-corrosion	NA
BS 7910	Standard	2013	corrosion-with-corrosion	NA
CSA Z662	Standard	2011	corrosion-with-corrosion	NA
PDAM	Standard	2003	corrosion-with-corrosion	NA

Table 21. Reference Related to Crack-with-Crack

Reference Number	Standard, Technical Report, or Journal Article	Year of Publication	Interaction Type	Experimental or Analytical of Both
32	Technical Report	1997	crack-with-crack	Analytical
33	Journal Article	1993	crack-with-crack	Analytical
34	Journal Article	2004	crack-with-crack	Experimental
35	Journal Article	2004	crack-with-crack	Experimental
36	Journal Article	1982	crack-with-crack	Analytical
37	Journal Article	1990	crack-with-crack	Both
38	Journal Article	1996	crack-with-crack	Experimental
39	Journal Article	1994	crack-with-crack	Analytical
40	Technical Report	1990	crack-with-crack	Analytical
41	Journal Article	2008	crack-with-crack	Experimental
42	Journal Article	2006	crack-with-crack	Analytical
43	Journal Article	2010	crack-with-crack	Analytical
44	Journal Article	2010	crack-with-crack	Analytical
45	Journal Article	2006	crack-with-crack	Analytical
46	Journal Article	1999	crack-with-crack	Analytical
47	Journal Article	2003	crack-with-crack	Analytical
48	Journal Article	2007	crack-with-crack	Experimental
50	Journal Article	1996	crack-with-crack	Analytical
51	Journal Article	2000	crack-with-crack	Analytical
52	Journal Article	2002	crack-with-crack	Analytical
API 579-1	Standard	2007	crack-with-crack	NA
BS 7910	Standard	2013	crack-with-crack	NA
CSA Z662	Standard	2011	crack-with-crack	NA
API 1104	Standard	2013	crack-with-crack	NA
FITNET	Standard	2006	crack-with-crack	NA
PDAM	Standard	2003	crack-with-crack	NA
CEPA	Standard	2007	crack-with-crack	NA
BS 7910	Standard	1999	crack-with-crack	NA
R6/4	Standard	2001	crack-with-crack	NA
ASME	Standard	1980	crack-with-crack	NA
BSI PD6493	Standard	1991	crack-with-crack	NA
ASME	Standard	1992	crack-with-crack	NA
BS 7910	Standard	2005	crack-with-crack	NA

Table 22. Reference Related to Mechanical Damage

Reference Number	Standard, Technical Report, or Journal Article	Year of Publication	Interaction Type	Experimental or Analytical of Both
56	Technical Report	2003	dent-with-gouge/crack/corrosion	Both
58	Technical Report	1999	dent-with-weld	Analytical
64	Journal Article	2000	dent-with-gouge	Experimental
65	Journal Article	2013	dent-with-crack	Experimental
66	Technical Report	1995	dent-with-gouge	Both
67	Technical Report	1995	dent-with-gouge	Both
68	Technical Report	1995	dent-with-gouge	Both
69	Technical Report	1995	dent-with-gouge	Both
70	Technical Report	1995	dent-with-gouge	Both
71	Technical Report	1994	dent-with-gouge/weld	Experimental
72	Technical Report	1997	dent-with-dent/weld/corrosion	Experimental
73	Journal Article	1998	dent-with-crack	Both
76	Journal Article	2007	dent-with-gouge	Experimental
77	Journal Article	2006	dent-with-crack	Analytical
78	Journal Article	2006	dent-with-crack	Analytical
80	Journal Article	2002	dent-with-dent	Analytical
81	Journal Article	2008	dent-with-dent	Analytical
82	Technical Report	2007	dent-with-weld	Analytical
83	PhD Thesis	2010	dent-with-dent/weld/corrosion	Analytical
84	Technical Report	2013	dent-with-weld	Experimental
85	Journal Article	2010	dent-with-weld/corrosion	Both
86	Technical Report	Ongoing	dent-with-weld/corrosion	Experimental
87	Technical Report	Ongoing	dent-with-gouge	Analytical
88	Technical Report	Ongoing	dent-with-weld	Experimental
ASME B31.4	Standard	2012	dent-with-corrosion/crack	NA
ASME B31.8	Standard	2010	dent-with-crack/gouge	NA
CSA Z662	Standard	2011	dent-with-corrosion/crack	NA
PDAM	Standard	2003	dent-with-gouge/crack/weld	NA

US DOT - PHMSA

Final Report No. 16-025

Final Report

Threat/Anomaly Mitigation Decision-Making Process – Annex B. Deterministic and Probabilistic Approaches for Scheduling Mitigations of Corrosion Regions

Jing Ma

February 23, 2016

0339-1402

Kiefner and Associates, Inc. is an Applus RTD company.

Intentionally blank

Final Report No. 16-025

Final Report

on

THREAT/ANOMALY MITIGATION DECISION-MAKING PROCESS
ANNEX B. DETERMINISTIC AND PROBABILISTIC APPROACHES FOR SCHEDULING MITIGATIONS OF CORROSION REGIONS
DTPH5614H00005

to

U.S. DEPARTMENT OF TRANSPORTATION – PIPELINE AND HAZARDOUS MATERIALS SAFETY ADMINISTRATION

February 23, 2016

by

Jing Ma

Kiefner and Associates, Inc.
5115 Parkcenter Avenue, Suite 200
Dublin, OH 43017

0339-1402

DISCLAIMER

This document presents findings and/or recommendations based on engineering services performed by employees of Kiefner and Associates, Inc. The work addressed herein has been performed according to the authors' knowledge, information, and belief in accordance with commonly accepted procedures consistent with applicable standards of practice, and is not a guaranty or warranty, either expressed or implied.

The analysis and conclusions provided in this report are for the sole use and benefit of the Client. No information or representations contained herein are for the use or benefit of any party other than the party contracting with Kiefner. The scope of use of the information presented herein is limited to the facts as presented and examined, as outlined within the body of this document. No additional representations are made as to matters not specifically addressed within this report. Any additional facts or circumstances in existence but not described or considered within this report may change the analysis, outcomes and representations made in this report.

TABLE OF CONTENTS

INTRODUCTION 1

BACKGROUND 1

DETERMINISTIC SCHEDULE OF CORROSION REMEDIATION 2

PROBABILISTIC SCHEDULE OF CORROSION REMEDIATION 11

OTHER SPECIFICATIONS OF ASME B31.8S 23

LIST OF FIGURES

Figure 1. Timing for Scheduled Responses: Time-Dependent Threats, Prescriptive Integrity Management Plan (A reproduction of ASME B31.8S-2010, Figure 4) 3

Figure 2. Burst Stress Relative to Flow Stress vs. Anomaly Length 7

Figure 3. Response Time Comparison between Anomalies with Finite and Infinite Length at MAOP=72%SMYS 7

Figure 4. Response Time Comparison between Anomalies with Finite and Infinite Length at MAOP=50%SMYS 8

Figure 5. Response Time Comparison between Anomalies with Finite and Infinite Length at MAOP=30%SMYS 8

Figure 6. Overlaid Response Curves with the Identical Corrosion Growth Rate 9

Figure 7. Probability Density Function for Actual WT/Nominal WT 12

Figure 8. Probability Density Function for Actual Yield Strength/SMYS 13

Figure 9. Probability Density Function for Actual Anomaly Depth Having 50%WT Reported by In-line Inspection 13

Figure 10. Probability Density Function for Actual Anomaly Length Having 6.36*Sqrt(Dt) Reported by In-line Inspection 14

Figure 11. Burst Pressure Prediction Error of Modified B31G Model 14

Figure 12. Failure Probability vs. Nominal Failure Pressure Ratio 16

Figure 13. Relative Failure Probability vs. Nominal Failure Pressure Ratio 17

Figure 14. Overlaid Response Curves as a Function of Failure Pressure Ratio 18

LIST OF TABLES

Table 1. Integrity Assessment Intervals: Time-Dependent Threats, Internal and External Corrosion, Prescriptive Integrity Management Plan (A reproduction of ASME B31.8S-2010, Table 3) 4

Table 2. Integrity Re-assessment Interval for the Same Growth Rate 10

Table 3. Probability Density Functions used in Calculations 12

Table 4. Probability of Failure at FPR=1.1 for Different MAOPs.....15
Table 5. Required FPR to Achieve Normalized POF=1.0.....16
Table 6. Integrity Re-assessment Interval for the Same Growth Rate and the Same POF for Immediate Repair.....18
Table 7. POF Based on Normal Growth Rate Distributions.....21
Table 8. POF Based on Lognormal Growth Rate Distributions.....22
Table 9. Required FPR and Re-assessment Interval to Maintain the Same POF.....23

Threat/Anomaly Mitigation Decision-Making Process – Annex B. Deterministic and Probabilistic Approaches for Scheduling Mitigations of Corrosion Regions

Jing Ma

INTRODUCTION

Pipeline operators must excavate and examine anomalies discovered through ILI, ECDA, ICDA, or SCCDA in a timely manner to assure that critical flaws are repaired before they can become large enough to cause a pipeline to fail at its maximum operating pressure. Pipeline operators must also periodically re-assess their pipelines that are located in or could affect high consequence areas. While prescriptive regulations often require examinations of anomalies or re-assessments to be carried out after specific time periods, a more rational way to schedule excavations or to conduct re-assessments would be to schedule them based on the sizes of anomalies remaining after the most recent assessment, the applicable rate of deterioration, and sizes of anomalies that would cause the pipeline to fail at its maximum operating pressure. Three types of anomalies and their related interaction criteria will be addressed in consecutive interim reports. The mitigation scheduling of corrosion areas will be specifically discussed in this report by following both deterministic and probabilistic approaches.

BACKGROUND

Part 192 and Part 195 of U.S. Code of Federal Regulations Title 49: Transportation incorporate the pipeline integrity management for gas and hazardous liquid transmission pipelines respectively. These regulations state the types of anomalies pipeline operators must address, they prescribe the types of assessment techniques that operators can employ to locate and evaluate anomalies, and they prescribe re-assessment intervals for continued monitoring and remediation. This project was conceived to develop a more flexible approach to pipeline integrity management that would allow pipeline operators to base re-assessments and remediation intervals on the actual rates of anomaly growth determined from measurements and experience. Both deterministic and probabilistic approaches are to be considered.

DETERMINISTIC SCHEDULE OF CORROSION REMEDIATION

CFR 192 Subpart O references ASME B31.8S for managing gas pipeline integrity. Liquid operators implement ASME B31.8S on a voluntary basis. The immediate response and re-assessment intervals for corrosion anomalies are defined in Section 7 Figure 4 and Section 5 Table 3 in ASME B31.8S-2010 for the mitigation of time-dependent growth of internal and external metal loss, as illustrated in Figure 1 and Table 1. These schedules warrant safety in a prescriptive-based manner. Additionally, a performance-based integrity management plan can extend the repair or re-inspection interval in conjunction with a sound engineering critical assessment. It is shown below that the criteria embodied in ASME B31.8S-2010, Figure 4 can offer flexibility in scheduling re-assessment of corrosion anomalies provided that a pipeline operator uses an actually-measured corrosion rate determined for a particular pipeline.

As shown in Figure 1 (a reproduction of ASME B31.8S-2010, Figure 4), the immediate response criteria are the same for all the operating pressure levels, i.e. any indications characterized with a failure pressure level less than 1.1 times the MAOP as predicted by ASME B31G or equivalent require an immediate response. An operator must determine any temporary reduction in operating pressure required using ASME B31G or AGA Pipeline Research Committee Project PR-3-805 RSTRENG, or reduce the operating pressure to a level not exceeding 80 percent of the level at the time the condition was discovered, or shut down the pipeline until the repair is completed.

From the deterministic perspective, the failure pressure ratio (FPR) of 1.1 in terms of the burst pressure calculated from ASME B31G or RSTRENG substantiates a sufficient safety margin for imminent action irrespective of the operating stress level. From the probabilistic perspective, the probability of failure with an FPR of 1.1 is relatively small for an operating pressure level corresponding to 72% of SMYS but the failure probability associated with an FPR of 1.1 increases with decreasing operating stress levels below 72% of SMYS. The implications of this are discussed later in this report.

Table 1 contains the re-assessment intervals for hydrostatic testing, in-line inspection (ILI) and direct assessment. It embodies the content equivalent to Figure 1. The maximum re-assessment interval is 20 years, 15 years and 10 years for operating pressure no greater than 30%SMYS, between 30%SMYS and 50%SMYS, and greater than 50%SMYS. To achieve the same re-assessment interval for the subsequent hydrostatic test or ILI, the pipeline with lower operating pressure has to be hydrostatically tested to a higher level of FPR, or to carry a larger value of FPR predicted from ILI anomalies. The corrosion growth is assumed as linear with respect to the elapsed time. No time-dependent kinetics model is considered.

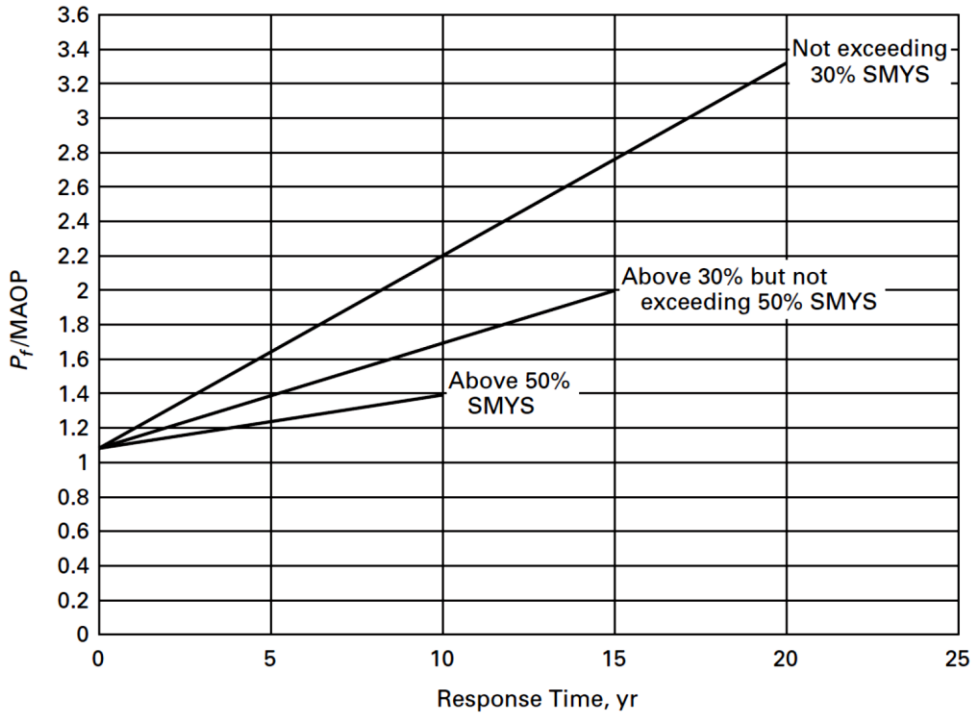

Figure 1. Timing for Scheduled Responses: Time-Dependent Threats, Prescriptive Integrity Management Plan (A reproduction of ASME B31.8S-2010, Figure 4)

Table 1. Integrity Assessment Intervals: Time-Dependent Threats, Internal and External Corrosion, Prescriptive Integrity Management Plan (A reproduction of ASME B31.8S-2010, Table 3)

		Criteria		
Inspection Technique	Interval, yr [Note (1)]	Operating Pressure Above 50% of SMYS	Operating Pressure Above 30% But Not Exceeding 50% of SMYS	Operating Pressure Not Exceeding 30% of SMYS
Hydrostatic testing	5	TP to 1.25 times MAOP [Note (2)]	TP to 1.39 times MAOP [Note (2)]	TP to 1.65 times MAOP [Note (2)]
	10	TP to 1.39 times MAOP [Note (2)]	TP to 1.65 times MAOP [Note (2)]	TP to 2.20 times MAOP [Note (2)]
	15	Not allowed	TP to 2.00 times MAOP [Note (2)]	TP to 2.75 times MAOP [Note (2)]
	20	Not allowed	Not allowed	TP to 3.33 times MAOP [Note (2)]
In-line inspection	5	P_f above 1.25 times MAOP [Note (3)]	P_f above 1.39 times MAOP [Note (3)]	P_f above 1.65 times MAOP [Note (3)]
	10	P_f above 1.39 times MAOP [Note (3)]	P_f above 1.65 times MAOP [Note (3)]	P_f above 2.20 times MAOP [Note (3)]
	15	Not allowed	P_f above 2.00 times MAOP [Note (3)]	P_f above 2.75 times MAOP [Note (3)]
	20	Not allowed	Not allowed	P_f above 3.33 times MAOP [Note (3)]
Direct assessment	5	Sample of indications examined [Note (4)]	Sample of indications examined [Note (4)]	Sample of indications examined [Note (4)]
	10	All indications examined	Sample of indications examined [Note (4)]	Sample of indications examined [Note (4)]
	15	Not allowed	All indications examined	All indications examined
	20	Not allowed	Not allowed	All indications examined

NOTES:
(1) Intervals are maximum and may be less, depending on repairs made and prevention activities instituted. In addition, certain threats can be extremely aggressive and may significantly reduce the interval between inspections. Occurrence of a time-dependent failure requires immediate reassessment of the interval.
(2) TP is test pressure.
(3) P_f is predicted failure pressure as determined from ASME B31G or equivalent.
(4) For the Direct Assessment Process, the intervals for direct examination of indications are contained within the process. These intervals provide for sampling of indications based on their severity and the results of previous examinations. Unless all indications are examined and repaired, the maximum interval for reinspection is 5 yr for pipe operating above 50% SMYS and 10 yr for pipe operating up to but not exceeding 50% of SMYS.

Consider an example. Assume an initial flaw representing a failure stress of 100%SMYS irrespective of the actual operating pressure level, i.e. FPR=3.3 for MAOP=30%SMYS; FPR=2.0 for MAOP=50%SMYS; FPR=1.39 for MAOP=72%SMYS. To guarantee the same safety margin FPR=1.1, the final flaw size is larger for lower operating pressure, which means that it takes a longer time to grow and leads to a longer allowable re-assessment interval. By the same token, for the same FPR, a pipeline with lower operating pressure has to be re-inspected earlier than the one carrying higher operating pressure as a result of the smaller absolute allowable pressure difference from 1.1MAOP.

These response curves were generated by Kiefner in 2002[1]. For each curve, a hypothetical case of a very long (infinite) corrosion region with uniform depth was assumed. The remaining wall thickness required to barely survive a certain operating stress can be calculated by:

$$rwt = t\left(\frac{\alpha \cdot \mathrm{SMYS}}{\mathrm{SMYS}+10}\right), \qquad \text{Equation 1}$$

Where rwt is the remaining wall thickness, t is the nominal wall thickness, SMYS is the specified minimum yield strength for pipe material in units of ksi, SMYS+10 (also in units of ksi) is the flow stress (assumed to be the failure stress) of the material, and α is the ratio of the operating stress level to SMYS. The corrosion growth rate R relative to the nominal wall thickness per year is listed individually for three typical operating conditions, 72% of SMYS, 50% of SMYS, and 30% of SMYS[2]:

$$R_{72} = 0.028\frac{\mathrm{SMYS}}{\mathrm{SMYS}+10}, \qquad \text{Equation 2}$$

$$R_{50} = 0.033\frac{\mathrm{SMYS}}{\mathrm{SMYS}+10}, \qquad \text{Equation 3}$$

$$R_{30} = 0.035\frac{\mathrm{SMYS}}{\mathrm{SMYS}+10}. \qquad \text{Equation 4}$$

It is noticeable that the inherent corrosion rates in three curves are not equal to each other. For properly using the criteria embodied in Figure 1, the actual rate associated with a particular pipeline has to be lower than the above values.

A wide range of pipe geometry, pipe grade, anomaly length and depth, along with pipeline design factor was explored to calculate the growth rate satisfying the ASME B31.8S-2010, Figure 4. The metal loss growth was assumed to occur in the depth direction only. The initial and final depths stand for the failure stress equal to 100%SMYS and 1.1MAOP. Therefore the rate is calculated for 10 years for Class 1 and Class 2, 15 years for Class 3, and 20 years for Class 4. It is noted that the failure consequence belonging to different class locations is not taken into account from the risk mitigation perspective. As a rule of thumb, the critical rate per year is 0.022t. This value is consistent with the Equation 2 prediction, in the sense that the required growth rate is smaller for a lower pipe grade. Particularly, the pipe of Grade B would

[1] Kiefner, J.F., "Criteria for Reinspection Intervals for Low-Stress Steel Pipelines", American Gas Association, January 8, 2002.

[2] The original formula was based on 1.0 MAOP as the immediate condition rather than 1.1 MAOP.

produce the lower bound $0.028 \cdot 35/45 \approx 0.022$, which matches up with the finite length studies.

Three questions arise from the prior investigation as below.

(1) Will the curves remain straight for a corrosion area with finite length?

The Modified B31G model is widely used for corrosion-caused burst pressure prediction. The formula is expressed as:

$$\sigma_f = \bar{\sigma}\left(\frac{1-0.85\frac{d}{t}}{1-0.85\left(\frac{d}{tM_T}\right)}\right) \qquad \text{Equation 5}$$

$$M_T = \left(1+0.6275\frac{L^2}{Dt}-0.003375\frac{L^4}{D^2t^2}\right)^{0.5} \text{ for } \frac{L^2}{Dt} \le 50 \qquad \text{Equation 6}$$

$$M_T = 0.032\left(\frac{L^2}{Dt}\right)+3.3 \text{ for } \frac{L^2}{Dt} > 50 \qquad \text{Equation 7}$$

Where,

σ_f is the predicted hoop stress at failure, psig
$\bar{\sigma}$ is the flow stress of the material (SMYS + 10 ksi)
t is the nominal wall thickness of the pipe, inch
D is the outside diameter of the pipe, inches
d is the depth of the anomaly, inch
L is the length of the anomaly, inches

In terms of the bulging factor $6.36\sqrt{Dt}$ is the theoretical maximum effective length as illustrated in Figure 2, whereby any additional corroded length would not affect the burst pressure. Figure 3, Figure 4 and Figure 5 exhibit the response time variation between infinite-length anomaly and finite-length anomaly for MAOP equal to 72%SMYS, 50%SMYS, and 30%SMYS respectively. To generate these results, the pipe material was assumed to be Grade B, and the corrosion growth rates were calculated from each maximum allowable re-assessment interval, i.e. 10 years for 72%SMYS, 15 years for 50%SMYS, and 20 years for 30%SMYS. The difference is fairly negligible accounting for the finite length effect. However, the difference magnitude turns to be larger for lower operating pressure, which has a maximum of roughly half a year for MAOP equal to 30%SMYS at FPR close to 2.25. In other words, this justifies

$6.36\sqrt{Dt}$ is a reliable length estimator for a very long but finite corrosion region. For this reason, the following calculations are all based on this length assumption.

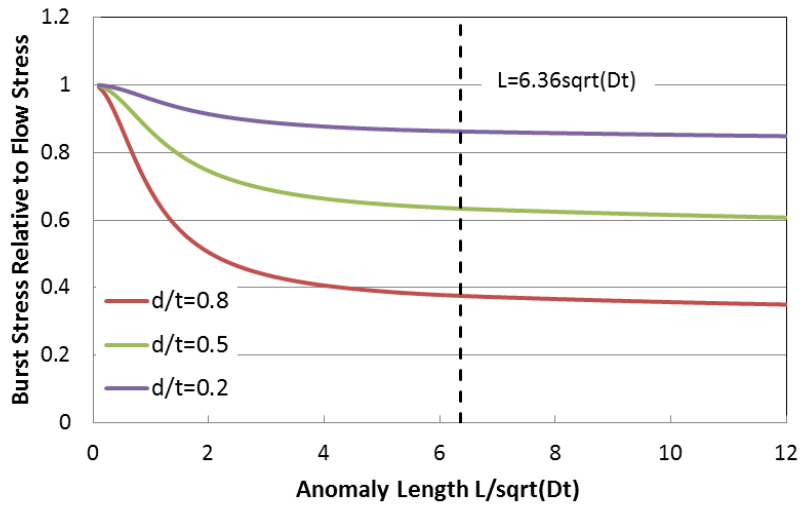

Figure 2. Burst Stress Relative to Flow Stress vs. Anomaly Length

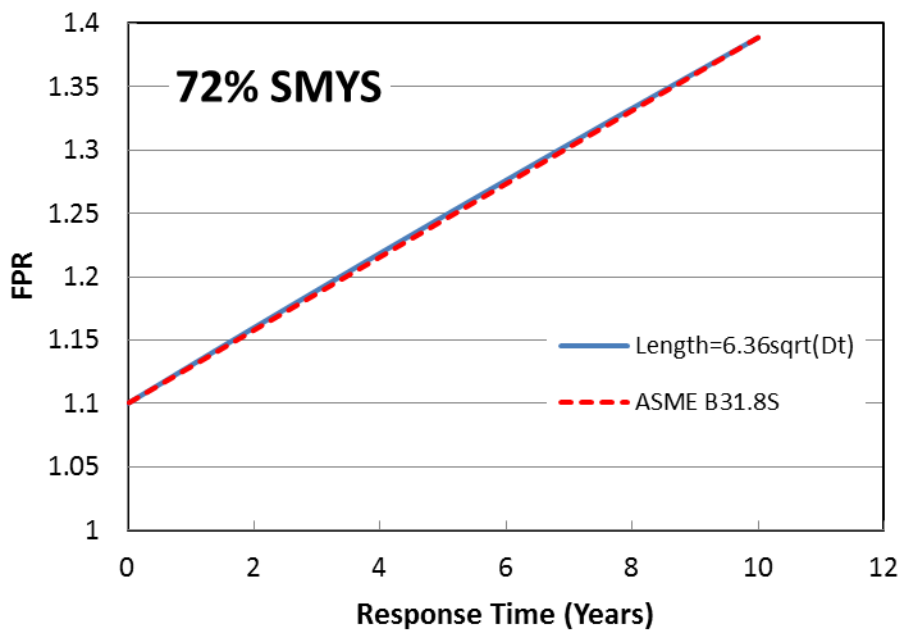

Figure 3. Response Time Comparison between Anomalies with Finite and Infinite Length at MAOP=72%SMYS

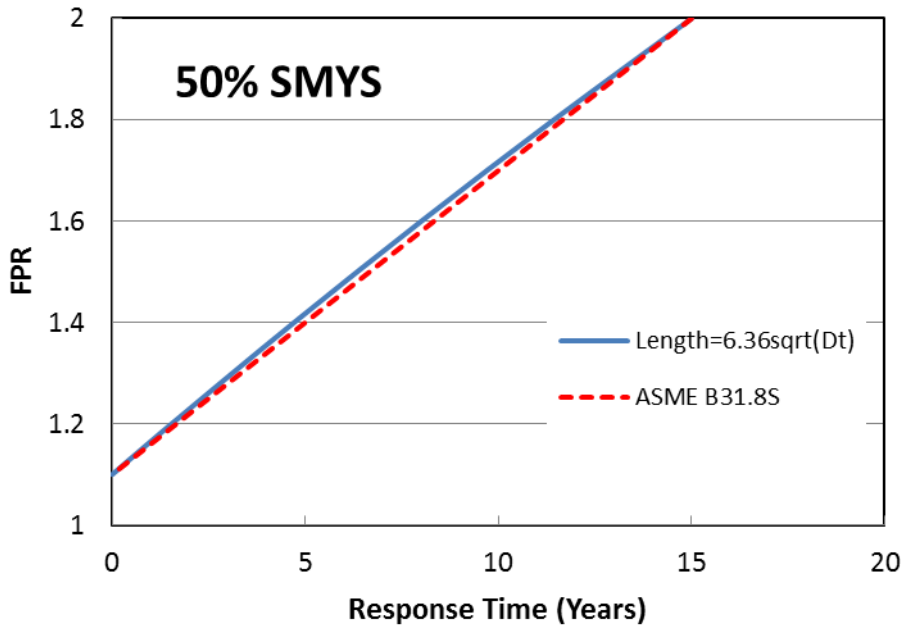

Figure 4. Response Time Comparison between Anomalies with Finite and Infinite Length at MAOP=50%SMYS

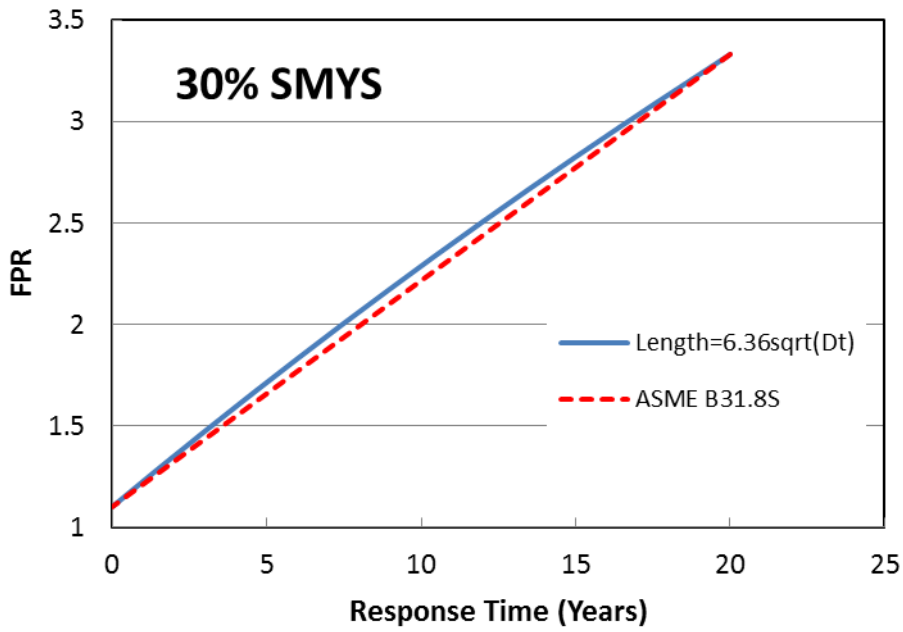

Figure 5. Response Time Comparison between Anomalies with Finite and Infinite Length at MAOP=30%SMYS

(2) What would the curves look like with the exact same growth rate?

As discussed above, the corrosion growth rates intrinsic to the ASME B31.8S-2010, Figure 4 are different from curve to curve. The lower bound of 2.2% of wall thickness per year was

introduced by the AGA report listed in Reference [1]. In the context of an identical growth rate, the response curves are plotted as dashed lines and overlaid to the original solid lines in Figure 6. Given that the lower bound is essentially suggested from MAOP equal to 72%SMYS, that response curve remains the same. The other response curves representing MAOP equal to 50%SMYS and 30%SMYS deviate from the original and move towards the longer re-assessment interval direction. This mitigation gain with respect to time is compromised by the decreased allowable corrosion growth rate.

ASME B31.8S-2010, Table B-1 gives average corrosion rates as follows:

3 mils per year for soil resistivity greater than 15,000 ohm-cm and no active corrosion
6 mils per year for soil resistivity between 1,000 and 15,000 ohm-cm and/or active corrosion
12 mils per year for soil resistivity less than 1,000 ohm-cm

In terms of the 2.2% of wall thickness limit, 12 mils per year would indicate that response times for any pipeline with a wall thickness greater than 0.545 inch could be evaluated according to Figure 6. For thinner wall pipes, if the actual corrosion rate does not exceed 2.2% of wall thickness, the dashed lines in Figure 6 are applicable. Table 2 captures the required pressure levels achieved from hydrostatic testing or predicted by in-line inspection for every 5 year interval increase. As can be seen in Figure 6, a small change of corrosion growth rate leads to substantial differences in re-assessment intervals. For example, when the growth rate decreases 0.5% of wall thickness, the maximum interval increases from 20 years to 30 years for pipelines operating at 30%SMYS.

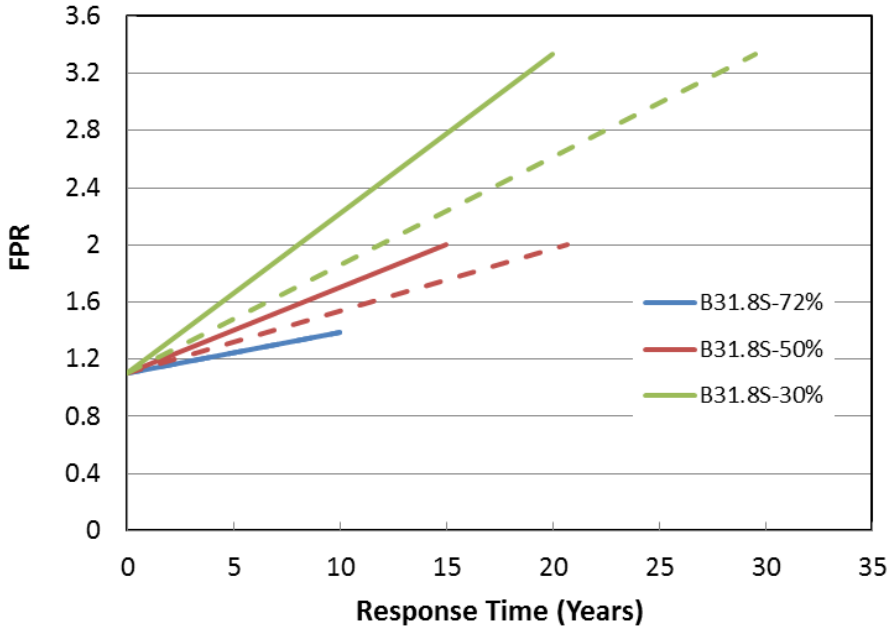

Figure 6. Overlaid Response Curves with the Identical Corrosion Growth Rate

Table 2. Integrity Re-assessment Interval for the Same Growth Rate

Interval (year)	Criteria for Hydrostatic Test or ILI Predicted Failure Pressure (MAOP)		
	Operating Pressure Above 50% of SMYS	Operating Pressure Above 30% of SMYS Not Exceeding 50% of SMYS	Operating Pressure Not Exceeding 30% of SMYS
0	1.10	1.10	1.10
5	1.25	1.32	1.48
10	1.39	1.54	1.86
15	Not allowed	1.75	2.23
20	Not allowed	1.97	2.61
25	Not allowed	Not allowed	2.99
30	Not allowed	Not allowed	3.33

(3) What is the effect of interaction between corrosion areas on response schedule?

The potential interaction between corrosion areas after growth is not taken into account in the ASME B31.8S-2010, Figure 4. If specifying a growth rate to be 2.2% of wall thickness, after the maximum allowed 20 years, the corrosion growth is 0.44 times wall thickness. This value compared with the interaction criteria of 6.0 times wall thickness is only 7.33%. The conservatism of 6.0 times wall thickness as the critical interaction distance along the axial as well as circumferential direction was ascertained in Task 2 of this project. In this way, it illustrates that with 6t as the interaction criteria for immediate repair, flaws not interacting at present will be unlikely to interact until the end of the maximum re-assessment interval for all operating conditions. It also validates the underlying depth-only growth postulation during the derivation of the ASME B31.8S-2010, Figure 4. The rationale is that 0.44t is only a tiny amount of square root of D·t, such that the growth along the axial direction won't affect the burst pressure through the bulging factor.

The use of the ASME B31.8S-2010, Figure 4 (Figure 1 of this report) allows some flexibility for operators to calculate re-assessment intervals that may differ from the prescriptive and arbitrary re-assessment intervals associated with the ASME B31.8S-2010, Table 3 (Table 1 of this report). In cases where corrosion rates are found to be lower than 2.2% of wall thickness per year (the basis of the 72%-of-SMYS sloping line on Figure 1), the re-assessment intervals could be longer than indicated by the prescribed sloping lines.

PROBABILISTIC SCHEDULE OF CORROSION REMEDIATION

Failure pressure ratio plays the role of safety factor from a deterministic aspect. However, the parameters and the model algorithm are subject to uncertainty by their nature. For instance, the actual pipe yield strength varies from SMYS, the actual wall thickness varies from the nominal value, and the anomaly size varies from reported by in-line inspection, etc. Consequently the actual failure pressure may not be the one calculated from the above deterministic procedure with fixed inputs. From a probabilistic perspective, the confidence level of each nominal failure pressure ratio can be described by the failure probability of the actual burst pressure being less than MAOP[3]. Over the 10-year period of use of ASME B31.8S criteria, no failure has occurred because of an inadequate or late response on the part of a pipeline operator who based their response on sound ILI data. Nonetheless, the probability of failure at the MAOP is not zero for an FPR of 1.1 or for any FPR for that matter.

Probability Distributions of the Key Input Parameters

The degree of uncertainty is reflected by some probability density functions. The applied functions in the following calculation are listed in Table 3 with the explanation of sources. The distributions are visualized in Figure 7 through Figure 11 with the highlights of 90% confidence level.

[3] Kariyawasam, S. and Huang, T., "How Safe Failure Pressure Ratios Are Related to %SYMS", IPC 2014-33647, Proceedings of the 2014 10th International Pipeline Conference, September 29-October 3, 2014, Calgary, Alberta, Canada.

Table 3. Probability Density Functions used in Calculations

Variable	Function Type	Function Parameters	Source
Wall thickness	Normal	μ=1.01*nominal, COV=1%	CSA Z662 Annex O[4,5]
SMYS	Normal	μ=1.09*SMYS, COV=4.4%	Mill test reports[6]
Anomaly depth	Normal	μ=indicated %WT, σ=7.8%WT	Typical ILI spec.[7]
Anomaly length	Normal	μ=indicated length, σ=0.61 inch	Typical ILI spec.[8]
Model error	Gamma	α=2.175, β=0.225, shift=0.914	Advantica report[9]

Note: For the normal distribution, μ is the mean value, COV is the coefficient of variance, and σ is the standard deviation. For the Gamma distribution, α is the shape parameter, β is the scale parameter, and γ is the shift amount.

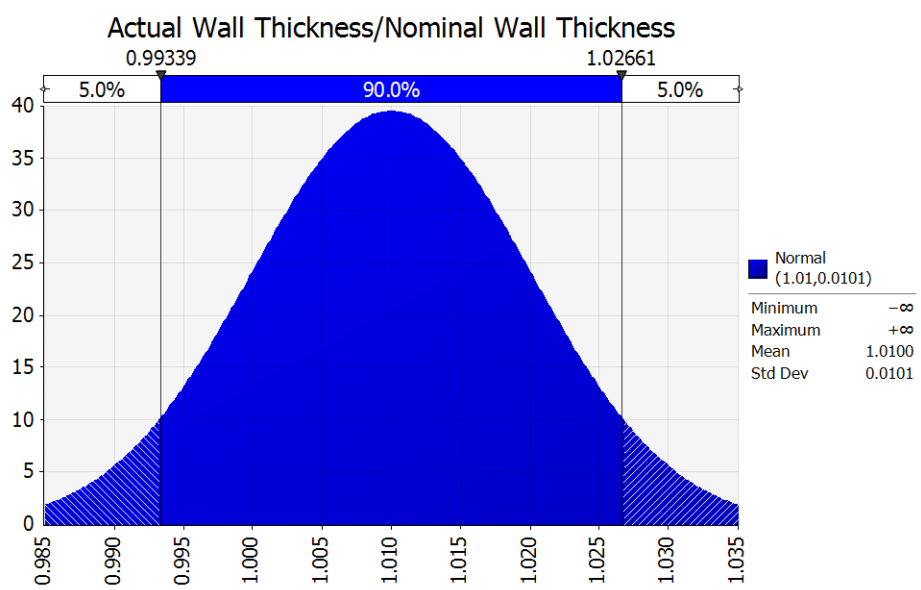

Figure 7. Probability Density Function for Actual WT/Nominal WT

[4] CSA Z662-11, "Oil and Gas Pipeline Systems", Annex O, "Reliability-based design and assessment (RBDA) of onshore non-sour service natural gas transmission pipelines".
[5] Zimmerman, T.J.E., Cosham, A., Hopkins, P., and Sanderson, N., "Can Limit States Design be Used to Design a Pipeline Above 80% SMYS?", OMAE98-902, 1998, Proceedings of the Seventeenth International Conference on Offshore Mechanics and Arctic Engineering.
[6] 30 measured yield strength values for an X52 material from the Kiefner database were fitted to a normal distribution with an arithmetic mean of 56,766 psi and a standard deviation of 2,512 psi.
[7] The typical MFL vendor specified anomaly depth error is ±10% of the wall thickness with 80% confidence.
[8] The typical MFL vendor specified anomaly length error is ±20 mm with 80% confidence.
[9] Chauhan, V., Brister, J., and Dafea, M., "A Review of Methods for Assessing the Remaining Strength of Corroded Pipelines", Advantica Report No. 6781, to the Pipeline and Hazardous Materials Safety Administration, U.S. Department of Transportation, October, 2008.

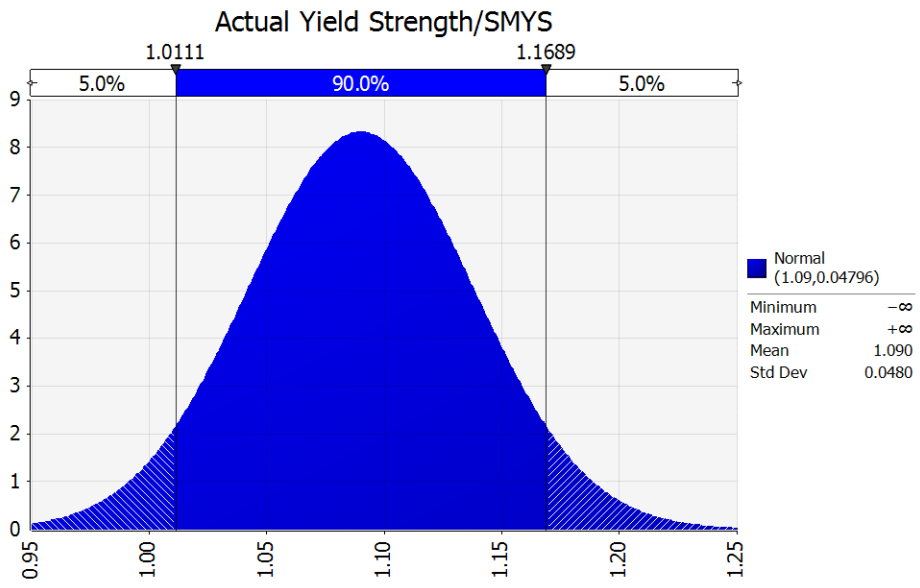

Figure 8. Probability Density Function for Actual Yield Strength/SMYS

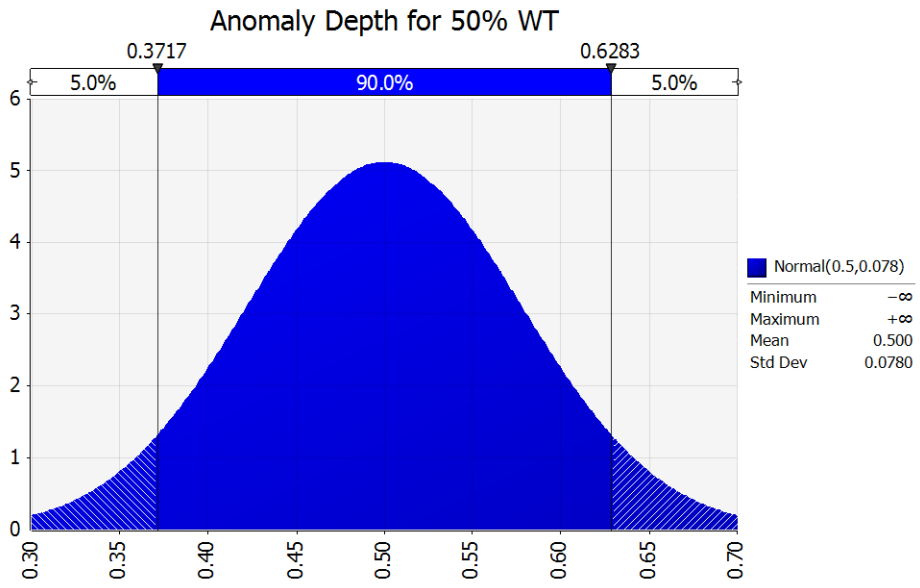

Figure 9. Probability Density Function for Actual Anomaly Depth Having 50%WT Reported by In-line Inspection

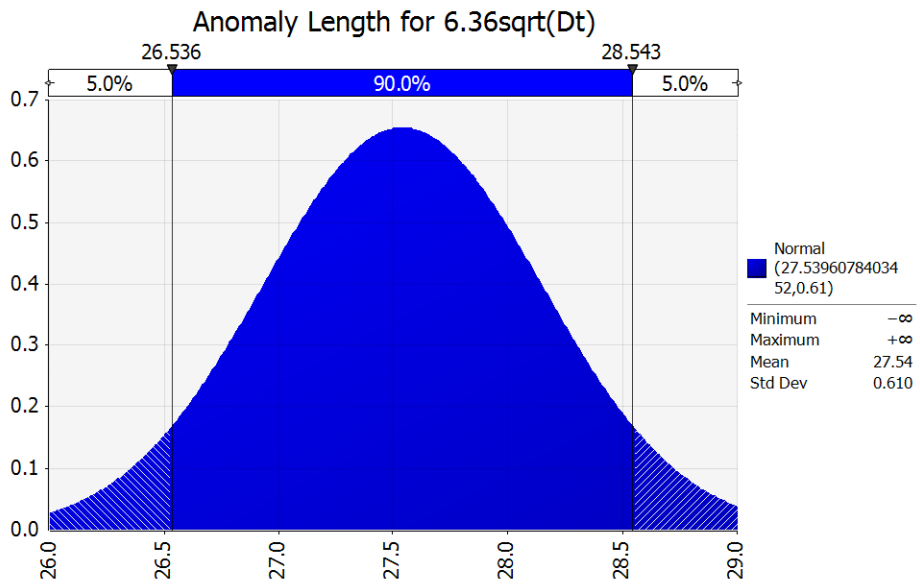

Figure 10. Probability Density Function for Actual Anomaly Length Having 6.36*Sqrt(Dt) Reported by In-line Inspection[10]

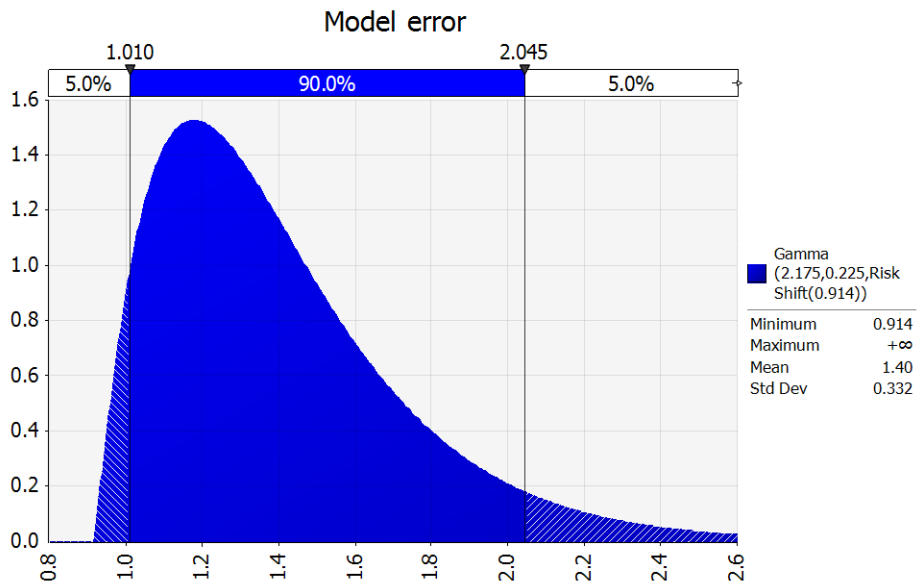

Figure 11. Burst Pressure Prediction Error of Modified B31G Model

Failure Probability of Immediate Condition

1.1MAOP is established as immediate repair across all the operating pressure conditions. The safety margin of 0.1MAOP is chosen for some arbitrary and subjective reason.

[10] Pipe is 30 inches in diameter and 0.625 inch in wall thickness.

Monte Carlo simulations were carried out for the likelihood of failure (POF) for actual burst pressure P_f less than 1.0 MAOP at any nominal burst pressure greater than 1.0 MAOP. P_f is calculated repeatedly using a value from each of the above distributions to generate a distribution of failure pressures. The probability of the failure pressure being less than the MAOP can then be assessed for any particular set of operating conditions and levels of FPR. To simplify the model, some assumptions are made based on the attributes of the Modified B31G equation.

- When the anomaly length is long enough to produce rupture dominant failures, the length has negligible influence on the failure probability at a particular FPR for a specific MAOP. As aforementioned, the anomaly length is fixed to a value normalized by the diameter and wall thickness, i.e. $6.36\sqrt{Dt}$.
- Only the ratio between flow stress and yield strength affect the failure probability, not the pipe grade. As an example, the ratio is fixed to be 1.19 by a Grade X52 material with SMYS of 52 ksi and flow stress of 62 ksi.

For each POF determination, a million Monte Carlo runs were conducted. The absolute POF values are demonstrated in Figure 12. At any particular MAOP, for a larger FPR, the POF decreases. At any particular FPR, for a smaller MAOP, the POF increases. If normalizing all the POFs by the value at FPR=1.1 for MAOP equivalent to 72%SMYS (6.17e-3), the relative POFs are shown in Figure 13. For the immediate condition at FPR=1.1, the relative POFs for MAOP corresponding to 60%SMYS, 50%SMYS, and 40%SMYS are roughly 2.23, 4.30, and 7.75 as listed in Table 4. In other words, to reach the same confidence as Class 1 for impending repair FPR=1.1, the pipeline operating in Class 2, Class 3 and Class 4 have to be predicted from ILI with FPR=1.144, 1.210, and 1.310 respectively as shown in Table 5. Similar trends have been brought forth by Reference [3]. The quantitative numbers derived from the simulations do not guarantee the "exact" relative failure probability measured in practice. Only the qualitative conclusion has the ultimate meaning.

Table 4. Probability of Failure at FPR=1.1 for Different MAOPs

MAOP equivalent to SMYS	FPR	Absolute POF	Normalized POF
72%	1.100	6.17E-03	1.00
60%	1.100	1.37E-02	2.23
50%	1.100	2.66E-02	4.30
40%	1.100	4.78E-02	7.75

Note: The normalized POF is the absolute POF for each MAOP at FPR=1.1 divided by the absolute POF for FPR=1.1 at MAOP equivalent to 72%SMYS, which is 6.17e-03.

Table 5. Required FPR to Achieve Normalized POF=1.0

MAOP equivalent to SMYS	FPR	FPR of ASME B31.8S-2010	FPR Difference from ASME B31.8S-2010	Normalized POF
72%	1.100	1.100	0.000	1.00
60%	1.144	1.100	0.044	1.00
50%	1.210	1.100	0.110	1.00
40%	1.310	1.100	0.210	1.00

Note: The normalized POF is the absolute POF for each MAOP at the listed FPR divided by the absolute POF for FPR=1.1 at MAOP equivalent to 72%SMYS, which is 6.17e-03.

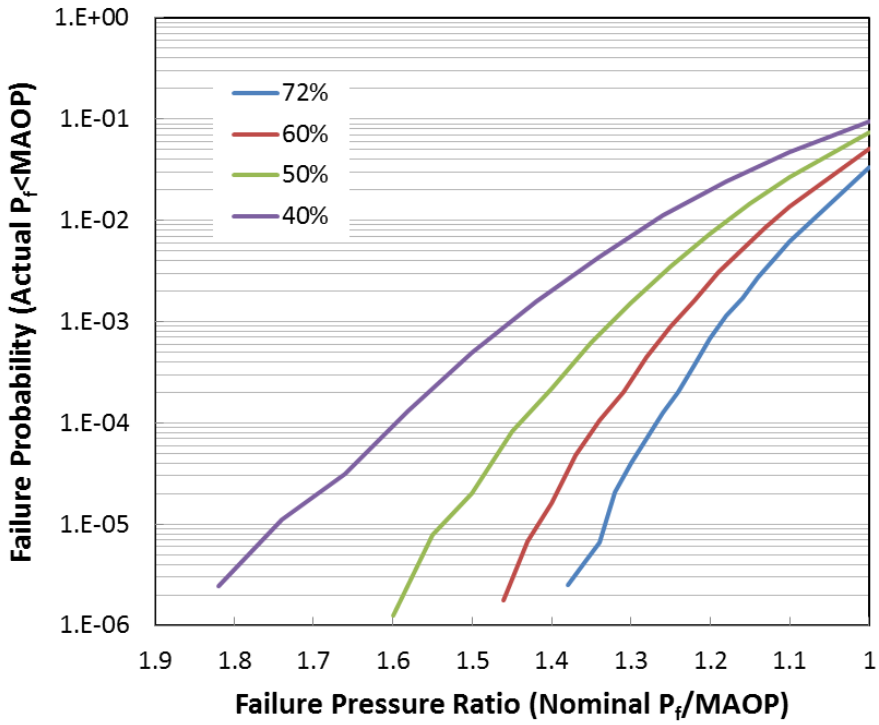

Figure 12. Failure Probability vs. Nominal Failure Pressure Ratio

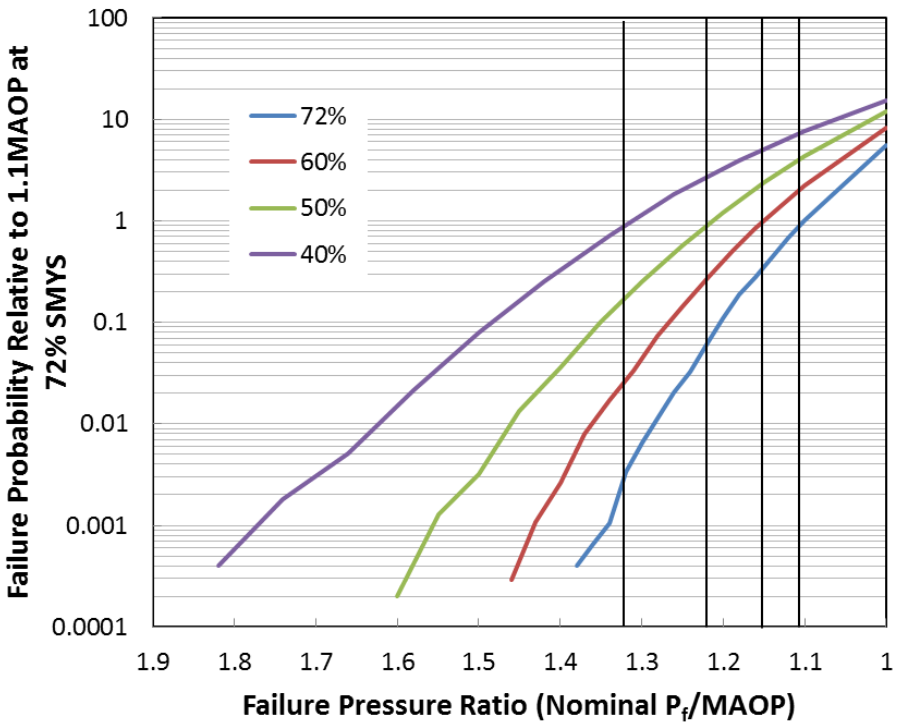

Figure 13. Relative Failure Probability vs. Nominal Failure Pressure Ratio

The response curves of the ASME B31.8S-2010, Figure 4 are plotted again in Figure 14 if adopting the FPRs carrying the same POF at imminent response time of zero years. The growth rates are presumed to be identical for three MAOPs, which is analogous to Figure 6. Table 6 gives the required FPR for every five year re-assessment interval increase. In Figure 14, it is evident that the immediate repair is more stringent for lower operating pressure. When this effect overweighs the decreased allowable identical corrosion growth rate, the necessary re-assessment is earlier than the ASME B31.8S-2010 requirement, such as FPR lower than 2.4 for MAOP equal to 30%SMYS. With the increasing FPR and the longer re-assessment interval, the smaller identical growth rate effect is a more dominant factor, and the re-assessment can be proceeded with on a later schedule than that the ASME B31.8S-2010 specifies. Consequently, crossing between dashed lines and solid lines takes place for MAOP equivalent to 50%SMYS and 30%SMYS. Moreover, this crossing happens around 5 year earlier for MAOP of 50%SMYS than for MAOP of 30%SMYS.

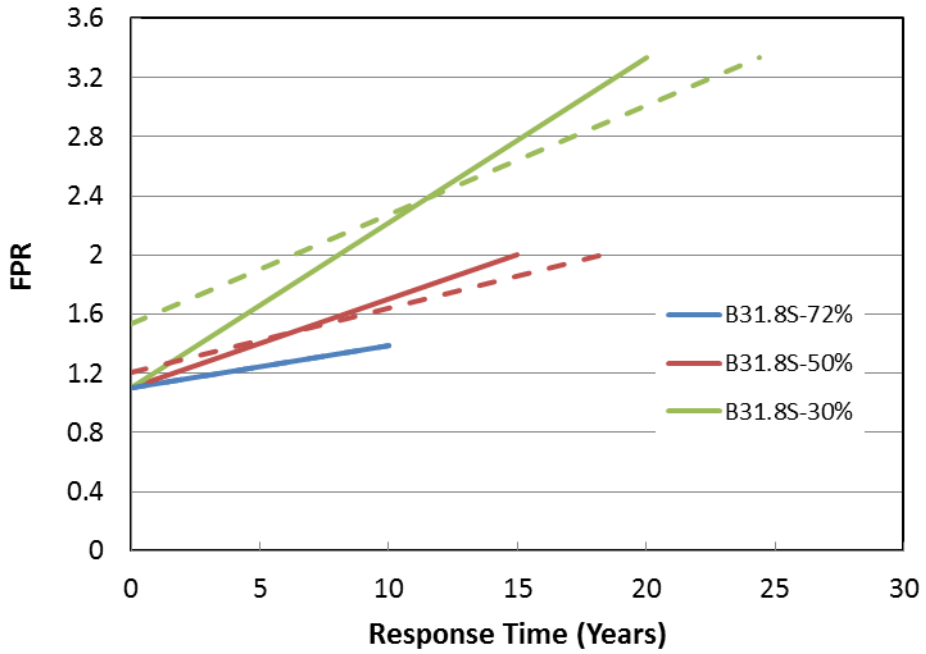

Figure 14. Overlaid Response Curves as a Function of Failure Pressure Ratio

Table 6. Integrity Re-assessment Interval for the Same Growth Rate and the Same POF for Immediate Repair

Interval (year)	Criteria for ILI Predicted Failure Pressure (MAOP)		
	Operating Pressure Above 50% of SMYS	Operating Pressure Above 30% of SMYS Not Exceeding 50% of SMYS	Operating Pressure Not Exceeding 30% of SMYS
0	1.10	1.21	1.53
5	1.25	1.43	1.90
10	1.39	1.64	2.27
15	Not allowed	1.86	2.64
20	Not allowed	Not allowed	3.01
25	Not allowed	Not allowed	Not allowed
30	Not allowed	Not allowed	Not allowed

Confidence Levels of 5-year, 10-year, 15-year and 20-year Conditions

In view of reliability, every entry in Table 1 is supposed to have the same failure probability when the required remediation time is approached. The Monte Carlo analyses were utilized to calculate the POF for every circumstance in the table. Two types of corrosion growth rate distribution were attempted, e.g. normal distribution and lognormal distribution, as these two options have been recommended by some prior researches[11, 12]. Despite the fact that the distribution shape and definition affect the numerical values in the ensuing calculation, the qualitative conclusion remains unchanged.

For each distribution, the mean growth rate μ was deterministically resolved from the ASME B31.8S-2010, Figure 4. For each mean μ, different amplitudes of coefficient of variation COV were practiced. The outcomes for normal and lognormal distributions are listed in Table 7 and Table 8 respectively. For the same value of μ, if the COV is less than 1.e-1, two distributions produce the close results. When the COV is as large as 1.0, the lognormal distribution leads to a substantial decrease of POF comparing to the normal distribution.

Multiple trends are observed, including (1) POF increases with a larger COV for the same MAOP and the same re-assessment interval; (2) POF decreases with a smaller re-assessment interval for the same MAOP and the same COV; (3) POF increases with a smaller MAOP for the same failure pressure relative to SMYS and the same COV.

Confidence levels vary significantly for every re-assessment requirement in the ASME B31.8S-2010, Table 3. Since the absolute POF at FPR=1.1 for MAOP equivalent to 72%SMYS is 6.17e-3 serving as a benchmark, the last columns of Table 7 and Table 8 give the relative POFs normalized by this value. When the COV is as small as 1.e-2 at every remediation interval, the relative POFs roughly equate to the 1.1MAOP immediate condition corresponding to the same MAOP (Table 4). As such, the degree of reliability of the ASME B31.8S-2010, Table 3 is not on the "equal" basis for every entry, which is a consequential point to be emphasized here.

Sensitivity investigations were undertaken to locate the equivalent FPR for achieving the same POF as the benchmark, i.e. 6.17e-3, after the prescribed re-assessment approaches. The assumed growth rate distribution is a lognormal function with a mean equal to the inherent values in the ASME B31.8S-2010, Table 3 and a COV equal to 1.e-1. The results are shown in Table 9. Apparently, the required FPR to achieve the same confidence level as immediate action at 1.1MAOP for MAOP of 72%SMYS is generally higher than those specified in the ASME

[11] F. Caleyo, A. Valor, V. Venegas, J. H. E. Hernandez, J. C. Velazquez, and J. M. Hallen, "PIPELINE INTEGRITY—1: Accurate corrosion modeling improves reliability estimations", Oil & Gas Journal, October 1, 2012.
[12] T. Bubenik, W.V. Harper, P. Moreno, and S. Polasik, "Identifying Locations of Active Corrosion Growth from Successive In-line Inspections", Pipeline Pigging and Integrity Management Conference, Houston, February 2015.

B31.8S-2010, Table 3. Two inclinations are identified: (1) The difference is higher for a lower operating pressure, which is consistent with Table 5. (2) For the same operating pressure, the difference is smaller for a shorter re-assessment interval. It is mainly the result of less accumulation of corrosion growth uncertainty. On average, the relative increase is 0.36% for MAOP of 72%SMYS, 7.47% for MAOP of 50%SMYS, and 19.35% for MAOP of 30%SMYS.

It is concluded that for lower operating stress levels, one should take into account the uncertainties in the various input parameters for calculating re-assessment intervals when utilizing the ASME B31.8S-2010, Table 3. The analyses conducted herein provide only qualitative guidance because the assumed distributions of corrosion growth rates have not been verified.

Table 7. POF Based on Normal Growth Rate Distributions

MAOP (SMYS)	Nominal Initial FPR	Nominal Final FPR	Schedule	Mean of Growth Rate	COV of Growth Rate	Actual Final FPR Mean	Actual Final FPR STD	Probability of Actual Final FPR less than 1.0	Normalized POF by POF of FPR=1.1 for MAOP=72% SMYS
0.72	1.39	1.1	10	0.0230	0.01	1.6968	0.4400	0.0064	1.04
0.72	1.39	1.1	10	0.0230	0.1	1.6966	0.4424	0.0072	1.17
0.72	1.39	1.1	10	0.0230	1	1.5418	0.5825	0.1507	24.42
0.72	1.25	1.1	5	0.0234	0.01	1.6976	0.4406	0.0065	1.05
0.72	1.25	1.1	5	0.0234	0.1	1.6975	0.4409	0.0065	1.05
0.72	1.25	1.1	5	0.0234	1	1.6251	0.4694	0.0470	7.61
0.5	2.00	1.1	15	0.0316	0.01	1.6950	0.4835	0.0271	4.39
0.5	2.00	1.1	15	0.0316	0.1	1.6932	0.5089	0.0416	6.74
0.5	2.00	1.1	15	0.0316	1	1.2998	1.1286	0.4123	66.80
0.5	1.65	1.1	10	0.0279	0.01	1.6962	0.4844	0.0271	4.38
0.5	1.65	1.1	10	0.0279	0.1	1.6956	0.4934	0.0319	5.17
0.5	1.65	1.1	10	0.0279	1	1.3796	0.8961	0.3085	49.98
0.5	1.39	1.1	5	0.0286	0.01	1.6963	0.4848	0.0269	4.35
0.5	1.39	1.1	5	0.0286	0.1	1.6960	0.4863	0.0282	4.57
0.5	1.39	1.1	5	0.0286	1	1.5350	0.6388	0.1617	26.20
0.3	3.33	1.1	20	0.0337	0.01	1.5897	0.7871	0.1417	22.96
0.3	3.33	1.1	20	0.0337	0.1	1.5449	0.9344	0.2058	33.35
0.3	3.33	1.1	20	0.0337	1	1.4691	1.8314	0.5349	86.65
0.3	2.75	1.1	15	0.0320	0.01	1.5922	0.7876	0.1406	22.78
0.3	2.75	1.1	15	0.0320	0.1	1.5642	0.8717	0.1779	28.83
0.3	2.75	1.1	15	0.0320	1	1.3291	1.5593	0.5111	82.80
0.3	2.20	1.1	10	0.0309	0.01	1.5925	0.7876	0.1407	22.79
0.3	2.20	1.1	10	0.0309	0.1	1.5791	0.8256	0.1578	25.56
0.3	2.20	1.1	10	0.0309	1	1.2364	1.3105	0.4683	75.87
0.3	1.65	1.1	5	0.0298	0.01	1.5923	0.7868	0.1404	22.75
0.3	1.65	1.1	5	0.0298	0.1	1.5897	0.7964	0.1444	23.40
0.3	1.65	1.1	5	0.0298	1	1.2623	1.0641	0.3637	58.92

Table 8. POF Based on Lognormal Growth Rate Distributions

MAOP (SMYS)	Nominal Initial FPR	Nominal Final FPR	Schedule	Mean of Growth Rate	COV of Growth Rate	Actual Final FPR Mean	Actual Final FPR STD	Probability of Actual Final FPR less than 1.0	Normalized POF by POF of FPR=1.1 for MAOP=72% SMYS
0.72	1.39	1.1	10	0.0230	0.01	1.6967	0.4393	0.0063	1.02
0.72	1.39	1.1	10	0.0230	0.1	1.6966	0.4423	0.0074	1.21
0.72	1.39	1.1	10	0.0230	1	1.6904	0.6250	0.0937	15.18
0.72	1.25	1.1	5	0.0234	0.01	1.6976	0.4401	0.0063	1.02
0.72	1.25	1.1	5	0.0234	0.1	1.6976	0.4412	0.0066	1.06
0.72	1.25	1.1	5	0.0234	1	1.6928	0.5069	0.0428	6.94
0.5	2.00	1.1	15	0.0316	0.01	1.6950	0.4836	0.0271	4.39
0.5	2.00	1.1	15	0.0316	0.1	1.6930	0.5090	0.0420	6.80
0.5	2.00	1.1	15	0.0316	1	1.8176	1.0881	0.2132	34.54
0.5	1.65	1.1	10	0.0279	0.01	1.6962	0.4845	0.0268	4.34
0.5	1.65	1.1	10	0.0279	0.1	1.6956	0.4933	0.0319	5.17
0.5	1.65	1.1	10	0.0279	1	1.7187	0.8621	0.1634	26.47
0.5	1.39	1.1	5	0.0286	0.01	1.6962	0.4843	0.0270	4.37
0.5	1.39	1.1	5	0.0286	0.1	1.6960	0.4868	0.0283	4.58
0.5	1.39	1.1	5	0.0286	1	1.6871	0.6650	0.1024	16.59
0.3	3.33	1.1	20	0.0337	0.01	1.5894	0.7866	0.1415	22.93
0.3	3.33	1.1	20	0.0337	0.1	1.5481	0.9311	0.2040	33.06
0.3	3.33	1.1	20	0.0337	1	2.3789	1.8752	0.2918	47.28
0.3	2.75	1.1	15	0.0320	0.01	1.5921	0.7883	0.1413	22.89
0.3	2.75	1.1	15	0.0320	0.1	1.5661	0.8708	0.1772	28.71
0.3	2.75	1.1	15	0.0320	1	2.0890	1.5733	0.2766	44.82
0.3	2.20	1.1	10	0.0309	0.01	1.5925	0.7884	0.1409	22.83
0.3	2.20	1.1	10	0.0309	0.1	1.5798	0.8253	0.1572	25.46
0.3	2.20	1.1	10	0.0309	1	1.8412	1.2962	0.2534	41.06
0.3	1.65	1.1	5	0.0298	0.01	1.5923	0.7873	0.1407	22.79
0.3	1.65	1.1	5	0.0298	0.1	1.5891	0.7961	0.1445	23.42
0.3	1.65	1.1	5	0.0298	1	1.6445	1.0227	0.2111	34.20

Table 9. Required FPR and Re-assessment Interval to Maintain the Same POF

MAOP (SMYS)	Reassessment Interval (Year)	Failure Pressure Ratio	Failure Pressure Ratio from ASME B31.8S-2010	Difference	Relative Difference
0.72	10	**1.40**	1.39	0.01	0.52%
0.72	5	**1.25**	1.25	0.00	0.19%
0.5	15	**2.14**	2.00	0.14	7.21%
0.5	10	**1.77**	1.65	0.12	7.27%
0.5	5	**1.50**	1.39	0.11	7.91%
0.3	20	**3.89**	3.33	0.56	16.77%
0.3	15	**3.20**	2.75	0.45	16.52%
0.3	10	**2.62**	2.20	0.42	19.17%
0.3	5	**2.06**	1.65	0.41	24.95%

OTHER SPECIFICATIONS OF ASME B31.8S

Chapter 7 of the ASME B31.8S-2010 is "Responses to Integrity Assessments and Mitigation (Repair and Prevention)". Except the major contents about internal and external corrosion, it is worthwhile to mention some other specifications listed below:

- Any metal loss indication affecting a detected longitudinal seam, if that seam was formed by direct current or low-frequency electric resistance welding or by electric flash welding, the operator shall take action by either examining them or reducing the operating pressure to provide an additional margin of safety, within a period not to exceed 5 days following determination of the condition.
- In lieu of developing assessment, response, and repair plans, an operator may elect to treat all indications of stress corrosion cracks as requiring immediate response, including examination or pressure reduction within a period not to exceed 5 days following determination of the condition.
- These could include dents with gouges. The operator shall examine these indications within a period not to exceed 5 days following determination of the condition.
- Indications requiring a scheduled response would include any indication on a pipeline operating at or above 30%SMYS of a plain dent that exceeds 6% of the nominal pipe diameter, mechanical damage with or without concurrent visible indentation of the pipe, dents with cracks, dents that affect ductile girth or seam welds if the depth is in excess of 2% of the nominal pipe diameter, and dents of any depth that affect nonductile

welds. The operator shall expeditiously examine these indications within a period not to exceed 1 year following determination of the condition.

US DOT - PHMSA

Final Report No. 16-025

Final Report

Threat/Anomaly Mitigation Decision-Making Process – Annex C. Deterministic and Probabilistic Approaches for Scheduling Mitigations of Crack-like Anomalies

Jing Ma and M.J. Rosenfeld

February 23, 2016

0339-1402

Kiefner and Associates, Inc. is an Applus RTD company.

Intentionally blank

Final Report No. 16-025

Final Report

on

THREAT/ANOMALY MITIGATION DECISION-MAKING PROCESS
ANNEX C. DETERMINISTIC AND PROBABILISTIC APPROACHES FOR SCHEDULING MITIGATIONS OF CRACK-LIKE ANOMALIES
DTPH5614H00005

to

U.S. DEPARTMENT OF TRANSPORTATION – PIPELINE AND HAZARDOUS MATERIALS SAFETY ADMINISTRATION

February 23, 2016

by

Jing Ma and M.J. Rosenfeld

Kiefner and Associates, Inc.
4480 Bridgeway Avenue, Suite D
Columbus, OH 43219

0339-1402

DISCLAIMER

This document presents findings and/or recommendations based on engineering services performed by employees of Kiefner and Associates, Inc. The work addressed herein has been performed according to the authors' knowledge, information, and belief in accordance with commonly accepted procedures consistent with applicable standards of practice, and is not a guaranty or warranty, either expressed or implied.

The analysis and conclusions provided in this report are for the sole use and benefit of the Client. No information or representations contained herein are for the use or benefit of any party other than the party contracting with Kiefner. The scope of use of the information presented herein is limited to the facts as presented and examined, as outlined within the body of this document. No additional representations are made as to matters not specifically addressed within this report. Any additional facts or circumstances in existence but not described or considered within this report may change the analysis, outcomes and representations made in this report.

TABLE OF CONTENTS

INTRODUCTION 1
BACKGROUND 1
DETERMINISTIC SCHEDULING OF CRACK REMEDIATION 2
Failure Pressure Prediction 2
Fatigue-Crack Growth Analysis 3
Interaction between Seam Weld Cracks 5
Interaction effect on the re-assessment interval prediction 7
Possible interacting patterns of hook cracks 10
Combination of SCC and Fatigue Growth 11
PROBABILISTIC SCHEDULING OF CRACK REMEDIATION 15
Pressure Spectrum 15
Material Strength 16
Crack-like Defect Size 17
Material Toughness 22
Burst Model Error 23
Probability of Failure 25
Comparison with Deterministic Analysis 27
Conclusion 28

LIST OF FIGURES

Figure 1. UT Inspection of ERW Pipe Made in 1958 6
Figure 2. Hydrostatic Testing Failure from a Couple of Interlinking Hook Cracks 7
Figure 3. Hydrostatic Testing Failure from Two Hook Cracks on ID and OD 7
Figure 4. Possible Configurations of Two Hook Cracks 11
Figure 5. Fatigue Growth Rate for a Crack as Deep as 20%-40%WT in a Gas Pipeline 13
Figure 6. Fatigue Growth Rate for a Crack as Deep as 20%-40%WT in a Liquid Pipeline 14
Figure 7. Discharge Pressure Spectrum of Pump Station C 16
Figure 8. Pipe Yield Strength Distribution Fitted from Mill Tests 17
Figure 9. In-ditch NDE Crack-like Indication Size for Segment from A to C 18
Figure 10. In-ditch NDE Crack-like Indication Size for Segment from C to E 18
Figure 11. Size Comparison of Crack-like Indications Detected by ILI for Two Segments 19
Figure 12. Size Comparison of Crack-like Indications Missed by ILI for Two Segments 19

Figure 13. Crack-like Indication Size Distribution for Segment from A to C 20
Figure 14. Crack-like Indication Size Distribution for Segment from C to E 21
Figure 15. Toughness Distribution Fitted From CVN Data in Kiefner Database.....23
Figure 16. Comparison between Predicted and Actual Failure Pressures.....24
Figure 17. Probability Density Distribution of Ratio between Actual Failure Pressure and Predicted Failure Pressure 24
Figure 18. Cumulative Probability Distribution of Ratio between Actual Failure Pressure and Predicted Failure Pressure 25
Figure 19. Relationship between POF and Deterministic Fatigue Life.....28
Figure 20. Comparison between Hydrostatic Testing and In-ditch NDT for the Segment between A and C 29
Figure 21. Comparison between Hydrostatic Testing and In-ditch NDT for the Segment between C and E.....29

LIST OF TABLES

Table 1. Sensitivity Study of Crack Growth for a Typical Liquid Pipeline..... 9
Table 2. Crack Life Including Both SCC Growth and Fatigue Growth for a Gas Pipeline 13
Table 3. Crack Life Including Both SCC Growth and Fatigue Growth for a Liquid Pipeline.....15
Table 4. Pressure Cycling Severity of Each Pump Station 16
Table 5. Fitted Distributions for Three Categories of Indications.....22
Table 6. POFs of Four Pump Segments 26
Table 7. Crack-like Indication Size with the Largest Depth 27
Table 8. Fatigue Life Determined by Deepest Indications.....27

Threat/Anomaly Mitigation Decision-Making Process – Annex C. Deterministic and Probabilistic Approaches for Scheduling Mitigations of Crack-like Anomalies

Jing Ma and M.J. Rosenfeld

INTRODUCTION

Pipeline operators must excavate and examine anomalies discovered through in-line inspection (ILI), or direct assessment (DA) for external corrosion, internal corrosion, or stress-corrosion cracking in a timely manner to assure that critical flaws are repaired before they can become large enough to cause a pipeline to fail at its maximum operating pressure. Pipeline operators must also periodically re-assess their pipelines that are located in or could affect high consequence areas (HCAs). While prescriptive regulations often require examinations of anomalies or re-assessments to be carried out after specific time periods, a more rational way to schedule excavations or to conduct re-assessments would be to schedule them based on the sizes of anomalies remaining after the most recent assessment, the applicable rate of deterioration, and sizes of anomalies that would cause the pipeline to fail at its maximum operating pressure. However, there are two challenges to employ performance-based assessment methods. First, one must account for the error inherent in all currently available in-situ technologies. Second, one must account for the interaction between coexisting anomalies. Three types of anomalies and their related interaction criteria will be addressed in a consecutive manner. As a part of this project, the mitigation scheduling of crack-like anomalies will be specifically dealt with in this interim report by following both deterministic and probabilistic approaches.

BACKGROUND

Part 192 and Part 195 of U.S. Code of Federal Regulations Title 49: Transportation incorporate pipeline integrity management regulations for gas and hazardous liquid transmission pipelines respectively. These regulations state the types of anomalies pipeline operators must address, and they prescribe maximum re-assessment intervals for continued monitoring and remediation within HCAs. This project was conceived to develop a more flexible approach to pipeline integrity management that would allow pipeline operators to base re-assessment and remediation intervals on the actual rates of anomaly growth determined from measurements and experience. In this project both deterministic and probabilistic methods are considered.

Deterministic methods tend to utilize fixed values of parameters such as material strength and toughness, crack-like defect length and depth (based on in-line or in-ditch inspection data) and crack-growth rate constants, and they typically employ standard failure pressure and remaining life calculation algorithms without considering the uncertainties associated with input parameters or the errors inherent in the algorithms. To account for possible variations, arbitrary factors of safety are applied to the calculations of failure pressure and remaining life to remediate critical flaws and to establish re-assessment intervals. In contrast, probabilistic methods utilize statistical distributions of the various parameters and consider the degree of error associated with the chosen pressure-calculating and remaining-life-calculating algorithms. The results are statistical distributions of failure pressure and remaining life, from which the user may select upper or lower bound values with a desired degree of confidence.

DETERMINISTIC SCHEDULING OF CRACK REMEDIATION

Crack-like anomalies are generally recognized to pose threats to the pipeline safety that depend on their size, the inherent resistance of the material to crack propagation, and the operating stress conditions on the pipeline. Two primary aspects of integrity assessment have to be taken into account, i.e. burst pressure and crack-growth life. The combination of these two elements constitutes the foundation of the mitigation planning, including the immediate repair and the re-assessment schedule.

Failure Pressure Prediction

Various models exist for the failure pressure calculation, such as the Modified Ln-Sec equation[1], PAFFC[2], CorLas™[3], Failure Assessment Diagram (FAD) methods of API 579[4] and BS 7910[5], and the Raju/Newman equation[6], etc. Endeavors have been undertaken to clarify the model dependence on failure mechanism, defect type, and material toughness, so that operators are able to make better decisions regarding the disposition of crack-like anomalies on a case-by-case basis.

[1] Kiefner, J.F., "Modified equation helps integrity management", Oil and Gas Journal, Oct 6, 2008, pp 76-82 and "Modified Ln-Secant equation improves failure prediction", October 13, 2008, pp 64-66.
[2] Leis, B. N., Brust, F. W., and Scott, P.M., "Development and Validation of a Ductile Flaw Growth Analysis for Gas Transmission Line Pipe", Final Report to American Gas Association, NG-18, Catalog No, L51543, 1991.
[3] Jaske, C. E., and Beavers, J. A., "Development and Evaluation of Improved Model for Engineering Critical Assessment of Pipelines", Proceedings of IPC 2002, 4th International Pipeline Conference, September 29-October 3, 2002, Calgary, Alberta, Canada.
[4] Fitness-for-Service, API Recommended Practice 579, First Edition, January, 2000 and Second Edition, June, 2007.
[5] Guide to Methods for Assessing the Acceptability of Flaws in Metallic Structures, BS 7910, First Edition, December 1999, Second Edition, July 2005, and Third Edition, December 2013.
[6] J.C. Newman, Jr. and I.S. Raju, "An Empirical Stress-Intensity Factor Equation for the Surface Crack". Engineering Fracture Mechanics, Vol. 15, No. 1-2, pp 185-192, 1981, printed in Great Britain.

Major conclusions drawn from prior research are: [7, 8, 9]

- The toughness of the bond line of a LF-ERW, DC-ERW, or flash-welded seam and possibly the heat-affected zone as well is sometimes much lower than that of the surrounding base metal. Defects residing in the bond line tend to fail in a brittle manner. The Raju/Newman equation describes this "elastic fracture" behavior and estimates a lower-bound of the actual failure pressure of cold welds with toughnesses in the range of a Charpy energy of 4 ft-lb to a Charpy energy of 0.4 ft-lb. The FAD methods can be used in these situations, but the use of the Modified Ln-Sec equation is inappropriate. The Modified Ln-Sec equation should not be used in situations where the Charpy upper-shelf energy is less than 15 ft-lb.

- The toughness of the pipe material is typically higher than that of the bond line region. Defects in the heat-affected zone adjacent to LF-ERW, DC-ERW, and flash-welded seams such as hook cracks and fatigue cracks tend to fail in a ductile manner unless the base metal itself is prone to brittle fracture initiation or the fracture jumps into the bond line. Therefore, it is appropriate to apply the ductile fracture models to predict the failure pressure for hook cracks and fatigue cracks. The Modified Ln-Sec equation is one such model. Other models likely would work equally well, e.g. PAFFC, CorLas™, or Level II FAD analysis.

In the context of this interim report, only defects having at least minimally ductile properties capable of supporting subcritical growth (e.g., as occurs with fatigue) are considered.

Fatigue-Crack Growth Analysis

The fatigue lives of remaining defects from the last assessment are usually determined by the Paris-Law method to account for the long-term integrity deterioration from the pressure cycles. The re-assessment interval is inferred from the fatigue life discounted by a certain safety factor, so as to guarantee the remediation attempted in a timely manner and to prevent the defects from growing large enough to fail in service.

The Paris-Law Equation is written as

[7] Kiefner, J.F. and Kolovich, K.M., "Models for Predicting Failure Stress Levels for Defects Affecting ERW and Flash-Welded Seams", Subtask 2.4 of U.S. Department of Transportation Other Transaction Agreement No. DTPH56-11-T-000003, January 3, 2013.
[8] Kiefner, J.F., and Kolovich, K.M., "ERW and Flash Weld Seam Failures", Subtask 1.4 of U.S. Department of Transportation Other Transaction Agreement No. DTPH56-11-T-000003, May 30, 2012.
[9] Kiefner, J.F. and Kolovich, K.M., "Predicting Times to Failure for ERW Seam Defects that Grow by Pressure-Cycle-Induced Fatigue", Subtask 2.5 of U.S. Department of Transportation Other Transaction Agreement No. DTPH56-11-T-000003, January 28, 2013.

$$\frac{da}{dN} = C(\Delta K)^n \qquad \text{Equation 1}$$

where

da/dN is an increment of crack growth, inch/cycle
C and n are constants for a particular material and environment
ΔK is the change in stress intensity factor at the fatigue crack tip during a cycle of changing applied stress, $\text{psi}\sqrt{\text{inch}}$

Fatigue-crack growth rate constants C and n rely on the material property, the environmental exposure, and the R-ratios, i.e. ratio of minimum to maximum stress. Their values have substantial influence on the fatigue life prediction. To obtain the most accurate and characteristic information of the Paris-Law coefficients, Compact Tension (CT) specimens can be machined from the pipe steel and cyclically loaded to failure. The testing can follow the procedure described in ASTM E647[10].

Two primary standardized sources of fatigue growth rate are widely used, BS 7910 and API 579. The data were collected from fatigue tests conducted for a variety of steel grades subjected to diverse working conditions. For ferritic steels such as line pipe steels operating in air, including seams, both standards recommend the same values as the simplified conservative parameters, i.e. C= 8.61E-19 and n=3 for da/dN in inch/cycle and ΔK in psi√inch, or equivalently C=5.21E-13 and n=3 for da/dN in mm/cycle and ΔK in $N/mm^{3/2}$. These values generate the fatigue growth rate similar to the mean plus twice the standard deviation curve for R≥0.5 in BS 7910[11]. Note that the growth rate constants recommended by these standards were selected to be conservative upper bounds, for design and assessment purposes. That is, they are well above "typical" rates as reported in the research literature or text books.

The draft of API RP 1176 collects the fatigue growth constants C and n from several references in the literature and from data produced from tests of certain vintage line pipe materials for a pipeline operator[12]. Likewise, C and n values recommended by BS 7910 and API 579 produce the upper bound of crack growth rate compared to other sources except very high ΔK regimes which are not representative of a typical fatigue analysis.

PIPELIFE is a software program used by Kiefner for performing incremental fatigue crack-growth time to failure calculations, in accordance with the Paris Law. The stress intensity factor

[10] ASTM E647, Standard Test Method for Measurement of Fatigue Crack Growth Rates, ASTM International.
[11] Aaron Dinovitzer, Improved Methods for Estimating Remaining Fatigue Life of ERW Pipelines, PRCI, Catalog No. PR-214-104505-R01, April 14, 2015.
[12] The Pipeline Research Council Inc. has recently conducted additional fatigue tests of a wide range of line pipe types. The report is not yet available for public reference, but the results generally are consistent with these, showing the API 579 or BS 7910 rates to be upper-bounding values.

K underlying the Kiefner's proprietary software PIPELIFE is the Raju/Newman solution for a longitudinal surface crack on a cylinder. It takes into account both the tensile stress from internal pressure and the bending stress resulting from the seam offset.

After establishing the initial defect size from inspection or hydrostatic testing, the analyst applies a pressure spectrum of the past or current operating condition to enlarge the defect until it fails at the maximum operating pressure or some transient pressure in the historical spectrum. The fatigue life is calculated as the ratio between total cycles experienced before the failure and the average pressure cycles per year in the pipeline.

Interaction between Seam Weld Cracks

The advancement of ILI crack detection technology makes it feasible to predict the sizes of crack-like anomalies. Although the sizing has a tangible amount of error, depending on the tool mechanism, seam weld geometry features such as the cap and root shapes, joint alignment, or ERW trim error, the ILI crack detection tools have proven robust enough to at least prioritize the severity of crack indications, according to the experience of several pipeline operators on their crack ILI validation programs.

Once the operators receive the inspection reports from vendors, they conduct the excavation program for immediate repairs and ILI tool validation. The in-ditch inspections, largely composed of shear wave UT, phased array and TOFD UT, and MPI, may reveal detailed information regarding the crack configuration, and support the ILI tool improvement on the anomaly detection and identification, and the signal analysis.

It is routinely observed that the vintage ERW and flash-welded seams may contain multiple hook cracks located close to each other. Figure 1 exhibits a 15-foot joint of 1958 vintage 12-inch OD × 0.250-inch WT ERW pipe material. The UT inspection found a total of 72 crack-like indications. Both OD and ID features exist, overlapping in some locations, and numerous ones exist in proximity to each other.

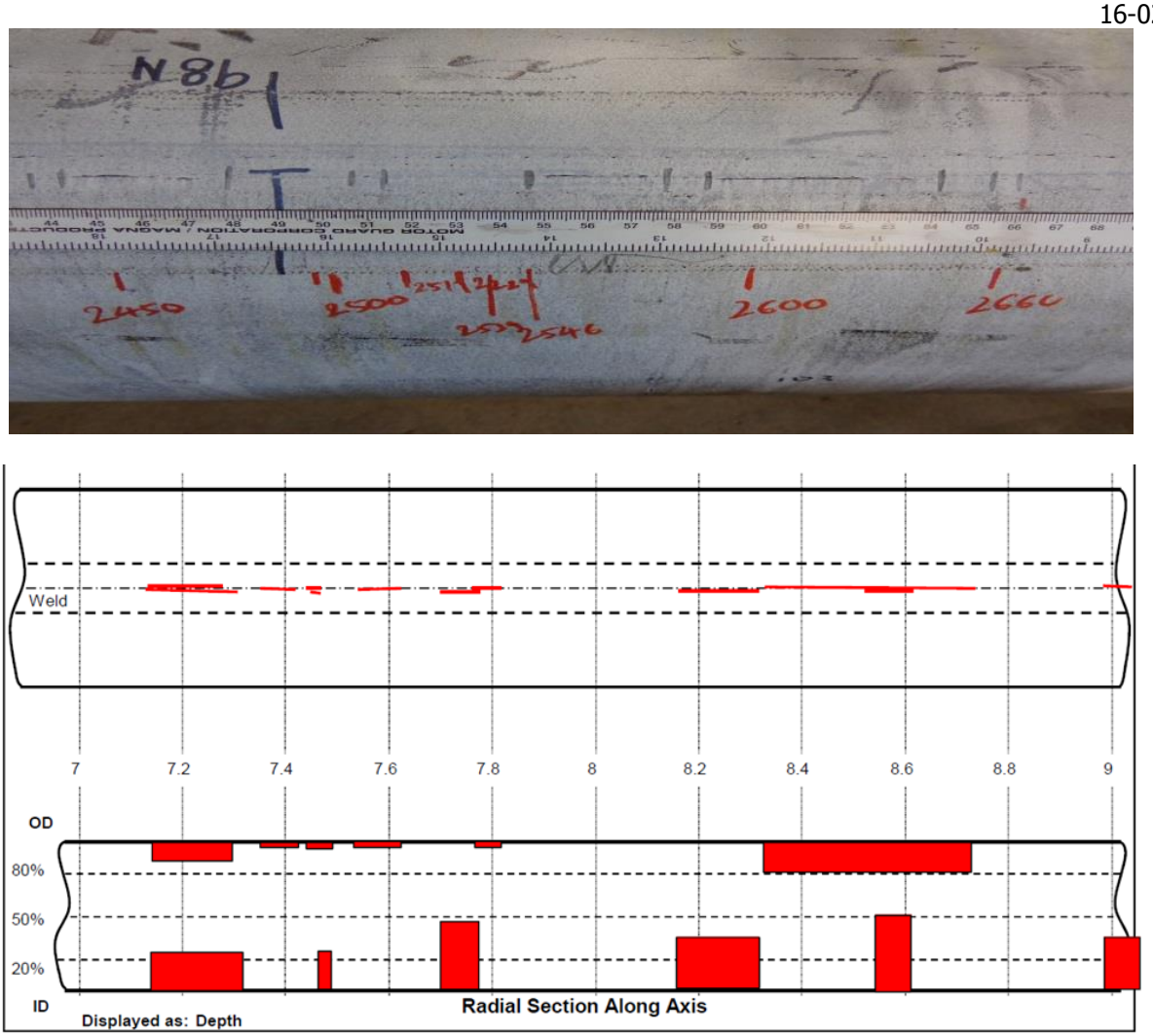

Figure 1. UT Inspection of ERW Pipe Made in 1958

Hydrostatic testing failures associated with the crack interaction are demonstrated in Figure 2 and Figure 3. These cases are extracted from the Kiefer failure analyses. Figure 2 is a 1972 vintage 16-inch OD × 0.250-inch WT high-frequency ERW pipe material. In total, there are eight hook cracks in the thickness cross section. The pattern is quite complex, i.e. four of them emanate from the pipe OD, two of them emanate from the pipe ID, and the remaining two emanate from inclusions or the layered microstructure in the mid wall. During the hydrostatic testing, the pipe failed as a rupture. Figure 3 is a hydrostatic test failure attributed to the interacting OD and ID hook cracks in a 12-inch OD × 0.250-inch WT Grade X52 pipeline manufactured by the low-frequency ERW process in 1961.

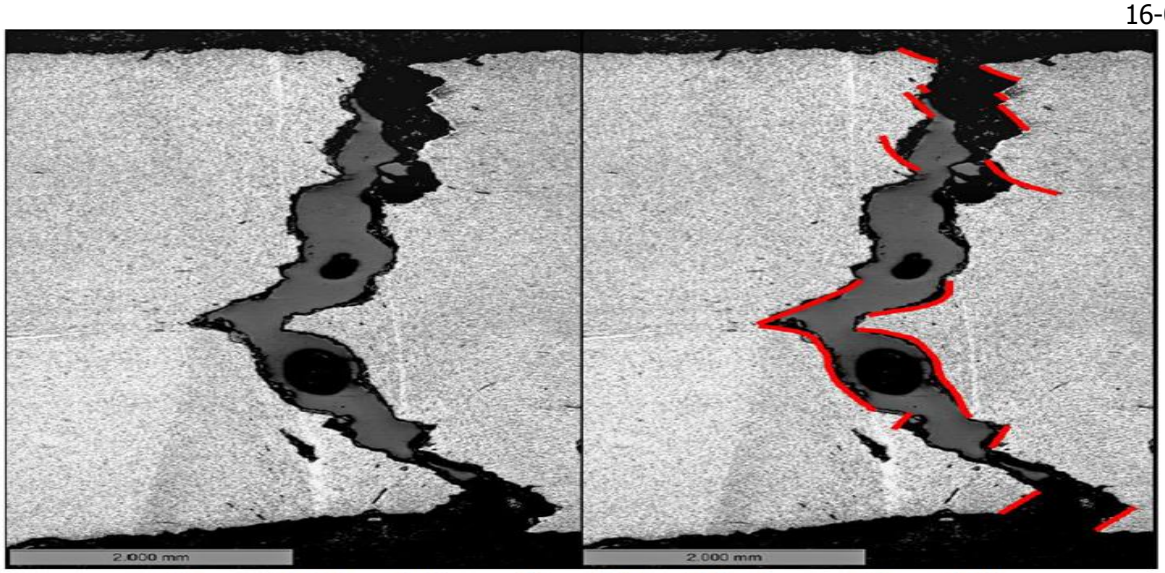

Figure 2. Hydrostatic Testing Failure from a Couple of Interlinking Hook Cracks

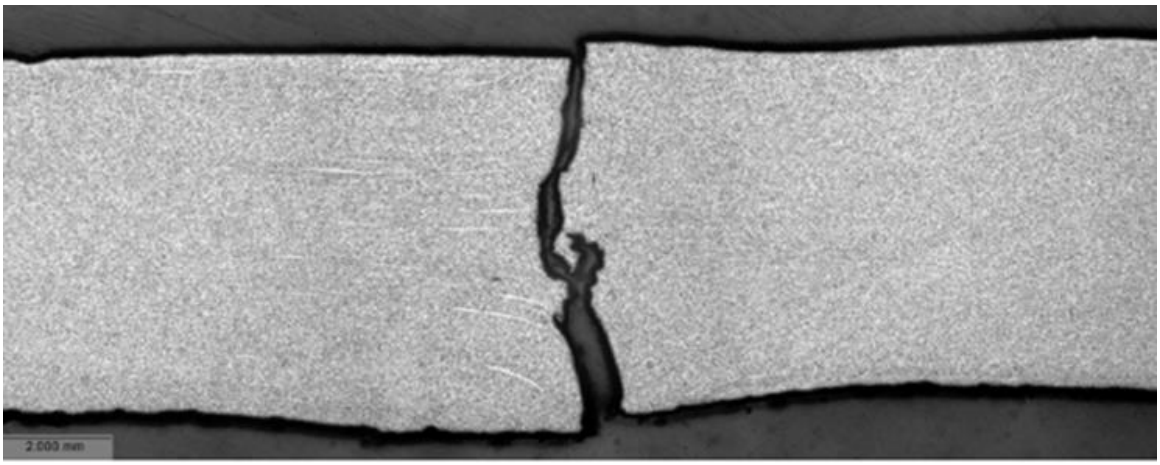

Figure 3. Hydrostatic Testing Failure from Two Hook Cracks on ID and OD

Interaction effect on the re-assessment interval prediction

As described in Task 2 of this project, the crack interaction criteria are best defined by BS 7910: 2013. Cracks are clustered according to the BS 7910 interacting rule, and the burst pressure is calculated. According to the Kiefner's experience, the re-assessment interval is determined by the shortest fatigue life of the cracks residing in the pipeline divided by a safety factor of 2. The interaction between cracks is not considered in the re-assessment interval determination. This is not consistent with the real pipeline condition as shown in Figure 1 through Figure 3. In other words, the re-assessment interval estimated from each individual crack may not reflect the actual crack growth picture in case that some cracks undergo pressure-induced-fatigue growth and gradually enlarge so as to approach each other and interact before the next re-assessment. So the burst pressure of the pipeline may decrease faster than if the individual cracks were non-interacting. Because a factor of safety of 2 on the calculated time to failure is

usually specified to define the re-assessment interval, it is possible that not considering interaction will have no consequence, but it would be better to consider interaction if feasible in the time-to-failure calculation.

Consequently, a more conservative interaction rule than BS 7910: 2013 may be required in order to assure that there is negligible possibility of hook crack interaction within the re-assessment interval, i.e. five years for liquid pipelines, if applied at the current stage. The extra conservatism compensates for the pressure-cycle-induced fatigue growth of cracks during five years.

To simplify the problem, all of the present cracks are projected to the same longitudinal plane to be coplanar. Since the width of ERW and flash-welded seams is very small and the fatigue growth usually keeps the crack plane straight, this process indicates the offset distance interaction criterion is always satisfied and stands on the conservative side. The in-plane distance is the only variable to be tracked during the fatigue growth.

A sensitivity study was performed using PIPELIFE to analyze the crack size extension in both depth and length directions before reaching the re-assessment interval and to learn the possibility of defect interaction. A liquid pipeline comprised of 8.625-inch OD, 0.220-inch WT, and Grade X46 pipe, and operating at MOP equal to 1,440 psi was considered. The fatigue life calculations were terminated when the growth time exceeded five years. The toughness of pipe material was set to be 15 ft-lb.

To facilitate the calculations, an annualized number of equivalent MOP pressure cycles was used to characterize the pressure fluctuation severity in lieu of the precise time-dependent pressure spectrum. The uniform pressure spectrum was derived by using the Palmgren-Miner relationship to produce the same overall cumulative damage.

$$N_{eq} = \sum_{i=1} N_i \left(\frac{\Delta P_i}{\text{MOP}} \right)^3 \frac{365.25}{\text{Days}} \qquad \text{Equation 2}$$

where

N_{eq} is the annual equivalent MOP cycles
N_i is the cycles of pressure differential ΔP_i from the Rainflow calculation
Days is the time span of a historical pressure spectrum to calculate N_{eq}

The impacts of initial crack size and pressure fluctuations on fatigue-crack growth are illustrated in Table 1.

Table 1. Sensitivity Study of Crack Growth for a Typical Liquid Pipeline

Equivalent MOP Cycles per Year	Initial Depth (inch)	Initial Length (inch)	Final Depth (inch)	Final Length (inch)	Fatigue Life (years)	Depth Growth/ WT	Length Growth/ WT
20	0.044	2	0.044459	2.000007	6	2.082E-03	3.359E-05
20	0.044	4	0.044475	4.000003	6	2.156E-03	1.264E-05
20	0.044	6	0.044482	6.000002	6	2.184E-03	7.041E-06
20	0.044	8	0.044485	8.000001	6	2.200E-03	4.629E-06
20	0.132	2	0.136281	2.000726	5.89	1.942E-02	3.295E-03
20	0.132	4	0.141641	4.000673	5.34	4.373E-02	3.054E-03
20	0.132	6	0.132614	6.000000	0.26	2.785E-03	0.000E+00
20	0.132	8	0.132614	8.000000	0.20	2.785E-03	0.000E+00
100	0.044	2	0.045502	2.000035	5.85	6.810E-03	1.606E-04
100	0.044	4	0.045590	4.000013	5.79	7.211E-03	6.110E-05
100	0.044	6	0.045624	6.000008	5.77	7.367E-03	3.417E-05
100	0.044	8	0.045643	8.000005	5.76	7.450E-03	2.251E-05
100	0.132	2	0.153503	2.004811	5.00	9.753E-02	2.182E-02
100	0.132	4	0.143769	4.000846	1.27	5.338E-02	3.835E-03
100	0.132	6	0.132614	6.000000	0.05	2.785E-03	0.000E+00
100	0.132	8	0.132614	8.000000	0.04	2.785E-03	0.000E+00
200	0.044	2	0.046877	2.000075	5.41	1.305E-02	3.402E-04
200	0.044	4	0.047073	4.000029	5.38	1.394E-02	1.304E-04
200	0.044	6	0.047150	6.000016	5.37	1.429E-02	7.315E-05
200	0.044	8	0.047191	8.000011	5.36	1.447E-02	4.827E-05
200	0.132	2	0.175350	2.011691	4.39	1.966E-01	5.303E-02
200	0.132	4	0.143630	4.000834	0.63	5.275E-02	3.785E-03
200	0.132	6	0.132614	6.000000	0.03	2.785E-03	0.000E+00
200	0.132	8	0.132614	8.000000	0.02	2.785E-03	0.000E+00

Certain trends are observed: (1) more frequent pressure cycling results in a shorter fatigue life and faster crack size enlargement for the same initial crack; (2) crack growth along the depth direction is generally greater than that along the length direction within five years; (3) with certain pressure cycling for the same initial crack depth, axially shorter cracks grow faster in the length direction than longer cracks; for the same initial crack length, deeper cracks grow faster in the length direction than do shallower cracks. This suggests that cracks having a larger shape aspect ratio, i.e. depth to half of length (a/c), have a greater length extension.

In BS 7910: 2013, the critical in-plane spacing between two cracks to interact is half of the maximum crack depth, $a_{max}/2$, which is by no means larger than half of the pipe wall thickness,

t/2. As a generic example, Table 1 proves the crack length growth, equivalent to the crack spacing decrease within five years is definitely less than half of the wall thickness. These discussions bring up the evidence to support a more conservative crack interaction rule for re-assessment interval prediction based on the single crack fatigue life calculation.

If applied with **twice the pipe wall thickness 2t** as an interaction spacing threshold to cluster crack-like defects, those which don't interact at the present time will unlikely interact by the end of five years. The safety factor of '2' allows for the uncertainty from the fact that BS 7910 interaction criterion builds on fatigue tests and brittle fracture tests but has no ductile tearing experiments supporting it. Note that the appropriateness of this criterion on ILI crack-like indications essentially depends on the tool performance, the length size tolerance in particular. For instance, one UT ILI specification prescribes that the length error be 0.8 inch for indications shorter than 4.0 inches, and otherwise 20% at 90% confidence. This uncertainty causes a substantial amount of influence on the ILI applicable interaction criteria. These ILI performance specifications were developed under controlled pull-test conditions, most likely using artificial defects. Actual performance with naturally occurring defects may differ.

Possible interacting patterns of hook cracks

There are four possible configurations for two hook cracks coexisting at a seam weld. Some specialists from the Kiefner failure analysis group ranked the relative frequency of occurrence of four hook cracking patterns in Figure 4. Two hook cracks on the same side of the seam weld and individually located on the ID and OD is the most common. This matches the hydrostatic testing failure in Figure 3. The hydrostatic testing failure in Figure 2 is represented by the pattern ranked as the second-most frequent, with individual hook cracks on the ID and OD and on separate sides of the bond line. On the other hand, two hook cracks each on OD and ID separately are more detrimental than both cracks on either OD or ID, because the projections of two crack planes to the seam weld reduce net thickness in the former case but have some extent of overlap for the latter case.

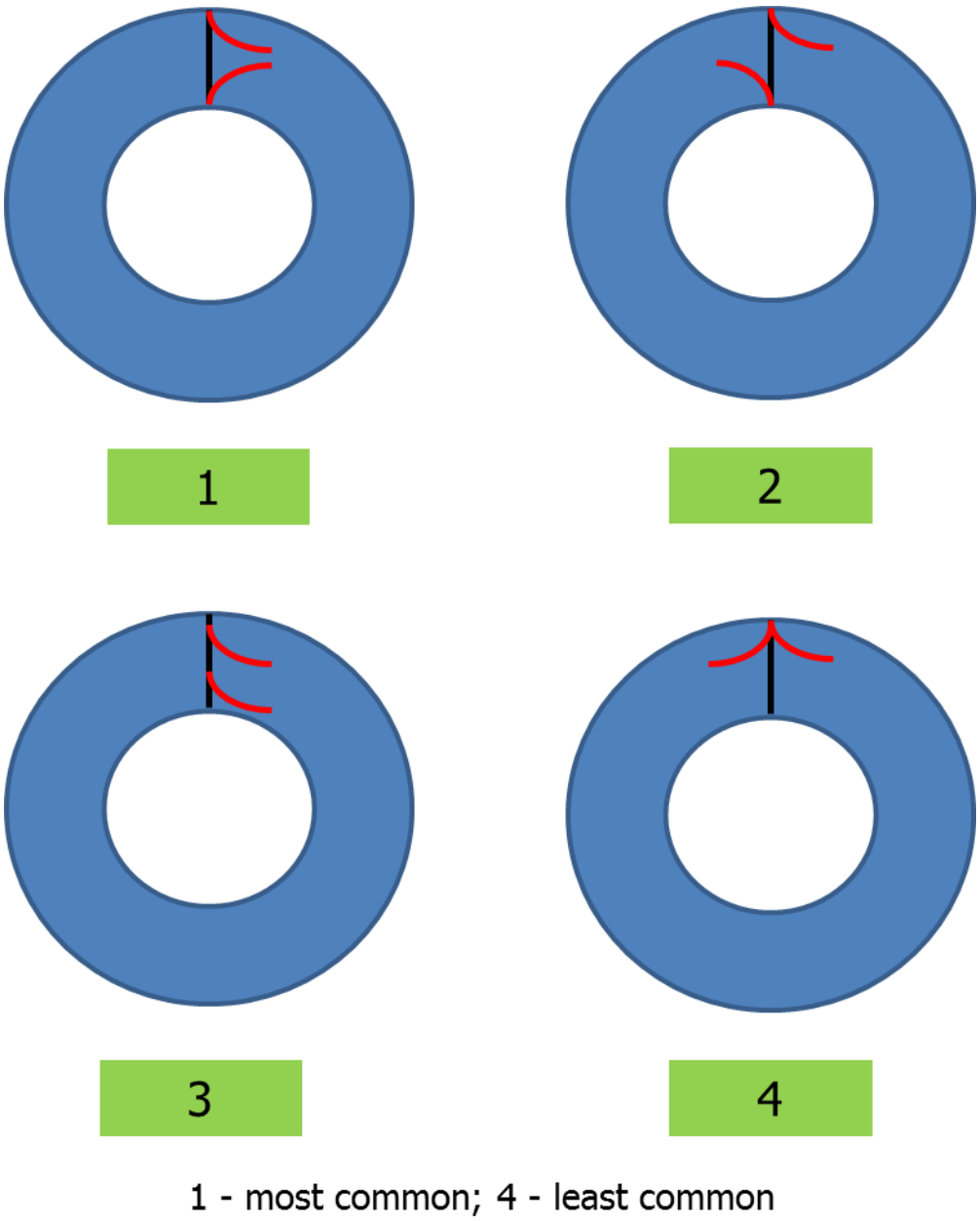

Figure 4. Possible Configurations of Two Hook Cracks

Combination of SCC and Fatigue Growth

For stress corrosion cracking in the pipe body, the environment-driven SCC growth has to be considered along with mechanical-driven fatigue growth. A composite model was proposed to depict the complex behavior as the linear superposition of SCC and fatigue[13]:

[13] Lambert, S.B., Beavers, J.A., Delanty, B., Sutherby, R., and Plumtree, A., "Mechanical Factors Affecting Stress Corrosion Crack Growth Rates in Buried Pipelines", Proceedings of IPC 2000: The International Pipeline Conference 2000, October 1-5, 2000, Calgary, Alberta, Canada.

$$\left.\frac{da}{dN}\right|_{Total} = \left.\frac{da}{dN}\right|_{Fatigue} + \frac{1}{f}\left.\frac{da}{dt}\right|_{SCC} \qquad \text{Equation 3}$$

The cyclic loading tests on single notch bending and compact tension specimens in near-neutral pH electrolyte demonstrated two stages of crack growth. At the beginning, cracks grow at a constant SCC rate independent of ΔK until fatigue growth takes over. Therefore, a conservative remaining life estimation of a crack with an initial depth d_0 is

$$\text{total remaining life} = \frac{d_{transit} - d_0}{\text{SCC growth rate}} + \text{fatigue life for } d_{transit} \qquad \text{Equation 4}$$

where $d_{transit}$ is the crack depth at which the fatigue growth starts to be faster than the SCC growth.

PIPELIFE was exercised to output the crack depth growth rate. Here, as an example: a gas pipeline has the attributes of 30-inch OD, 0.375-inch WT, and Grade X52 operated at MOP equivalent to 72% SMYS. The toughness was chosen to be 15 ft-lb in the calculation as well. The annual equivalent MOP cycles were assumed to be 10, which is greater than that for typical gas transmission pipelines. Figure 5 plots the growth rate every year for a fatigue crack with a fixed length equal to 6.0 inches and a varying depth in an increasing order before eventually reaching the failure. The growth rate escalates sharply at the very end of life, reflecting the cubic relationship between da and a in the Paris-Law equation. Since the crack doesn't grow very much along the length direction, the final depths at the failure are very close for all three initial depths, and then the growth rates are similar to each other before consuming the fatigue longevity. As a comparison, the initial growth rates are drastically different, i.e. a larger value for a deeper crack.

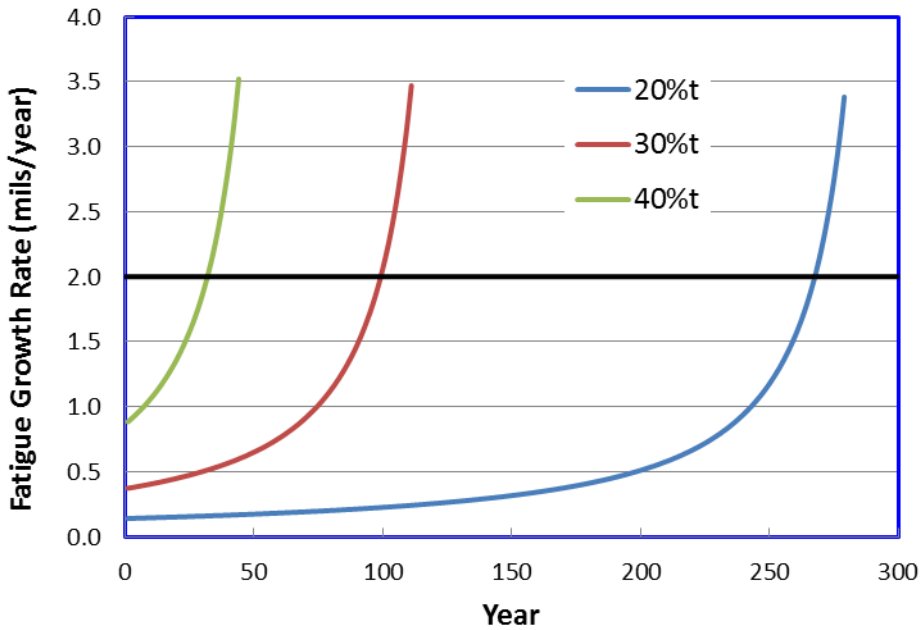

Figure 5. Fatigue Growth Rate for a Crack as Deep as 20%-40%WT in a Gas Pipeline

Furthermore, if this crack is a SCC and the SCC growth rate is 2.0 mils per year, the total lives for three depths are listed in Table 2 where $d_{transit}$ is the crack depth having the fatigue growth rate of 2.0 mils per year from the PIPELIFE calculation. According to Equation 4, the total life is concluded to integrate the SCC and fatigue growth. Since for most of the life span the crack is grown by the linear SCC mechanism, the difference of the total life is approximately in inverse proportion to the initial depth. For this specific pipeline, if the SCC growth rate is greater than about 3.5 mils per year, there won't be any fatigue growth to take place according to the hybrid model.

Table 2. Crack Life Including Both SCC Growth and Fatigue Growth for a Gas Pipeline

d_0 (WT)	$d_{transit}$ (WT)	SCC Growth between d_0 and $d_{transit}$ (year)	Fatigue Life of d_0 (year)	Fatigue Growth between d_0 and $d_{transit}$ (year)	Fatigue Life of $d_{transit}$ (year)	Total Life for d_0 (year)
20%	51%	59	279	268	11	70
30%	52%	41	111	100	11	52
40%	51%	21	44	32	12	33

Results differ significantly for a liquids pipeline. In parallel, a similar crack growth analysis was conducted on the same pipe geometry, but under much more severe pressure fluctuation, i.e. the annual equivalent MOP cycles is assumed to be 100. This is the upper bound cycling representing the liquid pipeline. In Figure 6 the fatigue growth rates are a lot higher than those in a gas pipeline. If the crack is a SCC and the SCC growth rate is 2.0 mils per year, on the contrary to the gas pipeline, the crack growth is primarily driven by fatigue rather than by SCC. Only the crack with an initial depth of 20% of the wall thickness has the portion of SCC growth, and the cracks with an initial depth of 30% of the wall thickness and greater won't be affected by SCC at all and only affected by fatigue. As another example, if the SCC growth rate is 12 mils per year, the overall life of cracks are listed in Table 3. The fatigue life of d_0 and total life of d_0 are closer to each other than those shown in Table 2. This demonstrates some examples of the fatigue dominant behavior in liquid pipelines and the SCC dominant behavior in gas pipelines.

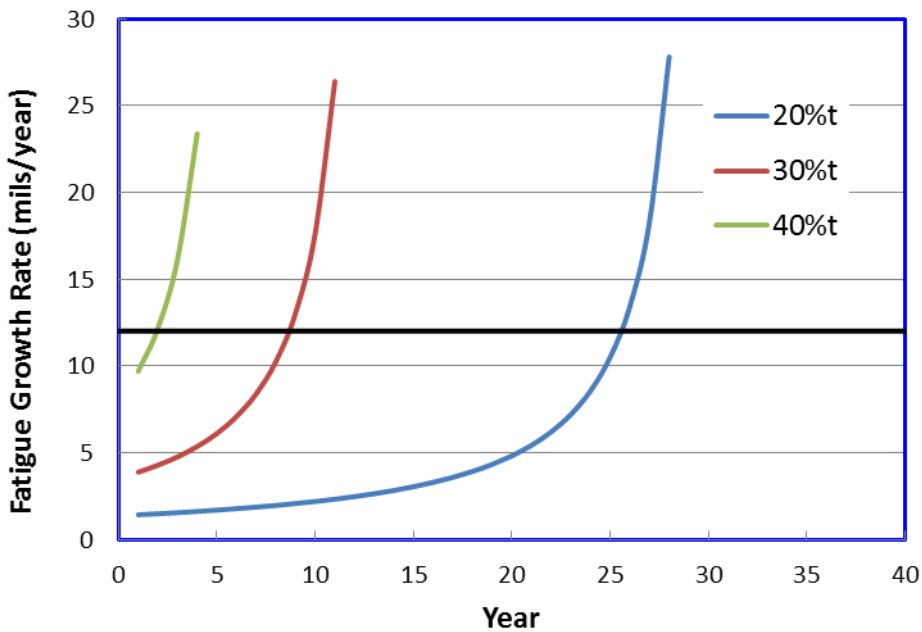

Figure 6. Fatigue Growth Rate for a Crack as Deep as 20%-40%WT in a Liquid Pipeline

Table 3. Crack Life Including Both SCC Growth and Fatigue Growth for a Liquid Pipeline

d_0 (WT)	$d_{transit}$ (WT)	SCC Growth between d_0 and $d_{transit}$ (year)	Fatigue Life of d_0 (year)	Fatigue Growth between d_0 and $d_{transit}$ (year)	Fatigue Life of $d_{transit}$ (year)	Total Life for d_0 (year)
20%	47%	9	28	26	2	11
30%	47%	5	11	9	2	7
40%	46%	2	4	2	2	4

PROBABILISTIC SCHEDULING OF CRACK REMEDIATION

Values of each parameter taken into deterministic analyses such as those specified ones may not be the actual values that characterize the pipeline. The probabilistic simulations were explored in this section to take into account the variability of input parameters in order to develop the distribution of fatigue life. The most confining aspect of a deterministic fatigue life calculation arises in conjunction with having to assume that the worst-case defect actually exists and is located in the location subjected to the most severe pressure cycles. Probabilistic analyses using distributions of possible defects along with distributions of other parameters can be used to assess probability distributions of remaining life.

Pressure Spectrum

A real case example is presented herein. An 8.625-inch OD, 0.220-inch WT and Grade X46 liquid pipeline is operated at the 1,440 psi MOP. It is comprised of two segments, i.e. from A to C and from C to E. Another pump station B is located between A and C; another pump station D is located between C and E. Historical pressure spectrums of four pump stations A, B, C and D were processed using the Rainflow cycle counting technique. Thereafter the annual equivalent MOP cycles were derived from the comprehensive pressure cycles for each pump station in Table 4. The most severe pressure cycling occurs at the discharge of pump station C, whose spectrum is graphically shown in Figure 7.

Table 4. Pressure Cycling Severity of Each Pump Station

Segment	Annual Equivalent MOP Cycles
A to B	33
B to C	30
C to D	66
D to E	36

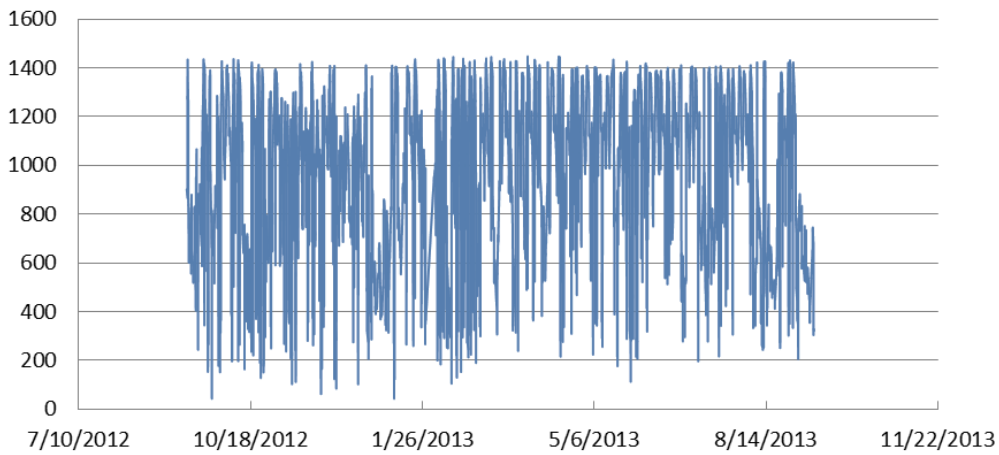

Figure 7. Discharge Pressure Spectrum of Pump Station C

Material Strength

Mill test documents were gathered to establish the material strength distribution. The yield strength of this Grade X46 pipe indicates a generalized β distribution with a mean value of 52,290 psi and a standard deviation of 3,596 psi illustrated in Figure 8 with highlights for the 90% confidence level. The SMYS value of 46,000 psi is below 5th percentile of the true material strength variation.

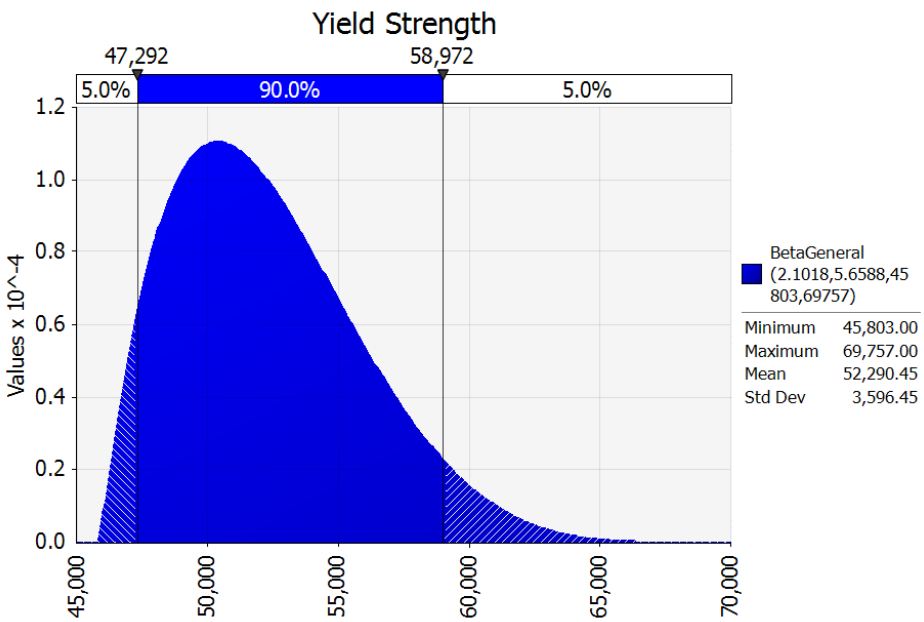

Figure 8. Pipe Yield Strength Distribution Fitted from Mill Tests

Crack-like Defect Size

The in-ditch excavation and NDT inspection, for example, during repair and ILI validation program provided information concerning the possible defect size. The presumption is that AUT such as the PA and TOFD combination produces more accurate crack size than ILI and circumvents the over conservatism from the ILI size in conjunction with the considerable tool tolerance.

The size distributions for three categories of crack-like defects were used for the fatigue life analysis, e.g. detected by ILI, missed by ILI, and total found in the ditch. Figure 9 and Figure 10 respectively demonstrate the discrete sizing for two segments.

The comparisons between two segments are shown in Figure 11 and Figure 12. From another perspective, these two plots also display the size difference between defects detected by ILI and missed by ILI. As expected, the defects found by ILI spread out to be deeper and longer. Since there are quite a few very long defects missed by ILI, the ILI detection capability is more driven by depth than by length. Comparison of two segments implies that ILI performance is consistent. The defects located within the segment between C and E, regardless whether detected or missed, are smaller than those located within the segment between A and C. The fitted distributions are shown in Figure 13 and Figure 14 and are summarized in Table 5.

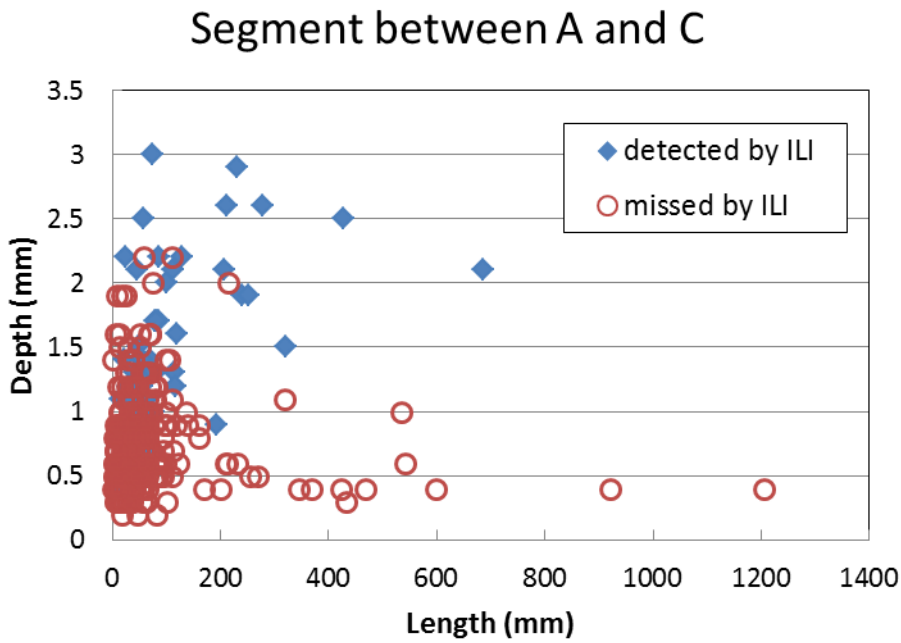

Figure 9. In-ditch NDE Crack-like Indication Size for Segment from A to C

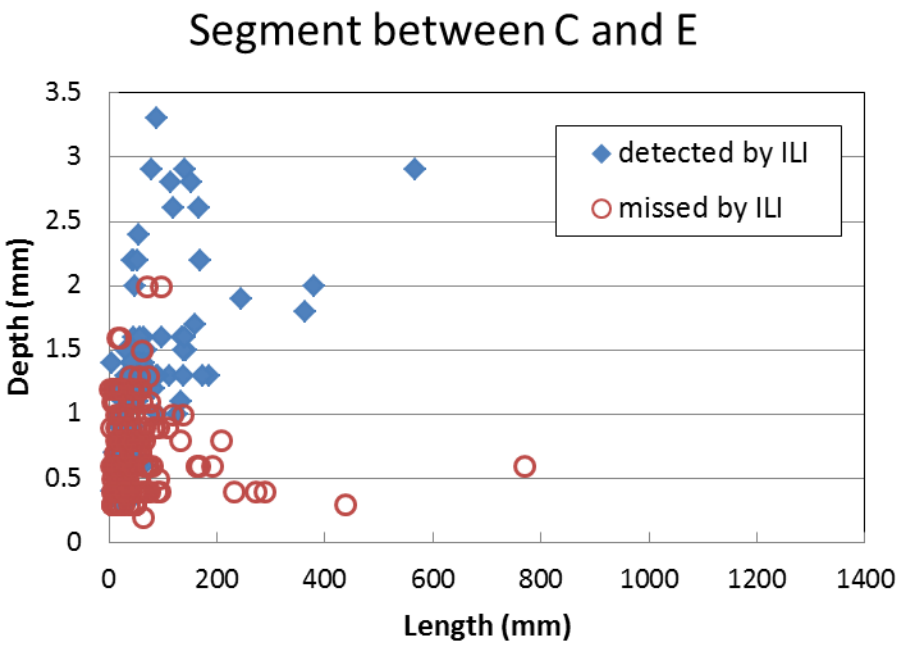

Figure 10. In-ditch NDE Crack-like Indication Size for Segment from C to E

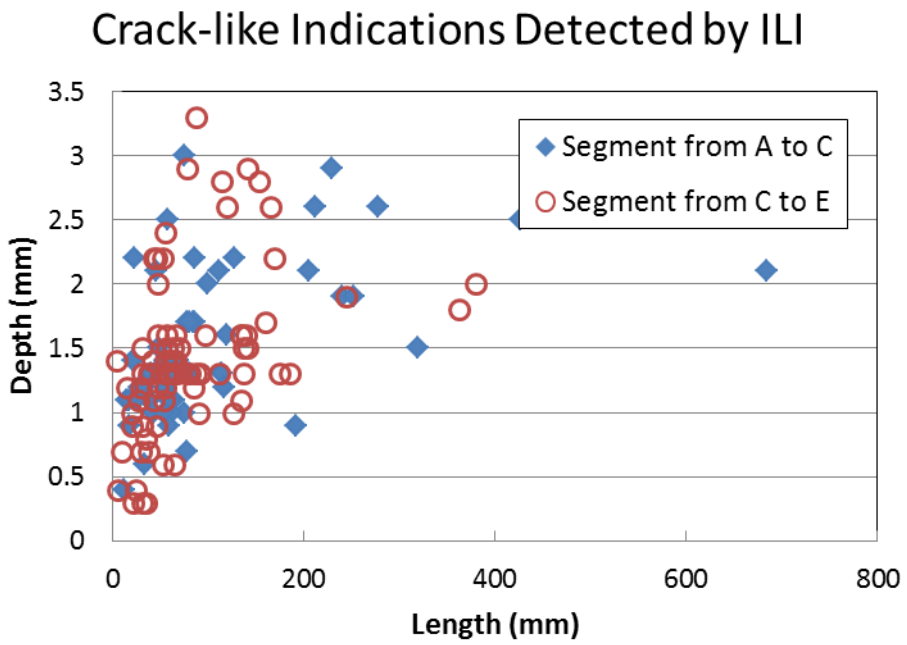

Figure 11. Size Comparison of Crack-like Indications Detected by ILI for Two Segments

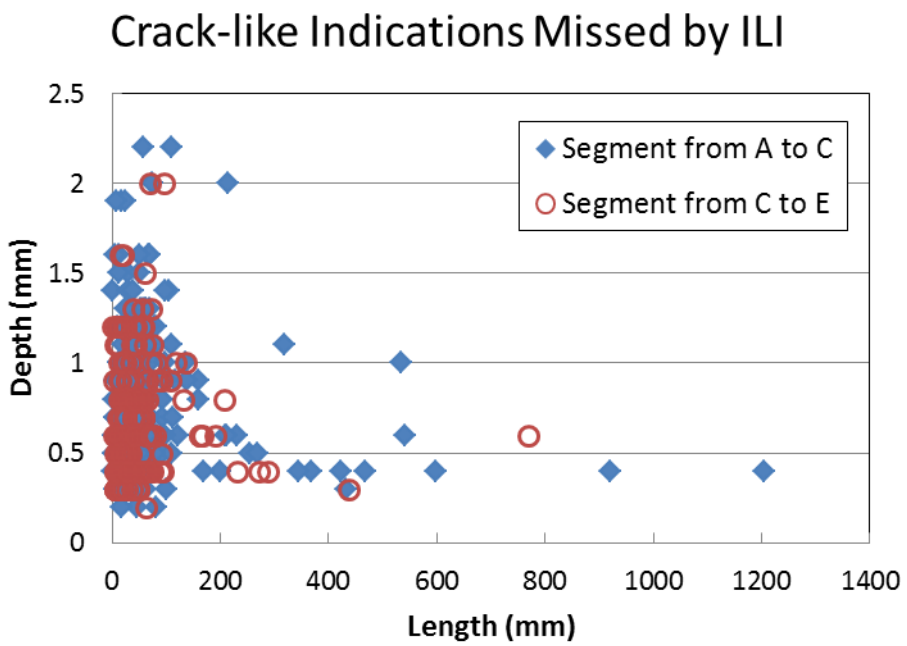

Figure 12. Size Comparison of Crack-like Indications Missed by ILI for Two Segments

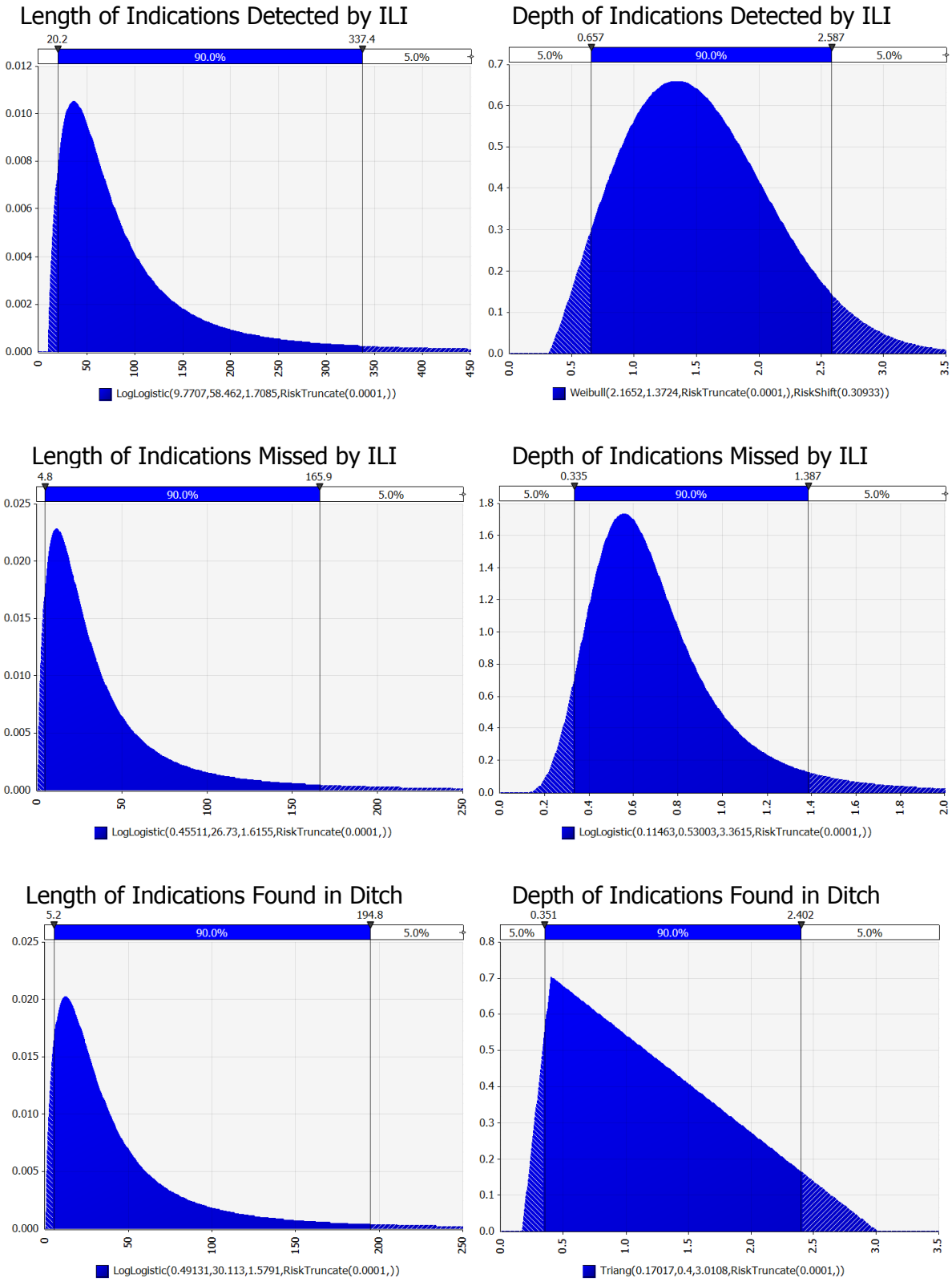

Figure 13. Crack-like Indication Size Distribution for Segment from A to C

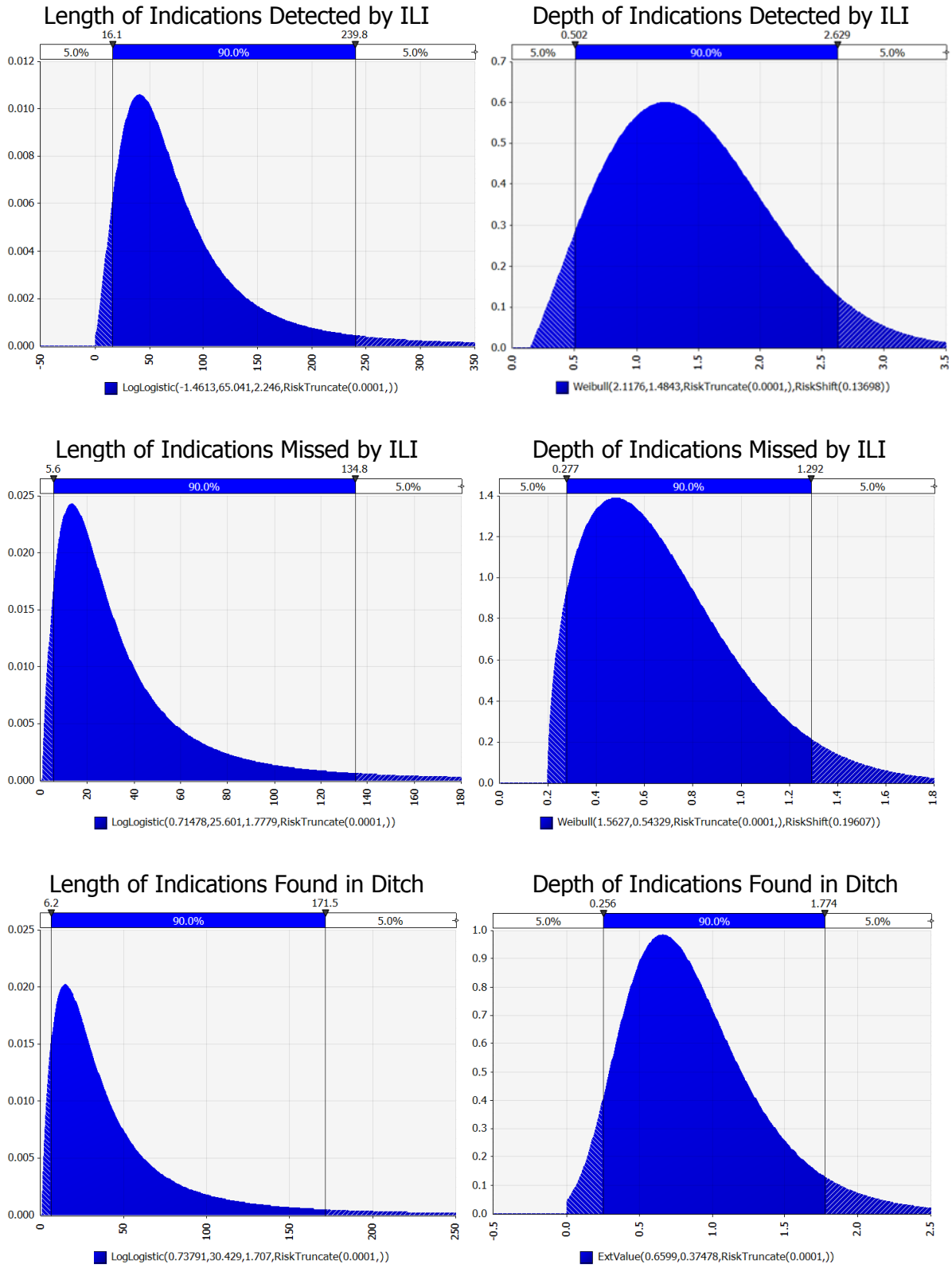

Figure 14. Crack-like Indication Size Distribution for Segment from C to E

Table 5. Fitted Distributions for Three Categories of Indications

Segment	Indication Type	Length/ Depth	Distribution Type	Mean (mm)	Std. (mm)	Shift (mm)
A to C	Detected by ILI	Length	Log Logistic	121.25	N/A	0.00
	Detected by ILI	Depth	Weibull	1.52	0.59	0.31
	Missed by ILI	Length	Log Logistic	56.29	N/A	0.00
	Missed by ILI	Depth	Log Logistic	0.73	0.41	0.00
	Total Found	Length	Log Logistic	66.06	N/A	0.00
	Total Found	Depth	Triangle	1.19	0.64	0.00
C to E	Detected by ILI	Length	Log Logistic	91.29	151.16	0.00
	Detected by ILI	Depth	Weibull	1.45	0.65	0.14
	Missed by ILI	Length	Log Logistic	46.84	N/A	0.00
	Missed by ILI	Depth	Weibull	0.68	0.32	0.20
	Total Found	Length	Log Logistic	58.84	N/A	0.00
	Total Found	Depth	Extreme Value	0.88	0.48	0.00

Material Toughness

ILI vendors normally use a single level of toughness to calculate the failure stresses for all detected and sized anomalies. The dilemma associated with this process is that the toughness of the material is usually not known and that true toughness is likely to vary from one batch of pipe to another. The application of lower-bound toughness estimates for predicting failure stress will possibly result in unnecessary excavations and examinations of many anomalies that may not be as injurious as those really needing to be repaired[7].

The Modified Ln-Sec equation describes the condition of ductile fracture initiation. Combined with a Charpy energy of 15 ft-lb, it gave reasonable and often conservative predictions of the failure stress levels of 31 of 32 fatigue-enlarged defects[7]. Since the Modified Ln-Sec model is an empirical model validated against a particular set of full scale tests[14], it may not be plausible to represent materials having the upper-shelf Charpy energy below 15 ft-lb in a full-size CVN specimen.[7]

From the Kiefner material property database, the full-size equivalent upper-shelf Charpy values were fitted to be a Log-logistic distribution with mean of 41 ft-lb and 5th percentile of 19 ft-lb

[14] Kiefner, J.F., Maxey, W.A., Eiber, R.J., and Duffy, A.R., "Failure Stress Levels of Flaws in Pressurized Cylinders", Progress in Flaw Growth and Fracture Toughness Testing, ASTM STP 536, American Society for Testing and Materials, pp 461-481, 1973.

shown in Figure 15. This fact supports 15 ft-lb as a lower bound ductile toughness to properly represent real pipe material, irrespective of pipe grades.

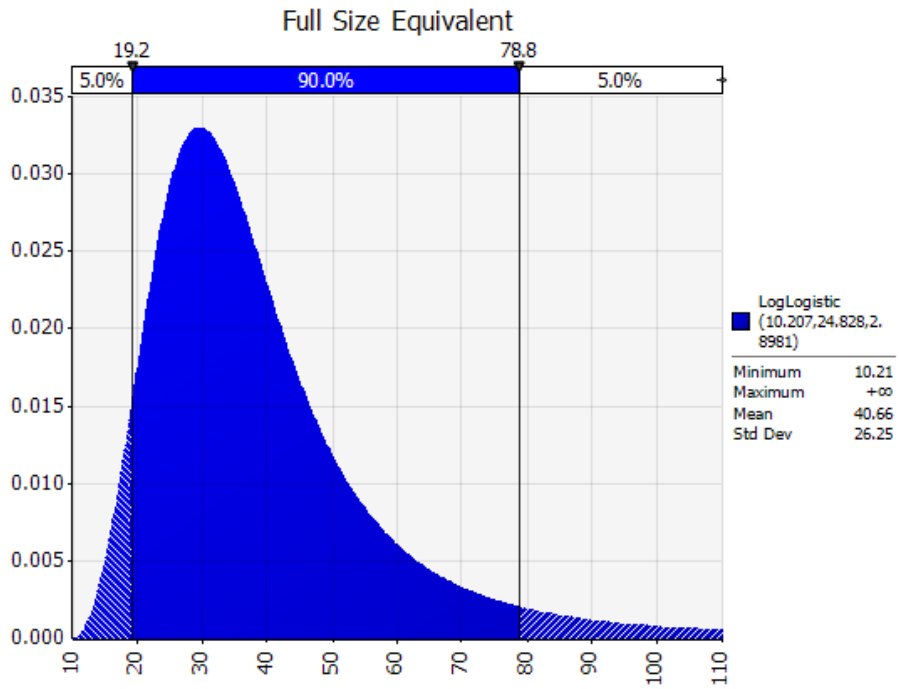

Figure 15. Toughness Distribution Fitted From CVN Data in Kiefner Database

Burst Model Error

The Modified Ln-Sec equation was validated by in-service failures, hydrostatic failures and burst tests on pieces of pipes removed from service, as depicted in Figure 16[15]. The model accuracy was explored through the ratio between actual failure pressure and predicted failure pressure. The statistical fitting of this ratio produced a Log-logistic distribution as illustrated in Figure 17 with mean of 1.089. The corresponding cumulative probability is plotted in Figure 18. When the ratio is equal to 1.0, there is 23% possibility that the Modified Ln-Sec equation is not conservative when using actual material properties. The model becomes more conservative when specified minimum yield strength (SMYS) values are used, since most pipe is stronger than the specified minimum value for the corresponding grade.

[15] Kiefner, J.F. and Leewis, K., "Guidance for the Assessment of Pipeline Defects", Pipeline Research Council International, Inc., Catalog No. PR-218-05404-R01, May 2010.

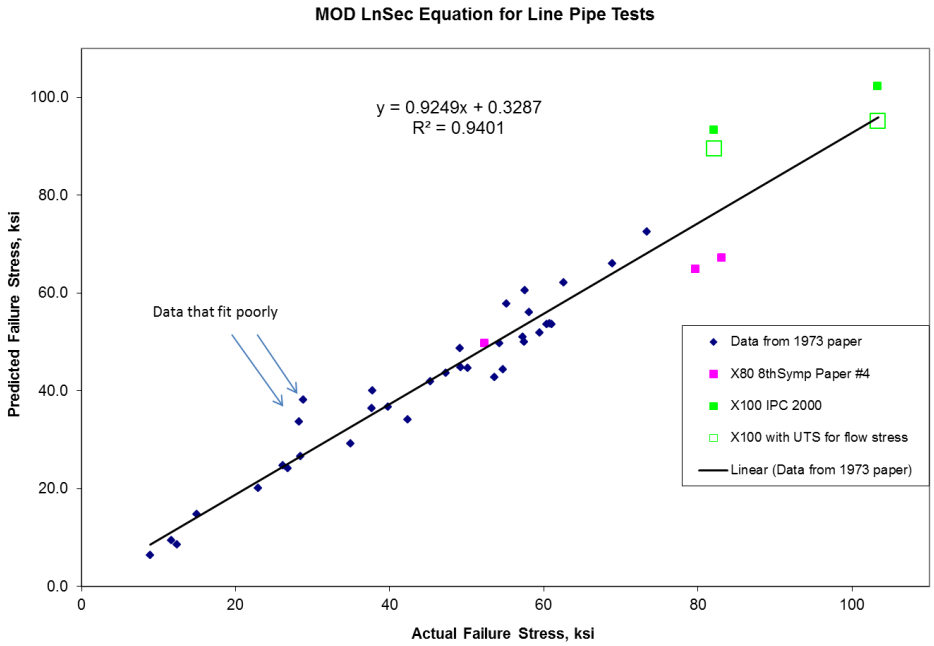

Figure 16. Comparison between Predicted and Actual Failure Pressures

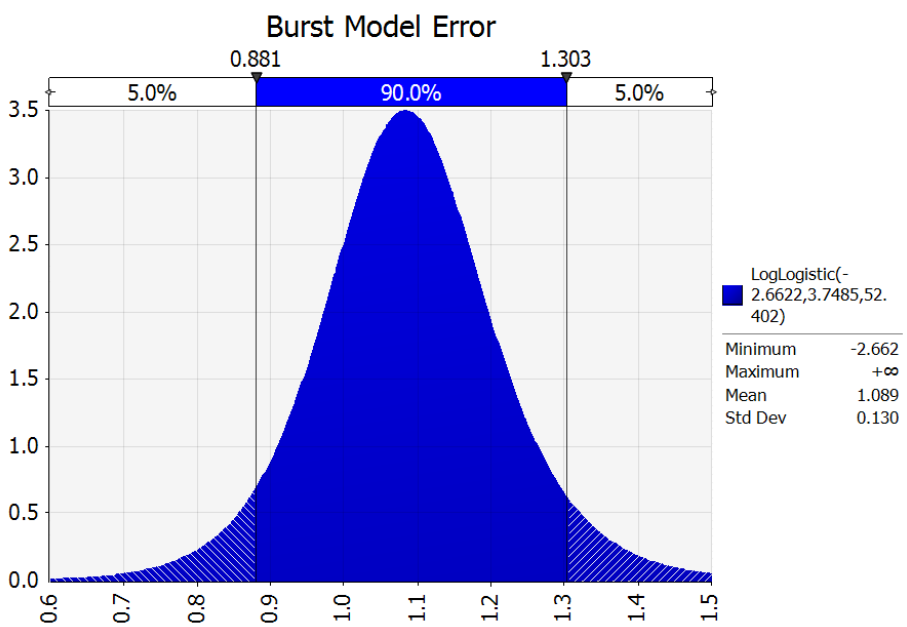

Figure 17. Probability Density Distribution of Ratio between Actual Failure Pressure and Predicted Failure Pressure

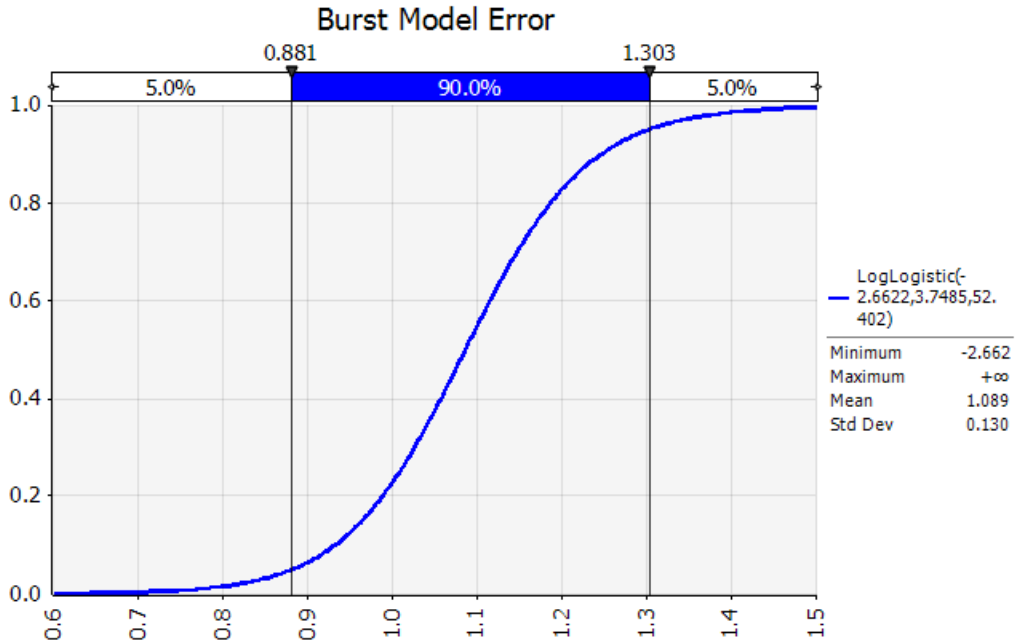

Figure 18. Cumulative Probability Distribution of Ratio between Actual Failure Pressure and Predicted Failure Pressure

Probability of Failure

Monte Carlo simulations were performed to generate the fatigue life with respect to material strength, toughness, defect size, and model prediction variations from the deterministic values. Probability of Failure (POF) is defined as the number of iterations having fatigue life less than 10 years, equivalent to a 5-year re-assessment interval, divided by the total number of iterations, which is chosen to be 100,000 in this study. The POFs for each indication size distribution and each discharge pressure are listed in Table 6. For every individual pump station, the unanimous conclusion is that the defects detected by ILI brought forth the highest POFs, missed by ILI led to the lowest POFs, and the POFs caused by the complete set of in-ditch indications (encompassing both those detected by ILI and those missed) was in-between. This observation is anticipated from Figure 9 through Figure 12.

Since both the fatigue growth and the burst capacity of cracks are more sensitive to the depth dimension than to the length dimension, deeper cracks most likely have a shorter fatigue life than shallower ones for comparable lengths. Such as shown in Figure 10, on average, the fatigue life of crack-like defects detected by ILI is shorter than that of those missed by ILI. When the crack length is longer than $6\sqrt{Dt}$, about 224 mm, the burst condition approaches approximately being length-independent. In Figure 9, even though some defects missed by ILI have a longer length than those detected, they have smaller depth in the range of length less than $6\sqrt{Dt}$. Deeper defects tend to grow more quickly than shallower defects. Therefore, the

defects not indicated by ILI generally have a longer fatigue life and produce a smaller failure probability in the studied pipeline.

When the pressure fluctuation has similar amplitudes, such as the section between A and B and the section between D and E, the POF is controlled by the defect size distribution. As three categories of defects (i.e., detected by ILI, missed by ILI, all found) are regularly smaller in the segment from C to E than in the segment from A to C, POFs of the section between D and E are lower than those of the section between A and B. When the pressure cycling increases, e.g. the section between C and D, it overrides the effect of smaller defect size, and produces greater POFs than the section between A and B for the defects detected by ILI.

Table 6. POFs of Four Pump Segments

Start	End	Indication Type	Probability of Life Less Than 10 Years
A	B	**Missed by ILI**	1.34E-03
A	B	Detected by ILI	1.30E-02
A	B	Total Found	2.47E-03
B	C	**Missed by ILI**	1.28E-03
B	C	Detected by ILI	1.17E-02
B	C	Total Found	1.94E-03
C	D	**Missed by ILI**	1.17E-04
C	D	Detected by ILI	2.44E-02
C	D	Total Found	1.42E-03
D	E	**Missed by ILI**	1.04E-04
D	E	Detected by ILI	1.11E-02
D	E	Total Found	6.54E-04

Table 6 offers insight regarding how to wisely deploy mitigation efforts to this pipeline from a risk-based standpoint. The POFs calculated from the crack-like defects missed by ILI in effect denotes the pipeline condition after the inspection and the repair program. The segment between C and E has lower POFs by about one order of magnitude than the segment between A and C. Mitigation efforts ought to be focused on the first segment under a financial budget constraint every year. Over time, the risk of fatigue crack failure may be decreased or increased depending on the balance between the mitigation effort and the crack growth rate. If the repair program following the next ILI re-assessment demonstrates the defects missed by ILI have overall smaller sizes, it is most likely that the POF would drop under a similar pressure cycling. This means the excavation efforts currently conducted outweigh the fatigue crack enlargement, and the mitigation is effective. On the other hand, if the missed defects

discovered by the next ILI validation program tend to be larger, POF would increase, which means more stringent excavation criteria or maybe hydrostatic testing are required in the future.

Comparison with Deterministic Analysis

The probabilistic results reported above were compared with the fatigue lives for four pump segments deterministically calculated as in Table 8 according to the deepest indications listed in Table 7.

Table 7. Crack-like Indication Size with the Largest Depth

Segment	Indication Type	Length (mm)	Depth (mm)
A to C	Detected by ILI	75	3.0
	Missed by ILI	110	2.2
C to E	Detected by ILI	88	3.3
	Missed by ILI	95	2.0

Table 8. Fatigue Life Determined by Deepest Indications

Start	End	Indication Type	Fatigue Life (year)
A	B	**Missed by ILI**	42
A	B	Detected by ILI	20
B	C	**Missed by ILI**	45
B	C	Detected by ILI	22
C	D	**Missed by ILI**	33
C	D	Detected by ILI	4
D	E	**Missed by ILI**	61
D	E	Detected by ILI	7

In general terms, Table 8 matches Table 6. A shorter fatigue life corresponds to a higher POF as shown in Figure 19 below. The trend is consistent, but there is not a direct relationship between deterministic and probabilistic results because of the defect sizing distributions shown in Figure 11 and Figure 12. Regardless of being detected or missed, the deepest defect of the segment from C to E is farther away from the medians of the defect size distributions than that of the segment from A to C.

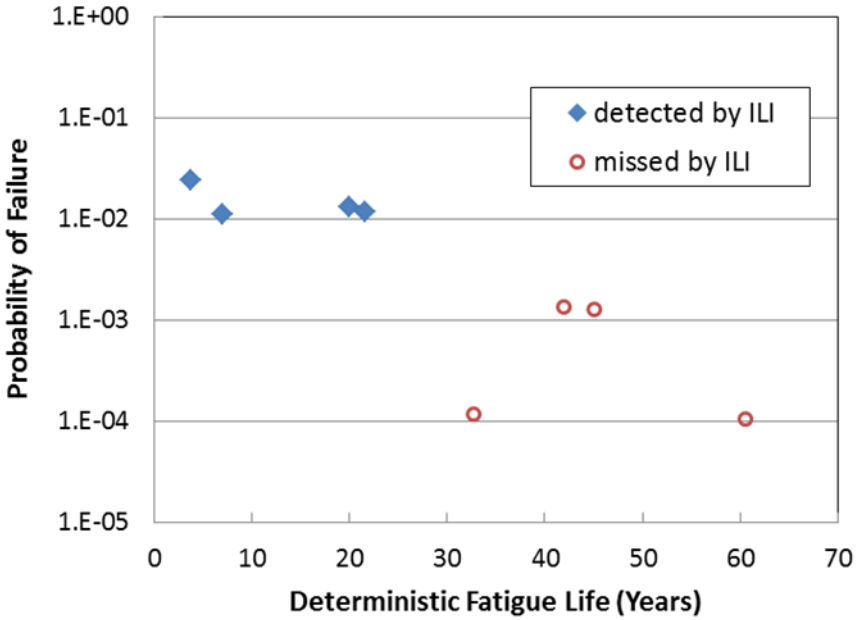

Figure 19. Relationship between POF and Deterministic Fatigue Life

Conclusion

Two types of fatigue life calculations are commonly pursued based on the means of the initial defect size determination. One is from inspection as investigated above; the other is from hydrostatic testing to infer the largest defects barely surviving the test. Without any historical hydrostatic test record, the manufacturers' minimum hydrostatic tests from API 5L point out that for this 1964 vintage, 8.625-inch OD, 0.220-inch WT, Grade X46 pipeline, the standard mill test pressure is equivalent to 75% SMYS, i.e. 1764 psig.

In PIPELIFE, the lengths of nine defects with minimum depth of 10%WT, maximum depth of 90%WT[16], and 10%WT consecutive increase are back-calculated from the Modified Ln-Sec equation with a burst pressure of 1764 psig. Considering those nine defects, one finds that the shortest remaining life is the fatigue life of the pipeline, which is about 10 years. Comparing to Table 8, hydrostatic testing at 75% SMYS in the studied pipeline is only capable of exposing fewer than thirteen defects detected by ILI, not a single one missed by ILI, and even the size of most defects detected by ILI is smaller than the size of those barely surviving the hydrostatic test. This is indicated graphically in Figure 20 and Figure 21 below. Even with a hydrostatic test level equal to 100% SMYS, only five defects missed by ILI could have been exposed, and

[16] Owing to the way ERW seams are made, it is likely that an initial crack will not exceed 50% or perhaps 60% of the pipe wall thickness. This is supported by extensive failure investigations. However, if the pipeline has been in service for a long time, a fatigue life evaluation based on a more recent hydrostatic pressure test must consider the possibility of a deeper flaw due to prior growth. Therefore, it is necessary to calculate times to failure for surviving flaws having a depth between 70% and 80% of the pipe wall thickness.

similarly many small defects detected by ILI are below the 100% SMYS curve. In other words, fatigue life is better characterized by inspection than by hydrostatic testing if in-ditch NDT proves to be reliable.

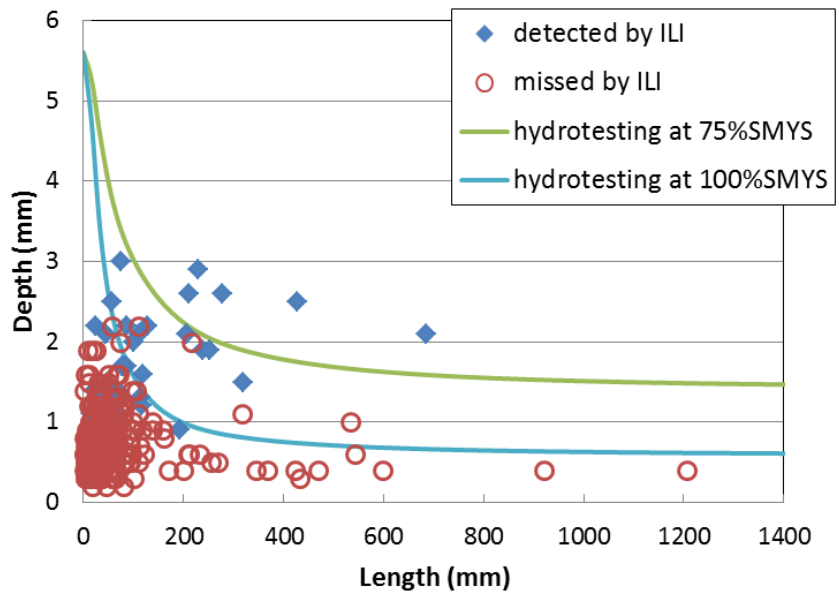

Figure 20. Comparison between Hydrostatic Testing and In-ditch NDT for the Segment between A and C

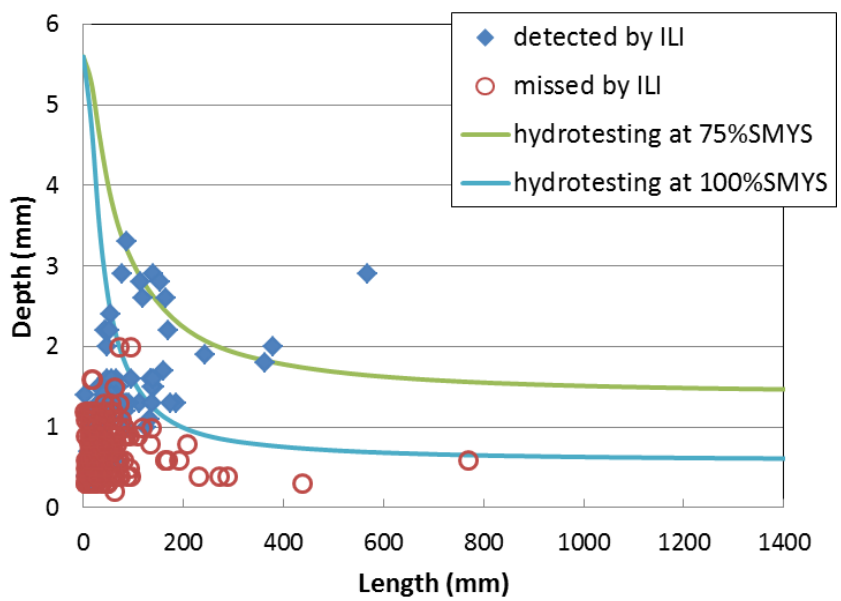

Figure 21. Comparison between Hydrostatic Testing and In-ditch NDT for the Segment between C and E

If one uses the deterministic analysis results as evidence of mitigation criteria, the fatigue lives of missed defects from ILI have approximately comparable scales for all four sections, i.e. 42,

45, 33, and 61. Discounted by a safety factor of '2' for the re-assessment interval, they are even closer, i.e. 21, 22, 16, and 30. The mitigation efforts would be placed on the section between C and D, which dramatically divert from the results of the probabilistic analysis. As elucidated in Table 6, POFs for the segment between C and E is about one order of magnitude less than the segment between A and C. The mitigation would be concentrated on the section between A and B.

Probabilistic fatigue life analysis stems from a broader picture of the pipeline condition by taking into account the variations for pipe material, defect size, etc. It demonstrates its own value related to risk ranking which assists the mitigation planning, particularly when the fatigue lives from the deterministic calculation for all the segments cannot be differentiated based on the worst-case scenario. The POF provides the clue as to the prioritization of segments and suggests the effectiveness of mitigation efforts over time.

US DOT - PHMSA

Final Report No. 16-025

Final Report

Threat/Anomaly Mitigation Decision-Making Process – Annex D. Deterministic and Probabilistic Approaches for Scheduling Mitigations of Mechanical Damage

Jing Ma, PhD and Fan Zhang, PhD
Kiefner and Associates Inc.
Guy Desjardins, Consultant
Desjardins Integrity Ltd.

February 23, 2016

0339-1402

Kiefner and Associates, Inc. is an Applus RTD company.

Intentionally blank

Final Report No. 16-025

Final Report

THREAT/ANOMALY MITIGATION DECISION-MAKING PROCESS ANNEX D. DETERMINISTIC AND PROBABILISTIC APPROACHES FOR SCHEDULING MITIGATIONS OF MECHANICAL DAMAGE

DTPH5614H00005

to

U.S. DEPARTMENT OF TRANSPORTATION – PIPELINE AND HAZARDOUS MATERIALS SAFETY ADMINISTRATION

February 23, 2016

Prepared by

Jing Ma
Senior Engineer I, PhD

Approved by

John F. Kiefner, PhD, P.E.

Kiefner and Associates, Inc.
4480 Bridgeway Avenue, Suite D
Columbus, OH 43219

0339-1402

DISCLAIMER

This document presents findings and/or recommendations based on engineering services performed by employees of Kiefner and Associates, Inc. The work addressed herein has been performed according to the authors' knowledge, information, and belief in accordance with commonly accepted procedures consistent with applicable standards of practice, and is not a guaranty or warranty, either expressed or implied.

The analysis and conclusions provided in this report are for the sole use and benefit of the Client. No information or representations contained herein are for the use or benefit of any party other than the party contracting with Kiefner. The scope of use of the information presented herein is limited to the facts as presented and examined, as outlined within the body of this document. No additional representations are made as to matters not specifically addressed within this report. Any additional facts or circumstances in existence but not described or considered within this report may change the analysis, outcomes and representations made in this report.

TABLE OF CONTENTS

INTRODUCTION 1
WORK SCOPE 1
BACKGROUND 2
PHMSA INCIDENT DATA AND STATISTICS 4
MITIGATION OF IMMEDIATE FAILURES 5
MITIGATION OF DELAYED FAILURES 11
Reportable Incident Risk Prediction 13
POE-Based Mitigation Plan 16
Bayesian-Based Mitigation Plan 22

LIST OF FIGURES

Figure 1. Probability Density Function for Actual Diameter/Nominal Diameter 8
Figure 2. Probability Density Function for Actual WT/Nominal WT 8
Figure 3. Probability Density Function for Actual UTS/SMTS 8
Figure 4. Probability Density Function for Resistance Model Error 9
Figure 5. Probability Density Function for Excavator Weight 9
Figure 6. Cumulative Probability Function for Excavator Weight 9
Figure 7. Probability Density Function for Tooth Length 10
Figure 8. Probability Density Function for Tooth Width 10
Figure 9. Significant Incident Probability per Feature per Year 15
Figure 10. Cumulative Probability of Occurrence of Dent Features from ILI 16
Figure 11. Predictions of Fatigue Life of Plain Dents by the EPRG Model[16] 19
Figure 12. Student's t-Distribution with 44 Degrees of Freedom 19
Figure 13. Probability of Unsafe vs ILI Anomaly Severity 23
Figure 14. Severity of Each of Fifty ILI Indications 26

LIST OF TABLES

Table 1. PHMSA Incidents between 1995 and 2014 4
Table 2. Probability Density Functions used in Calculations 7
Table 3. Comparison between Deterministic and Probabilistic Analysis 11
Table 4. Categories of Delayed-Failure Incidents by Mechanical Damage 1985-1997 12

Table 5. Statistics of Dents for Different Pipeline Systems.....13
Table 6. 2010-2014 Significant Incidents Caused by Excavation Damage 14
Table 7. "Significant" Incident Rate for Mechanical Damage and Rock Dent 14
Table 8. Risk Levels Associated with Repair Criteria 16
Table 9. ILI Information on Dents in Working Example.....20
Table 10. Probability of Dent Fatigue Failure 21
Table 11. After the 2nd Excavation 28
Table 12. After the 3rd Excavation.....29
Table 13. After the 14th Excavation.....30

Threat/Anomaly Mitigation Decision-Making Process – Annex D. Deterministic and Probabilistic Approaches for Scheduling Mitigations of Mechanical Damage

Jing Ma, PhD, Fan Zhang, PhD, and Guy Desjardins

INTRODUCTION

Pipeline operators must excavate and examine anomalies discovered through in-line inspection (ILI), or direct assessment (DA) for external corrosion, internal corrosion, or stress-corrosion cracking in a timely manner to assure that critical defects are repaired before they become large enough to cause a pipeline to fail at its maximum operating pressure. Pipeline operators must also periodically reassess their pipelines that are located in or could affect the high consequence areas (HCAs). While prescriptive regulations often require examinations of anomalies or re-assessments to be carried out after specific time periods, a more rational way to schedule excavations or to conduct re-assessments would be to schedule them based on the sizes of anomalies remaining after the most recent assessment, the applicable rate of deterioration, and the sizes of anomalies that would cause the pipeline to fail at its maximum operating pressure. However, there are two challenges to performance-based assessment approaches. First, one must account for the error inherent in all currently available in-situ technologies. Second, one must account for the interaction between coexisting anomalies. Three types of anomalies and their related interactions will be addressed in a consecutive manner. As a part of this project, the mitigation scheduling of mechanical damage will be specifically dealt with in this interim report by following both deterministic and probabilistic approaches.

WORK SCOPE

For this quarterly report, the mitigation of mechanical damage was mainly approached from the risk standpoint. This is in conjunction with the fact that the assessment methods of mechanical damage are generally not as robust as those for cracks and corrosion. Three different angles have been pursued for case studies, including (1) significant and serious incident probability based on the most up-to-date PHMSA reportable incident rate; (2) decision-making process based on the full knowledge of POE function; (3) decision-making process without knowledge of POE function based on excavation. These investigations shed light on circumstances of

remediation of in-line inspection anomalies and can be easily tailored to other called-out features, such as corrosion anomalies, crack anomalies, etc.

BACKGROUND

Part 192 and Part 195 of U.S. Code of Federal Regulations Title 49: Transportation incorporate pipeline integrity management regulations for gas and hazardous liquid transmission pipelines respectively. These regulations state the types of anomalies pipeline operators must address and they prescribe maximum re-assessment intervals for continued monitoring and remediation within HCAs. This project was conceived to develop a more flexible approach to pipeline integrity management that would allow pipeline operators to base re-assessment and remediation intervals on the actual rates of anomaly growth determined from measurements and experience.

The U.S. Federal Pipeline Safety Regulations have specific requirements regarding dents on pipelines, particularly in High Consequence Areas. For instance:

U.S. Code of Federal Regulations Title 49 Transportation, Part 192 – Transportation of Natural Gas and Other Gas by Pipeline, Subpart O—Gas Transmission Pipeline Integrity Management

§192.933 What actions must be taken to address integrity issues?

(d) *Special requirements for scheduling remediation*—(1) *Immediate repair conditions.*

(ii) A dent that has any indication of metal loss, cracking or a stress riser.

(2) *One-year conditions.*

(i) A smooth dent located between the 8 o'clock and 4 o'clock positions (upper $^2/_3$ of the pipe) with a depth greater than 6% of the pipeline diameter (greater than 0.50 inches in depth for a pipeline diameter less than Nominal Pipe Size (NPS) 12).

(ii) A dent with a depth greater than 2% of the pipeline's diameter (0.250 inches in depth for a pipeline diameter less than NPS 12) that affects pipe curvature at a girth weld or at a longitudinal seam weld.

(3) *Monitored conditions.*

(i) A dent with a depth greater than 6% of the pipeline diameter (greater than 0.50 inches in depth for a pipeline diameter less than NPS 12) located between the 4 o'clock position and the 8 o'clock position (bottom $^1/_3$ of the pipe).

(ii) A dent located between the 8 o'clock and 4 o'clock positions (upper $^2/_3$ of the pipe) with a depth greater than 6% of the pipeline diameter (greater than 0.50 inches in depth for a pipeline diameter less than Nominal Pipe Size (NPS) 12), and engineering analyses of the dent demonstrate critical strain levels are not exceeded.

(iii) A dent with a depth greater than 2% of the pipeline's diameter (0.250 inches in depth for a pipeline diameter less than NPS 12) that affects pipe curvature at a girth weld or a longitudinal seam weld, and engineering analyses of the dent and girth or seam weld demonstrate critical strain levels are not exceeded. These analyses must consider weld properties.

U.S. Code of Federal Regulations Title 49 Transportation, Part 195 – Transportation of Hazardous Liquids by Pipeline, §195.452 Pipeline integrity management in high consequence areas

(4) *Special requirements for scheduling remediation*—(i) *Immediate repair conditions.*

(C) A dent located on the top of the pipeline (above the 4 and 8 o'clock positions) that has any indication of metal loss, cracking or a stress riser.

(D) A dent located on the top of the pipeline (above the 4 and 8 o'clock positions) with a depth greater than 6% of the nominal pipe diameter.

(ii) *60-day conditions.*

(A) A dent located on the top of the pipeline (above the 4 and 8 o'clock positions) with a depth greater than 3% of the pipeline diameter (greater than 0.250 inches in depth for a pipeline diameter less than Nominal Pipe Size (NPS) 12).

(B) A dent located on the bottom of the pipeline that has any indication of metal loss, cracking or a stress riser.

(iii) *180-day conditions.*

(A) A dent with a depth greater than 2% of the pipeline's diameter (0.250 inches in depth for a pipeline diameter less than NPS 12) that affects pipe curvature at a girth weld or a longitudinal seam weld.

(B) A dent located on the top of the pipeline (above 4 and 8 o'clock position) with a depth greater than 2% of the pipeline's diameter (0.250 inches in depth for a pipeline diameter less than NPS 12).

(C) A dent located on the bottom of the pipeline with a depth greater than 6% of the pipeline's diameter.

These regulations provide the clear guidance for operators to respond once they receive the in-line inspection results. It is noticeable that within the gas regulations, engineering analyses are deemed legitimate to extend the one-year conditions to be the monitored conditions. However, there is no counterpart with regard to the liquid pipelines. In essence, the same considerations should be given as long as pressure-cycle-induced fatigue does not become an issue.

PHMSA INCIDENT DATA AND STATISTICS

According to the most up-to-date PHMSA data and statistics on their website as indicated in Table 1, for 20 years ranging from 1995 to 2014, for the 301,732 miles of gas transmission pipelines, excavation damage occupies 30.4% of the serious incidents and 16.4% of significant incidents; for the 199,210 miles of hazardous liquid pipelines, excavation damage occupies 31.6% of the serious incidents and 15.6% of the significant incidents. On the whole, excavation damage is the leading cause of serious incidents and ranks third for significant incidents following material/weld/equipment failure and corrosion. Those data will be referenced in the later sections to serve as the basis for risk assessment on excavation damage.

Table 1. PHMSA Incidents between 1995 and 2014

Pipeline System	Incident Type	Mileage up to 2014	Number of All Incidents	Number of Excavation Damage	Percentage of Excavation Damage
gas transmission	serious[1]	301,732	102	31	30.4%
gas transmission	significant[2]	301,732	1265	207	16.4%
hazardous liquid	serious	199,210	76	24	31.6%
hazardous liquid	significant	199,210	2697	421	15.6%
total	serious	500,941	178	55	30.9%
total	significant	500,941	3962	628	15.9%

[1] Fire First Incidents are Gas distribution incidents with a cause of Other Outside Force Damage and sub-cause of Nearby Fire/Explosion as Primary Cause of Incident. Serious Incidents are those including a fatality or an injury requiring in-patient hospitalization, but Fire First incidents are excluded.

[2] Fire First Incidents are Gas distribution incidents with a cause of Other Outside Force Damage and sub-cause of Nearby Fire/Explosion as Primary Cause of Incident. Significant Incidents are those including any of the following conditions, but Fire First incidents are excluded: 1) Fatality or injury requiring in-patient hospitalization; 2) $50,000 or more in total costs, measured in 1984 dollars; 3) Highly volatile liquid releases of 5 barrels or more or other liquid releases of 50 barrels or more; 4) Liquid releases resulting in an unintentional fire or explosion.

MITIGATION OF IMMEDIATE FAILURES

As emphasized in a PRCI report[3], it is difficult to state that the defects described as 60-day, 180-day, or 1-year conditions can always be distinguished so precisely in terms of their effects on the integrity or longevity of the affected pipe. This is so even though the regulations strive to identify distinct levels of severity in order to prioritize the urgency of the operator's response based on the perceived severity of the damage.

Mechanical damage incidents are typically classified as "immediate" (those that occur immediately upon impact of an external force) and "delayed" (those in which the pipeline sustains an impact of an external force but does not fail until later). According to Kiefner[4], equipment-induced damage fails immediately 83% of the time in the hazardous liquid pipelines and 90% of the time in the natural gas pipelines. It is noted that delay failures are relevant to mitigation, the subject of this report, whereas immediate failures can only be addressed by preventative measures and design efforts.

Preventative measures are commonly adopted to protect the pipelines from both immediate and delayed pipeline failures from mechanical damage. A reliability-based model was proposed by C-FER Technologies for PRCI in 1999[5]. Risk factors were extracted from the survey of North American and international pipeline companies. Fifteen responses to the survey were received, representing 36,661 miles of gas transmission pipelines. The reliability assessment is comprised of two parts: (1) the impact probability model described by the fault tree method; and (2) the puncture failure model comparing the impact load exerted by the excavation equipment and the pipeline resistance capacity.

The key parameters of puncture resistance are pipe diameter, wall thickness, mechanical strength, and bucket tooth size[6, 7]. The failure mechanism involves two modes: for a large ratio of diameter to wall thickness, the membrane action dominates; for a small ratio of diameter to wall thickness, the shear punching governs.

---

[3] Kiefner, J.F. and Leewis, K., "Pipeline Defect Assessment – A Review & Comparison of Commonly Used Methods", Pipeline Research Council International, Inc., Catalog PR218-05404, 2011.
[4] Kiefner, J.F., "Pipeline Incidents Caused by Mechanical Damage", Mechanical Damage Technical Workshop, Houston, Feb. 28 to Mar. 1, 2006.
[5] Chen, Q. and Nessim, M., "Reliability-based Prevention of Mechanical Damage to Pipelines", Catalog PR-244-9729, Pipeline Research Council International, Inc., August 1999.
[6] Spiekhout, J., Gresnigt, A.M. and Kusters, G.M.A., "The Behaviour of a Steel Cylinder Under the Influence of a Local Load in the Elastic and Elasto-Plastic Area", Proceedings of the International Symposium on Shell and Spatial Structures: Computational Aspects (July, 1986), Leuven, Belgium. Springer-Verlag Berlin, Germany, pp. 329-336, 1987.
[7] Corbin, P. and Vogt, G., "Future Trends in Pipelines", Proceedings of the Banff/97 Pipeline Workshop: Managing Pipeline Integrity – Planning for the Future, Banff, Alberta, 1997.

A deterministic equation for puncture resistance was derived based on fitting a set of experimental data[8].

$$R_p = \left(1.17 - 0.0029 \times \left(\frac{OD}{WT}\right)\right) \times (L + w) \times (WT \times \sigma_U) + E_R \qquad \text{Equation 1}$$

where

R_p is puncture resistance, lbf
OD is pipe outer diameter, inches
WT is pipe wall thickness, inch
L is length of tooth, inches
w is width of tooth, inches
σ_U is pipe ultimate tensile strength, psi
E_R is resistance model error, lbf

This equation has been validated by puncture failure tests conducted by European Pipeline Research Group (EPRG) and Battelle. The test-to-predicted ratios are generally close to 1.0 with a standard deviation of 0.092. It is worthy to note that the puncture resistance is independent of internal pressure. The bucket digging force is a function of excavator weight as described by:

$$F_p = 1.5 \times \left(1444 \times W^{0.826007}\right) \qquad \text{Equation 2}$$

where

F_p is digging force, lbf
W is excavator weight, tons

As recommended by the EPRG, a safety factor of 1.5 is applied to take into account the possible force increase caused by the heavier machines, e.g. those weighting more than 22 tons. Information was collected on the characteristics of excavators from construction machinery sales data, including equipment manufactures[9] and the US Department of Commerce[10]. The best fit distribution for excavator weight is a shifted Gamma function with a mean value of 31.2 tons and a standard deviation of 17.2 tons.

Two examples of the puncture analysis are illustrated below in both deterministic and probabilistic manners. One is a 16-inch OD, 0.250-inch WT, Grade X52 pipeline (Line 1); the

[8] Driver, R.G. and Playdon, D.K., "Limit States Design of Pipelines for Accidental Outside Force", Submitted to the National Energy Board, C-FER Report 96042, Edmonton, Alberta, Canada, 1997.
[9] Zimmerman, T.J.E., Chen, Q. and Pandey, M.D., "Limit States and Reliability-based Pipeline Design", Submitted to the Pipeline Research Committee International, Project PR-244-9517, C-FER Technologies, Edmonton, Alberta, Canada, 1997.
[10] USDOC 1979 – 1996, Statistics on Construction Machinery, Current Industrial Report MA35D, US Bureau of Census, Department of Commerce, Washington, D.C.

other is a 30-inch OD, 0.375-inch WT, Grade X52 pipeline (Line 2). These two represent typical liquid and gas pipeline configurations. To be conservative, deterministic assessments were conducted by applying the nominal values of pipe geometry and tensile strength. The bucket tooth cross-section size information was collected from six equipment manufacturers. The length is between 1.575 inches and 5.748 inches; the width is between 0.079 inch and 0.197 inch[5]. Hence, a lower-bound excavator tooth perimeter was assumed to be 3.307 inches. Since about one quarter of equipment encountered on pipelines are excavators, the probability of puncture was calculated to be 1.67E-01 and 7.77E-02 for these two pipelines. For 100 excavation hits from the outside, there are about 17 chances for Line 1 and 8 chances for Line 2 to be penetrated.

In parallel, probabilistic analyses took into account other variabilities for multiple variables, such as outer diameter, wall thickness, tensile strength, puncture resistance model error, and bucket tooth length and width. The corresponding distributions are summarized in Table 2 and plotted in Figure 1 through Figure 8 for demonstration purposes.

Table 2. Probability Density Functions used in Calculations

Variable	Function Type	Function Parameters	Source
Pipe Diameter	Normal	μ=1.0*nominal, COV=0.06%	CSA Z662 Annex O[11,12]
Wall Thickness	Normal	μ=1.01*nominal, COV=1%	CSA Z662 Annex O[11,12]
Tensile Strength	Normal	μ=1.19*SMTS, COV=11.05%	Kiefner material database
Resistance Model Error	Normal	μ=187, COV=32	EPRG and Battelle
Bucket Tooth Length	Uniform	min=1.575, max=5.748	six equipment manufacturers
Bucket Tooth Width	Uniform	min=0.079, max=0.197	six equipment manufacturers
Excavator Weight	Gamma	α=0.632, β=21.638, shift=17.53	Manufacturer and USDOC[9, 10]

Note: For the normal distribution, μ is the mean value and COV is the coefficient of variance. For the extreme value distribution, α is the location parameter and β is the shape parameter. For the Gamma distribution, α is the shape parameter and β is the scale parameter.

[11] CSA Z662-11, "Oil and Gas Pipeline Systems", Annex O, "Reliability-based Design and Assessment (RBDA) of Onshore Non-sour Service Natural Gas Transmission Pipelines".
[12] Zimmerman, T.J.E., Cosham, A., Hopkins, P., and Sanderson, N., "Can Limit States Design be Used to Design a Pipeline Above 80% SMYS?", OMAE98-902, 1998, Proceedings of the Seventeenth International Conference on Offshore Mechanics and Arctic Engineering.

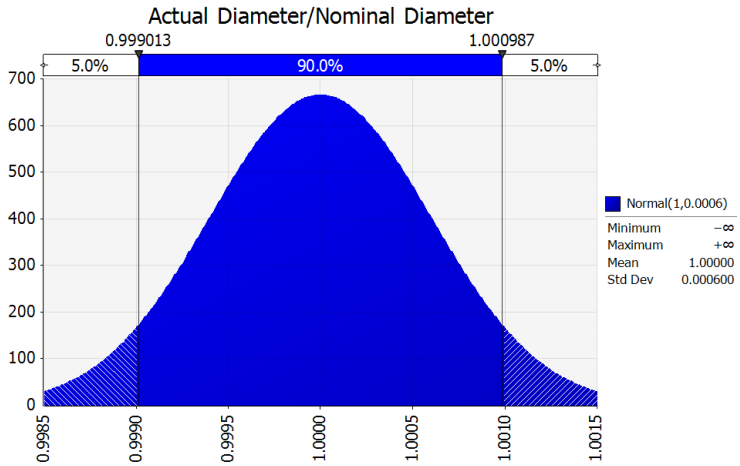

Figure 1. Probability Density Function for Actual Diameter/Nominal Diameter

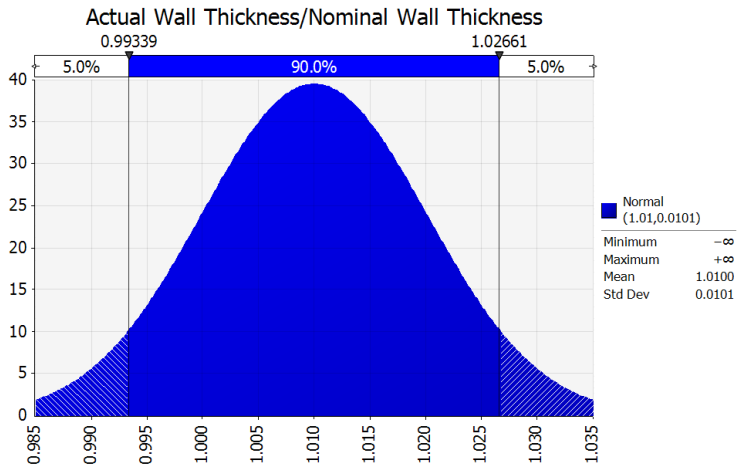

Figure 2. Probability Density Function for Actual WT/Nominal WT

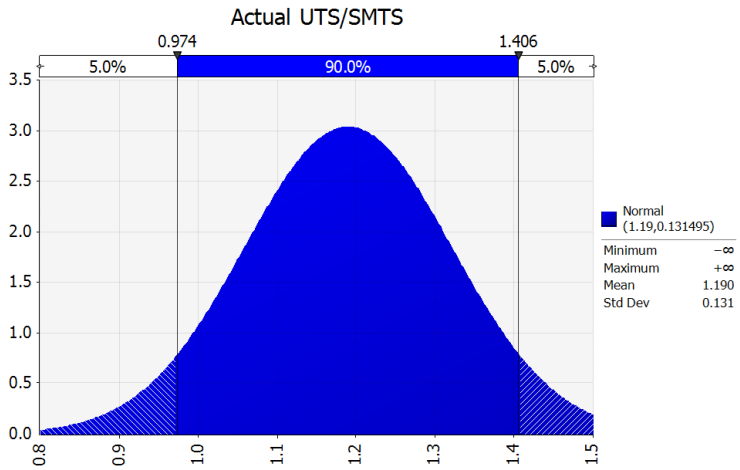

Figure 3. Probability Density Function for Actual UTS/SMTS

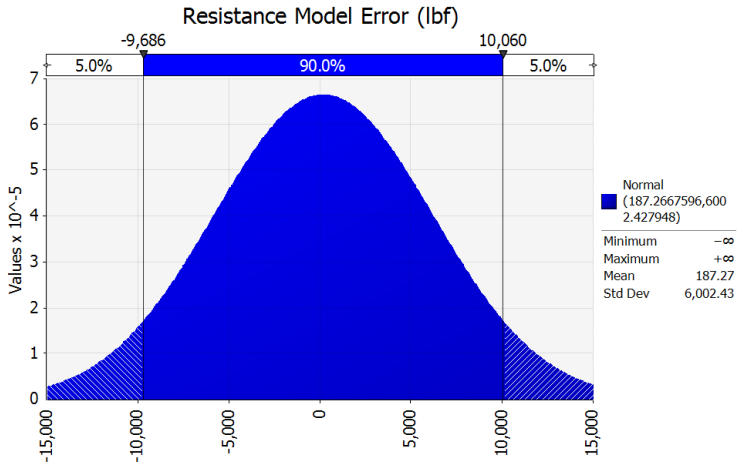

Figure 4. Probability Density Function for Resistance Model Error

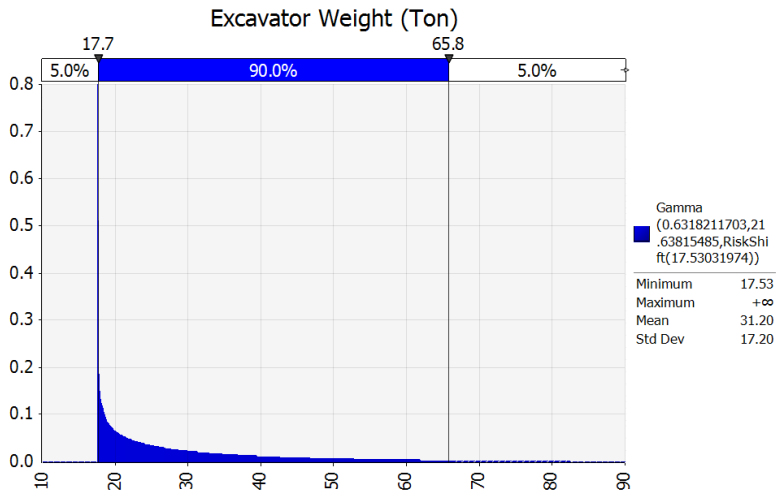

Figure 5. Probability Density Function for Excavator Weight

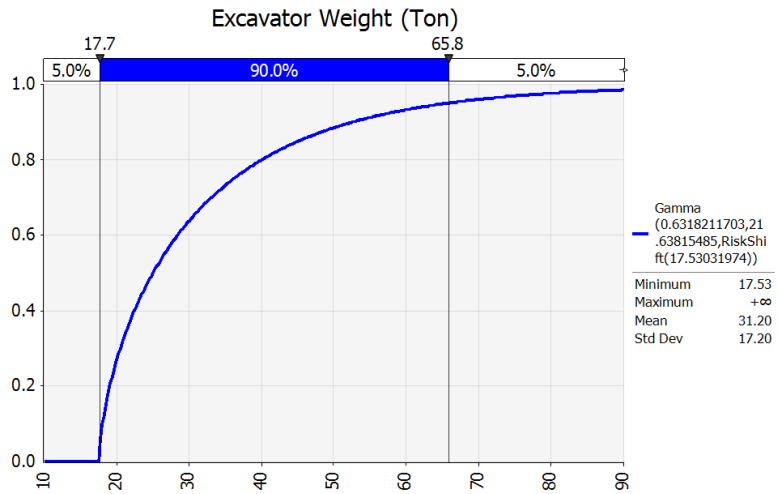

Figure 6. Cumulative Probability Function for Excavator Weight

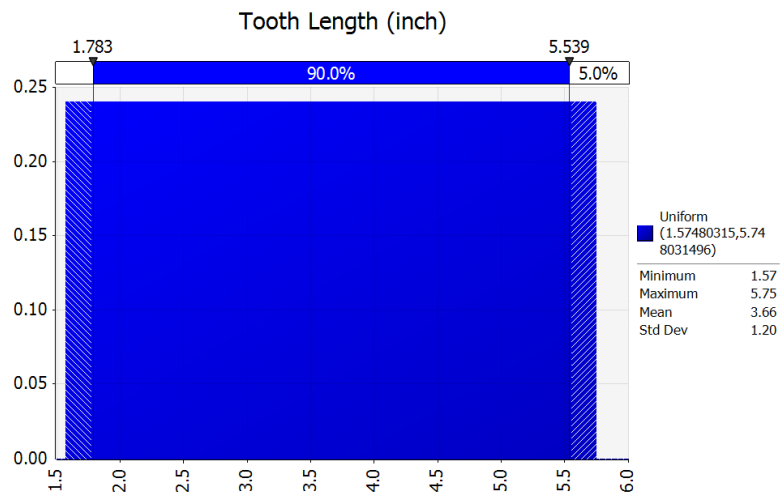

Figure 7. Probability Density Function for Tooth Length

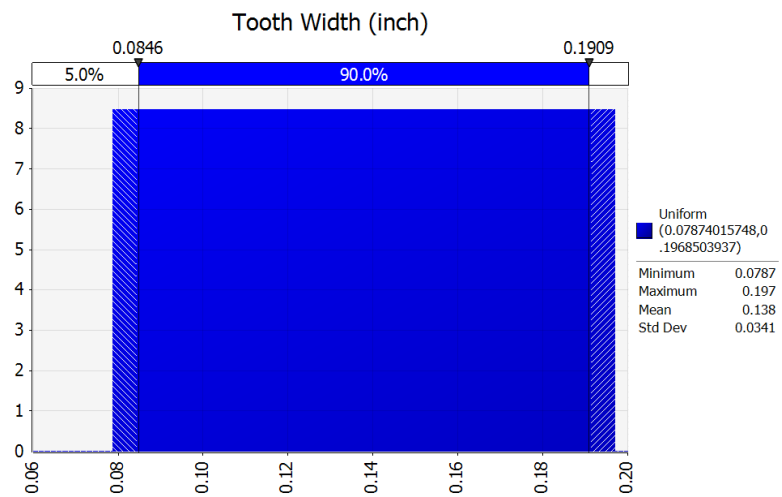

Figure 8. Probability Density Function for Tooth Width

Monte Carlo simulations were applied to find the possibility that puncture load is greater than the puncture capacity. For each case, 10^5 iterations of calculation were conducted based on the above defined distributions. Since all the parameters related to the pipeline resistance are either equal to or larger than nominal values chosen in the deterministic analysis, the probability of puncture drops to 2.37E-02 and 7.26E-03 for Line 1 and 2 respectively. For every one thousand hits from the outside, there are about 24 chances for Line 1 to be penetrated but only 7 chances for Line 2 to be penetrated. Note that this is largely due to Line 1 being only 2/3 as thick as Line 2. Table 3 compares the deterministic and probabilistic results. More than one order of magnitude decrease of puncture probability is attributed to the actual properties of pipelines more desirable than the claimed nominal conditions, and also the actual excavator tooth cross section size is generally larger than the lower bound assumption. There is no

essential difference between gas and liquid pipelines, e.g. operating condition. Only the pipe geometry matters. When the wall thickness is greater, the probability of puncture is much less.

Table 3. Comparison between Deterministic and Probabilistic Analysis

Pipeline	OD (inches)	WT (inch)	Grade	Deterministic POF	Probabilistic POF	Ratio between Probabilistic and Deterministic
Line 1	16	0.250	X52	1.67E-01	2.37E-02	14.25%
Line 2	30	0.375	X52	7.77E-02	7.26E-03	9.33%

These two case studies exemplify the procedure of reliability-based assessment and its functionality in the pipeline design to prevent incidents from mechanical damage. To reduce the possibility of excavation activities interfering with the pipeline right-of-way, prevention methods were recommended[4, 5], including public education, one-call system, buried markers, physical barriers, quick response to the notification, on-site supervision of excavation, signs at all crossing, magnetic or electronic pipeline locators, frequent patrol, cover depth increased to 5 feet, etc. With minimizing the pipeline exposure to nearby excavation activities through a prevention program and increasing the pipeline designed capacity to resist puncture, the risk of immediate mechanical damage failures can be reduced.

MITIGATION OF DELAYED FAILURES

Delayed incidents caused by mechanical damage were analyzed by Kiefner for the Gas Research Institute GRI-99/0050[4]. The viability of in-line inspection as a preventative alternative was discussed for several types of delayed incidents. The investigation was based upon the PHMSA reportable incidents between 1985 and 1997, in which 183 delayed failures were reported and 68 failures provided useful information.

Table 4. Categories of Delayed-Failure Incidents by Mechanical Damage 1985-1997

Type of Incidents	Number of Incidents (gas and liquid)	Percentage of Incidents	In-line Inspection to Avoid Delayed Failures
Type 1- short time to failure (hours to days)	4	5.90%	ILI is no value.
Type 2- occurred after ≥10% pressure increase	5	7.40%	ILI before an intentional increase in MOP could prevent.
Type 3- suspected corrosion, fatigue, SCC at old damage	17	25.00%	ILI can prevent through the types and schedules used by operators.
Type 4- old damage, age documented*	29	42.60%	An arbitrary schedule for ILI would prevent some, but not all.
Type 5- rock dents	13	19.10%	ILI is not justified.**

*Although it said the age documented, it probably means the age undocumented.
**Although this was stated in Reference [4], it is not necessarily the case. The reportable incident data reveal multiple cases of leaks developing at rock dents. Such dents can be found via in-line inspection, and the potential to prevent leaks of this type could justify an in-line inspection.

From Table 4, it is evident that in-line inspection can be used to prevent delayed-failure incidents in some cases. About 51.5% of all delayed-failure incidents, including Type 2, Type 3, Type 5, may be preventable via ILI and subsequent timely and appropriately mitigation. About 42.6%, such as Type 4, also is possibly preventable. With the recent development of new technologies, ILI is evolving to be an effective reliable method to locate and size existing mechanical damage, and to differentiate the severity of each indication.

In the following, three individual risk-based methodologies are proposed to determine the repair criteria to mitigate mechanical damage reported from ILI: (1) risk factors extracted from the most recent PHMSA incident database; (2) probability of failure calculated from the EPRG probabilistic model; (3) Bayesian approach to account for the inconsistency of ILI.

Reportable Incident Risk Prediction

Dawson, et al.[13] reported the frequency of occurrence of various types of damage detected by ILI. They estimated that, on average, pipelines exhibit 2.3 dents/mile with 73% of the features being located on the bottom. As shown in Table 5, these estimated quantities suggest that there are approximately 1,152,165 dents all together residing in 500,941 miles of gas transmission and hazardous liquid pipelines. Among those, 841,081 are rock dents located in the bottom half and 311,085 are mechanical damage located in the upper half.

Table 5. Statistics of Dents for Different Pipeline Systems

Pipeline System	2014 Mileage	Dents /Mile	Rock Dents/Total Indication	Total Dents	Total Rock Dents (Bottom)	Total Mechanical Damage (Top)
gas transmission	301,732	2.3	0.73	693,983	506,607	187,375
hazardous liquid	199,210	2.3	0.73	458,183	334,473	123,709
total	500,941	2.3	0.73	1,152,165	841,081	311,085

Since 2010, Reported Cause of Incidents of "Excavation Damage" is comprised of three sub-types, i.e. operator/contractor excavation damage, previous damage due to excavation, and third party excavation damage. According to PHMSA, the first and third types are meant for immediate failures, and the second type is meant for delayed failures. The compilation of significant incidents caused by excavation damage from 2010 to 2014 in Table 6 implies the ratio between immediate and delayed failures[14]. There are 14.6% delayed incidents in gas transmission pipelines and 13.3% delayed incidents in hazardous liquid pipelines. Those numbers are slightly different from the Kiefner prior study for GRI[4], i.e. 10% in gas transmission pipelines and 17% in hazardous liquid pipelines.

[13] Dawson, S.J., Russell, A. and Patterson, A., "Emerging Techniques for Enhanced Assessment and Analysis of Dents", IPC 2006-10264, 6th IPC, Calgary, Canada, 2006.
[14] There is no delayed failure caused by excavation damage in PHMSA serious incidents during five years from 2010 through 2014.

Table 6. 2010-2014 Significant Incidents Caused by Excavation Damage

Significant Incidents Caused by Excavation Damage (2010-2014)	Operator/ Contractor Excavation Damage	Previous Damage due to Excavation	Third Party Excavation Damage	Total Number	Delayed Incidents/ Total Incidents
gas transmission	6	7	35	48	14.6%
hazardous liquid	10	8	42	60	13.3%
total	16	15	77	108	13.9%

According to Kiefner's experience, excluding hydrostatic test-induced failures of latent damage and excavation puncture, the ratio between top half damage and bottom half damage is 0.83 to 0.17. The above statistics provide the reference to infer the probability of reportable incidents in association with mechanical damage (MD) features or rock dent (RD) features left in place and not repaired.

Note that since the consequence of risk assessment was not analyzed herein, the differentiation between "significant" and "serious" incidents was not taken into account. Moreover, the significant incidents include serious incidents in the reporting criteria, so in the following calculation only significant incident rate was used.

The delayed failure rates for reportable incident, i.e. per feature per year, are calculated in Table 7 and plotted in Figure 9 for each pipeline type, e.g. gas transmission (GT), hazardous liquid (HL), and total. The highlighted values of "Delayed MD Failures per Feature per Year" and "Delayed RD Failures per Feature per Year" are essential to determine the risk reduction associated with repairing more indications.

Table 7. "Significant" Incident Rate for Mechanical Damage and Rock Dent

system	total MD failures from 1995 to 2014	total MD failures per year	delayed MD failures per year	total MD features	**delayed MD failures per feature per year**	delayed RD failures per year	total RD features	**delayed RD failures per feature per year**
GT	207	10.35	1.51	187,375	8.06E-06	0.30	506,607	5.96E-07
HL	421	21.05	2.81	123,709	2.27E-05	0.56	334,473	1.68E-06
TOTAL	628	31.4	4.36	311,085	1.40E-05	0.87	841,081	1.04E-06

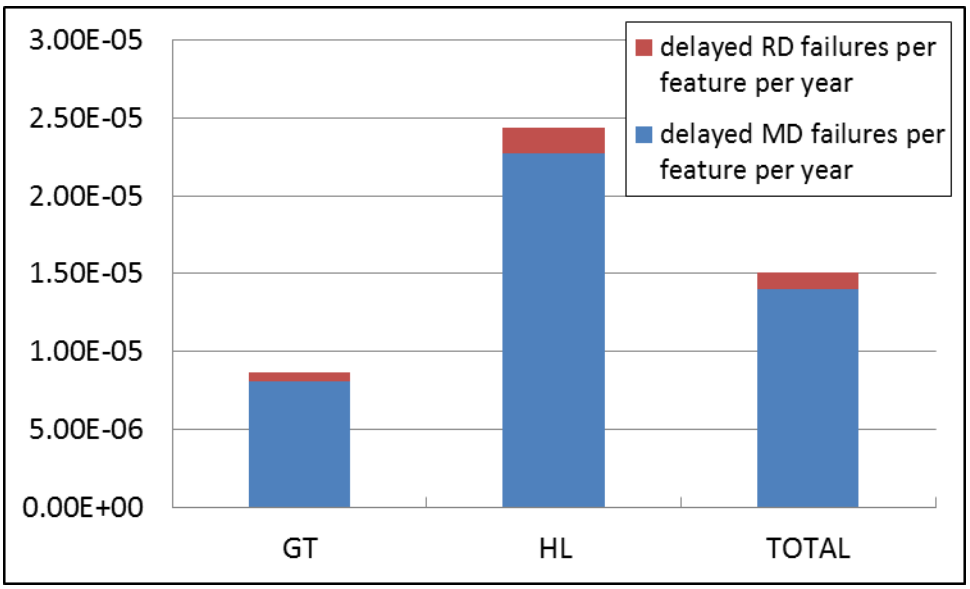

Figure 9. Significant Incident Probability per Feature per Year

Comparing the gas transmission to hazardous liquid pipelines, within significant incidents, the hazardous liquid pipelines has more frequent failures, around one order of magnitude, than the gas transmission pipelines. This observation might be attributed to smaller D/t ratios for liquid pipelines than gas pipelines in general terms. Over and above, the probability of delayed MD failures is one order of magnitude greater than that of delayed RD failures.

A hypothetical example is given below to demonstrate repair criteria determination from the risk perspective. The cumulative frequency of dent severity from ILI, for instance, depth/pipe diameter (d/D), is shown in Figure 10. To simplify the problem, the density of dent indications is assumed to be 10 per mile. The annual risk levels of incidents per mile accompanying different repair criteria are listed Table 8. By and large, the expected incident rates are on the order of 1.0E-5 or less except the incident risk caused by mechanical damage on liquid pipelines.

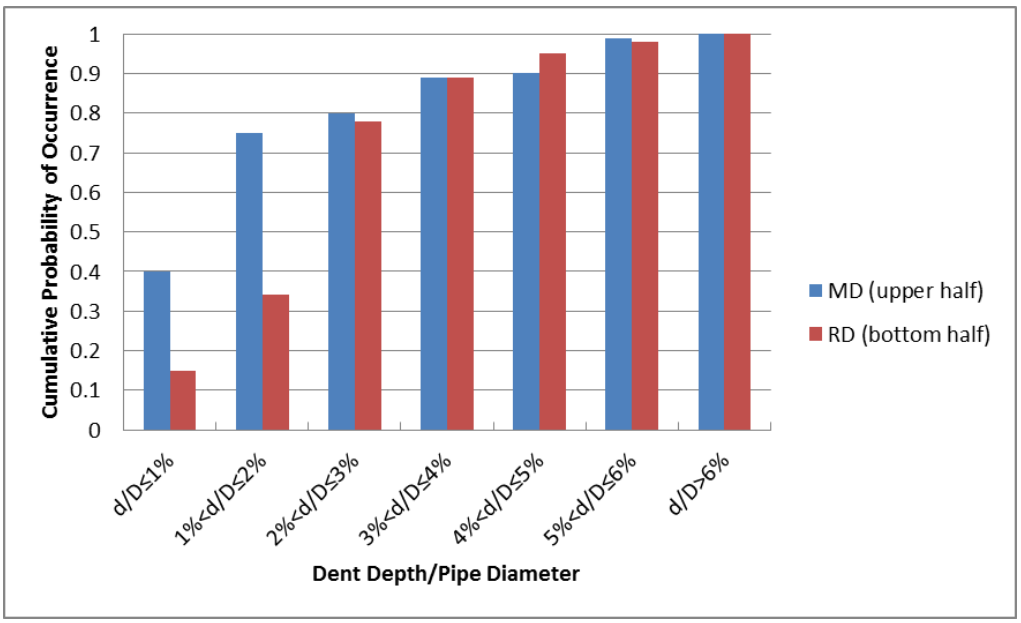

Figure 10. Cumulative Probability of Occurrence of Dent Features from ILI

Table 8. Risk Levels Associated with Repair Criteria

Feature Type	Repair	Leave in Place	Cumulative Percentage	Number of Features per Mile	Incident Risk per Mile per Year (gas)	Incident Risk per Mile per Year (liquid)
MD	d/D>6%	d/D≤6%	0.99	10	7.97E-05	2.25E-04
MD	d/D>5%	d/D≤5%	0.9	10	7.25E-05	2.04E-04
MD	d/D>4%	d/D≤4%	0.89	10	7.17E-05	2.02E-04
MD	d/D>3%	d/D≤3%	0.8	10	6.44E-05	1.82E-04
MD	d/D>2%	d/D≤2%	0.75	10	6.04E-05	1.70E-04
MD	d/D>1%	d/D≤1%	0.4	10	3.22E-05	9.08E-05
RD	d/D>6%	d/D≤6%	0.98	10	5.84E-06	1.64E-05
RD	d/D>5%	d/D≤5%	0.95	10	5.66E-06	1.59E-05
RD	d/D>4%	d/D≤4%	0.89	10	5.30E-06	1.49E-05
RD	d/D>3%	d/D≤3%	0.78	10	4.65E-06	1.31E-05
RD	d/D>2%	d/D≤2%	0.34	10	2.03E-06	5.71E-06
RD	d/D>1%	d/D≤1%	0.15	10	8.94E-07	2.52E-06

POE-Based Mitigation Plan

As another example, Probability of Exceedance (POE) analysis was shown here to explain a decision-making process for mitigating a fairly large number of dents on a pipeline. If the failure probability at the ith dent is p_i, the probability of no failure at the ith dent is $1 - p_i$.

Assuming there are n dents in total, the probability of no failure at any dents in the entire pipeline is $(1-p_1)(1-p_2)\ldots(1-p_i)$, hence the probability of failure for this particular pipeline is

$$P = 1-(1-p_1)(1-p_2)\ldots(1-p_n) = 1-\prod_{i=1}^{n}(1-p_i) \qquad \text{Equation 3}$$

One of the probabilistic dent fatigue life models is the European Pipeline Research Group (EPRG) model developed in 1995[15]. The approach was later recommended in the Pipeline Defect Assessment Manual (PDAM)[16]. The fatigue life of an unconstrained plain dent, N, with 50% probability of failure is given by

$$N = 1000\left(\frac{\sigma_U - 50}{2\sigma_A K_s}\right)^{4.292} \qquad \text{Equation 4}$$

$$2\sigma_A = \sigma_U[B(4+B^2)^{0.5} - B^2] \qquad \text{Equation 5}$$

$$B = \frac{\frac{\sigma_a}{\sigma_U}}{\left[1-\left(\frac{\sigma_a}{\sigma_U}\right)\left(\frac{1+R}{1-R}\right)\right]^{0.5}} \qquad \text{Equation 6}$$

$$\sigma_a = \sigma_{max} - \sigma_{min} \qquad \text{Equation 7}$$

$$R = \frac{\sigma_{min}}{\sigma_{max}} \qquad \text{Equation 8}$$

where

σ_U is ultimate tensile strength of pipe steel, ksi
σ_a is equivalent cyclic hoop stress range, ksi
R is stress ratio
σ_{min} is minimum hoop stress, ksi
σ_{max} is maximum hoop stress, ksi

[15] Corder, I., and Chatain, P., "EPRG Recommendations for the Assessment of the Resistance of Pipelines to External Damage", Proc. of the EPRG/PRC 10th Biennial Joint Technical Meeting on Line Pipe Research, Cambridge, UK, April 1995.
[16] Cosham, A. and Hopkins, P., "Pipeline Defect Assessment Manual (PDAM)", 2002.

The dent stress concentration factor K_S is determined by

$$K_S = 2.871\sqrt{K_d} \qquad \text{Equation 9}$$

$$K_d = C_u d_0 \frac{t}{D} \qquad \text{Equation 10}$$

$$d_0 = 1.43 d_p \qquad \text{Equation 11}$$

where

d_0 is dent depth measured at zero pressure, inches
t is wall thickness of pipe, inch
D is diameter of pipe, inches
C_u is unit conversion factor as 1.0 for d_0 in millimeters and 25.4 for d_0 in inches
d_p is dent depth under pressure after rebounding, inches

The comparison of fatigue life from above EPRG model with existing experiment data is shown in Figure 11. The ratio of model-predicted to actual number of cycles to failure exhibits a considerable amount of scatter. The model prediction error is described by

$$\ln \hat{N} = \ln N + \left[\hat{\beta}_0 - t_{n-r-1}(\alpha)\sqrt{s^2 + Var(\hat{\beta}_0)}\right] \qquad \text{Equation 12}$$

where

$\hat{N}$ is the fatigue life of an unconstrained plain dent with the $(100\alpha)^{\text{th}}$ percentile probability of failure
$t_{n-r-1}(\alpha)$ is the upper $(100\alpha)^{\text{th}}$ percentile (i.e. one-tail confidence level) of a t-distribution with $n - r - 1$ degrees of freedom

This formula was derived from the linear regression analysis on 45 full scale tests. The remaining parameters in Equation 12 were determined as $\hat{\beta}_0 = 0.0168$, $\mathrm{Var}(\hat{\beta}_0) = 0.0522$, $s^2 = 2.35$ and $n - r - 1 = 44$. For 5% of failure probability, i.e. a 95% confidence of survival, $t_{44}(0.05) = 1.680$.

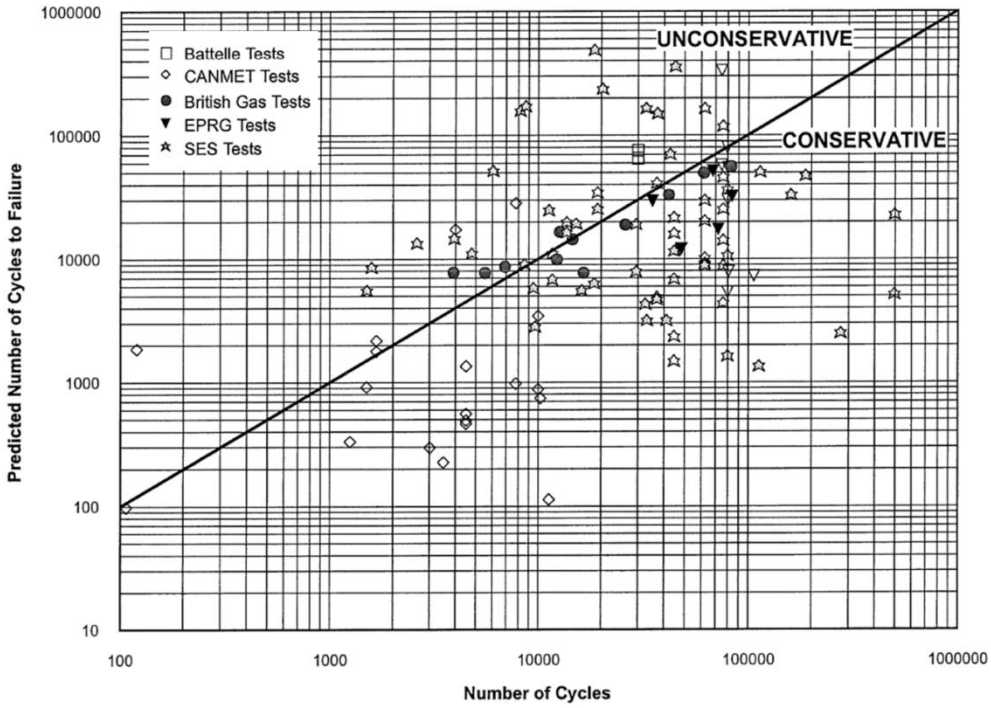

Figure 11. Predictions of Fatigue Life of Plain Dents by the EPRG Model[16]

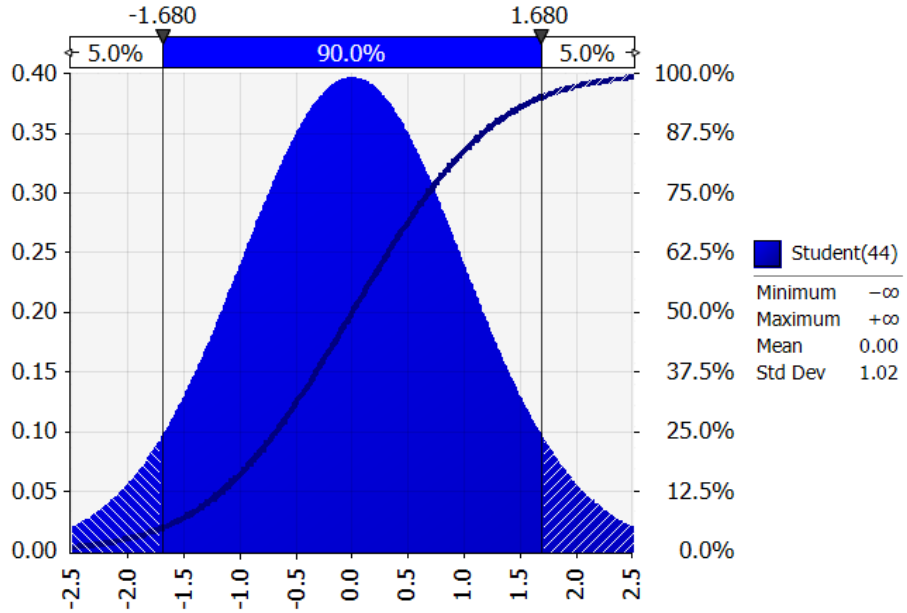

Figure 12. Student's t-Distribution with 44 Degrees of Freedom

Note that this model is also applicable to constraint dents. Though only a limited number of experimental data about the fatigue life of constraint dents is available, based on these data and general experience from the industry, a constrained plain dent should have a fatigue life which is at least that of an unconstrained plain dent of the same depth. Consequently, the above model can be applied to constraint dents as a conservative approach.

Below is a working example for the dent fatigue life POE analysis. A recent in-line inspection in a pipeline found a series of dent anomalies. After several very deep dents had been repaired, nine mild and shallow dents were left in place as shown in Table 9. This pipeline consists of 30-inch diameter and 0.625-inch wall thickness Grade X60 line pipes. It was constructed between 1976 and 1977. In 1990, a short segment was replaced with line pipes having the same grade and dimensions. The construction year and pipe dimensions at each dent location are also included in Table 9. The maximum operating pressure (MOP) of the pipeline is 1,806 psig, equivalent to a design factor of 0.72. No historical records are available relevant to when those dents were formed. All of the nine dents are located at or near the bottom half of the pipeline. It is planned to re-assess the pipeline in 10 years, i.e. the year of 2025. To have a 95% confidence level none of the dents left in place will fail during the 10 years; until the next re-assessment, the operator needs to determine which dents in the list should be remediated at this time. The remediation list can be developed following the approach below.

Table 9. ILI Information on Dents in Working Example

Dent No.	Installation Year of Pipeline Segment	Pipe OD (inches)	Pipe Wall Thickness (inches)	Dent Depth from ILI (inches)
1	1976	30	0.625	0.445
2	1976	30	0.625	0.525
3	1976	30	0.625	0.240
4	1977	30	0.625	0.222
5	1990	30	0.625	0.233
6	1977	30	0.625	0.168
7	1977	30	0.625	0.194
8	1977	30	0.625	0.329
9	1977	30	0.625	0.221

As all of these dents are at or near the bottom half of the pipes; they are likely constrained rock dents. As mentioned before, the EPRG model is applicable for both constrained and unconstrained dents. An accurate fatigue analysis should follow the pressure spectrum history at each exact dent location, and the information about any potential changes in pressure cycles in the future should be considered. For an illustration purpose, it is assumed that the pressure spectrum is universally equivalent to two MOP cycles per year and the pipeline will be operated in a similar fashion for the next 10 years. For a full MOP cycle, $\sigma_a = 0.72\sigma_Y$ and $R = 0$. The yield strength and tensile strength are chosen to be specified minimum values for Grade X60, i.e. $\sigma_Y = 60\ \mathrm{ksi}$ and $\sigma_U = 75.4\ \mathrm{ksi}$. Following Equation 4 through Equation 11, the fatigue life in cycles with 50% probability of failure, N for each dent was calculated. The results are shown in Table 10.

Although there is no historical record about the forming time of the dents, rock dents are generally formed during the initial construction or the replacement activity. Solve the equation

$$t_{n-r-1}(\alpha) = \frac{\left[\hat{\beta}_0 - \ln\left(\frac{\widehat{N}}{N}\right)\right]}{\sqrt{s^2 + Var(\hat{\beta}_0)}} \qquad \text{Equation 13}$$

with $\widehat{N}$ equal to twice the pipeline age until the year of 2025 due to a pressure fluctuation of two MOP cycles per year. The probability of dent fatigue failure α can be back calculated from the value of $t_{n-r-1}(\alpha)$. The age and probability of failure by the year of 2025 of each dent are listed in Table 10.

Table 10. Probability of Dent Fatigue Failure

Dent No.	Dent Depth at Zero Pressure (inches)	Fatigue life with 50% Probability of Failure (Cycles)	Age of Dent by 2025 (Years)	Probability of Failure by 2025
1	0.636	780	49	9.56%
2	0.751	547	49	13.90%
3	0.343	2936	49	1.72%
4	0.317	3473	48	1.30%
5	0.334	3113	35	0.94%
6	0.240	6333	48	0.50%
7	0.277	4658	48	0.82%
8	0.470	1492	48	4.28%
9	0.315	3516	48	1.27%

Without any remediation to any dents, the probability of failure in entire pipeline before the re-assessment by Equation 3 is

$$P = 1 - (1 - 0.0956)(1 - 0.1390)(1 - 0.0172) \ldots (1 - 0.0127) = 30.2\% \qquad \text{Equation 14}$$

This failure probability is much higher than the targeted 5%. The remediation has to be applied right away. As shown in Table 10, Dent No. 2 has the highest probability of failure, thus the highest priority to be repaired. After this dent is mitigated, the probability of failure in the entire pipeline is recalculated as

$$P = 1 - (1 - 0.0956)(1 - 0.0172)(1 - 0.0130) \ldots (1 - 0.0127) = 19.0\% \qquad \text{Equation 15}$$

Repeat this process by mitigating other dents in the decreasing order of probability of failure and calculating the P values each time. The process continues until $P \leq 5\%$. Eventually dents 1, 2, 3 and 8 are added to the current remediation list, and the probability of failure for the entire pipeline in the year of 2025 based on the remaining five dents is 4.8%.

Bayesian-Based Mitigation Plan

In the above example, the POE function of dent fatigue life is known. So the failure probability of entire pipeline in the future can be calculated straightforwardly. There are other situations where the failure probability function is unknown or partially known. Additionally, the in-line inspection may have undefined reliability and exhibits inconsistency with the in-ditch findings. A pipeline operator can hypothesize an initial function and, based on excavations or experiments, derive the best estimates of the parameters inherent in the function. The Bayesian method is exercised here to exhibit its capability to foster the decision-making process.

For example, a relatively large number of very minor mechanical damage features (MDF) occurred on a pipeline. This kind of circumstance was investigated from the fitness-for-service standpoint and the characteristics of remaining features left in the pipeline were assumed tantamount to those excavated features. It was concluded that none of the remaining unexcavated features posed a significant risk to the pipeline [17, 18] after the operator conducted quite a few excavations to build enough information about the real condition in pipeline. However, one piece of critical judgement is missing from those prior studies. The question would be, "*how many excavations would be required to determine the safety of the remaining features?".*

A Bayesian-based conceptual approach is proposed here to strive to answer this question. To describe the approach, suppose n MDF anomalies exists, $A_1, A_2, \ldots A_n$ which have been identified using ILI. Based on the analysis of the ILI data, the severity of each anomaly is given by $x_1 \ldots x_n$. Furthermore, it is assumed that the x_i's are related to the ultimate safety of the MDF's. When an MDF is excavated, a full assessment of the feature is conducted, and the feature is repaired if it is unsafe. The probability that the MDF is unsafe is postulated to be a function of x as

[17] Rosenfeld, M.J., Beckett, A., Neogi, B., Baskurt, U.J. and Johnson, E., "Deterministic Assessment of Minor Mechanical Damage on Pipelines," IPC 2006-10513, Proceedings of IPC2006, 6th International Pipeline Conference, September 25-29, Calgary, Alberta, Canada, 2006.

[18] Vieth, P.H., Maier, C.J., Harper, W.V., Johnson, E., Neogi, B., Baskurt, U.J., and Beckett, A., "Probabilistic Assessment of Minor Mechanical Damage", IPC 2006-10409, Proceedings of IPC2006, 6th International Pipeline Conference, September 25-29, Calgary, Alberta, Canada, 2006.

$$p(x) = 1 - e^{-\lambda x}$$ Equation 16

The shape of the relationship between the ILI severity of the MDF and the probability of an unsafe condition is illustrated in Figure 13 for $\lambda = 5$ and $0 \leq x \leq 1$. x can stand for the damage severity being such that the MDF is not able to withstand the pressure of 1.1MOP. Note that the probability of an unsafe anomaly is highest for large x and approaches zero for small x. The cumulative probability function implies the probability density of x is an exponential distribution as

$$f(x) = \lambda e^{-\lambda x}$$ Equation 17

Starting with a population of anomalies with a uniform distribution of x, some of those anomalies will be safe and some will be unsafe. The safe anomalies will tend to have smaller values of x, and the unsafe anomalies will tend to have higher values of x.

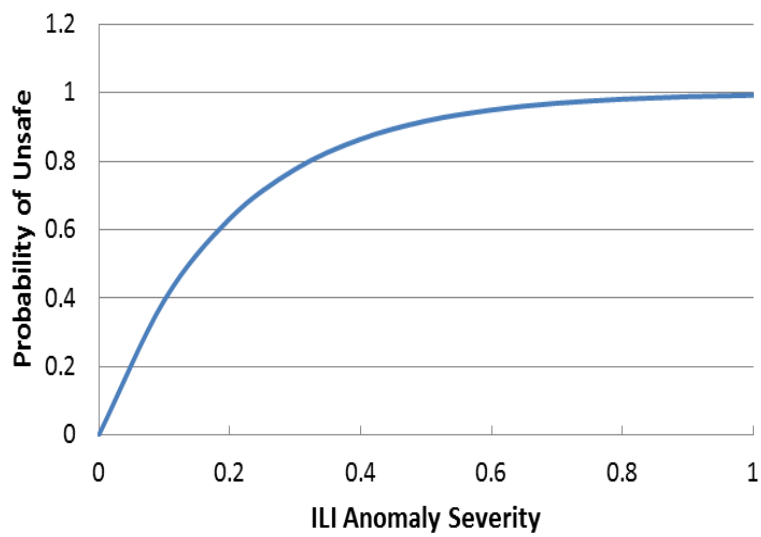

Figure 13. Probability of Unsafe vs ILI Anomaly Severity

Initially, the value of λ is unknown, but its value is determined from the results of the excavations. With each excavation, the value of λ is updated using a Bayesian estimator. Yang, et al.[19] proposes that λ can be estimated where the prior distribution is a non-informative Gamma distribution:

$$\lambda \sim \mathrm{Gamma}(\lambda; \alpha, \beta)$$ Equation 18

[19] Yang, L., Zhou, H., and Yuan, S., "Bayes Estimation of Parameter of Exponential Distribution under a Bounded Loss Function," Research Journal of Mathematics and Statistics, pp. 28-31, 2013.

It is also proposed prior distribution to be $\lambda \sim \mathrm{Gamma}(\lambda;\ \alpha_0, \beta_0)$, where $\alpha_0 = 0$ and $\beta_0 = 0$. $\mathrm{Gamma}(\lambda;\ 0, 0)$ is a non-informative improper distribution. An improper distribution is one which does not integrate to one. However these distributions can be used as prior distributions, and they become proper once data is received.

A non-informative prior distribution may be the best choice for the time being, but eventually, the relationship between the severity x and the probability of exceedance $p(x)$ may be known for a number of different pipelines. Once a reasonable range of values is known for λ, then the prior distribution can be designed to reflect this knowledge.

The Bayesian procedure updates the values of α and β with each data point received. For the current problem, if m excavations have found safe features, then the estimate of α and β are:

$$\alpha = \alpha_0 + m \qquad \text{Equation 19}$$

and

$$\beta = \beta_0 + \sum_{i=1}^{m} x_i \qquad \text{Equation 20}$$

The expected value and variance of λ are given by

$$E[\lambda] = \frac{\alpha}{\beta} \qquad \text{Equation 21}$$

$$\mathrm{Var}[\lambda] = \frac{\alpha}{\beta^2} \qquad \text{Equation 22}$$

Note that if $\alpha_0 = 0$ and $\beta_0 = 0$ then the estimate of $1/\lambda$ is the simple average of the values of safe x_i's. Another conservative estimator, i.e. 90% upper bound value, of λ is:

$$\lambda = \frac{\alpha}{\beta} \pm 1.96\sqrt{\frac{\alpha}{\beta^2}} \qquad \text{Equation 23}$$

The procedure is outlined below by three alternative stopping conditions:

1. Identify the MDF anomalies, $A_1 \ldots A_n$

2. Estimate x_i for each anomaly A_i from the ILI data so that the probability that the anomaly will fail within some predetermined period of time is given by

$$p(x_i) = 1 - e^{-\lambda x_i} \qquad \text{Equation 24}$$

3. Initialize
   a. Set $k \leftarrow 1$
   b. $\alpha = \alpha_0$
   c. $\beta = \beta_0$
4. Excavate anomaly A_k
5. If anomaly A_k is safe then go to step 8
6. Set $k \leftarrow k + 1$
7. Go to step 4
8. Update
   a. $\alpha \leftarrow \alpha + 1$
   b. $\beta \leftarrow \beta + x_k$
   c. λ:
      i. The best estimate of $\lambda \leftarrow \alpha/\beta$ or
      ii. A conservative estimate of $\lambda \leftarrow \alpha/\beta + 1.96\sqrt{\alpha/\beta^2}$ (90% upper bound value)
9. Calculate stopping criteria:
   a. The probability of the next MDF to be excavated being unsafe is

$$p(x_{k+1}) = 1 - e^{-\lambda_k x_{k+1}} \qquad \text{Equation 25}$$

   b. Update the estimated number of unsafe and unexcavated MDF anomalies. The probability that there is at least one unsafe unexcavated MDF on the pipeline is

$$P_k = 1 - \prod_{i=k+1}^{n} e^{-\lambda_k x_i} \qquad \text{Equation 26}$$

   c. Update the estimated number of unsafe and unexcavated MDF anomalies. The total expected number of remaining unexcavated unsafe anomalies is

$$N_k = \sum_{i=k+1}^{n} (1 - e^{-\lambda_k x_i}) \qquad \text{Equation 27}$$

10. Check for stopping condition and STOP if it is satisfied. The stopping criterion may be any one of the following:
    a. $p(x_{k+1}) < \alpha_1$,
    b. $P_k < \alpha_2$, or
    c. $N_k < \alpha_3$,

    where α_1, α_2, α_3 are the levels of confidence.
11. Set $k \leftarrow k + 1$
12. Go to step 4

An example is given for an illustrative purpose. Suppose that an ILI inspection has identified a total of 50 MDF anomalies on a pipeline. The ILI signal of each feature has been examined and given a severity value. The anomalies are then sorted from most severe to the least severe in Figure 14. This is a completely hypothetical example, but if such a distribution of severities were to be observed, the operator might wonder if the only the first three anomalies pose a threat. On the other hand, perhaps the first dozen anomalies are potential threats. In either case, it might be expected that a large portion of very small MDF anomalies really pose no threat. The question is *where the cut off is between those anomalies which do pose a threat and which do not.*

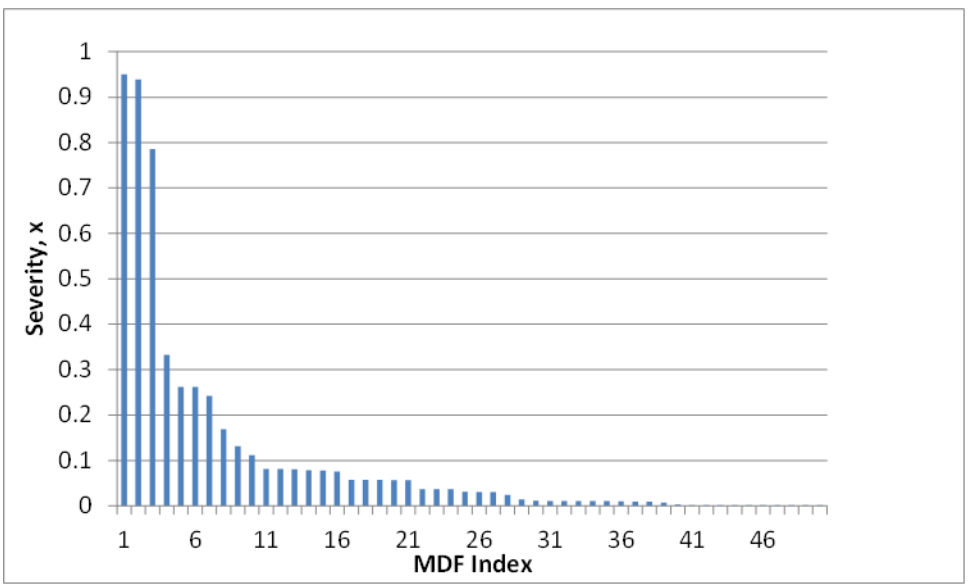

Figure 14. Severity of Each of Fifty ILI Indications

Initializing the Procedure

The procedure starts by defining α_0 and β_0. As described above α and β are used to estimate the value of λ and its potential range. The value of λ in turn is used to calculate the probability that any given anomaly is safe or unsafe. Possible starting values are $\alpha_0 = 0$ and $\beta_0 = 0$. These starting values are non-informative, which means that there is no expected value of λ;

and the unsafe probability of the anomalies cannot be estimated. The value of λ is only estimated from the x values of safe anomalies.

Excavating the Anomalies

- After the Excavation of No. 1 Indication

The procedure starts with the anomalies in order of decreasing severity. The most severe anomaly is excavated first. If the excavated anomaly is unsafe, meaning that it might be expected to fail within some predetermined time period, then α and β are left unchanged. In this experiment, suppose that the first excavation reveals an unsafe MDF anomaly. As stated, the α and β values are left unchanged. Turn to the next anomaly for excavation.

- After the Excavation of No. 2 Indication

Suppose that the second anomaly is safe. From this excavation result, now update α and β:

$$\alpha = \alpha_0 + 1 = 1$$

and

$$\beta = \beta_0 + x_2 = 0.939$$

The expected value of $\lambda = \frac{\alpha}{\beta} = 1.064$. The current situation is summarized in Table 11 with the information of only the first 15 anomalies. The excavation results found that the first anomaly was unsafe, but the second anomaly was safe. The safe anomaly enabled the update of α and β to estimate $\lambda = 1.064$. With that value of λ the probability that the remaining anomalies are unsafe can be estimated. The expected number of unsafe MDF anomalies is 3.141, and the probability of at least one unexcavated anomaly being unsafe is 0.974. Because both values are high, continue excavating other anomalies.

Table 11. After the 2nd Excavation

Expected Number of Unsafe MDF		**3.141**
Probability of Unsafe MDF		0.974
	λ	1.064
Index	**ILI Measurement**	**Probability of Exceedance**
1	0.950	Excavation result = unsafe
2	0.939	Excavation result = safe
3	0.786	0.567
4	0.334	0.299
5	0.263	0.243
6	0.263	0.243
7	0.243	0.228
8	0.169	0.164
9	0.131	0.130
10	0.112	0.112
11	0.082	0.084
12	0.082	0.084
13	0.082	0.083
14	0.079	0.079
15	0.079	0.080

- After the Excavation of No. 3 Indication

The third anomaly is safe. Therefore, α and β are similarly updated as

$$\alpha = \alpha + 1 = 2$$

and

$$\beta = \beta + x_3 = 1.724$$

The expected value of $\lambda = \frac{\alpha}{\beta} = \frac{2}{1.724} = 1.160$.

Table 12. After the 3rd Excavation

Expected Number of Unsafe MDF		**2.776**
Probability of Unsafe MDF		0.952
	λ	1.160
Index	**ILI measurement**	**Probability of Exceedance**
1	0.950	Excavation result = unsafe
2	0.939	Excavation result = safe
3	0.786	Excavation result = safe
4	0.334	0.320
5	0.263	0.261
6	0.263	0.262
7	0.243	0.245
8	0.169	0.177
9	0.131	0.141
10	0.112	0.122
11	0.082	0.091
12	0.082	0.091
13	0.082	0.090
14	0.079	0.086
15	0.079	0.087

- After the Excavation of No. 14 Indication

Suppose that after 14 excavations three anomalies have been found unsafe: No. 1, 11 and 12. The α and β would be updated with each safe anomaly. The parameter α is the number of safe anomalies.

$$\alpha = \alpha_0 + 11 = 11,$$

and β is the sum of the x_i of the safe anomalies.

$$\beta = \beta_0 + 0.939 + 0.786 + 0.333 + 0.262 + 0.263 + 0.242 + 0.168 + 0.132 + 0.112 + 0.081 + 0.078 = 3.393$$

The expected value of $\lambda = \frac{\alpha}{\beta} = \frac{11}{3.393} = 3.242$.

Table 13. After the 14th Excavation

Expected Number of Unsafe MDF		**2.386**
Probability of Unsafe MDF		0.923
	λ	3.242
Index	**ILI measurement**	**Probability of Exceedance**
1	0.950	Excavation result = unsafe
2	0.939	Excavation result = safe
3	0.786	Excavation result = safe
4	0.334	Excavation result = safe
5	0.263	Excavation result = safe
6	0.263	Excavation result = safe
7	0.243	Excavation result = safe
8	0.169	Excavation result = safe
9	0.131	Excavation result = safe
10	0.112	Excavation result = safe
11	0.082	Excavation result = unsafe
12	0.082	Excavation result = unsafe
13	0.082	Excavation result = safe
14	0.079	Excavation result = Safe
15	0.079	0.224

After 14 excavations, the expected number of unsafe anomalies left in ground based on the best estimate of λ is still more than 2.

Stop the Procedure

- After the Excavation of No. 33 Indication

If there are actually only three anomalies unsafe in the pipeline, finally, after 33 excavations,

$$\alpha = 30$$

and

$$\beta = 4.117$$

The expected value of $\lambda = \frac{\alpha}{\beta} = \frac{30}{4.117} = 7.286$. This value of λ implies an estimate of the number of remaining unsafe anomalies to be less than 0.5 ($N_k < 0.5$). It is regarded as a suitable stopping condition.

Alternate Prior Distributions

Since a non-informative Gamma distribution was initially assumed for λ in this study, such a distribution is often appropriate to avoid any bias of the results from a preconceived idea of what λ should be. The disadvantage of this approach is that the number of excavations required to converge on the correct value of λ may be large. If this procedure were to be used then, over time, a range of values of λ may be known. From this range, initial values of α_0 and β_0 could be set to incorporate the range of λ and quicken the rate at which the procedure converges to the correct value.